
# Regulating stem cell behaviour using bioengineered culture substrates

Thesis submitted in accordance with the requirements of the University of Liverpool for the degree of Doctor in Philosophy

by

Christopher James Hill

October 2016

# Acknowledgements

First, I would like to thank my supervisors Prof. Trish Murray and Prof. Olga Mayans for creating such an engaging and diverse project, and seeing the potential in me to fulfil it. I am very grateful for all of the support and guidance they have given me throughout this PhD. I am also thankful to Prof. Edward Draper and Dr. Sarrawat Rehman for their input and advice.

I would like to acknowledge the many people I have met and worked with over the last four years, particularly members of the Stem Cell Group, Lab C and the Mayans Group for their academic support and friendship. A special thanks has to go to Dr. Barbara Franke for her patience in teaching a rookie structural biologist the ropes, and for always finding the time to help out when things went wrong. I would also like to thank Dr. Jennifer Fleming, Dr. Svetomir Tsokov, Alison Beckett, Dr. Mark Morgan and Masoumeh Mousavinejad for their expert advice and contributions to this thesis. Additional thanks are due to the AJ's crowd for all the laughs on Friday nights and for their encouragement when PhD life seemed hard!

Last, but by no means least, I would like to extend my gratitude to my family and friends, who have supported me throughout my studies and beyond. I am truly fortunate to have them.

# Abstract

Stem cells hold enormous potential for the treatment of injuries and degenerative diseases. In the pursuit of stem cell therapies, a plethora of biomaterials have been developed to induce lineage-specific differentiation or support cell propagation for research and clinical applications. However, the use of stem cells is hindered by the cost of scale-up and risk of zoonotic transmissions from animal-derived culture components. Here, we utilise a recombinant protein scaffold composed of self-assembling nanofibres, termed ZT, and assess the systems adaptability for *in vitro* applications. Protein-based scaffolds offer distinct advantages over conventional materials such as the display of peptidic motifs with near-native stoichiometries and control of the spatial density and nanotopographical distribution of genetically-encoded bioactivities.

Herein, the functionalisation potential of the ZT system is explored via the generation of chimeric protein building blocks that exhibit the integrin-binding RGD motif. Specific sites within the building blocks were found to tolerate diversification, in the form of exogenous peptides or a fused protein domain, without structural perturbation or inhibition of assembly. The bioactivity of functionalised ZT nanofibres was assessed using murine mesenchymal stem cells (mMSCs), which recognised the integrin-binding moieties. The ability of one ZT nanofibre variant to induce mMSC chondrogenesis was investigated, which proved unsuccessful in the current context. A second generation of ZT variants were generated by the incorporation of chondroinductive motifs for future applications in cartilage tissue engineering. Additionally, the capacity of functionalised ZT nanofibres to act as culture substrates for human embryonic stem cell (hESC) self-renewal was explored.

It was found that a ZT variant containing a domain from fibronectin could support attachment of hESCs, and that cells maintained a pluripotent phenotype over multiple passages. Intriguingly, cell attachment to the recombinant substrate induced morphological changes and specific integrin activation. These findings hold promise for the future utility of the ZT system as a customisable biomimetic substrate for stem cell culture.

# Table of Contents

# List of figures

## List of tables



## List of equations

# Abbreviations

| | |
|---|---|
| **Å** | Angstrom |
| **AEC** | Anion exchange chromatography |
| **BSA** | Bovine serum albumin |
| **DAPI** | 4',6-diamidino-2-phenylindole |
| **$D_{max}$** | Maximum particle dimension |
| **DMEM** | Dulbecco's Modified Eagle's Medium |
| **dn/dc** | Differential index of refraction |
| **EB** | Embryoid body |
| **EDTA** | Ethylenediaminetetraacetic acid |
| **ESC** | Embryonic stem cell |
| **FCS** | Foetal calf serum |
| **FnIII** | Fibronectin type III domain |
| **$His_6$** | Hexahistidine tag |
| **IF** | Immunofluorescence |
| **Ig** | Immunoglobulin |
| **iPSC** | Induced pluripotent stem cell |
| **IMAC** | Immobilised metal affinity chromatography |
| **IPTG** | Isopropyl-β-D-1-thiogalactopyranoside |
| **kDa** | Kilodalton |
| **LB** | Luria-Bertani |
| **MALLS** | Multi-angle laser light scattering |
| **MM** | Molecular mass |
| **MSC** | Mesenchymal stem cell |
| **nm** | Nanometres |
| **OD** | Optical density |
| **PBS** | Phosphate buffered saline |
| **PCR** | Polymerase chain reaction |
| **PDB** | Protein Data Bank |
| **PEG** | Polyethylene glycol |
| **PSC** | Pluripotent stem cell |
| **$R_g$** | Radius of gyration |

| | |
|---|---|
| **RT-qPCR** | Real-time quantitative polymerase chain reaction |
| **SAXS** | Small angle X-ray scattering |
| **SD** | Standard deviation |
| **SDS-PAGE** | Sodium dodecyl sulphate polyacrylamide gel electrophoresis |
| **SEC** | Size exclusion chromatography |
| **SEM** | Standard error of the mean |
| **TCT** | Tissue culture-treated |
| **Tel** | Telethonin |
| **Tel$^{C\text{-}RGD}$11** | Telethonin with a C-terminal RGD motif in the pETM-11 vector |
| **Tel$^{C\text{-}RGE}$11** | Telethonin with a C-terminal RGE motif in the pETM-11 vector |
| **Tel$^{C\text{-}RGD}$13** | Telethonin with a C-terminal RGD motif in the pETM-13 vector |
| **Tel$^{C\text{-}RGE}$13** | Telethonin with a C-terminal RGE motif in the pETM-13 vector |
| **Tel$^{N\text{-}RGD}$13** | Telethonin with a N-terminal RGD motif in the pETM-13 vector |
| **Tel$^{N\text{-}RGE}$13** | Telethonin with a N-terminal RGE motif in the pETM-13 vector |
| **TEM** | Transmission electron microscopy |
| **TEV** | Tobacco etch virus |
| **Tris** | Tris-(hydroxymethyl)-aminomethane |
| **UV** | Ultraviolet |
| $V_M$ | Matthews coefficient |
| **Z1Z2** | Ig domains (Z1 and Z2) from the N-terminus of titin |
| **Z1Z2-Tel** | Palindromic complex of two Z1Z2 Ig doublets and telethonin |
| **Z1Z2$^{Fn}$** | Z1Z2 with the FnIII 10 domain fused at the C-terminus |
| **Z1Z2$^{HAVD}$** | Z1Z2 with the HAVD motif in the CD loop of Z1 |
| **Z1Z2$^{KLER}$** | Z1Z2 with the KLER motif in the CD loop of Z1 |
| **Z1Z2$^{RGD}$** | Z1Z2 with the RGD motif in the CD loop of Z1 |
| **Z1Z2$^{RGE}$** | Z1Z2 with the RGE motif in the CD loop of Z1 |
| **$Z_{1212}$** | Two Z1Z2 modules joined by an engineered linker |
| **$Z_{1212}^{Fn}$** | $Z_{1212}$ with the FnIII 10 domain fused at the C-terminus |
| **$Z_{1212}^{HAVD}$** | $Z_{1212}$ with the HAVD motif in the β-strand B of one Z1 domain |
| **$Z_{1212}^{KLER}$** | $Z_{1212}$ with the KLER motif in the CD loop of one Z1 domain |
| **$Z_{1212}^{RGD}$** | $Z_{1212}$ with the RGD motif in the CD loop of one Z1 domain |
| **$Z_{1212}^{RGE}$** | $Z_{1212}$ with an RGE control motif in the CD loop of one Z1 domain |
| **ZT** | Wild type nanofibres |

| | |
|---|---|
| **ZT$^{Fn}$** | Assembly product of $Z_{1212}{}^{Fn}$ and Tel |
| **ZT$^{HAVD}$** | Assembly product of $Z_{1212}{}^{HAVD}$ and Tel |
| **ZT$^{KLER}$** | Assembly product of $Z_{1212}{}^{KLER}$ and Tel |
| **ZT$^{RGD}$** | Assembly product of $Z_{1212}{}^{RGD}$ and Tel |
| **ZT$^{RGE}$** | Assembly product of $Z_{1212}{}^{RGE}$ and Tel |

# Chapter 1

# Introduction

## 1.1 Stem cells and regenerative medicine

Stem cells have received tremendous attention in recent years due to their potential use in regenerative medicine. The hallmark traits of stem cells are their capacity to self-renew and ability to undergo differentiation. These attributes have enabled scientists to translate stem cell research into tissue engineering strategies for the treatment of diseases and injuries (Ivanova *et al.*, 2002). Such strategies often require the use of biomaterial scaffolds for stem cell propagation, cellular delivery or to induce lineage-specific differentiation (Sakiyama-Elbert, 2008). In the regenerative medicine field, mesenchymal stem cells (MSCs) and embryonic stem cells (ESCs) feature prominently for reasons discussed below.

### *1.1.1 Mesenchymal stem cells*

The term "mesenchymal stem cell" was devised in 1991 by Arthur Caplan (Caplan, 1991) to describe a population of bone-marrow-derived stromal precursor cells first isolated by Alexander Friedenstein and colleagues (Friedenstein *et al.*, 1974). MSCs are a heterogeneous population of cells that are plastic-adherent and can differentiate into lineages from bone, fat and cartilage tissues *in vitro* by the addition of appropriate inductive agents (Horwitz *et al.*, 2005). Thus, MSCs represent an infinite pool of these cell types for use in regenerative medicine (Pittenger *et al.*, 1999). As well as cells of mesodermal origin, MSCs can

differentiate into lineages from unrelated tissues such as myocytes, neurones and hepatocytes (Petersen *et al.*, 1999; Mezey *et al.*, 2000; Jackson *et al.*, 2001). Thus, MSCs have become invaluable in tissue engineering strategies due to their multilineage potential. Additionally, MSCs can be sourced from a variety of tissues including bone marrow, umbilical cord tissue (Wharton's jelly and blood), peripheral blood and adipose tissue, therefore circumventing the danger of causing further damage when harvesting cells from a site of injury (Csaki *et al.*, 2008). The chondrogenic and osteogenic differentiation potential of MSCs have been their most exploited characteristic thus far, with vast numbers of studies describing their use in bone and cartilage repair (Gupta *et al.*, 2012; Knight and Hankenson, 2013). Understanding the regulators and mechanisms of cartilogenesis during skeletogenesis is extremely important in MSC-based cartilage tissue engineering, since such strategies aim to recapitulate the *in vivo* situation for effective neocartilage formation (Richardson *et al.*, 2015).

### *1.1.2 Mechanisms of chondrogenesis and cartilogenesis*

During skeletogenesis in the early embryo, invasion and proliferation of chondroprogenitor cells in the skeletal blastema and subsequent formation of cartilaginous nodules leads to joint formation (Goldring *et al.*, 2006). In the developing limb bud, the differentiation of mesenchymal progenitor cells to the chondrogenic lineage is a multifactorial process tightly regulated by a myriad of transcription factors and extracellular matrix (ECM) proteins. It is worth noting that in the developing embryonic skeleton, bone formation in the limbs and pelvis (by endochondral ossification) is preceded by cartilage anlage deposition, of which only articular cartilage remains after bone maturation. Thus, establishment of a cell niche

that is highly sensitive to microenvironmental changes promotes chondrogenic differentiation of progenitor cells (Djouad *et al.*, 2007). Key mediators in the main stages of chondrogenesis (summarised in Figure 1) include the following exogenous and endogenous cell signalling molecules: mitogenic fibroblast growth factors (FGFs) (Hellingman *et al.*, 2010), morphogens of the hedgehog signalling pathway, serine-threonine kinases, transcription factors of the RUNX and SOX families, and cytokines (Molténi *et al.*, 1999; Goldring *et al.*, 2006; Shimizu *et al.*, 2007).

Chondrogenic differentiation of progenitor cells begins by mass aggregation to form cellular condensations. This process is facilitated in part by increased hyaluronidase and metalloprotease activity to degrade the surrounding hyaluronan and collagen type I-rich ECM (Goldring *et al.*, 2006; Djouad *et al.*, 2007). Genes encoding the cell adhesion proteins N-cadherin and neural cell adhesion molecule (N-CAM) are upregulated by members of the transforming growth factor β (TGF-β) family of cytokines and support cell-cell interactions (Chimal-Monroy and De León, 1999). Once compressed, intercellular signalling between ECM proteoglycans, such as syndecans, glypicans, laminin, tenascins and cartilage oligomeric protein (COMP) activate signalling cascades which ultimately lead to chondrocyte maturation (DeLise *et al.*, 2000). An example of intercellular signalling activation in early chondrogenesis is the interaction of the α5β1 integrin ectodomain with fibronectin (Tavella *et al*., 1997; Nagae *et al*., 2012). Fibronectin has been shown to be essential for cellular condensation both in vitro and in vivo (Gehris *et al*., 1997).

Each successive step in chondrogenic differentiation is modulated by transcription factors (Figure 1), of which the most important are *SOX* genes. SOX transcription factors are expressed throughout the maturation process and SOX9 is crucial for condensation (Akiyama *et al.*, 2002). Although the role of FGFs in

chondroprogenitor cell condensation has not been fully defined, FGF2 has been shown to increase *SOX9* expression and promote chondrogenic differentiation of human MSCs *in vitro* (Handorf and Li, 2011). FGF receptor 3 (FGFR3) signalling is implicated in pre-chondrocyte proliferation and has an established role in chondrogenic aberration during late embryonic development (Ornitz and Marie, 2002). FGF9 and FGF18 signalling is important for both the promitogenic and hypertrophic effects of FGFR3, as mice lacking both growth factors show reduced chondrocyte proliferation and hypertrophy (Hung *et al*., 2007; Liu *et al*., 2007). Bone morphogenetic proteins (BMPs) also contribute to pre-cartilaginous condensation (Yoon *et al.*, 2005; Shimizu *et al.*, 2007). Following the proliferation of pre-chondrocytes, their differentiation to mature chondrocytes is dependent on SOX9, L-SOX5, SOX6 and BMP signalling (Akiyama *et al.*, 2002; Goldring *et al.*, 2006; Dy *et al.*, 2010). Completed differentiation is associated with the secretion of cartilage ECM composed primarily of collagen types II, IX and XI and the chondroitin sulphate proteoglycan, aggrecan (Goldring *et al.*, 2006). SOX9 is required for upregulation of the collagen type II gene and its coactivators, L-SOX5 and SOX6 (the SOX trio), promote aggrecan production as well as other ECM components (Ng *et al.*, 1997; Smits *et al.*, 2001). An alteration in the equilibrium of growth factor and cytokine signalling is responsible for chondrocyte proliferation, specifically involving BMPs and FGF1, 2 and 3-mediated upregulation of parathyroid hormone-related protein (PTHrP) and Indian hedgehog (IHH) which in turn stimulates mitosis (Minina *et al.*, 2002). Finally, in the case of chondrocytes constituting the long bone cartilaginous anlage, hypertrophy and cell death ensue. This process is positively modulated by members of the RUNX family of transcription factors; RUNX1, RUNX2 and RUNX3, which activate matrix

metalloprotease 13 and other downstream target genes including IHH (Enomoto *et al.*, 2000; Yoshida *et al.*, 2004; Goldring *et al.*, 2006). Hypertrophic chondrocytes drastically increase in volume and are positive for collagen type X, BMP-2, BMP-6 and alkaline phosphatase expression before apoptosis and ossification of the cartilage matrix by osteoblasts (Goldring *et al.*, 2006). FGFR1 signalling has been shown to be important in chondrocyte hypertrophy, as conditional FGFR1 knockout mice exhibit diminished hypertrophy during early development (Hung *et al*., 2007).

Many soluble signalling molecules involved in chondrogenesis, such as FGFs, are known to interact with heparan sulphate (HS) proteoglycans (HSPGs). The HSPG perlecan has been shown to play a pivotal role in cartilogenesis, as perlecan deficient mice exhibit abnormal cartilage formation and impaired endochondral ossification (Arikawa-Hirasawa *et al*., 1999; Costell *et al*., 1999). Furthermore, the HS-bearing domain of perlecan alone is sufficient to induce chondrogenic differentiation *in vitro*, suggesting that the glycosaminoglycan (GAG) component is responsible for the chondroinductive effect of perlecan (French *et al*., 2002). Perlecan may also be involved in adult cartilage homeostasis by sequestering FGF2, which is subsequently released in response to injury for activation of the ERK signalling pathway (Ellman *et al*., 2013). Syndecan-3, a transmembrane HSPG that also carries chondroitin sulphate chains, is highly expressed in precartilaginous mesenchyme and is required for cellular condensation (Gould *et al*., 1992; Koyama *et al*., 1996; Chimal-Monroy and Diaz de Leon, 1999). Functional blocking of syndecan-3 causes a reduction in FGF2-mediated proliferation of chondrocytes, which is indicative of a promitogenic role for syndecan-3 by modulation of FGF signalling pathways (Kirsch *et al*., 2002).

In summary, although the molecular mechanisms governing chondrocyte

differentiation, hypertrophy and endochondral ossification have been well documented, details of the unique developing joint microenvironment in which the articular phenotype is retained remain undefined. Thus, further clarification of key players in articular maintenance will greatly enhance efforts in regenerative medicine for cartilage tissue repair.

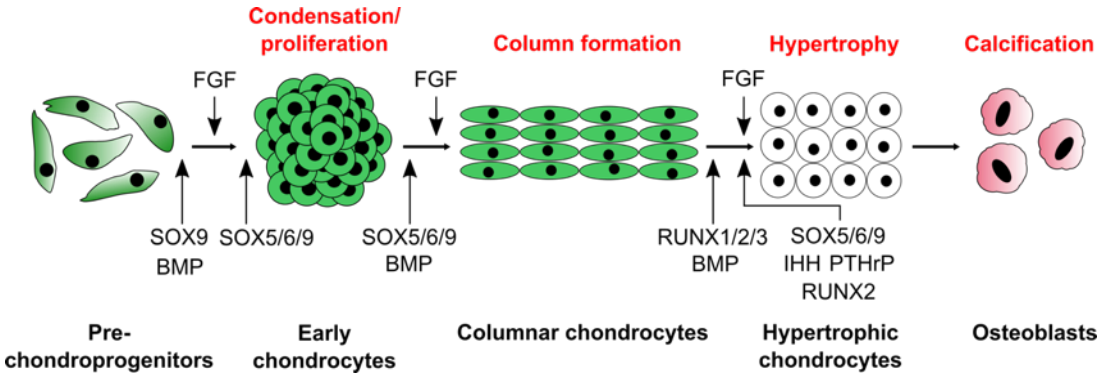


**Figure 1. Stages in chondrocyte differentiation and hypertrophy from the perspective of anlage formation and bone maturation in the developing limb bud**. All abbreviations are detailed in the main text. Figure adapted from Shimizu *et al*. (2007).

### *1.1.3 Pluripotent stem cells*

Pluripotent stem cells (PSCs) can give rise to any cell type of the body and are derived from the inner cell mass of the blastocyst. When isolated and cultured *in vitro*, they are termed embryonic stem cells (ESCs) and can self-renew indefinitely. ESCs were first isolated from the inner cell mass of mouse blastocysts in 1981 (Evans and Kaufman, 1981; Martin, 1981) and in 1998 the first human ESC (hESC) lines were established by the group of James Thomson (Thomson *et al.*, 1998). The ability of ESCs to differentiate into any somatic or germ cell lineage has generated enormous interest in their use for developmental biology, drug discovery and cellular therapies.

Aside from nuclear transfer or pluripotent cell fusion, somatic cells can be

stimulated to adopt an embryonic phenotype by inducing the expression of pluripotency-associated transcription factors. In 2006, the first induced pluripotent stem cell (iPSC) lines were generated by retroviral transduction of 24 candidate genes in mouse fibroblasts. Sequential trials revealed that as few as four genes (Oct3/4, c-Myc, Klf4 and Sox2) were required to reprogram somatic cells to a pluripotent phenotype (Takahashi and Yamanaka, 2006). A year later, the same group demonstrated that human dermal fibroblasts could be transformed into iPSCs (hiPSC) by expression of these four factors (Takahashi *et al.*, 2007). Shinya Yamanaka was awarded the Nobel Prize in Physiology or Medicine for his discovery that adult cells can be reverted to an embryonic state by the enforced expression of pluripotency associated transcription factors. Many adult cell types have been used to derive iPSC lines including hepatocytes, keratinocytes, neural stem cells and adipose-derived stem cells (Stadtfeld and Hochedlinger, 2010). The generation iPSCs circumvents two major drawbacks of ESCs; ethical protests from the use/destruction of human embryos and immune rejection of allogenic donor cells.

Many clinical trials are now underway to realise the potential of PSC research and therapies. The London Project to Cure Blindness, established in 2007, was the first approved UK clinical trial for application of hESCs and focused on the treatment of age-related macular degeneration. The project aims to transplant hESC-derived retinal pigment epithelial cells into the retina and the first patient was treated in 2015. Relatedly, autologous iPSC-derived dopaminergic neurons have now been successfully transplanted in a cynomolgous monkey model of Parkinson's disease with positive effects (Hallett *et al.*, 2015). As well as transplanting PSC-derived lineages to replace lost or damaged tissue, such cells could be used as screening platforms to evaluate the safety and efficacy of novel pharmaceuticals.

Unanticipated side-effects are the major cause for new and approved drugs being removed from the market, effectively wasting vast sums of money and research time. A prevalent example of such side-effects is cardiotoxicity, which accounts for 28% of pharmaceutical withdrawals in the USA (Gwathmey *et al.*, 2009). Current safety platforms for identifying negative cardiovascular effects are limited by the use of genetically modified non-cardiac-derived cell lines, which fail to recapitulate cardiac events and yield misleading information. Since primary human cardiomyocytes are effectively senescent and are prone to dedifferentiation *in vitro*, another model system is needed. The elucidation of specific factors required to differentiate PSCs to a cardiac phenotype, in combination with enhanced sorting techniques to obtain pure populations, now means that billions of cardiomyocytes can be produced for *in vitro* toxicity screening (Denning *et al.*, 2016).

## 1.2 Biomaterials

### *1.2.1 Fundamentals*

Cells are surrounded by an ECM, which provides structural support as well as modulating essential chemical and physical stimuli that are necessary for tissue and organ homeostasis. The ECM is a conglomerate of fibrous proteins with modular architectures such as fibronectin, tenascin, collagens and laminins. Proteoglycans including aggrecan and the GAG polysaccharides HS, chondroitin sulphate and hyaluronic acid are also present at varying ratios in different tissues. It is the tissue-specific composition and spatial arrangement of the ECM which gives each organ its mechanical and biochemical characteristics through mediation of cell attachment, migration, and differentiation. Furthermore, the ECM can guide tissue

organisation and function through binding and sequestering soluble growth factors and governing their release in response to stimuli (Frantz *et al.*, 2010). Thus, the tissue-specific physical and chemical cues imposed on cells by the ECM regulates phenotype and cell fate by engaging specific signalling pathways. These differences have been harnessed for the design of ECM-mimetic biomaterials that can direct the differentiation of stem cells to desired lineages for tissue engineering and regenerative medicine applications (Shekaran and Garcia, 2011).

In general, tissue engineering requires the combination of a biocompatible scaffold, a cell population and inductive agents (either as additional factors or incorporated into the scaffold) to drive differentiation to the required lineage or maintain cell phenotype (Figure 2). Scaffolds are typically composed of polymers, peptides, proteins or combinations of components to yield nanocomposite materials. Supramolecular polymers may be classified as ordered or disordered structures and assemble by non-covalent interactions. These mutable interactions bestow unique attributes on polymeric biomaterials such as the ability to reversibly switch their physicochemical properties by external stimuli (Dong *et al.*, 2015). Peptidic systems employ the self-associating properties of certain peptides to create defined structures such as fibres, rods and sheets. The resulting nanostructures are readily amenable to chemical modifications that imbue biological functionality (Nisbet and Williams, 2012). Like polymer-based materials, peptides can be easily modified to form three-dimensional structures, such as hydrogels, for cell encapsulation (Zhou *et al.*, 2009). The inherent biocompatibility of proteins makes them highly attractive as building blocks for biomaterials. They may also offer advantages over polymer and peptide-derived counterparts in terms of bottom-up functionalisation potential and controlled nanotopographical distribution of genetically engineered bioactive moieties. In

polymer/peptide systems, functionality is often endowed top-down following assembly by coating, saturating or chemically conjugating active factors. However, such approaches can result in the heterogeneous distribution of functional groups and inadequate potency due to clustering or undesirable stoichiometric presentation (Bruning *et al.*, 2010). Thus, protein-composed scaffolds represent a useful alternative to traditional, synthetic biomaterials.

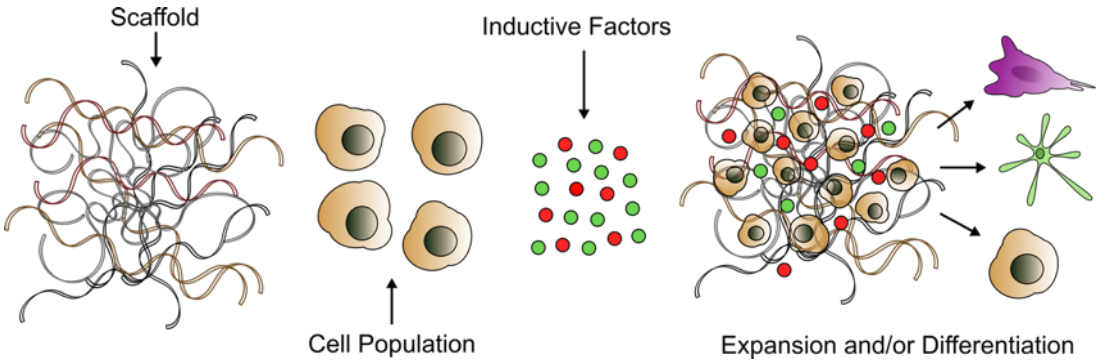


**Figure 2. Fundamentals of tissue engineering.** The principle of tissue engineering requires three components: a biocompatible scaffold, the cell type of interest or stem/progenitor cells capable of differentiation to the required phenotype, and inductive factors that can drive differentiation.

### *1.2.2 Self-assembling peptides and proteins as biomaterials*

A specific goal of protein nanotechnology is to develop scaffolds that mimic the ECM, thus the generation of fibrous assemblies is desirable since the ECM itself is a meshwork of polymeric proteins with modular architectures. Many natural polyproteins of the ECM have been utilised as scaffolds for *in vitro* applications including vitronectin, fibronectin, laminins and collagens. However, the majority of these proteins are extracted from animal sources by methods that may cause heterogeneous sampling, resulting in batch-to-batch inconsistencies. Further, immunoreactivity and zoonotic transmission are also cause for concern when using xenogeneic materials (Gomes *et al.*, 2012). The next generation of biomaterials is

likely to include more chimeric protein assemblies and nanocomposites sparked by advances in recombinant protein and synthetic biology technologies (Sørensen and Mortensen, 2005; Assenberg *et al.*, 2013). Multicomponent ECM proteins such as collagens have been recombinantly produced in eukaryotic expression systems and used as substrates for directed stem cell differentiation. However, production of full-length proteins with complex architectures is often challenging and requires the co-expression of chaperones or post-translationally-modifying enzymes for correct domain folding and quaternary structure assembly. For example, 4-hydroxylase must be co-expressed with collagen chains in yeast for assembly of triple-helical fibrils (Myllyharju *et al.*, 2000). In the case of fibrinogen, protease-deficient yeast must be used since *N*-glycosylation is a prerequisite for successful association of the Aα, Bβ and γ chains (Tojo *et al.*, 2008). Bulk recombinant protein production is most commercially viable when expressed in *E. coli*, however, this route is often confounded by the absence of eukaryotic post-translational modification machinery that is required for the synthesis of proteins identical to the native form (Gomes *et al.*, 2012). Therefore, there is a great need for alternative biomatrices that can circumvent the complications associated with natural ECM derivatives.

In Nature, many proteins exhibit self-assembly properties that have evolved to generate supramolecular functional complexes. These systems have allowed researchers to dissect the principles of protein self-association and develop methodologies for the rational design of synthetic nanostructures (King and Lai, 2013). Prominent examples of such structures are viral capsids, in which symmetry defines the assembly mode. Understanding the importance of symmetry in design concepts has led to the generation of novel protein cages and lattices by fusion of proteins that naturally oligomerise (Padilla *et al.*, 2001; Sinclair *et al.*, 2011).

Introducing self-association properties in proteins using bottom-up approaches and genetic engineering has pioneered the advent of a new generation of nanomaterials that surpass natural protein assemblies in terms of biological properties and customisation potential.

The *de novo* design of self-assembling peptide systems has seen much success in the fabrication of supramolecular structures for use in bionanotechnology. The majority of polypeptide-based assemblies incorporate small fragments of proteins (also called tectons) such as α helices in bundled or coiled-coil conformations, polyproline helices and β-sheet assemblies. To this end, many studies have utilised tectons derived from natural supramolecular assemblies such as silk, elastin and resilin that retain the polymerisation capacities of the parental protein domains (Cai and Heilshorn, 2014). Similarly, β-sheet-forming peptides have been derived from both amyloidogenic sequences and rationally designed peptides based on the fundamentals of β-sheet formation. The peptides may be assembled into fibrils or hydrogels and attempts have been made to functionalise these systems with integrin binding motifs for enhanced cell attachment and survival. Gras *et al.* (2008) functionalised a self-assembling peptide from transthyretin by incorporating the fibronectin RGD motif at the C-terminus and demonstrated the attachment of mouse fibroblasts to the modified fibres. A β-sheet peptide-based hydrogel has also been functionalised by integration of a linear RGD peptide, which increased human umbilical vein endothelial cell (HUVEC) adhesion without negatively effecting the mechanical properties of the gel (Jung *et al.*, 2009). However, peptide-derived materials are limited by their capacity to support a finite number of functionalities and exogenous peptides are often displayed in linear, non-native conformations due to a lack of spatial segregation between diversifiable sites and assembly interfaces

(Bruning *et al*., 2010).

Examples of folded protein domains exhibiting defined three-dimensional structures in bottom-up design strategies are relatively sparse in the literature. However, the utilisation of protein domains in self-assembling systems may overcome several limitations of tecton-based materials, namely the regulation of morphology, spatial separation of assembly interfaces with sites amenable to functionalisation and atomic level structural modification. Nevertheless, endowing protein domains with polymerisation properties is challenging due to the complex and highly reactive architecture of protein surfaces, which may respond in unpredictable and undesirable ways upon modification.

Recent advances in molecular modelling and the routine application of biophysical techniques, such as NMR (nuclear magnetic resonance spectroscopy) and X-ray crystallography, to the analysis of protein structures have allowed for the elucidation of structural features necessary for the logical design of supramolecular protein assemblies with defined features. Broadly speaking, there are three design strategies for the bottom-up generation of protein nanomaterials; domain fusion, site-directed mutagenesis and complementation (King and Lai, 2013). In domain fusion, proteins that naturally oligomerise are genetically fused and expressed as recombinant chimeras that assemble via homotypic interactions. This approach has been utilised to build tetrahedral protein cages by fusion of the trimeric bromoperoxiadase with the dimeric M1 matrix protein (Padilla *et al.*, 2001). Site directed mutagenesis can be used to introduce novel binding interfaces in monomeric proteins to form homo-oligomers. Grueninger *et al.* (2008) used this strategy to produce a trimeric urocanase and octameric L-rhamnulose-1-phosphate aldolase by extracting contact information from crystal structures and mutating

residues to induce self-association. Complementation involves the incorporation of non-biological moieties such as ligands or metal ions. In this fashion, hollow nanotubes were formed from the tetradecameric chaperonin GroEL by modification with 1'-(maleimidoethyl)spirobenzopyran, which coordinates divalent cations to connect GroEL monomers (Biswas *et al.*, 2009). It is also possible to combine different design avenues to achieve assembly. For example, filamentous assemblies have been fashioned using a combination of domain fusion and complementation strategies. In a specific example, human Erbin PDZ domains were fused to each subunit of the tetrameric superoxide reductase (SOR) from *Pyrococcus furiosus*. A second construct was generated by replacing the PDZ domains fused to SOR with a PDZ-binding ligand, which in the presence of the first chimera would self-assemble in an abutting manner (Usui *et al.*, 2009).

In summary, there is great need for novel ECM mimetics that can be tailored to imitate niche microenvironments by multiunctionalisation. Scaffolds generated from whole protein domains may represent the ideal materials for such applications; however, their rational design remains challenging.

## 1.3 The ZT nanofibre system

### *1.3.1 Concept and design*

This project is centred around a self-assembling protein system developed by the research group of Professor Olga Mayans (Bruning *et al.*, 2010). The system was inspired by the mode of titin dimerisation in the muscle sarcomere. Titin is a giant filamentous protein composed of approximately 300 domains, the majority of which comprise a fibronectin type III (FnIII) or immunoglobulin (Ig) fold (Meyer and

Wright, 2013). The sarcomere can be divided into several discrete zones, of which titin spans the entirety and is embedded N-terminally at the Z-disk and C-terminally at the M-line (Granzier and Labeit, 2004). The N-terminus of titin comprises two intermediate (I)-type Ig domains, Z1 and Z2, which interact with a crosslinking protein called telethonin (Tel). Structural elucidation of the Z1Z2-Tel complex has revealed that Tel forms an intermolecular β-sheet between two antiparallel Z1Z2 molecules to generate a unique palindromic assembly (Figure 3a). Within the complex, the four Ig-Tel interfaces are formed by two antiparallel β-sheets comprising β-strand G of each opposing Ig domain and the β-hairpin motifs of Tel (Figure 3b) (Zou *et al.*, 2006). The association is highly robust, as significant force is exerted upon the complex during passive muscle stretch (Bertz *et al.*, 2009). The structural ingenuity of this load-bearing assembly was harnessed for protein engineering purposes by Bruning *et al*. (2010). By combining domain fusion and complementation strategies, the Z1Z2-Tel complex was engineered to induce the propagative assembly of a self-associating protein copolymer. To accomplish this, the Z1Z2 doublet was fused in tandem to generate a four Ig chain (henceforth $Z_{1212}$, Figure 3c) joined centrally by a linker comprising the sequence **VQ**GETT**QA** (residues in bold are integral to the flanking Z1 and Z2 Ig domains). The linker was considered suitable since both threonine residues were calculated to be free from interaction with flanking modules by *in silico* modelling, thus allowing for interdomain motion at this site (Bruning *et al*., 2010). Both $Z_{1212}$ and Tel could be recombinantly expressed in *E. coli* at high yields. Hypothetically, each $Z_{1212}$ tandem interfaces with two Tel molecules, thus permitting the sequential recruitment of building blocks in an adjoining manner to form fibrillar assemblies (Figure 3c). The resulting nanofibres, termed ZT, were predicted to follow two assembly modes by

molecular simulations. Indeed, two distinct morphologies were observable by transmission electron microscopy (TEM); “tapelike” fibres with apparent helicity and “curly” fibres with high flexibility (Figure 3d,e). Tapelike fibres are formed by transverse association of building blocks perpendicular to the fibre axis, and have a diameter of ~14 nm. Curly fibres are generated by longitudinal stacking and have a diameter of ~7 nm. The alternative stacking arrangements can be expected to impart characteristic properties on the resulting nanofibres. In tapelike fibres, the engineered linker of $Z_{1212}$ is situated at the centre of the fibril, thus flexibility from this point would be sterically hindered and result in a semi-rigid arrangement (Figure 3d). Conversely, longitudinal stacking in curly fibres allows for intermodular motion around the engineered linker as demonstrated by the high flexibility and kinking propensity of this morphology (Figure 3e).

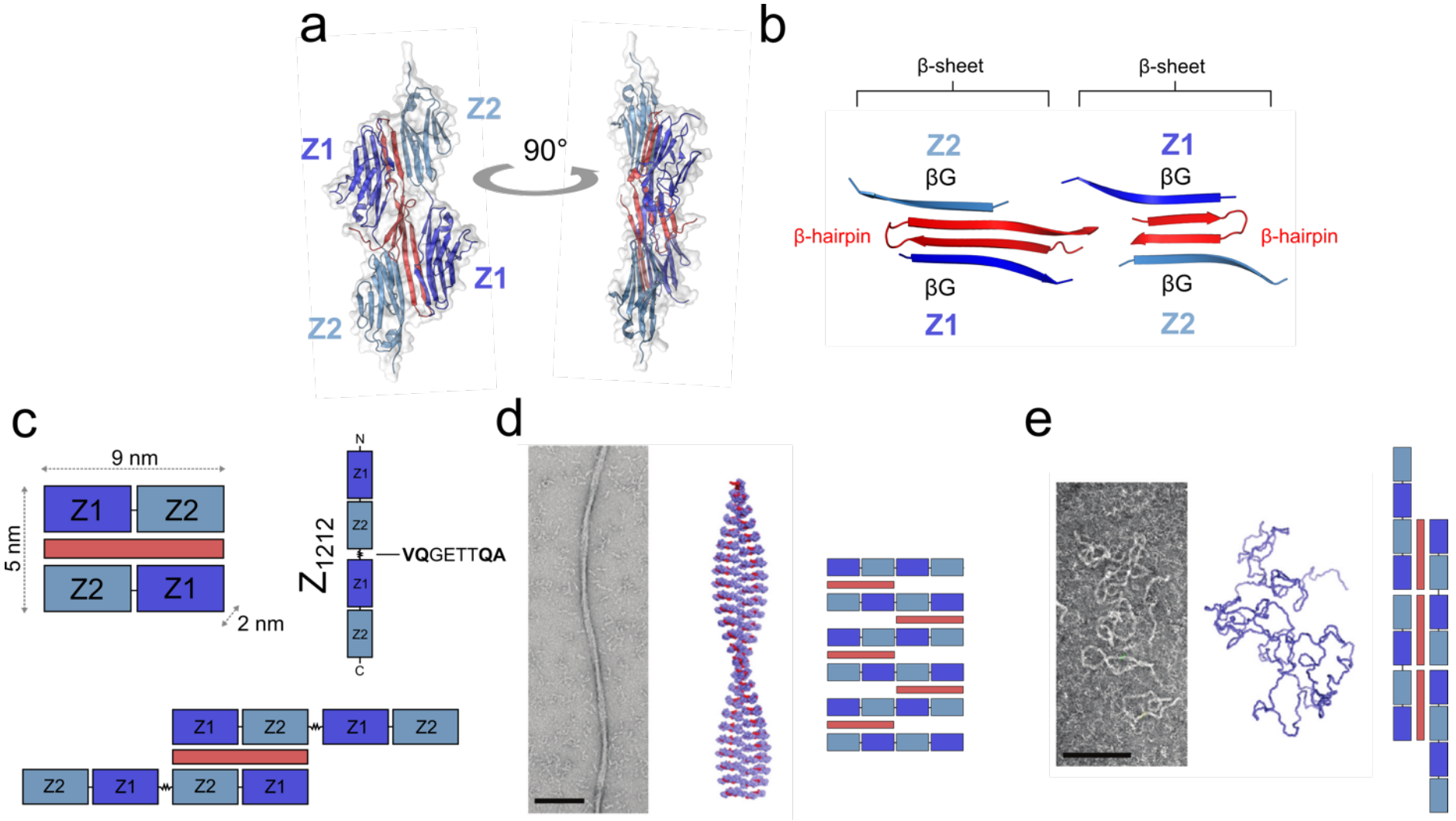
a
Z2
Z1
90°
Z1
Z2
b
β-sheet
β-sheet
Z2
Z1
βG
βG
β-hairpin
β-hairpin
βG
βG
Z1
Z2
c
9 nm
5 nm
Z1
Z2
Z2
Z1
2 nm
N
Z1
Z2
Z1
Z2
C
Z1212
VQGETTQA
Z1
Z2
Z1
Z2
Z2
Z1
Z2
Z1
d
e

**Figure 3. Building blocks and assembly modes of ZT nanofibres.** (a) Crystal structure (PDB: 1YA5, Zou *et al*., 2006) of the "sandwich-like" biological complex formed by two Z1Z2 Ig-doublets from titin (Z1; *blue*, Z2; *light blue*) and telethonin (*red*) in human muscle. This complex represents the repeating unit of ZT nanofibres. (b) Intermolecular antiparallel β-sheet formation in the Z1Z2-Tel complex. The schematic shows β-strand G from each opposing Ig domain and the two β-hairpin motifs of telethonin as observed in the crystal structure. (c) Schematic representations of fibre building blocks showing the Z1Z2-Tel complex with dimensions labelled (*top left*), $Z_{1212}$ and position of the engineered linker (*top right*) and the propagative assembly mode of $Z_{1212}$ with Tel (*bottom*). In the engineered linker, residues integral to the flanking Ig domains are highlighted (*bold*). Nanofibres exhibit two morphologies: "tapelike" (d) and "curly" (e) due to differential stacking arrangements of the individual components. Each panel shows a TEM micrograph (*left*), an *in silico* simulation-generated model (*middle*) and a schematic representation of the assembly (*right*). Scale bars = 100 nm. Figure taken in part and adapted from Bruning *et al*. (2010).

### *1.3.2 Functionalisation potential of ZT nanofibres*

ZT nanofibres could display functional groups with nanoscale periodicity via recruitment of gold nanoparticles to an N-terminal hexahistidine tag on Tel, thus confirming the functionalisation potential of the system (Bruning *et al*., 2010). However, several other sites were identified that are spatially segregated from the assembly interface and may permit the display of exogenous peptides. Flexible loops on the surface of the Z1 and Z2 Ig domains are promising candidates for functionalisation since they represent the most variant regions of the (I)-type Ig domains of titin in terms of amino acid composition (Bruning *et al*., 2012). Ig domains are composed of 70-100 residues and share a β-sandwich framework. The tertiary structure is composed of antiparallel β-strands (βA – βG) ordered into two β-sheets, which pack against each other to form the β-sandwich. Different Ig subtypes can be classified by the topology of the β-strands; (I)-type Ig domains are typically composed of one β-sheet formed by β-strands A, B, E and D, and another β-sheet formed by β-strands G, F and C (Bodelón *et al.*, 2013) (Figure 4a). Each strand is connected by a loop, the nomenclature of which is based upon the strands it

connects. For example, the CD-loop connects β-strands C and D (Figure 4b).

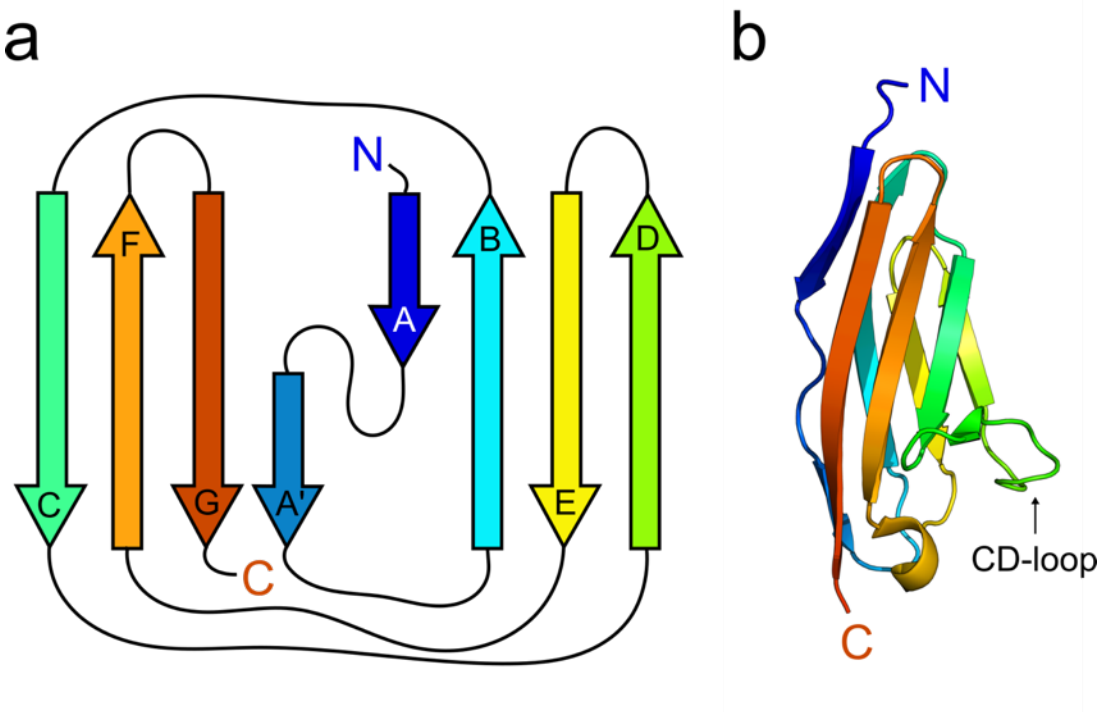


**Figure 4. Structure and topology of (I)-type Ig domains.** (a) Topological schematic of the (I)-type Ig fold and β-strand nomenclature. (b) Crystal structure of the Z1 Ig domain from titin (PDB: 1YA5, Zou *et al.*, 2006). The position of the CD-loop is indicated (*arrow*). Figure adapted from Meyer and Wright, (2013).

Previous work has shown that the Z1 domain can tolerate drastic diversification of the CD-loop by insertion of the FLAG affinity tag (DYKDDDDK) and the native PxxP SH3-interaction motif (Bruning *et al.*, 2012). The CD-loop was chosen because it is a region of low sequence conservation between the Ig domains of titin, thus residue composition has a low requirement for correct fold architecture. Despite moderately destabilising Z1 as evidenced by thermal denaturation, the exogenous sequences did not cause misfolding nor decrease protein yield. Analysis of these chimeric Z1 domains by NMR and Fourier transform infrared (FTIR) spectroscopy concluded that correct folding of the domain is not compromised by alterations to the CD-loop. Further, the FLAG sequence was shown to be exposed in

the context of Z1 and could actively bind an anti-FLAG M2 antibody as demonstrated by pull-down and isothermal titration calorimetry (ITC) (Bruning *et al.*, 2012).

The ZT nanofibre system was designed to support bottom-up functionalisation by spatial separation of diversifiable sites and assembly interfaces. Furthermore, the system is amenable to multifunctionalisation strategies through the utilisation of numerous customisable sites. These sites include the N- and C-termini of Tel, the CD-loops of Z1 and Z2, the N-terminus of Z1 and the C-terminus of Z2 (Figure 5). The Z1Z2-Tel complex was purposely chosen as a building block because the association of the individual components is main-chain mediated and largely independent of sequence composition. Indeed, various truncated and/or mutated variants of Tel have been shown to retain their capacity to bind Z1Z2 (Zou *et al.*, 2003).

Multifunctionalisation may be achievable via the incorporation of cell adhesive and substrate adhesive moieties at different sites, or by coupling enzymatic and catalytic modules for orthogonal recognition. Since foreign peptides and/or domains would be genetically encoded, the periodicities of functional moieties are defined and customisable at the nanoscale (Bruning *et al*., 2010).

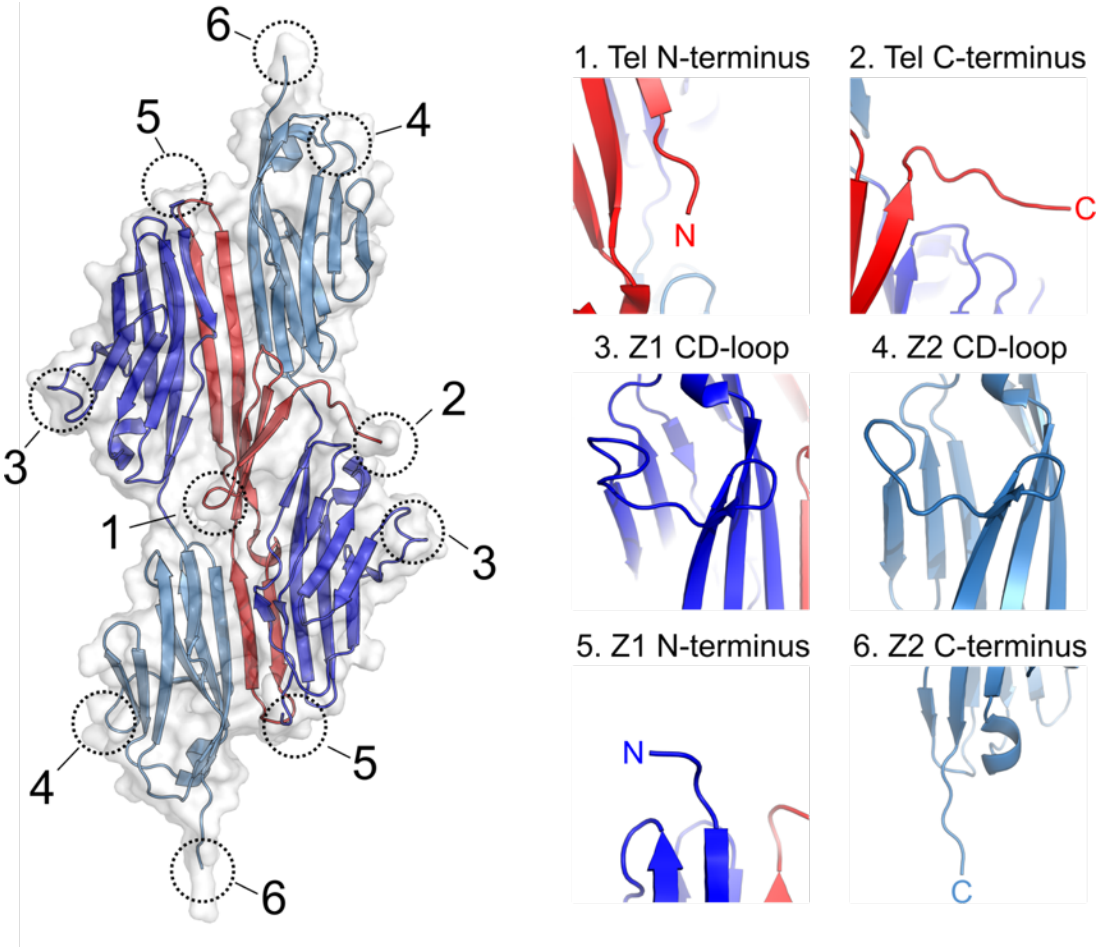


**Figure 5. Functionalisation potential of ZT nanofibres.** The crystal structure of the titin-telethonin complex is shown to the left and potential sites for functionalisation are circled and numbered. Zoomed views of the numbered sites are shown to the right and a description is given above each image.

## 1.4 Aims

The biomaterials field encompasses a plethora of research on materials science and biotechnology, with novel substrates and translational approaches reported daily. However, biomaterials composed of folded protein domains in ordered, modular arrays are somewhat underrepresented as scaffolds for stem cell culture or differentiation. The aim of this work was to explore the functionalisation potential of ZT nanofibres and assess the applicability of the system to act as an ECM mimetic for stem cell applications. For this, the following steps were taken:

1. To assess the functionalisation capacity of the system, individual components of ZT nanofibres were genetically engineered to generate protein chimeras displaying exogenous peptide motifs with biological activities.
2. To ensure that domain integrity and polymerisation capacity were maintained following mutation, the chimeric proteins were heterologously expressed and structurally characterised.
3. In order to validate the bioactivity of functional moieties, the ability of nanofibre variants to promote MSC adhesion was assessed. Further, the chondroinductive potential of an integrin-binding ZT variant was investigated.
4. To demonstrate the ability of functionalised nanofibres to act as recombinant substrates for hESC propagation, HUES7 cell attachment, self-renewal and pluripotency were characterised when cultured on a ZT variant.

# Chapter 2

# Materials and methods

## 2.1 Molecular biology

### *2.1.1 Materials*

All restriction endonucleases were purchased from New England Biolabs (NEB) and digestions were performed according to the manufacturer's guidelines in the recommended buffer system. Primers were purchased from Sigma Aldrich. Primer-specific amplification of DNA fragments by PCR used Q5 High-Fidelity DNA Polymerase (NEB). PCR reaction cleanup and extraction of DNA from agarose gels used the ISOLATE II PCR and Gel Kit (Bioline).

### *2.1.2 QuikChange site-directed mutagenesis*

For QuikChange site-directed mutagenesis (Braman *et al.*, 1996), primers were designed using the QuikChange Primer Design Program (Agilent Technologies). Following whole plasmid amplification with KOD Hot Start DNA Polymerase (Merck Millipore), methylated (non-mutated) DNA was digested by the addition of 10 U DpnI (Thermo Scientific) for 1 h at 37°C. Next, 1 µL of linear DpnI-treated DNA was added to a reaction mixture comprising 5 U T4 Polynucleotide Kinase (NEB), 0.5 µL T4 buffer and nuclease-free water to a total volume of 5 µL. The reaction was incubated for 30 min at 37°C before addition of 200 U T4 DNA Ligase (NEB), 0.5 µL T4 buffer and nuclease-free water to a final volume of 10 µL. Following incubation for 1 h at room temperature (RT;

approximately 22°C), all of the reaction mixture was used to transform chemically-competent *Escherichia coli* (*E. coli*) cells (section 2.1.4).

### *2.1.3 Ligation*

Ligation of endonuclease-digested DNA fragments and plasmid vectors used T4 DNA Ligase (NEB) according to the manufacturer's protocol. Typically, a 3:1 molar ratio of insert to vector DNA was used and ligations were allowed to occur for 30 min at RT.

### *2.1.4 Bacterial transformation*

*E. coli* DH5α (Invitrogen) or BL21 (DE3) (Novagen) RbCl-chemically competent cells were transformed with plasmid DNA as follows; 50 µL aliquots of cells stored at -80°C were mixed with plasmid DNA and incubated for 30 min on ice. Cells were subsequently heat-shocked at 42°C for 45 s and rested on ice for 1 min. 500 µL of Luria-Bertani (LB) medium was added and the cells were incubated at 37°C with shaking for 1 h, after which the suspension was spread on LB agar plates supplemented with the appropriate antibiotic and incubated overnight at 37°C.

### *2.1.5 Mutant verification*

Following transformation of plasmid DNA, antibiotic-resistant colonies were screened for correct construct size by PCR; a sterile pipette tip was used to touch each colony and then transferred to a 0.2 mL tube containing 25 µL MyTaq™ Red Mix (Bioline) mastermix (Table 1). Vigorous mixing was used to displace the bacteria from the tip and disperse the cells throughout the reaction mixture. After thermocycling (Table 1), amplicon size was determined by agarose gel

electrophoresis with reference to a molecular mass (MM) marker (HyperLadder™ 1kb, Bioline). Colonies containing plasmids with the correct insert size were used to inoculate 10 mL Luria-Bertani broth and grown overnight at 37°C. Cells were collected by centrifugation and plasmid DNA was extracted using the ISOLATE II Plasmid Mini Kit (Bioline). All constructs were verified by Sanger sequencing (Source BioScience Sequencing Service) using T7 forward and reverse primers (Table 2).

**Table 1.** Reaction components and PCR cycling conditions for transformant screening using MyTaq™ Red Mix.

| Reaction Components | Volume (µL) | | Cycling Conditions |
|---|---|---|---|
| | | 1X | 95°C, 5 min |
| MyTaq™ Red Mix | 12.5 | | 95°C, 15 s |
| Sense (5') primer (10 µM) | 1 | 30X | 50°C, 10 s |
| Antisense (3') primer (10 µM) | 1 | | 72°C, 15 s/kb |
| Nuclease-free water | 10.5 | 1X | 72°C, 2 min |

## 2.2 Protein cloning

The nucleic acid sequences of all protein constructs produced during the course of this project are given in the Appendix.

### *2.2.1 $Z_{1212}$ grafted fibronectin chimera cloning*

Mutant proteins were produced from wild type (*wt*) $Z_{1212}$ tandem template (described by Bruning *et al*., 2010). Insertion of the RGD motif into the second Z1 domain of $Z_{1212}$ ($Z_{1212}^{RGD}$) was by overlap extension PCR; two fragments were created from the $Z_{1212}$ template DNA (corresponding to native residues 1-242 and 242-391) which overlapped by additional bases coding for the RGD motif generated

during fragment amplification. The first fragment (residues 1-242) was generated using the primers 1 and 4, and the second fragment (residues 242-391) using primers 2 and 3 (Table 2). Individual fragments were hybridised and amplified using a two-stage thermocycling protocol, the first cycle with the fragments alone and the second in the presence of primers 1 and 2 (note: the T7 forward and reverse primers complement sites upstream and downstream of the multiple cloning site and are integral to the pETM plasmid vectors). The grafted insert was seven amino acids in length and replaced residues 243-246 with four non-native residues flanking the RGD motif (SGRGDSS). An RGE variant ($Z_{1212}^{RGE}$) was produced using the QuikChange method to replace aspartic acid with glutamic acid. Constructs were ligated into the pETM-11 vector (EMBL Plasmid Collection) via the NcoI and KpnI restriction sites so as to incorporate an N-terminal hexahistidine ($His_6$) tag and a tobacco etch virus (TEV) cleavage site.

### *2.2.2 Telethonin grafted fibronectin chimera cloning*

All Tel mutants were produced from a C-terminally truncated cysteine-null Tel template (residues 1-87, UniProt O15273, Bruning et al., 2010). Four mutants were produced in the pETM-13 vector (EMBL Plasmid Collection) as follows; a Tel amplicon containing a GRGDSGRGD sequence and $His_6$-tag at the N-terminus was generated using primers 2 and 5 (Table 2), which was inserted into the pETM-13 vector via the NcoI and KpnI restriction sites ($Tel^{N\text{-}RGD}13$). A control construct containing a GRGESGRGE sequence ($Tel^{N\text{-}RGE}13$) was produced in the same fashion using primers 2 and 6 (Table 2). Two similar constructs containing motifs at the C-terminus ($Tel^{C\text{-}RGD}13$ and $Tel^{C\text{-}RGE}13$ ) were generated using primers 1 and 7 or 1 and 8 (Table 2) for $Tel^{C\text{-}RGD}13$ and $Tel^{C\text{-}RGE}13$, respectively.

Two Tel mutants were produced in the pETM-11 vector as follows; a Tel amplicon containing a GRGDS motif at the C-terminus was generated using primers 1 and 9 (Table 2), which was inserted into the pETM-11 vector via the NcoI and KpnI restriction sites ($Tel^{C\text{-}RGD}11$). A control construct containing a GRGES motif ($Tel^{C\text{-}RGE}11$) was produced in the same fashion using primers 1 and 10 (Table 2).

**Table 2. Primers for the generation of $Z_{1212}$ and Tel fibronectin chimeras.** Non-native bases are shown in *red* and restriction sites are highlighted (*bold, underlined*).

| Primer | Description | Restriction enzyme | Sequence (5' – 3') |
|---|---|---|---|
| 1 | T7 Forward | - | TAATACGACTCACTATAGGG |
| 2 | T7 Reverse | - | GCTAGTTATTGCTCAGCGG |
| 3 | $Z_{1212}^{RGD}$ Forward | - | GTGATTTCCAGTGGTCGCGG CGATAGCAGTCC |
| 4 | $Z_{1212}^{RGD}$ Reverse | - | CACGCCGGGACTGCTATCGC CGCGAC |
| 5 | $Tel^{N\text{-}RGD}13$ Forward | NcoI | ATG**CCATGG**GTCATCATCATC ATCATCATCGCGGCGATAGC GGCCGCGGCGATATGGCTAC CTCAGA |
| 6 | $Tel^{N\text{-}RGE}13$ Forward | NcoI | ATG**CCATGG**GTCATCATCATC ATCATCATCGCGGCGAAAGC GGCCGCGGCGAAATGGCTAC CTCAGA |
| 7 | $Tel^{C\text{-}RGD}13$ Reverse | KpnI | GATC**GGTACC**TTAATGATGAT GATGATGATGCGGATCGCCG CGGCCGCTATCGCCGCGCTG GTAGGG |
| 8 | $Tel^{C\text{-}RGE}13$ Reverse | KpnI | GATC**GGTACC**TTAATGATGAT GATGATGATGCGGTTCGCCG CGGCCGCTTTCGCCGCGCTG GTAGGG |
| 9 | $Tel^{C\text{-}RGD}11$ Reverse | KpnI | **GGTACC**TCAGGGGCTATCGC CGCGACCACTCTGGTAGGG |
| 10 | $Tel^{C\text{-}RGE}11$ Reverse | KpnI | **GGTACC**TCAGGGGCTTTCGC CGCGACCACTCTGGTAGGG |

### *2.2.3 $Z_{1212}$ fibronectin fusion chimera cloning*

The region of fibronectin encoding type III domains 8 to 11 (residues 1269-1638, UniProt P02751) was amplified from human cDNA (a kind gift from Dr. Andrew Marriott, University of Liverpool) with primers 11 and 12 (Table 3) and used for subcloning. A fusion protein comprising $Z_{1212}$ and the tenth type III domain of fibronectin (FnIII 10) joined C-terminally was produced by Golden Gate Assembly (Engler *et al.*, 2009); sequence corresponding to FnIII 10 (residues 1448-1543) was amplified with an N-terminal BbsI restriction site using primers 13 and 14 (Table 3). A $Z_{1212}$ amplicon with a C-terminal BbsI site was made in the same fashion using primers 15 and 16 (Table 3) and both fragments were ligated after digestion with BbsI. Primers were designed to introduce a GETTQ linker sequence between the C-terminal residue of $Z_{1212}$ (Q389) and start residue of FnIII 10 (S1448). The full-length fusion protein ($Z_{1212}^{Fn}$) was ligated into the pETM-11 vector via the NcoI and KpnI restriction sites.

**Table 3. Primers for the generation of fibronectin constructs.** Non-native bases are shown in *red* and restriction sites (*bold, underlined*) are highlighted. Overhangs produced by the Type IIS restriction endonuclease BbsI (for Golden Gate assembly) are shown in *bold italics*.

| Primer | Description | Restriction enzyme | Sequence (5' – 3') |
|---|---|---|---|
| 11 | Fn-III 8-11 Forward | NcoI | CG**CCATGG**ATCATCCCAGCTGTT |
| 12 | Fn-III 8-11 Reverse | KpnI | GA**GGTACC**TCACAGTCCTTTAGGGCG |
| 13 | Fn-III$^{10}$ Forward | BbsI | TATTAA**GAAGAC*ACTCAG***TCTGATGTTCCGAGGGAC |
| 14 | Fn-III$^{10}$ Reverse | KpnI | GA**GGTACC**TCAGTCAATTTCTGTTCG |
| 15 | $Z_{1212}$ Forward | NcoI | GCG**CCATGG**CAACTCAAGCA |
| 16 | $Z_{1212}$ Reverse | BbsI | GTGGTG**GAAGAC*CT***CTGATGTTTCACCTTGAAC |

### *2.2.4 Generation of the Z1Z2 doublet and chimeric variants*

A construct comprising the dual Z1Z2 Ig domains from titin (residues 1-196, UniProt Q8WZ42) was amplified from the $Z_{1212}$ template DNA using primers 17 and 18 (Table 4) and cloned into the pETM-11 vector via the NcoI and KpnI restriction sites. The process was repeated for $Z1Z2^{RGD}$, $Z1Z2^{RGE}$ and $Z1Z2^{Fn}$ variants using the corresponding $Z_{1212}$ chimeras as templates.

**Table 4. Primers for the generation of Z1Z2 chimeras.** Non-native bases are shown in *red* and restriction sites are highlighted (*bold, underlined*).

| Primer | Description | Restriction enzyme | Sequence (5' – 3') |
|---|---|---|---|
| 17 | Z1Z2 Forward | NcoI | GCG***CCATGG***CAACTCAAGCA |
| 18 | Z1Z2 Reverse | KpnI | GA***GGTACC***TCATGTCTCGCC CTGCAC |

### *2.2.5 $Z_{1212}$ grafted N-cadherin and decorin chimera cloning*

Insertion of the N-cadherin HAVD motif in β-strand B or the decorin KLER motif in the CD-loop of Z1 used the QuikChange method. As the $Z_{1212}$ tandem contains two complementary sites for any specific primer, *wt* Z1Z2 (section 2.2.4) was used as a template for site-directed mutagenesis. The HAVD motif was inserted between residues A26 and F31 using primers 19 and 20 (Table 5), replacing native residues I28-G30 (H27 was retained) to produce $Z1Z2^{HAVD}$. For insertion of the KLER motif, several rounds of QuikChange mutagenesis were required to generate the desired constructs by sequential mutation/deletion of codons using primers 21-26 (Table 5). The KLER motif was placed between V45 and L51, replacing native residues I46-T50 to produce $Z1Z2^{KLER}$.

To fuse the mutated and *wt* Z1Z2 sequences in order to recreate the original tandem, *wt* $Z_{1212}$ in the pETM-11 vector was digested with unique (single site) restriction enzymes NcoI and SacI. The NcoI site is located upstream of the inserted construct in the multiple cloning site, whilst the SacI site is integral to the $Z_{1212}$ sequence (Figure 6). Digestion with these enzymes generates two fragments; 5934 bp and 569 bp. The 5934 bp fragment comprising the vector and secondary Z1Z2 module of $Z_{1212}$ was purified by agarose gel electrophoresis. Similarly, $Z1Z2^{HAVD}$ and $Z1Z2^{KLER}$ constructs were amplified with T7 forward and reverse primers (Table 2) and digested with NcoI and SacI. Finally, the 5934 bp and $Z1Z2^{HAVD}$/$Z1Z2^{KLER}$ fragments were ligated to produce $Z_{1212}{}^{HAVD}$ and $Z_{1212}{}^{KLER}$.

**Table 5. Primers used for the generation of N-cadherin and decorin chimeras.** Non-native bases incorporated by the QuikChange method are shown in *red*.

| Primer | Description | Sequence (5' – 3') |
|---|---|---|
| 19 | $Z1Z2^{HAVD}$ Forward | TGATTTCCAGTTCCTGAGGTG |
| 20 | $Z1Z2^{HAVD}$ Reverse | ACAGCGTGAGCCTCAAAGGTTGC |
| 21 | $Z1Z2^{K}$ Forward | AAAACTTCCACTCTGCCCGGC |
| 22 | $Z1Z2^{K}$ Reverse | CACCTGGCCATCCCTAAAC |
| 23 | $Z1Z2^{KL}$ Forward | CCAGGTGAAACTCTCCACTCTGCCCG |
| 24 | $Z1Z2^{KL}$ Reverse | CCATCCCTAAACCAGCTC |
| 25 | $Z1Z2^{KLER}$ Forward | GGTGAAACTCGAACGCCTGCCCGGCGTG |
| 26 | $Z1Z2^{KLER}$ Reverse | TGGCCATCCCTAAACCAG |

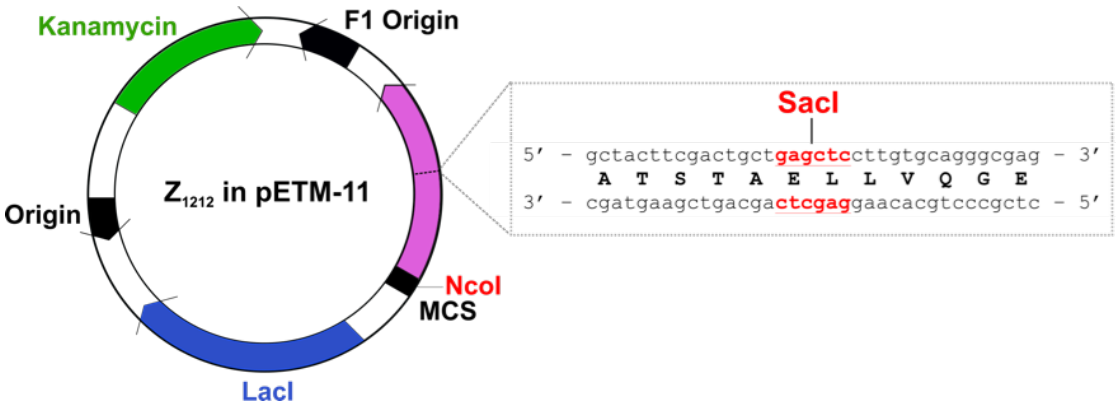


**Figure 6. Vector map of $Z_{1212}$ in the pETM-11 plasmid.** Key features of the map are labelled and the position of the unique SacI site between the Z1Z2 doublets of $Z_{1212}$ (*purple*) is shown to the right. The NcoI site in the multiple cloning site (MCS) is also highlighted.

### *2.2.6 Cloning for co-expression of protein complexes*

To permit the dual transformation of *E. coli* DH5α cells with plasmids encoding interacting proteins and their subsequent co-expression, Z1Z2 variants were subcloned into the pET-15b vector (Novagen) that contains an ampicillin resistance gene. Sequences encoding Z1Z2 variants were amplified using T7 forward and reverse primers (Table 2) to include the multiple cloning site from the pETM-11 vector. Fragments were digested with XhoI/KpnI and ligated into the pET-15b plasmid spliced with the same restriction endonucleases. The XhoI site omits the incorporation of an N-terminal $His_6$ tag and thrombin cleavage site encoded by the pET-15b vector, meaning that the recombinantly expressed protein is untagged and can only be isolated by immobilised metal affinity chromatography when complexed with a tagged binding partner.

## 2.3 Recombinant protein production

### *2.3.1 Protein expression*

Expression of all protein constructs was achieved by transformation of *E. coli* BL21 (DE3) RbCl chemically competent cells with construct-containing plasmids. Cultures were inoculated 1:100 and grown at 37°C with shaking to an $OD_{600}$ of 0.6 in Luria Bertani (LB) medium containing appropriate antibiotics (25 μg/mL kanamycin or 50 μg/mL ampicillin for constructs encoded by the pETM-11 and pET-15b vectors, respectively). Cultures were grown overnight at 18°C in the presence of 1 mM isopropyl-thio-β-D-galactopyranoside (IPTG; Bioline) to induce protein overexpression, after which cells were harvested by centrifugation at 6,600*g* for 20 min at 4°C and stored at -80°C until use.

### *2.3.2 Purification of Z1Z2 and $Z_{1212}$ chimeras*

The following proteins were isolated and purified using the method described below: *wt* Z1Z2, $Z1Z2^{HAVD}$, $Z1Z2^{KLER}$, *wt* $Z_{1212}$, $Z_{1212}^{RGD}$, $Z_{1212}^{RGE}$, $Z_{1212}^{Fn}$, $Z_{1212}^{HAVD}$ and $Z_{1212}^{KLER}$. Cell pellets were thawed on ice and resuspended in lysis buffer (50 mM Tris-HCl pH 7.4, 500 mM NaCl) supplemented with EDTA-free protease inhibitor cocktail (Roche) and 10 μg/mL DNAse I (Sigma Aldrich) before disruption by high pressure homogenisation. Lysates were clarified by centrifugation at 40,000*g* for 40 min at 4°C. The soluble fraction was filtered (0.22 μm polyethersulfone syringe filter) and applied to a 1 mL $Ni^{2+}$-NTA Hi-Trap column (GE Healthcare). Bound recombinant protein was eluted with an imidazole gradient and supplemented with approximately 20 μg of TEV protease per mL of protein solution. Samples were dialysed into 50 mM Tris-HCl pH 7.4, 100 mM NaCl (gel

filtration buffer) overnight at 4°C to allow for His-tag cleavage. Next, samples were applied once more to a $Ni^{2+}$-NTA Hi-Trap column to remove the protease, His-tag and uncleaved sample that remained bound to the column. The flow-through containing cleaved recombinant protein was concentrated before further purification by size-exclusion chromatography using either a Superdex 200 16/60 or 26/60 column (GE Healthcare) equilibrated in gel filtration buffer. Finally, proteins were dialysed overnight at 4°C in 50 mM Tris-HCl pH 8.0, 50 mM NaCl and applied to a Mono Q 5/50 GL anion-exchange column (GE Healthcare) equilibrated in dialysis buffer. Elution used a linear gradient of 50-500 mM NaCl and fractions were dialysed in gel filtration buffer to remove excess NaCl prior to concentrating the proteins to approximately 20 mg/mL. $Z_{1212}$ variants were used immediately or flash frozen in liquid nitrogen and stored at -80°C. Protein purity and quality was assessed at all stages of the purification process by Coomassie-stained sodium dodecyl sulphate polyacrylamide gel electrophoresis (SDS-PAGE). Protein concentration was estimated by absorbance at 280 nm using a NanoDrop 1000 spectrophotometer (Thermo Scientific).

### *2.3.3 Purification of Tel, Tel$^{C\text{-}RGD}$11 and Tel$^{C\text{-}RGE}$11*

Cell pellets were thawed at RT before resuspending in a lysis buffer containing 25 mM Tris-HCl pH 7.4 and 8 M urea supplemented with EDTA-free protease inhibitor cocktail and 10 μg/mL DNAse I. Cells were disrupted by high pressure homogenisation and the lysate clarified by centrifugation at 40,000*g* for 40 min at 20°C. The soluble fraction containing Tel was filtered (0.22 μm polyethersulfone syringe filter) before applying to a 1 mL $Ni^{2+}$-NTA Hi-Trap column. Bound protein was eluted with an imidazole gradient. Fractions containing

Tel were dialysed in 25 mM Tris-HCl pH 7.4, 8 M urea and concentrated to approximately 30 mg/mL. Tel preparations were stored at RT for up to 1 month before discarding.

### *2.3.4 Dual expression of protein complexes*

For *in vivo* complexation of Z1Z2 variants and Tel, proteins were co-expressed in *E. coli* BL21 (DE3) cells. To achieve this, competent cells were transformed with pETM-11 and pET-15b plasmids encoding Tel and Z1Z2 variants, respectively. Z1Z2 variants were as follows: *wt* Z1Z2, $Z1Z2^{RGD}$, $Z1Z2^{Fn}$, $Z1Z2^{KLER}$ and $Z1Z2^{HAVD}$. Dually-transformed clones were selected by antibiotic screening against kanamycin and ampicillin. Recombinant protein expression and purification was as described previously (sections 2.3.1 and 2.3.2).

## 2.4 Protein characterisation

### *2.4.1 Analytical size exclusion chromatography*

Analytical SEC was conducted on an ÄKTA pure system (GE Healthcare) using a Superdex 200 10/300 Tricorn column (GE healthcare) at a flow rate of 0.75 ml/min. The column was equilibrated in 50 mM Tris pH 7.4, 100 mM NaCl.

### *2.4.2 Size exclusion chromatography combined with multi-angle laser light scattering (SEC-MALLS)*

SEC-MALLS measurements were obtained on an ÄKTA pure system linked to an 8-angle light scattering detector ($\lambda$ = 658 nm) and a differential refractometer (Helios DAWN8+ and Optilab T-rEX, Wyatt Technology). A Superdex 200 Increase

10/300 GL column (GE Healthcare) equilibrated in 50 mM Tris pH 7.4, 100 mM NaCl was used at a flow rate of 0.75 mL/min. Protein samples of 100 µL were injected at a concentration of 0.6 mg/mL. A BSA (Sigma-Aldrich) sample was used as a calibration standard to establish detector delay volumes. Data analysis and MM calculations used the ASTRA 6.1 software suite (Wyatt Technology) with a refractive index increment (dn/dc) of 0.185 mg/mL.

## *2.5 Protein structural analysis*

### *2.5.1 Small-angle X-ray scattering (SAXS)*

SAXS data was collected by Dr. Barbara Franke (Universität Konstanz) at the P12 undulator beamline of the PETRA III Synchrotron (EMBL/DESY, Hamburg, Germany) using a Pilatus 2M detector (Dectris, Switzerland). $Z_{1212}$ samples were analysed at concentrations of 1.03, 3.50, 6.70, 10.20 and 14.50 mg/mL. $Z_{1212}^{RGD}$ samples were analysed at concentrations of 1.03, 3.52, 6.90, 9.60 and 15.10 mg/mL. Protein solutions (10 µL) were measured in 50 mM Tris-HCl pH 7.4, 100 mM NaCl at a temperature of 10°C. The scattering intensity ($I$) in the range of momentum transfer $0.01 < s < 0.45$ Å$^{-1}$, ($s = 4\pi \sin\theta/\lambda$, where the wavelength $\lambda$ = 1.24 Å and $2\theta$ is the scattering angle) was recorded at a sample-detector distance of 3.1 metres. Radiation damage, monitored by repetitive 0.05 s exposures, was negligible. Background scattering was subtracted and data reduced, normalised and extrapolated to infinite dilution using the program PRIMUS (Konarev *et al.*, 2003). The forward scattering $I(0)$, radii of gyration ($R_g$) and sample monodispersity were assessed using the Guinier approximation (Guinier, 1939). These parameters were also calculated from the entire scattering pattern using the program GNOM

(Svergun, 1992), which additionally provides the distance distribution function, p(r), and maximum particle dimension ($D_{max}$).

### *2.5.2 X-ray crystallography*

#### *2.5.2.1 Crystallogenesis screening*

Crystallogenesis screening was carried out at 22°C using an automated Screenmaker 98+8™ Xtal™ nanovolume-dispensing crystallisation robot (Innovadyne) and INTELLI-PLATE 96-2 shallow well plates (Art Robinson Instruments). The sitting drop vapour diffusion method was utilised with reservoirs containing 70 µL mother liquor and drops composed of a 1:1 ratio of protein to reservoir solution at a final volume of 200 nL. The following commercial crystallisation matrices were used for screening; MD Structure Screen, JCSG+, Morpheus, Cryo, Midas (Molecular Dimensions), Wizard Classic (Emerald BioSystems), SaltRx, PEGRx (Hampton Research) and NeXtal PACT (Qiagen).

#### *2.5.2.2 Wild type $Z_{1212}$ and $Z_{1212}^{RGD}$ crystallisation*

$Z_{1212}$ and $Z_{1212}^{RGD}$ were screened at 15 and 30 mg/mL, generating multiple crystal hits. The diffraction potential of initial crystals was tested on the tuneable microfocus beamline I24 (Diamond Light Source, Oxfordshire, UK). $Z_{1212}^{RGD}$ was crystallised in space group H3 at 15 mg/mL in 10% [w/v] 8000 kDa polyethylene glycol, 100 mM Tris HCl pH 7.0, 200 mM $MgCl_2$ (Wizard Classic screen). Initial crystals diffracted to low resolution (~3 Å) and the condition was varied in an attempt to improve resolution. Diffraction quality was not improved by optimisation, and crystals were used for microseed screening (Bergfors, 2003) using a 1:1:2 ratio of protein to seed stock to mother liquor. Screens were set up as previously

described (section 2.5.2.1) using Wizard Classic and Cryo matrices. A large number of crystal hits were generated and diffraction data was collected on beamline I03 (Diamond Light Source). The best crystals grew in 10% [v/v] isopropanol, 100 mM $Na_2HPO_4$ pH 4.2, 200 mM $LiSO_4$ (Wizard Classic screen) and were cryoprotected with 30% [v/v] glycerol prior to flash cooling in liquid nitrogen. X-ray diffraction data was collected to 2.4 Å resolution for one $Z_{1212}^{RGD}$ crystal.

#### *2.5.2.3 Z1Z2$^{HAVD}$ and Z1Z2$^{KLER}$ crystallisation*

$Z1Z2^{HAVD}$ and $Z1Z2^{KLER}$ were screened at 25 and 50 mg/mL; $Z1Z2^{HAVD}$ did not crystallise under any of the conditions assessed and one hit was identified for $Z1Z2^{KLER}$; 1 M $NH_4H_2PO_4$ pH 4.6, 100 mM sodium acetate (SaltRx). Attempts to recreate or improve the initial hit failed. Crystals were cryoprotected in 30% [v/v] glycerol and flash cooled in liquid nitrogen prior to data collection. X-ray diffraction data was collected on beamline I03 (Diamond Light Source) to 2.6 Å resolution.

#### *2.5.2.4 Structure calculation*

Diffraction data was processed using XDS (Kabsch, 2010) and estimation of the asymmetric unit content used the matthews_coef program of the CCP4 software suite (Winn *et al.*, 2011). For $Z_{1212}^{RGD}$, molecular replacement was conducted with Phaser (McCoy *et al.*, 2007) using Z1 and Z2 Ig domains as individual search models (PDB: 2A38; Marino *et al*., 2006). Structure refinement was conducted with PHENIX (Adams *et al.*, 2010). Manual building and the addition of water and solvent molecules used Coot (Emsley *et al.*, 2010). Model quality was assessed using MolProbity (Chen *et al.*, 2010). Refinement and building of the $Z_{1212}^{RGD}$ structure was carried out by Dr. Jennifer Fleming (Universität Konstanz).

## 2.6 ZT nanofibres

### *2.6.1 Nanofibre assembly*

Polymerisation of ZT nanofibres used a protocol developed by Bruning *et al*. (2010); a 3:1 molar excess of Tel to $Z_{1212}$ was mixed (final protein concentration of 10 mg/mL) and dialysed overnight (Slide-A-Lyzer™ MINI Dialysis Device 3.5 kDa MWCO; Thermo Fisher Scientific) at RT in 50 mM Tris-HCl pH 7.4, 100 mM NaCl (assembly buffer). Following initial assembly and removal of urea, nanofibre preparations were left for 1 week at RT in sterile Eppendorf tubes to allow polymerisation to proceed before use.

### *2.6.2 Transmission electron microscopy (TEM)*

#### *2.6.2.1 Grid preparation*

200 mesh copper grids were coated with either pioloform or pure carbon support films. Grids with a pioloform support film were carbon-coated before use and both grid types were either left unmodified or freshly glow discharged for 30 s prior to sample application. Pioloform grids were manufactured in-house (University of Liverpool) from 0.3 % [w/v] polyvinyl butyral dissolved in chloroform. Pure carbon-coated grids were either manufactured in-house (University of Sheffield) or purchased (C101/025; TAAB).

#### *2.6.2.2 Sample loading and staining*

Nanofibre samples at 10 mg/mL were diluted 1:10 or 1:100 with assembly buffer prior to loading onto carbon-coated or piloform-coated grids. Five µL of

diluted nanofibre solution was applied for 60 s. The nanofibre solution was removed and the grid washed three times with distilled water before staining twice with 5 µL of 2% [w/v] uranyl-acetate dissolved in distilled water (5 s and 45 s for the first and second stains, respectively). Fluid was removed from the grid between each washing and staining step by gently touching a piece of filter paper to the edge of the grid. A loading protocol that omitted the wash steps was also implemented. Imaging was performed at the University of Liverpool (assisted by Alison Beckett) or the University of Sheffield (assisted by Dr. Svetomir Tsokov) on a FEI 120 kV Tecnai G2 Spirit BioTWIN electron microscope operating at 100 kV.

### *2.6.3 Native polyacrylamide gel electrophoresis (PAGE)*

Protein samples were loaded on 15% [v/v] acrylamide gels in non-reducing loading buffer (without boiling) and SDS was excluded from both the gel and the running buffer. Gels were run at RT for 3 h at 20 mA and stained with Coomassie Brilliant Blue.

### *2.6.4 Nanofibre adsorption to plastic surfaces*

All ZT nanofibres were sterilised by UV irradiation for 15 min in 1.5 mL Eppendorf tubes. Stock solutions of sterile ZT nanofibre variants and control human plasma fibronectin (Merck Millipore) were diluted in culture-grade PBS (Sigma Aldrich) to achieve concentrations ranging from 0.1 – 10 µg/mL. Proteins were passively adsorbed onto non-tissue culture treated (TCT) 24-well suspension plates (Greiner) or non-TCT 8-well µ-Slides (ibidi) by adding 300 µL of protein solution to each well and incubating at 37°C for 2 h. The protein solution was removed and wells were immediately filled with the required medium prior to cell seeding.

## *2.7 Cell Culture*

### *2.7.1 Mouse mesenchymal stem cells*

Murine mesenchymal stem cell (mMSC) line D1 (ATCC) was cultured on standard TCT vessels in high glucose Dulbecco's Modified Eagle Medium (DMEM; Sigma-Aldrich) supplemented with 10% [v/v] foetal calf serum (FCS; Gibco), non-essential amino acids (Sigma-Aldrich), 2 mM L-glutamine (Invitrogen) and 55 μM β-mercaptoethanol (Gibco). Cells were subcultured at approximately 90% confluence using 1% trypsin (Sigma-Aldrich) and maintained at 37°C with 5% [v/v] $CO_2$.

### *2.7.2 Human embryonic stem cells*

Human embryonic stem (hESC) cell line HUES7 (Harvard University, HUES cells facility, Melton Laboratory, ME, USA) was cultured in serum-free mTeSR™1 medium (Stem Cell Technologies) on hESC-qualified Matrigel (Corning). For routine expansion, tissue culture treated plastic vessels (Corning) were coated with Matrigel according to the manufacturer's instructions; Matrigel was thawed on ice and diluted in DMEM/F-12 medium (Gibco). Diluted Matrigel was added to culture vessels at a volume sufficient to cover the growth surface (1 mL/well for a 6-well plate) and incubated for 1 h at RT. Prior to cell seeding, the diluted Matrigel was removed by aspiration (care was taken not to disturb the matrix) and fresh mTeSR™1 medium was added. For passaging on Matrigel, spent medium was removed and hESC colonies were detached by incubation with Gentle Cell Dissociation Reagent (Stem Cell Technologies) at RT; the appearance of gaps between cells at the periphery of colonies (observed under a microscope) was judged

to be the optimal incubation time (typically 5 – 7 min) and care was taken to avoid the generation of a single cell suspension by overexposure to the dissociation reagent. Following incubation, the dissociation reagent was removed and fresh mTeSR™1 medium added before removal of colonies using a cell scraper and transfer to a 15 mL falcon tube. The suspension was gently triturated to generate clumps of approximately 50 – 200 cells and split 1:6 onto Matrigel-coated vessels. Cells were cultured at 37°C with 5% [v/v] $CO_2$ and medium was exchanged daily.

### *2.8 CCK-8 assay*

The toxicity of the $Z_{1212}$ tandem was assessed by CCK-8 assay (Cell Counting Kit 8; Sigma-Aldrich) according to the manufacturer's guidelines. The assay utilises the reductive potential of WST-8 [2-(2-methoxy-4-nitrophenyl)-3-(4-nitrophenyl)-5-(2,4-disulfophenyl)-2H-tetrazolium, monosodium salt] to produce a formazan dye in the presence of metabolically active cells. Further, the extent of colour change is directly correlatable to the number of viable cells in a sample. To assess $Z_{1212}$ toxicity, $1 \times 10^4$ mMSCs were cultured for two days in the presence of 0.01 – 1 mg/mL $Z_{1212}$. Concentrations were created by sterile-filtering 15 mg/mL protein stocks (Ultrafree-MC Centrifugal Filter Units; Millipore) and diluting with cell medium. Standard medium and 0.1% (v/v) Triton-X 100 were included as negative and positive controls, respectively. Absorbance was measured at 450 nm using an LP400 microplate reader (Anthos Labtec Instruments) and results were expressed as a percentage of the activity of the positive control (100%). All conditions were run in triplicate.

### *2.9 Cell adhesion assays*

mMSCs cultured under standard conditions were serum-starved for 24 h post-seeding on ZT nanofibres; medium was removed and the cells washed twice with phosphate-buffered saline (PBS; Sigma-Aldrich) to remove remaining serum components before serum-free (SF) medium was added. SF medium was composed of Advanced DMEM (Gibco), 100 U/mL Penicillin-Streptomycin (Invitrogen), 2 mM L-glutamine and 55 μM β-mercaptoethanol. After 24 h, SF medium was removed and cells washed once with PBS before trypsinising to generate a single cell suspension. The suspension was diluted 1:1 with SF medium and centrifuged at 200 × g for 3 min to pellet the cells, and the supernatant was discarded. The cells were resuspended in fresh SF medium and the centrifugation step was repeated to remove residual trypsin. Finally, the cells were resuspended in SF medium, counted using a haemocytometer and seeded at $1 \times 10^4$ cells/cm$^2$ in non-TCT plates precoated with proteins.

HUES7 cells cultured on Matrigel were washed once with PBS and disaggregated by incubation with Accutase (Innovative Cell Technologies) at 37°C until all cells in colonies appeared rounded and began to lift from the dish (approximately 5 min). Cells were completely detached by shear force and the suspension was diluted 1:1 with mTeSR™1 medium followed by centrifugation at 200 g for 3 min. The supernatant was removed and the pellet resuspended in fresh medium by gentle trituration to generate a single cell suspension. Seeding on protein-coated wells was as described for mMSCs, with the exception that mTeSR™1 medium was used and Matrigel was also included as an additional control. At specific time points post-seeding, cells were fixed with 4% [w/v] paraformaldehyde (PFA) for 10 min to halt adhesion/spreading and wells were

washed with PBS to remove non-attached cells prior to analysis.

For quantification, phase contrast micrographs were acquired in 3 random fields of view per well (triplicate wells, $n$ = 9) using a Leica DM2500 inverted microscope and Leica DFC420C camera. Adhered cells in each field of view were counted and the average number for each condition calculated.

### *2.10 Peptide inhibition assay*

Peptide inhibition experiments essentially followed the same protocol as the cell adhesion assays. Following trypsinsation, mMSCs were incubated with 0, 2.5, 25 or 250 μM of integrin-binding GRGDS or 250 μM control GRGES pentapeptides (synthesised by Protein Peptide Research Fareham, UK) for 15 min at 37°C. Cells were then seeded in suspension culture plates precoated with control fibronectin or ZT nanofibres at 10 μg/mL as described previously (section 2.6.4). After 2 h incubation at 37°C, cells were fixed and imaged by phase contrast microscopy to quantify attachment and spreading.

### *2.11 Analysis of cell morphology*

Variations in cell morphology induced by different substrates were investigated by quantifying cell area, circularity, aspect ratio (AR) and solidity. For this, individual cells were outlined using ImageJ (Schneider *et al.*, 2012). Images were spatially calibrated (μm/pixel) and the parameters were calculated by the software.

Circularity was calculated using Equation 1:

$$Circularity = \frac{4\pi A}{P^2}$$

Where A and P represent cell area and perimeter, respectively.

Solidity was calculated using Equation 2:

$$Solidity = \frac{A}{CA}$$

Where A and CA represent area and convex area, respectively.

AR was calculated using Equation 3:

$$AR = \frac{LA}{SA}$$

Where LA and SA represent the long axis and short axis of the best-fitted ellipsis, respectively.

For each independent experiment, 50 cells were measured for each condition and in the case of the number of observable cells being less than 50, all attached cells were measured in the images available.

### *2.12 Live cell imaging*

For time lapse microscopy studies, cell cultures were transferred to a Cell-IQ live cell imaging system (CM Technologies) and maintained for the duration of the experiment at 37°C and 5% $CO_2$. Imaging cycles were initiated 2 h post-seeding to allow the system to equilibrate and cells to adhere sufficiently for automated focusing. For each condition, three random areas were imaged in triplicate wells using a 10× objective (the field of view is 800 $\mu m^2$). Each designated position was imaged once every 15 min and data was processed using Imagen analysis software (CM Technologies).

### *2.13 Chondrogenesis assays*

Induced chondrogenic differentiation of mouse MSCs *in vitro* used the pellet culture method (Peister *et al*., 2004); MSCs grown in monolayer culture were trypsinised and 2 x $10^5$ cells in standard medium (Section 2.7.1) were compacted by centrifugation at 200*g* for 5 min. Following incubation for 24 h, medium was replaced with chondroinductive medium; DMEM, 10 ng/mL TGFβ-3 (Sigma-Aldrich), 200 ng/μL BMP-7 (R & D Systems) 0.1 μM dexamethasone, 50 μg/mL ascorbic acid (Sigma-Aldrich), 40 μg/mL pyruvate and 50 mg/mL ITS (Invitrogen). Medium was exchanged every two days and pellets were cultured for up to 21 days at 37°C with 5% [v/v] $CO_2$. After 21 days, cell pellets were fixed with 4% [w/v] PFA, washed with PBS and incubated at 4°C for 12 h in 30% [w/v] sucrose solution. Next, pellets were suspended in Cryomatrix embedding resin (Thermo-Fisher Scientific) and flash-frozen on dry ice. Finally, pellets were sectioned using a cryotome (7 μm thickness) and stained with 0.1% [w/v] Safranin-O solution (Sigma-Aldrich) for 5 min. Slides were washed in distilled water and allowed to dry before imaging using a Leica DM2500 inverted microscope equipped with a Leica DFC420C camera.

### *2.14 Clonogenic assays*

HUES7 cells were dissociated with Accutase to generate a single cell suspension and seeded at a density of 2.5 × $10^3/cm^2$ on non-TCT plastic precoated with fibronectin or $ZT^{Fn}$ at 10 μg/mL, or control Matrigel as previously described (sections 2.6.4 and 2.7.2). Cells were cultured for 4 days under standard conditions to allow colonies to form. Next, cells were fixed with 4% [w/v] PFA and stained with 0.1% [w/v] crystal violet. The number of colonies per well and area of the

surface covered were calculated using ImageJ. All conditions were run in quadruplet. Clonogenic assays were carried out by Masoumeh Mousavinejad (University of Liverpool).

### *2.15 Human embryonic stem cell self-renewal*

HUES7 cells cultured on Matrigel were detached using the clump passaging procedure (section 2.7.2) and seeded onto non-TCT plates (Gibco) precoated with fibronectin or $ZT^{Fn}$ solutions at 10 μg/mL as previously described (section 2.6.4). Once confluent, cells were passaged onto fresh substrates using the same method. Cells were fixed with 4% [w/v] PFA after five and ten passages for analysis by immunofluorescence (section 2.18.3) or were lysed in TRI Reagent after one and five passages for gene expression analysis (section 2.20).

### *2.16 Embryoid body formation*

For embryoid body (EB) formation, HUES7 cells grown on fibronectin or $ZT^{Fn\text{-}III}$ for thirteen passages were dissociated with Accutase to generate a single cell suspension. Cultures maintained on Matrigel were used as a control. Cells were resuspended in STEMdiff™ APEL™ Medium (Stem Cell Technologies) and plated at $3 \times 10^3$ cells/well in 96-well round bottom Nunclon™ Sphera™ Microplates (Thermo Scientific). To promote aggregation, plates were centrifuged at 140*g* for 2 min and incubated at 37°C with 5% $CO_2$ to allow EBs to develop.

### *2.17 Pluripotency assays*

EBs were harvested after 7-10 days of development and transferred to plastic 8-well μ-Slides (ibidi) precoated with Matrigel. The EBs were allowed to attach and

spread in neutral STEMdiff™ APEL™ Medium. EBs were fixed after 7-10 days of attachment using 4% [w/v] PFA and stained for germ layer markers (section 2.18.3).

### *2.18 Immunocytochemistry*

For analysis by immunofluorescence, cells were washed twice with PBS, fixed with 4% [w/v] PFA for 10 min, permeabilised with 0.1% [v/v] Triton X-100 for a further 10 min and blocked with 1% [w/v] BSA for 30 min prior to the application of primary antibodies. All primary antibodies were incubated overnight at 4°C followed by secondary antibody application for 2 h at RT. All secondary antibodies were used at 1:1000 dilution. Observation of F-actin filaments used AlexaFluor488 or AlexaFluor594 Phalloidin (Invitrogen) and cell nuclei were counterstained with 4',6-diamino-2-diamino-2-phenylindole, dilactate (DAPI; Invitrogen).

#### *2.18.1 Chondrogenic and osteogenic markers*

Primary antibodies for differentiation marker detection in mMSCs were as follows; rabbit anti-osteocalcin (1:200, sc-30045; Santa Cruz Biotechnology) and mouse anti-collagen type II (1:25, CIIC1; Hybridoma Bank, NIH). Secondary antibodies were chicken anti-rabbit AlexaFluor594 and goat anti-mouse AlexaFlour594 (Invitrogen).

#### *2.18.2 Focal adhesion markers and integrins*

Primary antibodies for focal adhesion and integrin staining of mMSCs and HUES7 cells were as follows; rabbit anti-paxillin (1:500, ab32084; Abcam), mouse anti-zyxin (1:500, ab58210; Abcam) rabbit anti-fibronectin (1:1000, ab299; Abcam),

rat anti-α5 integrin subunit (1:200, 5H10-27; BD Biosciences), rat anti-α5 integrin subunit (1:1000, MAB11; non-commercial), rat anti-αV integrin subunit (1:200, RMV-7; BD Biosciences), mouse anti-αV integrin subunit (1:200, L230; ATCC), hamster anti-β3 integrin subunit (1:200, 2C9.G2; BD Biosciences), mouse anti-αVβ3 integrin (1:200, MAB1976; Merck Millipore), rabbit anti-β5 integrin subunit (1:1600, 3629; Cell Signaling Technology), rabbit anti-β1 integrin subunit (1:200, EP1041; ab52971 Abcam), mouse anti-β1 integrin subunit (1:200, MAB1987Z; Merck Millipore) and mouse anti-β1 integrin subunit (1:500, MAB1965; Merck Millipore). Secondary antibodies were goat anti-rabbit AlexaFluor594, goat anti-mouse AlexaFluor594, chicken anti-rat AlexaFluor488, donkey anti-rat AlexaFluor568 (Invitrogen) and goat anti-hamster AlexaFluor647 (Jackson ImmunoResearch). All integrin antibodies were kind gifts of Dr. Mark Morgan (University of Liverpool).

### *2.18.3 Pluripotency and germ layer markers*

Primary antibodies for pluripotency and germ layer marker detection in HUES7 cells were as follows; mouse anti-OCT3/4 (1:500, sc-5279; Santa Cruz Biotechnology), rabbit anti-NANOG (1:500, D73G4; Cell Signalling Technology), rabbit anti-GATA6 (1:500, sc-9055; Santa Cruz Biotechnology), rabbit anti-nestin (1:250, ab92391; Abcam) and goat anti-brachyury (1:500, sc-17743; Santa Cruz Biotechnology). Secondary antibodies were goat anti-mouse AlexaFluor594, donkey anti-goat AlexaFluor488 and chicken anti-rabbit AlexaFluor488/594 (Invitrogen).

## *2.19 Confocal microscopy*

For confocal imaging, single cell suspensions of mMSCs or HUES7 cells

were seeded at a density of $3 \times 10^4$ cells/well in 8-well μ-Slides (ibidi) precoated with protein solutions (ZT nanofibres or fibronectin at 10 μg/mL, section 2.6.4) or Matrigel (section 2.7.2). Following application of antibodies, imaging was conducted on a 3i Spinning Disk confocal microscope with a Zeiss autofocus system and Hamamatsu camera. Multicolour fluorescence imaging used 405 nm, 488 nm, 561 nm and 640 nm (50 mW) diode lasers (100 ms exposure time) and 20× air or 40× and 63× oil objectives. Z-stacks were acquired using a step size of 0.34 μm and projections were generated in ImageJ.

### *2.20 Real time-qPCR*

#### *2.20.1 RNA extraction and cDNA synthesis*

For RNA extraction, medium was removed and cells immediately lysed with TRI Reagent (Sigma-Aldrich). RNA was isolated by chloroform extraction (1:5 [v/v] chloroform followed by shaking for 15 s and centrifugation at 12,000*g* for 15 min at 4°C). The upper aqueous phase was separated and RNA precipitated by the addition of 1:1 [v/v] isopropanol and overnight incubation at -20°C to increase yield. RNA was pelleted by centrifugation at 12,000*g* for 10 min at 4°C and washed with 75% [v/v] ethanol. The ethanol was removed and the pellets were air-dried before dissolving in nuclease-free water. RNA concentration was measured using a NanoDrop 2000 spectrophotometer (Thermo Scientific) and 2 μg of RNA from each sample was used for cDNA synthesis; RNA was incubated with 1 μL of RQ1 DNase (Promega) at 37°C for 30 min and the reaction was stopped by the addition of 1 μL of Stop Solution (Promega) and incubation at 60°C for 15 min. One μg of DNase-treated RNA was reverse transcribed by the addition of 100 ng random hexamers

(Qiagen), 500 μM dNTPs (Invitrogen) and 200 U SuperScript III Reverse Transcriptase (Invitrogen) using the following incubation steps; 5 min at 25°C, 60 min at 50°C and 15 min at 70°C.

### *2.20.2 Gene expression analysis*

Template cDNA was diluted 1:25 with nuclease-free water for RT-qPCR experiments. Reaction mixtures were as follows; 1 μL cDNA, 500 nM forward/reverse primers (1 μL of a 10 μM stock), 10 μL 2X SYBR Green JumpStart Taq ReadyMix (Sigma-Aldrich) and nuclease-free water to a final volume of 20 μL. RT-qPCR was conducted on a CFX Connect Real-Time PCR Detection System (Bio-Rad) using the following cycling parameters; initial denaturation and enzyme activation at 95°C for 3 min followed by 40 3-step PCR cycles of 95°C for 10 s, 58°C (mouse gene targets) or 65°C (human gene targets) for 15 s and 72°C for 30 s. Melt curve analysis was performed post-amplification; 0.5°C temperature increments from 65°C - 95°C. Details of the primer pairs (synthesised by Sigma-Aldrich) used for RT-qPCR analysis of mouse and human cDNA are given in Tables 6 and 7, respectively. DNase-treated RNA and no template control reactions were run for all samples and primer pairs, respectively, to confirm the absence of contaminants. Individual samples were run in triplicate and the mean cycle threshold ($C_t$) value was used for gene expression analysis. Data was analysed using CFX-Manager 3.1 software (Bio-Rad) and verified in Excel (Microsoft). For mMSCs, gene expression was normalised using β-actin as the reference gene. For HUES7 cells, gene expression was normalised using the geometric mean $C_t$ values for reference genes GAPDH and HPRT1. Relative expression levels of target genes between control and experimental samples were calculated using the $2^{-\Delta\Delta Ct}$ method

(Livak and Schmittgen, 2001).

**Table 6.** Primers for RT-qPCR analysis of mouse mesenchymal stem cells

| Gene | Denomination | Direction | Primer sequence (5' – 3') | Size (bp) |
|---|---|---|---|---|
| ***Actb*** | β-actin | Forward | *CGTTGACATCCGTAAAGACC* | 154 |
| | | Reverse | *CAGGAGGAGCAATGATCTTGA* | |
| ***Bglap*** | Osteocalcin | Forward | *GACCATCTTTCTGCTCACTC* | 128 |
| | | Reverse | *TCACTACCTTATTGCCCTCC* | |
| ***Col2a1*** | Collagen type II | Forward | *CTGACCTGACCTGATGATACC* | 170 |
| | | Reverse | *CACCAGATAGTTCCTGTCTCC* | |
| ***Sox9*** | Sox9 | Forward | *TACGACTGGACGCTGGTGCC* | 305 |
| | | Reverse | *CCGTTCTTCACCGACTTCCTCC* | |

**Table 7.** Primers for RT-qPCR analysis of human embryonic stem cells

| Gene | Denomination | Direction | Primer sequence (5' – 3') | Size (bp) |
|---|---|---|---|---|
| ***GAPDH*** | Glyceraldehyde 3-phosphate dehydrogenase | Forward | *GTGGAAGGACTCA TGACCA* | 119 |
| | | Reverse | *GAGGCAGGGATG ATGTTCT* | |
| ***HPRT1*** | Hypoxanthine phosphoribosyltra-nsferase 1 | Forward | *GCAGCCCTGGCG TCGTGATTAG* | 143 |
| | | Reverse | *TCGAGCAAGACGT TCAGTCCTGTCC* | |
| ***NANOG*** | Nanog homeobox | Forward | *TCCAACATCCTGA ACCTCAGC* | 125 |
| | | Reverse | *GAGGCCTTCTGC GTCACA* | |
| ***OCT4*** | Octamer-binding transcription factor 4 | Forward | *ATGTGGTCCGAGT GTGGTTC* | 67 |
| | | Reverse | *TGTGCATAGTCGC TGCTTGA* | |
| ***SOX2*** | SRY (sex determining region Y)-box 2 | Forward | *TCAGGAGTTGTCA AGGCAGAG* | 60 |
| | | Reverse | *GGCAGCAAACTAC TTTCCCC* | |

### *2.21 Statistics*

For statistical evaluation, independent experiments were conducted a minimum of 3 times. Standard error of the mean (SEM), standard deviation (SD), coefficient of variation (CV) and skewness were calculated using Excel. Statistically significant differences between two groups were determined by Student's t-test using Minitab 17 software (www.minitab.com). A difference between samples was considered significant when $p < 0.05$ (*), highly significant when $p < 0.01$ (**) and very highly significant when $p < 0.001$ (***).

# Chapter 3

# Generation of fibronectin chimeras

## 3.1 Introduction

### *3.1.1 Fibronectin and RGD motifs*

The ECM is a conglomerate of molecules that acts as both a supportive scaffold and biochemical coordinator of fundamental cellular events including proliferation, polarisation, adhesion, movement and differentiation. A major component of the ECM is fibronectin, a dimeric glycoprotein that assembles into fibrils following interaction with cell surface integrins. Each fibronectin monomer is composed principally of homologous type I, II and III domains organised in modular repeats to form an elongated filament (Figure 7a) (Hynes and Yamada, 1982). Fibronectin interacts cooperatively with multiple ECM components including collages, fibrin, heparin and HS to initiate cellular responses (Xu and Mosher, 2011). However, the most well documented function of fibronectin is its role in integrin-mediated cell adhesion. The major integrin interaction site is the Arg-Gly-Asp (RGD) motif located within the tenth type III domain (FnIII 10) (Main *et al.*, 1992). The RGD motif is also found in other ECM proteins including vitronectin, collagens, fibrinogen and thrombospondin (Ruoslahti, 1996). In fibronectin, the RGD motif acts concomitantly with the synergistic Pro-His-Ser-Arg-Asn (PHSRN) motif in the ninth Type III domain (FnIII 9) to interact with integrins αVβ1, αVβ3, αVβ6, α8β1, α5β1 and αIIbβ3 (Figure 7a) (Mao and Schwarzbauer, 2005; Humphries *et al.*, 2006) (see section 6.1.2 for detailed discussion on integrin-mediated cell adhesion). The

RGD motif is positioned at the apex of a solvent exposed loop between β-strands F and G (Figure 7b).

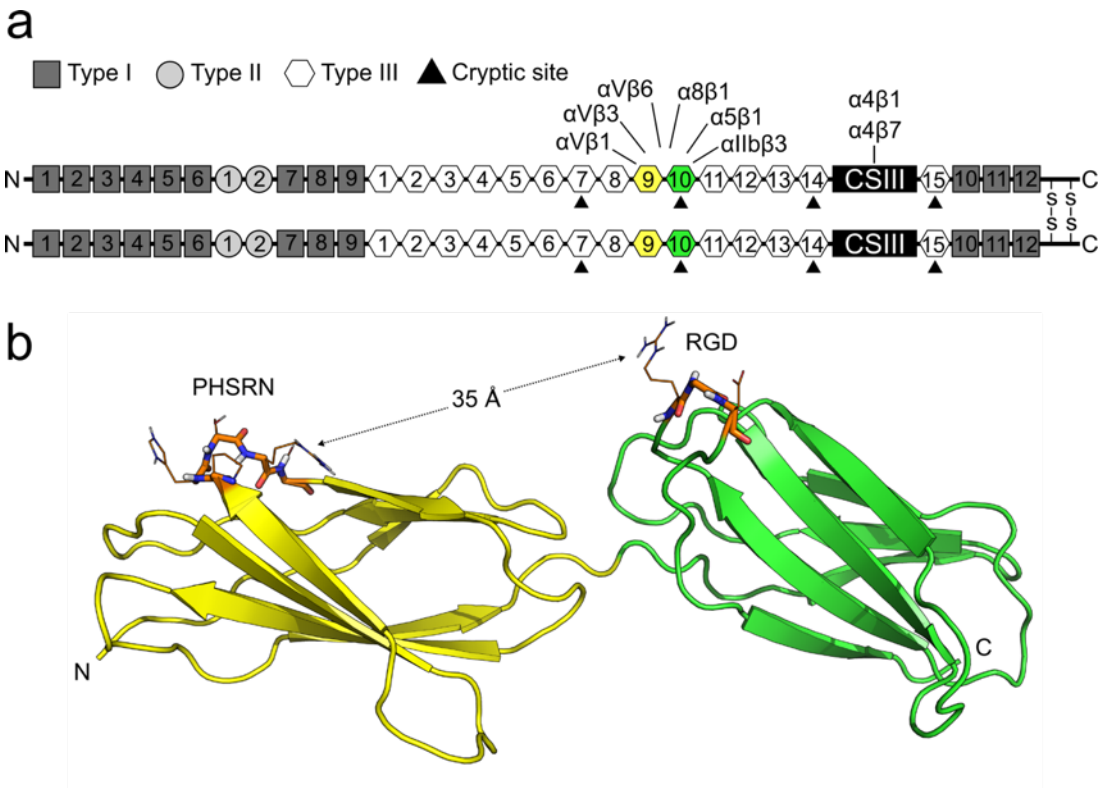


**Figure 7. The modular arrangement of fibronectin and structures of integrin-binding domains.** (a) Schematic representation of a fibronectin dimer formed by the joining of two monomers via two disulphide bridges at the C-terminus. Each monomer is composed of 12 type I (*squares*), 2 type II (*circles*) and 15 type III (*hexagons*) domains. The ninth and tenth type III domains containing the synergy site and RGD motif are highlighted and integrins known to interact with this region are specified. Also shown is the type III connecting segment III (*rectangle*) along with known integrin receptors. Domains containing cryptic binding sites are indicated (*triangles*). Schematic adapted in part from Aziz-Seible and Casey, (2011). (b) Crystal structure of the ninth (*yellow*) and tenth (*green*) type III domains harbouring the synergistic PHSRN and integrin-binding RGD motifs, respectively (PDB: 1FNF, Leahy *et al.*, 1996). Domains are coloured to match the schematic. Residues encompassing the motifs are shown as main chain sticks with side chain lines (*orange*).

Observations of FnIII 10 at atomic resolution have revealed that the FG loop adopts a β-hairpin-like conformation with a distorted morphology, and studies suggest that the specific residue stoichiometries adopted in this environment are

critical for RGD function (Hautanen *et al.*, 1989; Main *et al.*, 1992; Ruoslahti, 1996). In native fibronectin the synergy site is approximately 35 Å from the RGD motif, an arrangement that is essential for the binding of several integrins including α5β1 (Aota *et al.*, 1991; Mardon and Grant, 1994). However, fibronectin deformation upon cellular and/or ECM interaction can decouple PHSRN and RGD to a point beyond cooperative integrin engagement, although some integrins can still bind to the RGD motif independent of the synergy site such as αVβ3 (Krammer *et al.*, 2002; Zollinger and Smith, 2016). The discovery of RGD-mediated integrin engagement has inspired the development of biomaterials that incorporate the motif to promote cell attachment (Hersel *et al.*, 2003; Macneil *et al.*, 2008).

### *3.1.2 Protein engineering for molecular recognition*

For decades, protein domains that can display exogenous peptidic sequences for molecular recognition have been harnessed for biotechnological and medicinal applications (Skerra, 2000). Such proteins have been termed "scaffolds" to generalise a myriad of domain architectures with a common feature; the presence of non-contiguous loops that are not integral to stability of the tertiary structure of the domain and can thus tolerate diversity in sequence length and composition. The archetypal protein scaffolds found in nature are antibodies, of which the (V)-type Ig domains are able to bind innumerable antigens through a process of random recombination and consequent diversification of three hypervariable loops (Sela-Culang *et al.*, 2013). Strictly speaking, molecular recognition can be achieved by random or rational diversification. In the case of the former, randomised libraries are generated by combinatorial substitution of residues at target sites and the generated mutants are screened for desired binding specificities. Rational diversification

involves the incorporation of specific polypeptide sequences with defined bioactivity onto the scaffold fold using molecular biology techniques. Characteristic scaffold proteins include Ig domains, Fn domains, affibodies, PDZ domains, lipocalins, knottins and ankryin repeat domains (Skerra, 2000; Hosse *et al.*, 2006). Although conformational stability is intrinsic to archetypal protein scaffolds, local changes in residue composition may cause domain instability and lead to misfolding or aggregation. Therefore, sites targeted for diversification must first be carefully assessed for their tolerance to modification (Bruning *et al.*, 2012).

### *3.1.3 Genetic incorporation of integrin binding motifs in scaffolds*

Many studies have utilised integrin binding peptides to functionalise biomaterials for tissue engineering applications (Macneil *et al.*, 2008). Synthetic peptides, such as RGD, are often incorporated in linear conformations (Hersel *et al.*, 2003; Widhe *et al.*, 2013). However, cell adhesion to the linear fibronectin peptidomimetic GRGDSP has been shown to be ~1000-fold less efficient than native fibronectin (Hautanen *et al.*, 1989), possibly because the structurally-restrained conformation of the loop and its distorted morphology are required for robust integrin binding (Hautanen *et al.*, 1989; Leahy *et al.*, 1996; Ruoslahti, 1996). Therefore, grafting of RGD tripeptides in scaffold domains or self-assembling protein systems may be advantageous in mimicking the native environment of the motif, leading to increased binding affinity or specific integrin targeting. To this end, domains with and without scaffolding properties have been functionalised by RGD motif insertion at the genetic level. For example, RGD motifs have been grafted in recombinant silk fibroin from *Bombyx mori* (Yang *et al.*, 2008; Asakura *et al.*, 2011), Agouti-related protein of the cysteine-knot family (Silverman *et al.*, 2009)

and even lysozyme (Yamada *et al.*, 1995). In the case of RGD-grafted lysozyme, the potentially synergistic effect of lysozyme-heparin interaction (Boschetti *et al*., 1981) on cell adhesion was not explored, although native lysozyme was not found to support cell attachment. Others have taken an alternative approach to rationalised mutation by fusing regions of fibronectin to other proteins with distinctive properties, thus generating fibronectin chimeras. The fusion of fibronectin type III domains 9-14 with osteocalcin resulted in enhanced adhesion and osteogenic differentiation of a pre-osteoblastic cell line (Yun *et al.*, 2013). Roy *et al.* (2011) have explored the generation of ECM mimetics by fusing key functional domains from fibronectin to imitate the effects of the full length protein on cell adhesion. Domains responsible for heparin and integrin binding were combined to produce bacterially-expressed chimeras with cell adhesive properties comparable to native fibronectin.

### *3.1.4 Aims*

In this chapter, the functionalisation potential of the ZT nanofibre system is assessed by modification of Tel terminal regions, CD-loop diversification and domain fusion to impart cell-adhesive properties. For this, a fibronectin-inspired RGD motif was genetically incorporated at the C-terminus of Tel, or grafted in the Z1 CD-loop of $Z_{1212}$. These sites were selected because they had previously been shown to support functionalisation (Bruning *et al*., 2010, Bruning *et al*., 2012). The RGD motif was chosen due to its proven track record in biomaterial functionalisation and applicability to *in vitro* testing. The resulting chimeras were recombinantly expressed and characterised. Additionally, FnIII 10 from human fibronectin, which contains the native RGD motif, was fused with $Z_{1212}$ to explore

the exciting prospect of whole domain exhibition in a self-assembling system.

## 3.2 Results

### *3.2.1 Generation and Expression of Tel variants*

Tel acts as a molecular crosslinker to join two Z1Z2 molecules (or two $Z_{1212}$ molecules to form ZT nanofibres) and the majority of its surface is buried within the protein-protein interfaces (Figure 3b). However, the N- and C-termini protrude outwards from the complex and are free from interaction, thus permitting the exhibition of peptidomimetics in linear conformations. As standard, *wt* Tel was expressed in the pETM-11 vector that incorporates an N-terminal $His_6$ tag and TEV protease cleavage site, thereby increasing the length of the N-terminus by 26 amino acids. In an attempt to assess the functionalisation potential of the N- and C-termini of Tel in an unbiased manner, the first generation of variants were expressed in the pETM-13 vector with an engineered $His_6$ tag flanking the inserted peptide. For functionalisation, a dual RGD motif (RGDSGRGD) or control RGE motif (RGESGRGE) was grafted at the N- ($Tel^{N\text{-}RGD}13$ and $Tel^{N\text{-}RGE}13$) or C-terminus ($Tel^{C\text{-}RGD}13$ and $Tel^{C\text{-}RGE}13$) of Tel (Figure 8a). The resulting constructs were overexpressed in *E. coli* and whole cell lysates were subjected to SDS-PAGE analysis to observe protein yield (Figure 8b). A marked drop in yield was observed for all variants compared to *wt* Tel. Since yield was reduced in the pETM-13 vector following modification of protein termini, a second generation of Tel variants were created in the pETM-11 vector.

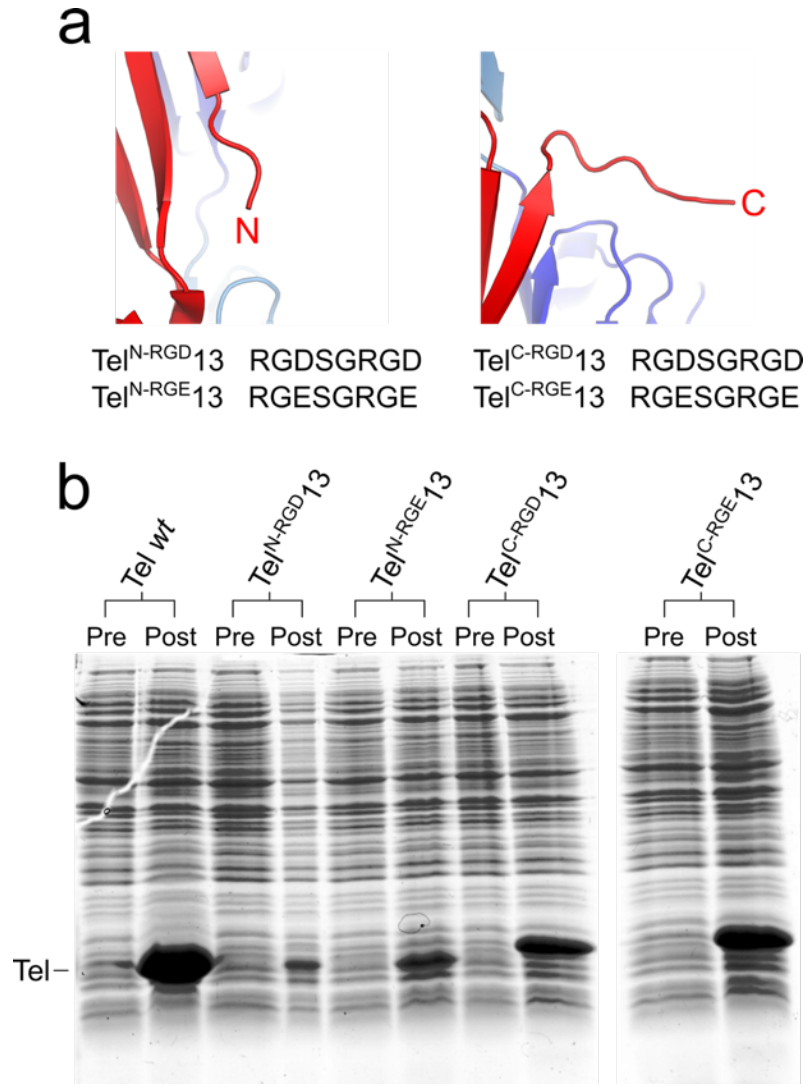


**Figure 8. Tel functionalisation and expression in the pETM-13 vector.** (a) The crystal structures of the N- (*left*) and C-termini (*right*) of Tel in the Z1Z2-Tel complex (PDB: 1YA5) are shown (*red*) and grafted amino acid sequences of the corresponding Tel variants in the pETM-13 vector are given below. (b) SDS-PAGE gel showing Tel expression pre- and post-induction of recombinant protein synthesis. The position of Tel is indicated.

Accordingly, a GRGDS motif was grafted at the C-terminus of Tel in pETM-11 ($Tel^{C\text{-}RGD}11$) and a second variant with an inactive GRGES motif ($Tel^{C\text{-}RGE}11$) was produced as a control (Figure 9a). To best mimic the motif of fibronectin, natural flanking residues glycine and serine were incorporated alongside the RGD tripeptide. Following overexpression of $Tel^{C\text{-}RGD}11$ and $Tel^{C\text{-}RGE}11$, whole bacterial lysate was subjected to SDS-PAGE analysis to observe yield. The quantity of $Tel^{C\text{-}}$

$^{RGD}$11 and Tel$^{C\text{-}RGE}$11 was noticeably lower than that of *wt* Tel and an unknown species of approximately 20 kDa was observed in both preparations (Figure 9b). Due to its disordered nature in the absence of a binding partner, heterologously-expressed recombinant Tel is sequestered in insoluble inclusion bodies, which necessitates the use of a strong denaturing buffer for solubilisation and subsequent isolation (Zou *et al.*, 2003). Therefore, bacterial cell pellets corresponding to *wt* Tel and variants were lysed in the presence of 8 M urea and purified by immobilised metal affinity chromatography (IMAC) using a nickel column. Applying this method, *wt* Tel could be purified to a high level of homogeneity without the need for further chromatographic techniques. However, the unknown 20 kDa species present in Tel$^{C\text{-}RGD}$11 and Tel$^{C\text{-}RGE}$11 preparations was co-eluted with the samples and became more enriched with increasing imidazole concentration, suggesting that it has a greater affinity for the nickel column than the $His_6$-tagged Tel variants (Figure 9c). Due to the relatively poor yields of terminally-modified Tel variants and presence of an unknown species in Tel$^{C\text{-}RGD}$11 and Tel$^{C\text{-}RGE}$11 preparations, priority was given to the generation of other RGD-functionalised constructs.

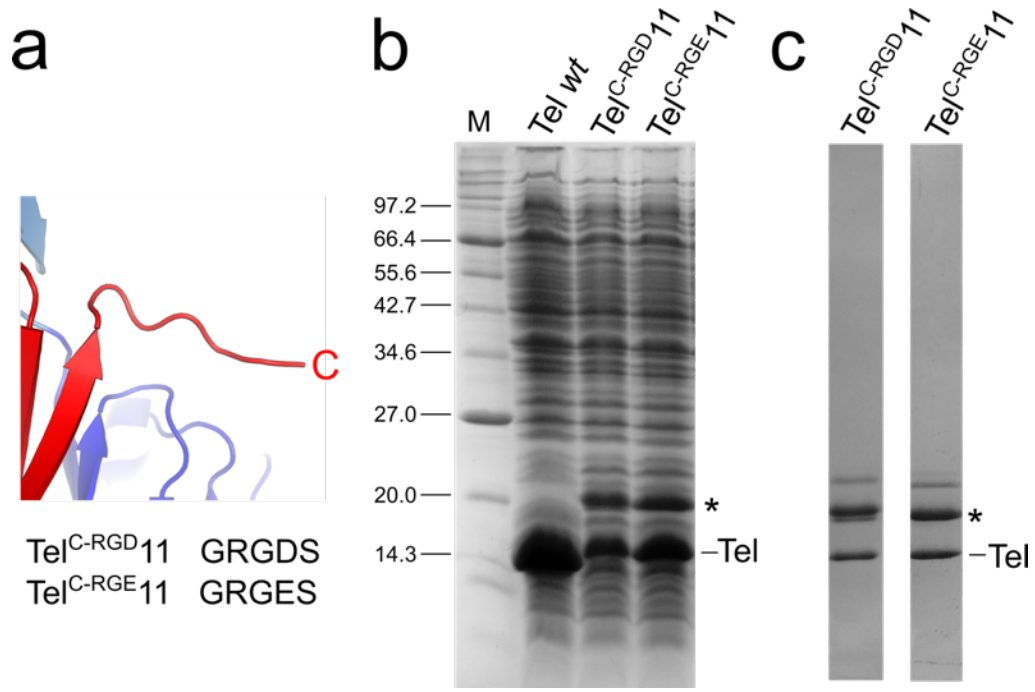


**Figure 9. Tel functionalisation and expression in the pETM-11 vector.** (a) The crystal structure of the Tel C-terminus in the Z1Z2-Tel complex (PDB: 1YA5) is shown in the schematic (*red*) and amino acid sequences grafted at the C-termini of Tel variants in the pETM-11 vector are shown below. (b) SDS-PAGE gel showing Tel expression post-induction of recombinant protein synthesis. The position of Tel is indicated and an unknown species present in the lysate corresponding to $Tel^{C\text{-}RGD}11$ and $Tel^{C\text{-}RGE}11$ is marked by an asterisk (*). A molecular mass marker (M) in kDa is shown to the left. (c) Samples of $Tel^{RGD}$ and $Tel^{RGE}$ at high imidazole concentration following purification by immobilised metal affinity chromatography.

### *3.2.2 Generation and characterisation of CD-loop-grafted variants*

#### *3.2.2.1 Design of protein constructs*

The integrin-binding RGD motif with flanking residues from fibronectin was inserted in the CD-loop of the second Z1 domain within $Z_{1212}$ ($Z_{1212}^{RGD}$), thereby permitting the assessment of the functionalisation potential of this site in the context of ZT nanofibres. In $Z_{1212}^{RGD}$, four naturally occurring residues were substituted and three non-native residues were inserted at the genetic level. Specifically, the amino acid sequence SGRGDSS was grafted, where the two residues flanking the RGD motif replaced native Z1 residues. An inactive RGE motif was also grafted ($Z_{1212}^{RGE}$) to act as a control (Figure 10). To best mimic the RGD motif of fibronectin, natural

flanking residues glycine and serine were included alongside non-native serine residues to extend the loop and increase flexibility.

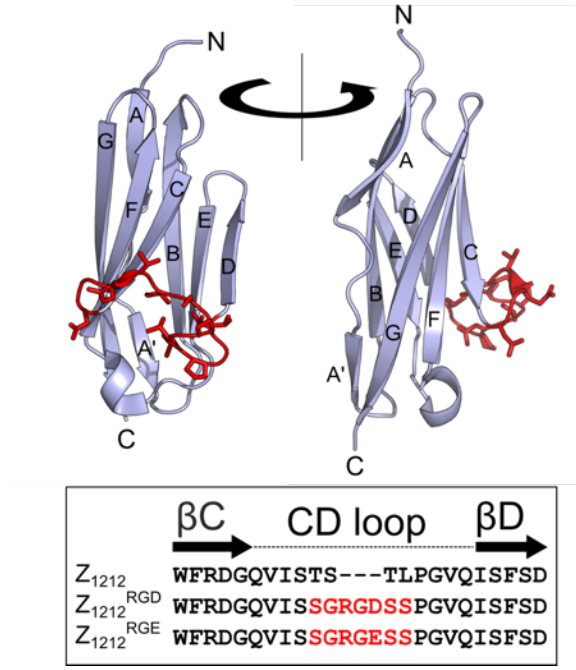


**Figure 10. Z1 domain functionalisation by CD-loop diversification.** Crystal structure of the titin Z1 Ig domain (PDB: 2A38, Marino *et al*., 2006) with secondary structural elements labelled. The side chains of residues comprising the native CD-loop are shown as sticks (*red*). The amino acid sequences of the CD-loop in *wt* $Z_{1212}$ and grafted mutants $Z_{1212}^{RGD}$ and $Z_{1212}^{RGE}$ are show below with non-native residues highlighted (*red*).

### *3.2.2.2 Purification and characterisation of the Z1Z2$^{RGD}$-Tel complex*

To confirm that insertion of the RGD motif in the Z1 domain did not negatively affect the ability of the Z1Z2 doublet to interact with Tel, a construct comprising Z1Z2 with an RGD-modified CD-loop (Z1Z2$^{RGD}$) was constructed and co-expressed with Tel to allow for *in vivo* complexation. The expression system was designed to include a $His_6$-tagged Tel and untagged Z1Z2$^{RGD}$, meaning that only Tel-bound Z1Z2$^{RGD}$ (Z1Z2$^{RGD}$-Tel) would co-elute when subjected to nickel affinity chromatography. Thus, purification of the Z1Z2$^{RGD}$-Tel complex was achieved by IMAC, followed by $His_6$ tag removal using targeted proteolysis and subsequent reverse affinity chromatography. Final purification was by size-exclusion (SEC) and

anion-exchange (AEC) chromatography. The complex eluted as multiple species by SEC (Figure 11a) and both Z1Z2$^{RGD}$ and Tel were present in the main peak (Figure 11b). Although the presence of Z1Z2$^{RGD}$-Tel in an intermediate peak suggests that a higher oligomeric state was formed, the same elution profile was observed for *wt* Z1Z2-Tel (data not shown). It should be noted that higher MM species were consistently observed by SDS-PAGE for Z1Z2-Tel complexes (Figure 11b,d). It is most likely that these species represent complexes that were not denatured by boiling prior to sample loading. Importantly, the recombinant complex was not present in the column void, confirming the absence of aggregation. Fractions from the main peak ($V_e$ = 85.45 mL) were further purified by AEC (Figure 11c,d) prior to additional analysis.

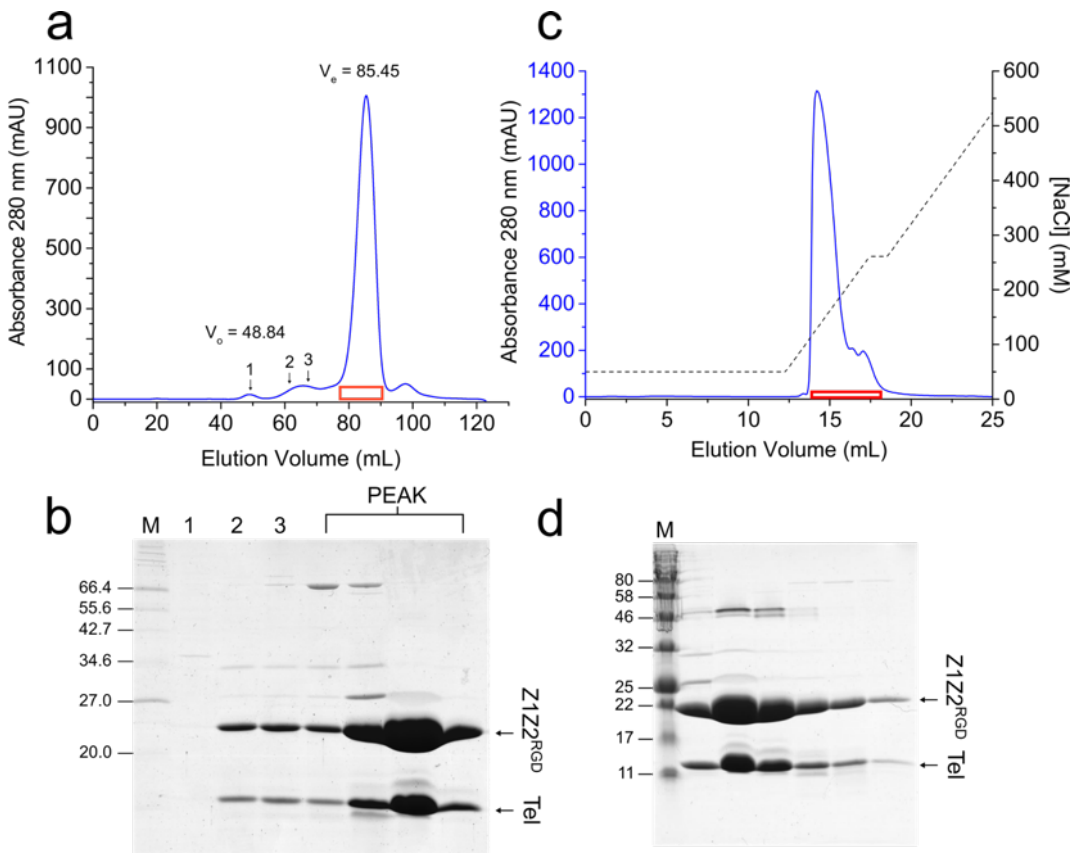


**Figure 11. Purification of the Z1Z2$^{RGD}$-Tel complex.** (a) Size-exclusion chromatogram from a Superdex 200 16/60 column. The void ($V_o$) and exclusion ($V_e$) volumes are indicated on the graph and the inset SDS-PAGE gel (b) shows fractions taken from individual peaks (*numbers*) and the boxed area (*red*). (c) Anion-exchange chromatogram from a MonoQ 5/50 GL column with inset SDS-PAGE gel (d) of fractions from the boxed area (*red*) of the peak. A molecular mass marker (M) in kDa is shown on each gel and individual protein components of the complex are indicated.

To ensure that the complex of Z1Z2$^{RGD}$-Tel reproduced that of *wt* Z1Z2-Tel, both samples were compared using analytical SEC (Figure 12a). The elution chromatograms of both samples were in exact agreement, reproducibly eluting at the same volume of exclusion ($V_e$ = 14.42 mL). To further confirm that the Z1Z2$^{RGD}$-Tel complex assembled in the expected 2:1 ratio, this sample was studied analytically using SEC coupled to multi-angle laser light scattering (SEC-MALLS). SEC-MALLS is a technique for determination of absolute protein molecular mass (MM) independent of shape. The experimentally measured MM of Z1Z2$^{RGD}$-Tel was 53.3 ± 0.7 kDa, in good agreement with a complex comprising one Tel and two Z1Z2$^{RGD}$

subunits (respective MM of 13.43 and 21.12 kDa as calculated from the sequence data) (Figure 12b).

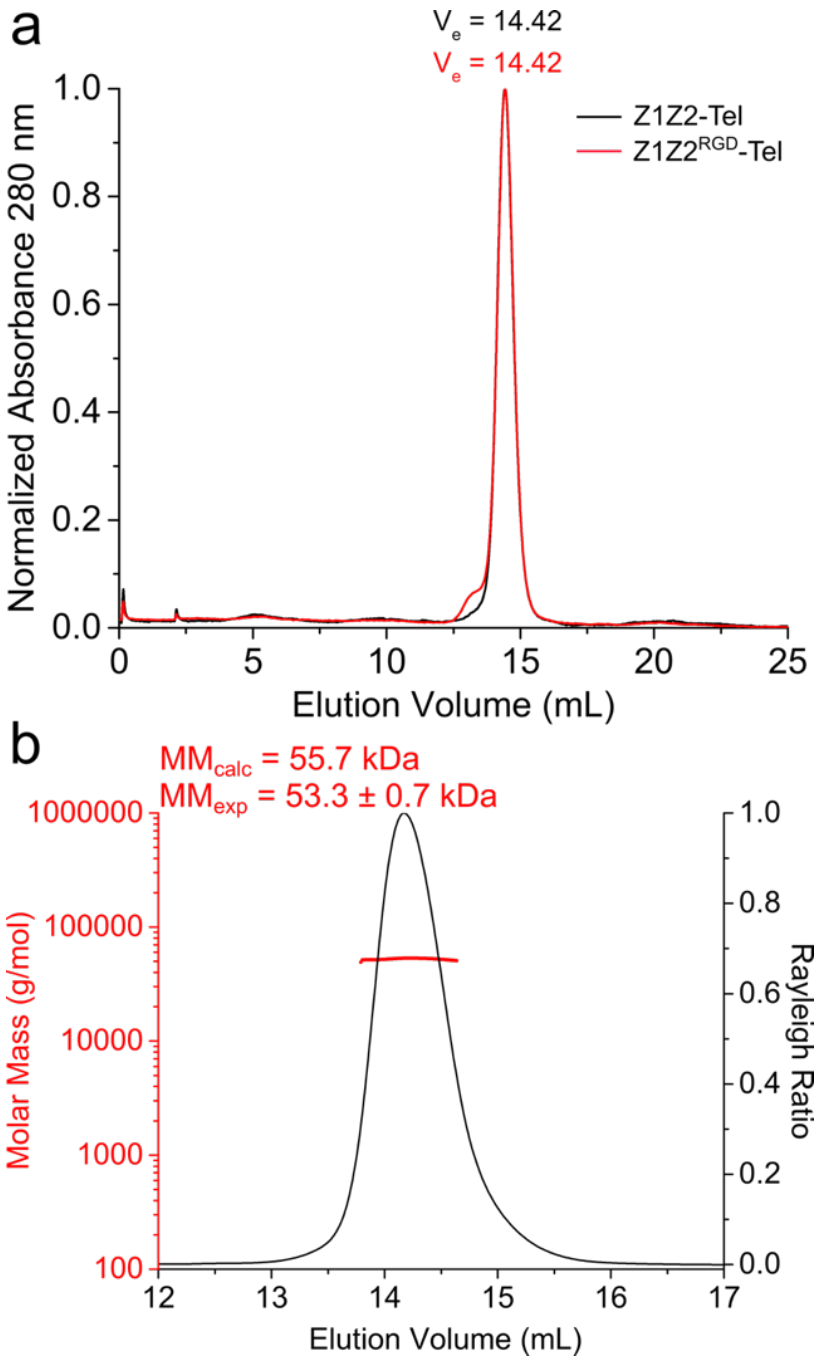


**Figure 12. Characterisation of the Z1Z2$^{RGD}$-Tel complex.** (a) Size-exclusion chromatogram overlays of Z1Z2-Tel (*black trace*) and Z1Z2$^{RGD}$-Tel (*red trace*) complexes on a Superdex 200 10/300 column. The exclusion volumes ($V_e$) are indicated. (b) SEC-MALLS analysis of Z1Z2$^{RGD}$-Tel complex. Normalised refractive index (*black trace*) is plotted against retention volume. The experimentally determined molecular mass ($MM_{exp}$) of the eluting material, calculated from the refractive index and light scattering measurements, is plotted as a *red line*. Values for both experimental and calculated ($MM_{calc}$) molecular masses are given above.

### *3.2.2.3 Purification and characterisation of $Z_{1212}^{RGD}$ and $Z_{1212}^{RGE}$*

After concluding that insertion of the RGD motif in the CD-loop of Z1 did not interfere with Tel association, CD-loop-grafted $Z_{1212}$ tandem chimeras were investigated for structural stability and polymerisation capacity. Both $Z_{1212}^{RGD}$ and $Z_{1212}^{RGE}$ proved unchallenging to produce in *E. coli* and expressed at yields comparable to *wt* $Z_{1212}$ (approximately 40 and 30 mg pure protein per litre of bacterial culture, respectively). $Z_{1212}^{RGD}$ eluted as a single peak by SEC (Figure 13a,b) and could be further purified to a high level of homogeneity by AEC (Figure 13c,d).

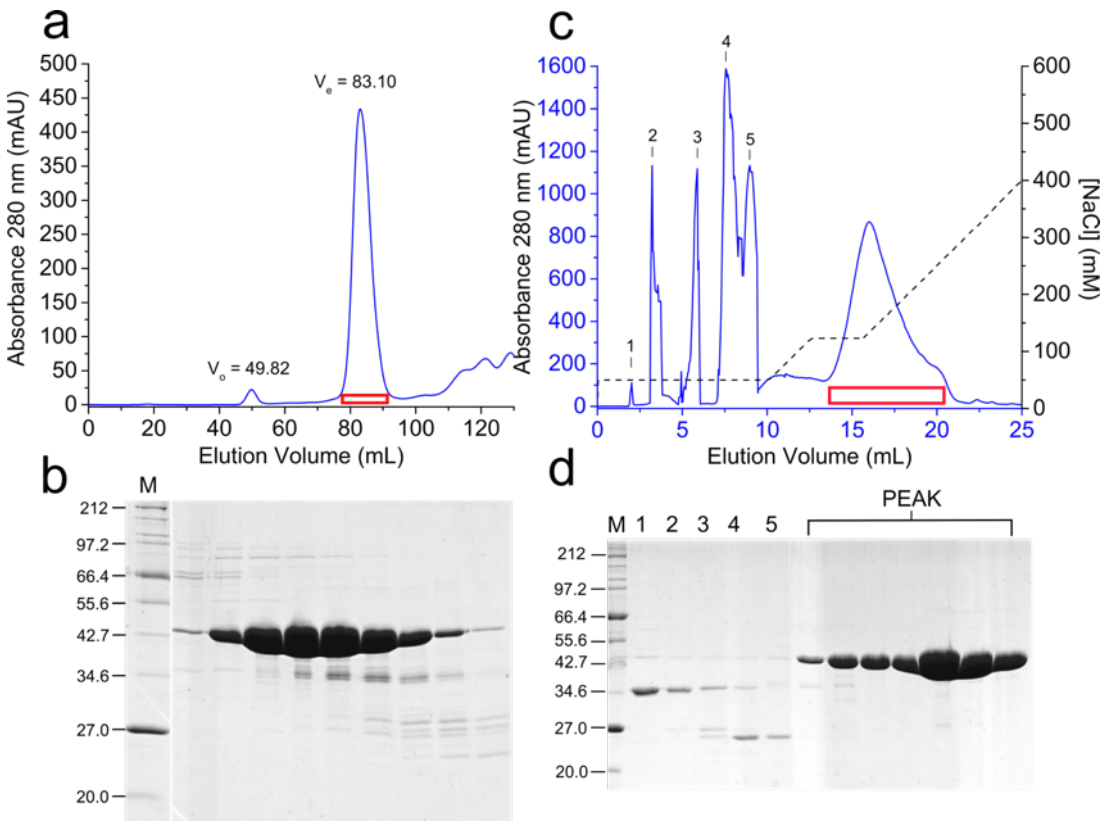


**Figure 13. Purification of $Z_{1212}^{RGD}$.** (a) Size-exclusion chromatogram from a Superdex 200 16/60 column. The void ($V_o$) and exclusion ($V_e$) volumes are indicated on the graph and the inset SDS-PAGE gel (b) shows fractions taken from the boxed area (*red*) of the peak. (c) Anion-exchange chromatogram from a MonoQ 5/50 GL column with inset SDS-PAGE gel (d) of fractions taken from individual peaks (*numbers*) or the boxed area (*red*). A molecular mass marker (M) in kDa is shown on each gel

Analytical SEC was used to assess the oligomeric state of $Z_{1212}^{RGD}$ and $Z_{1212}^{RGE}$. Both proteins gave identical elution profiles to *wt* $Z_{1212}$, confirming the absence of undesirable homophilic interactions in these variants (Figure 14).

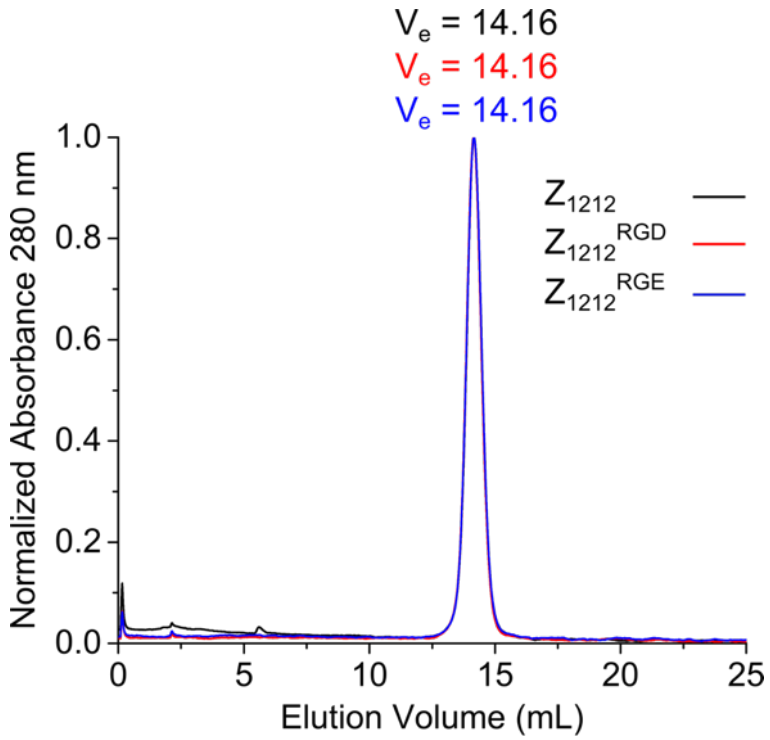


**Figure 14. $Z_{1212}^{RGD}$ and $Z_{1212}^{RGE}$ characterisation.** Size-exclusion chromatogram overlays of $Z_{1212}$ (*black trace*), $Z_{1212}^{RGD}$ (*red trace*) and $Z_{1212}^{RGE}$ (*blue trace*) on a Superdex 200 10/300 column. The exclusion volumes ($V_e$) are indicated.

### *3.2.2.4 Small-angle X-ray scattering analysis of $Z_{1212}$ and $Z_{1212}^{RGD}$*

Further insight into the molecular properties of $Z_{1212}^{RGD}$ was gained through small-angle X-ray scattering (SAXS) experiments. SAXS is a solution technique that can characterise the shape and conformation of macromolecules (Putnam *et al.*, 2007). SAXS data were collected at a concentration range of approximately 3.5 – 15 mg/mL for $Z_{1212}$ and $Z_{1212}^{RGD}$ to derive experimental scattering profiles (Figure 15a,b). All SAXS data was collected by Dr. Barbara Franke (Universität Konstanz) at beamline P12 of the PETRA III Synchrotron Source (EMBL/DESY, Hamburg, Germany). The scattering data shows that both $Z_{1212}$ and $Z_{1212}^{RGD}$ are monodisperse at the highest concentration tested and did not demonstrate a propensity to aggregate. Radius of gyration ($R_g$) values obtained by Guinier approximation were almost identical ($R_g$ = 45.6 ± 0.2 Å and 45.4 ± 0.2 Å for $Z_{1212}$ and $Z_{1212}^{RGD}$, respectively), suggesting that both samples have a similar conformation in solution. Pair-distance distribution functions calculated from the scattering profiles of $Z_{1212}$ and $Z_{1212}^{RGD}$ (Figure 15c,d) yielded a maximum particle size ($D_{max}$) of 180 Å. This value is in good agreement with the hypothetical size of a four Ig protein given that domains are approximately 44 Å in length (Marino *et al.*, 2005). The $D_{max}$ also indicates that domains attain an extended conformation along the the axial length of the construct. Taken together, analogous $R_g$ and $D_{max}$ values for $Z_{1212}$ and $Z_{1212}^{RGD}$ suggests that these proteins have near identical global conformations in solution.

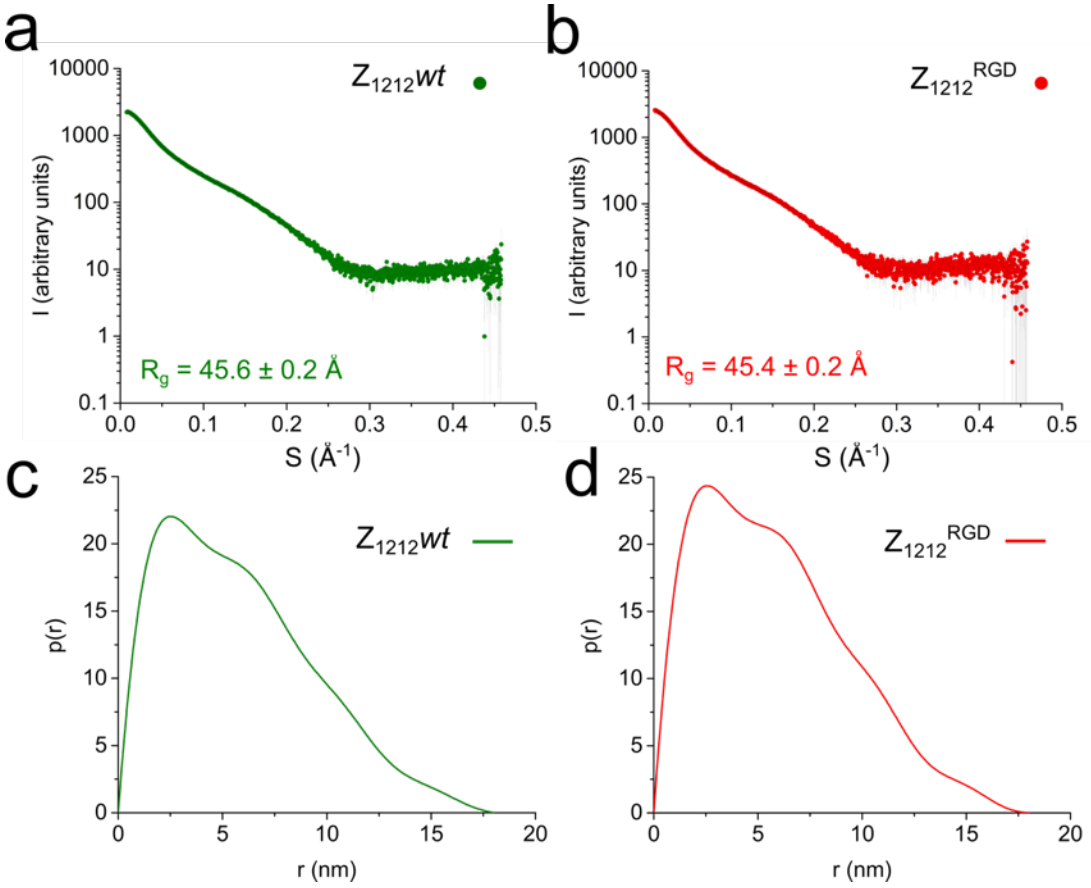


**Figure 15. SAXS analysis of $Z_{1212}$ and $Z_{1212}^{RGD}$.** Experimental scattering profiles of $Z_{1212}$ (a) and $Z_{1212}^{RGD}$ (b) are displayed as dots with error bars. The log scattering intensity (I) is plotted against scattering momentum (S). $R_g$ values obtained by Guinier approximation are stated on the graphs. Pair-distance distribution functions, p(r), of $Z_{1212}$ (c) and $Z_{1212}^{RGD}$ (d) were calculated from the experimental scattering curves using the program GNOM.

### *3.2.2.5 Polymerisation capacity of CD-loop-grafted variants*

In the presence of Tel, $Z_{1212}^{RGD}$ and $Z_{1212}^{RGE}$ were shown to assemble at levels comparable to *wt* $Z_{1212}$, as observed by native PAGE analysis (Figure 16a). $Z_{1212}$ and variants were observed to generate streaks on native PAGE gels, which suggested that a concentration-dependent aggregation of the proteins was occurring. Although the monodisperse nature of $Z_{1212}$ and $Z_{1212}^{RGD}$ at 15 mg/mL was confirmed by SAXS, considerably higher concentrations may be attained at the stacking and resolving gel interfaces, thus resulting in aggregation. The highly resolved unpolymerised $Z_{1212}$ from the assembly mixtures was supportive of this hypothesis,

since protein concentration was lower. Assemblies derived from $Z_{1212}^{RGD}$ ($ZT^{RGD}$) and $Z_{1212}^{RGE}$ ($ZT^{RGE}$) showed near identical electrophoretic mobility profiles with supramolecular species in the upper portion of the gel. An unidentified band was observed in lanes corresponding to ZT assemblies that ran further on the gel than unpolymerised $Z_{1212}$. It was hypothesised that this band represented a "blunt" by-product of the assembly process formed by the interaction of $Z_{1212}$ with a single Tel molecule (Figure 16b). Following seven days of polymerisation, two distinct phases were observable in the assembly mixtures; a clear upper layer and a turbid lower layer comprising insoluble material (Figure 16c).

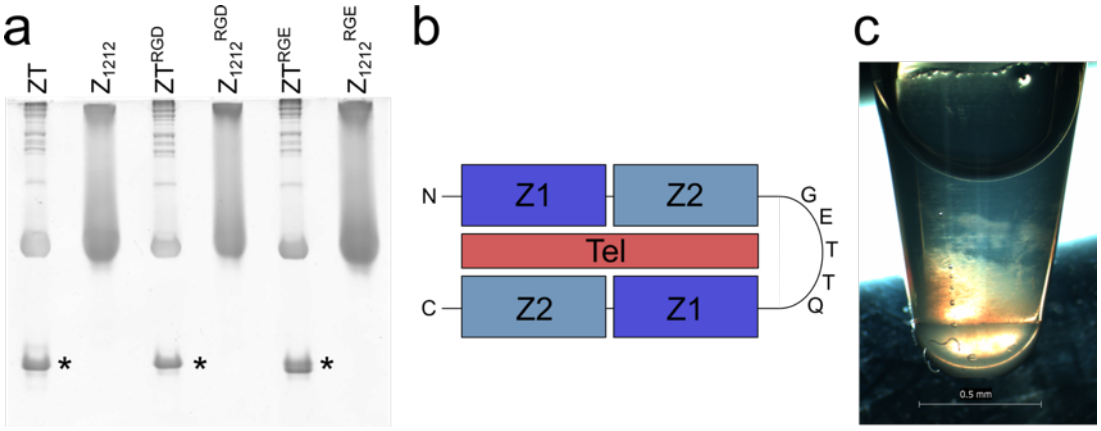


**Figure 16. $Z_{1212}$ CD-loop mutant polymerisation capacities.** (a) Native PAGE of individual tandem proteins and their corresponding assemblies in the presence of Tel (samples at 5 mg/mL) 24 hours post-mixing. Hypothetical "blunt" products are marked with asterisks (*). (b) Schematic representation of a non-propagative $Z_{1212}$-Tel interaction. (c) Nanofibre solution at 10 mg/mL in a 1.5 mL Eppendorf tube 7 days post-mixing at a 3:1 molar ratio of Tel to $Z_{1212}$. Scale bar = 0.5 mm.

### *3.2.2.6 Transmission electron microscopy*

During the original design and fabrication of the ZT system, nanofibres were visualised by transmission electron microscopy (TEM) using a negative staining method developed by Bruning *et al*. (2010) and carried out at the Biozentrum of the University of Basel, Switzerland. During the course of the current project, attempts

to image both unmodified and functionalised ZT nanofibres proved challenging and difficult to reproduce. To observe macromolecules by TEM, the sample must first be deposited onto a copper grid cast with a fine meshwork that has been coated with a support film. The nature of this support film varies depending on sample type and application, but is most often made from plastic (pioloform or formvar films that are stabilised with evaporated carbon) or pure carbon when working with protein-based samples. Furthermore, the surface chemistry of the support film can be modified to promote the adsorption of samples. Carbon support films are generally hydrophobic and must be glow discharged to make the surface hydrophilic and, thus, more accessible to the suspended sample. As described in Chapter 2 (section 2.6.2.1), both carbon-stabilised pioloform and pure carbon support films, with or without glow discharging, were tested in an attempt to consistently observe ZT nanofibres by TEM. However, samples were only visualised successfully when loaded on glow discharged pure carbon support films (manufactured in-house at the University of Sheffield) using the protocol established by Bruning *et al*. (2010). Visualisation of $ZT^{RGD}$ and $ZT^{RGE}$ by TEM confirmed the presence of nanofibres, with comparable distributions of curly and tapelike morphologies to *wt* ZT (Figure 17). Despite these promising observations, more thorough quantification of nanofibre morphology was not possible, since subsequent preparations of *wt* ZT, $ZT^{RGD}$ and $ZT^{RGE}$ were not observed when loaded onto grids using the same protocol.

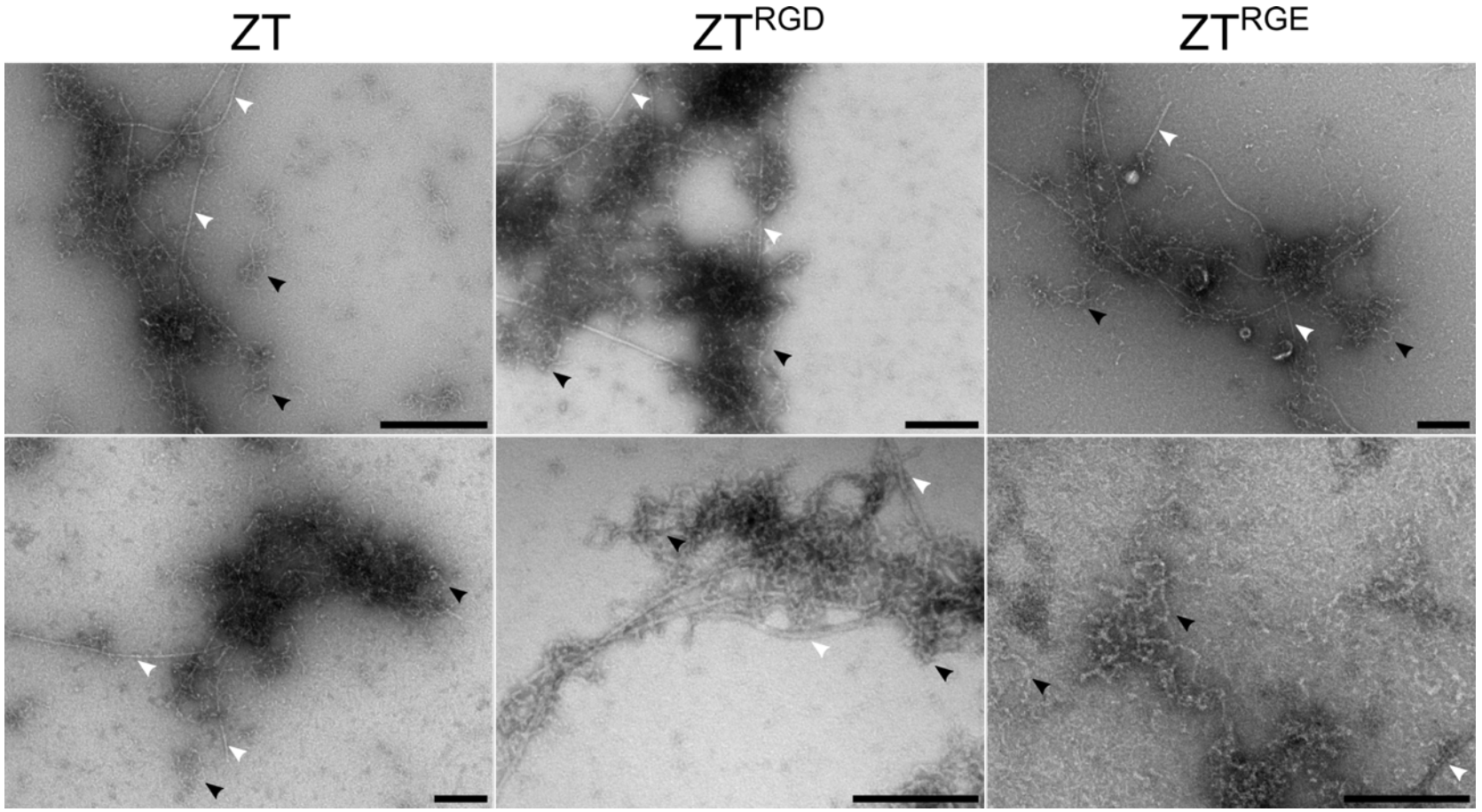


**Figure 17. Nanofibre morphology when assembled from Z1 CD-loop mutants.** Representative transmission electron micrographs of negatively stained *wt* ZT, $ZT^{RGD}$ and $ZT^{RGE}$ nanofibres. Tapelike (*white arrows*) and curly (*black arrows*) morphologies are highlighted. Nanofibres (day 7 post-assembly) were loaded onto grids at a concentration of 1 mg/mL and imaged using a FEI 120 kV Tecnai G2 Spirit BioTWIN electron microscope operating at 100 kV. Scale bars = 200 nm.

### *3.2.3 Generation and characterisation of the fibronectin fusion chimera*

#### *3.2.3.1 Protein construct design*

The FnIII 10 domain from human fibronectin, containing the RGD motif *in situ*, was fused to the C-terminus of $Z_{1212}$ by genetic engineering. Specifically, a GETTQ linker sequence was introduced between the C-terminal glutamine of $Z_{1212}$ and the N-terminal serine of FnIII 10 to create a five-domain chimera termed $Z_{1212}^{Fn}$ (Figure 18a). Computational modelling of the GETTQ linker in the context of $Z_{1212}$ predicted that interdomain flexibility is permitted (Bruning *et al.*, 2010), thus the linker was reused to permit movement of the FnIII domain for non-restricted interaction with receptors on the cell surface. It was hypothesised that the addition of FnIII 10 would not inhibit nanofibre polymerisation due to its positioning at the C-terminus of $Z_{1212}$, but would permit the periodic display of the RGD motif in both longitudinal (Figure 18b) and parallel (Figure 18c) assembly modes.

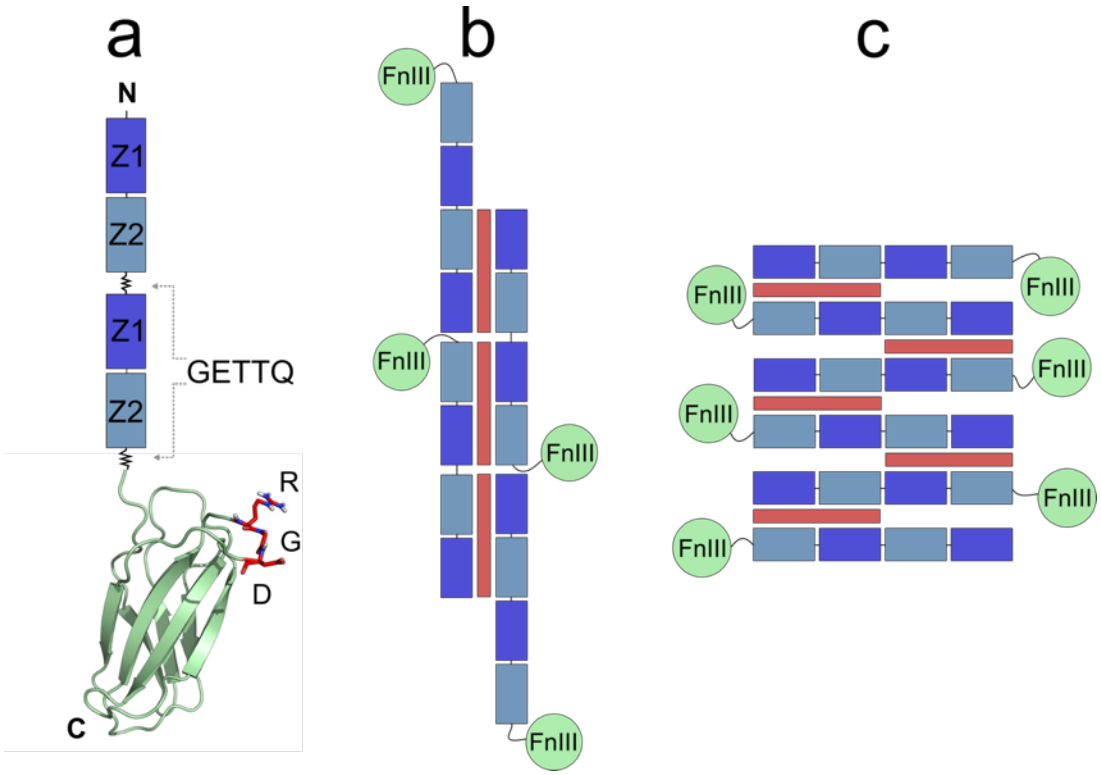


**Figure 18. $Z_{1212}$ functionalisation by domain fusion.** (a) Schematic representation of the $Z_{1212}$ tandem fused C-terminally to the FnIII 10 domain of human fibronectin (PDB: 1FNF, *green*) via the same GETTQ linker used to join the Z1Z2 pairs. The integrin binding RGD motif, as observed in the crystal structure, is highlighted (*red*). Z1 and Z2 domains are of approximately the same size as the fused FnIII domain; the domains are not shown to scale in the image for visual simplicity. The hypothesised self-assembly modes of $Z_{1212}^{Fn}$ and Tel into fibrous scaffolds along a "longitudinal" (b) or "parallel" (c) propagation path are portrayed to show the putative positioning of the FnIII domains (*green spheres*) in each assembly mode.

### *3.2.3.2 Purification and characterisation of the Z1Z2$^{Fn}$-Tel complex*

The effect of FnIII 10 fusion on Tel interaction was investigated using the same rational as CD-loop variants; an untagged construct comprising Z1Z2 fused to FnIII 10 (Z1Z2$^{Fn}$) was co-expressed with $His_6$-tagged Tel in bacteria to allow for complexation and co-purification. Recombinant proteins were purified by IMAC as previously described (section 3.2.2.2) and applied to a size-exclusion column. The complex eluted as multiple peaks by SEC (Figure 19a) and both Z1Z2$^{Fn}$ and Tel were present in the main peak (Figure 19b). As with *wt* Z1Z2-Tel, a small proportion

of Z1Z2$^{Fn}$-Tel appears to adopt a higher oligomeric state, but is not prone to aggregation. Fractions from the main peak ($V_e$ = 78.60 mL) were purified by AEC (Figure 19c,d) prior to additional analysis.

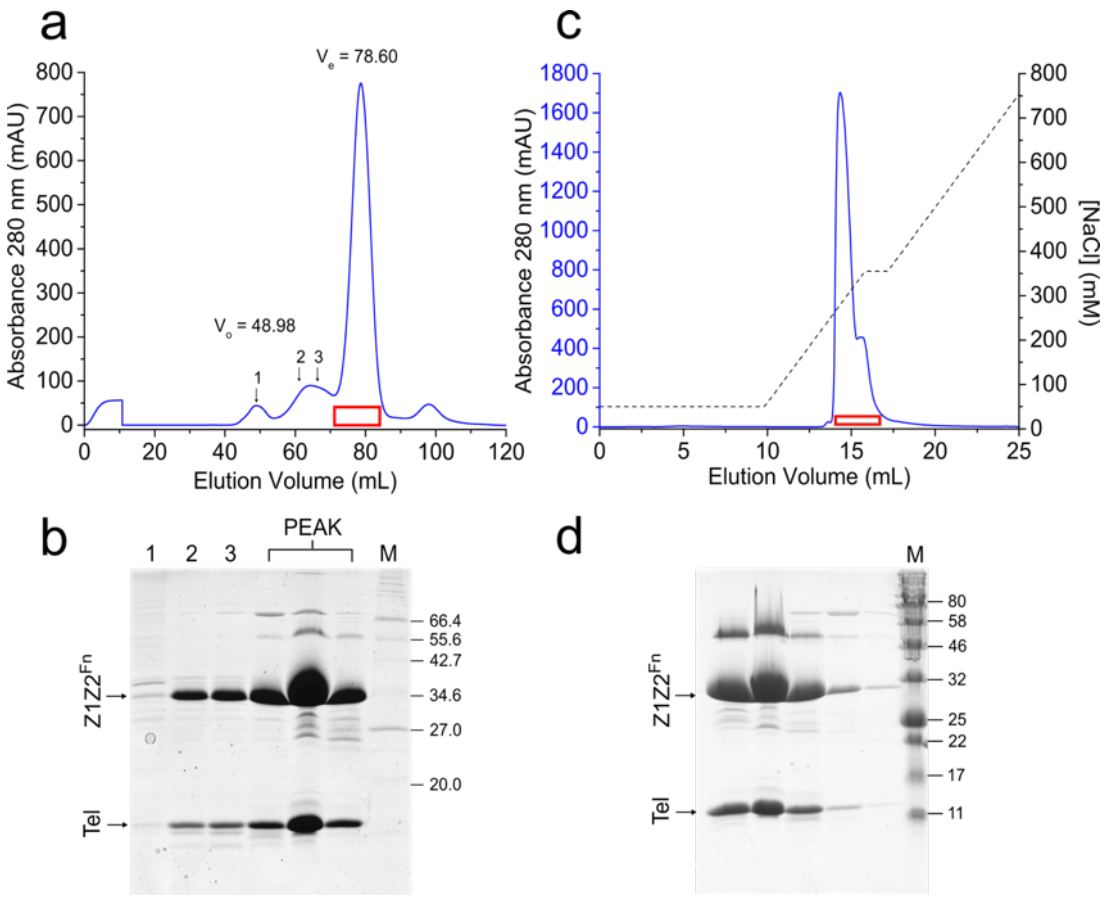


**Figure 19. Purification of the Z1Z2$^{Fn}$-Tel complex.** (a) Size-exclusion chromatogram from a Superdex 200 16/60 column. The void ($V_o$) and exclusion ($V_e$) volumes are indicated on the graph and the inset SDS-PAGE gel (b) shows fractions taken from individual peaks (*numbers*) and the boxed area (*red*). (c) Anion-exchange chromatogram from a MonoQ 5/50 GL column with inset SDS-PAGE gel (d) of peak fractions from the boxed area (*red*). A molecular mass marker (M) in kDa is shown on each gel and individual protein components of the complex are indicated.

Analytical SEC and SEC-MALLS were employed to investigate the stoichiometry of the Z1Z2$^{Fn}$-Tel complex. As expected, Z1Z2$^{Fn}$-Tel eluted as a larger species by analytical SEC compared to the *wt* Z1Z2-Tel complex and showed no indication of aggregation or oligomerisation (Figure 20a). SEC-MALLS measurements of Z1Z2$^{Fn}$-Tel yielded an average MM of 72.2 ± 0.8 kDa, in good

agreement with the theoretical MM of a 2:1 association between Z1Z2$^{Fn}$ and Tel (31.41 and 13.43 kDa, respectively) (Figure 20b).

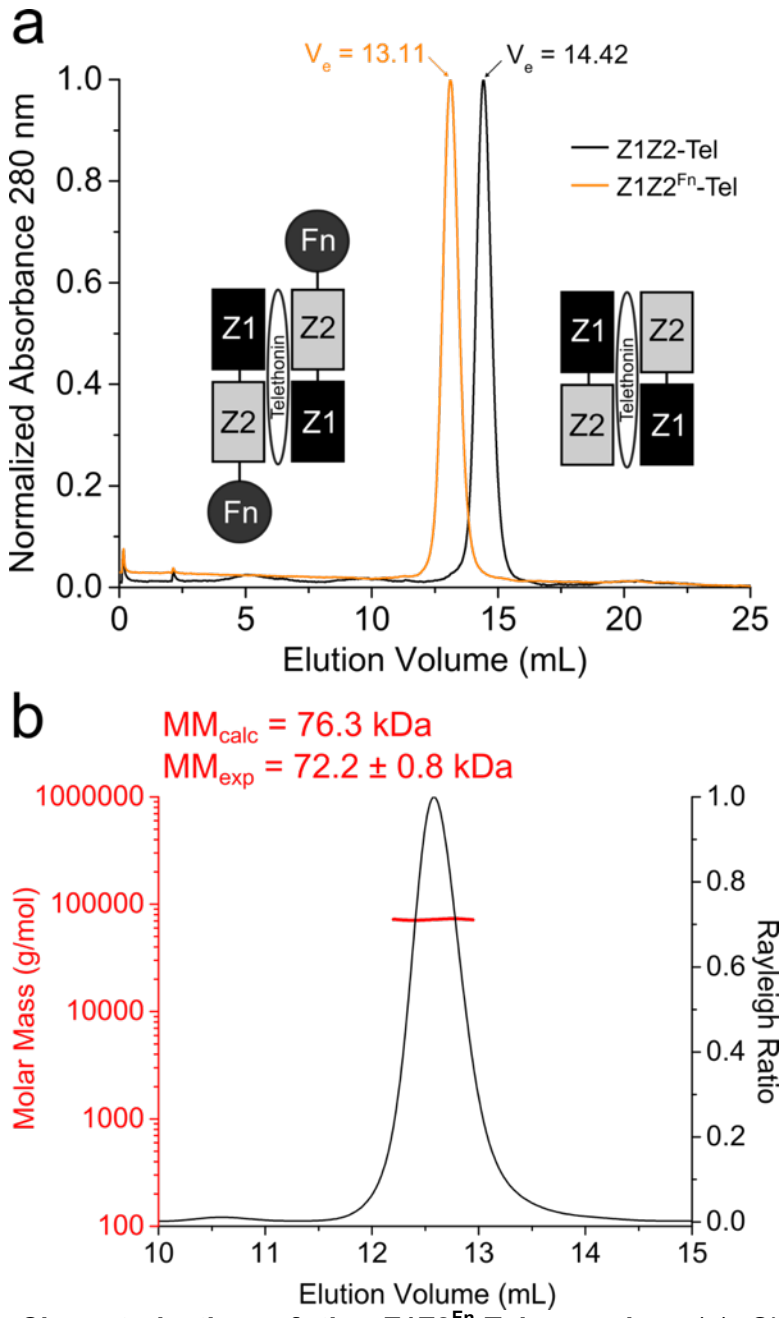


**Figure 20. Characterisation of the Z1Z2$^{Fn}$-Tel complex.** (a) Size-exclusion chromatogram overlays of Z1Z2-Tel (*black trace*) and Z1Z2$^{Fn}$-Tel (*orange trace*) complexes on a Superdex 200 10/300 column. The exclusion volumes ($V_e$) are indicated and schematic representations of complexes are shown to the left or right of their corresponding peaks. (b) SEC-MALLS analysis of the Z1Z2$^{Fn}$-Tel complex. Normalised refractive index (*black line*) is plotted against retention volume. The experimentally determined molecular mass ($MM_{exp}$) of the eluting material, calculated from the refractive index and light scattering measurements, is plotted as a *red line*. Values for both experimental and calculated ($MM_{calc}$) molecular masses are given above.

### *3.2.3.3 Purification and characterisation of $Z_{1212}^{Fn}$*

Overexpression of the five domain $Z_{1212}^{Fn}$ construct in *E. coli* was comparable in yield to *wt* $Z_{1212}$ (approximately 40 mg pure protein per litre of bacterial culture) and the fusion protein was isolated from crude lysate by IMAC. $Z_{1212}^{Fn}$ eluted as a largely enriched species by SEC (Figure 21a,b) and was further purified by AEC (Figure 21c,d).

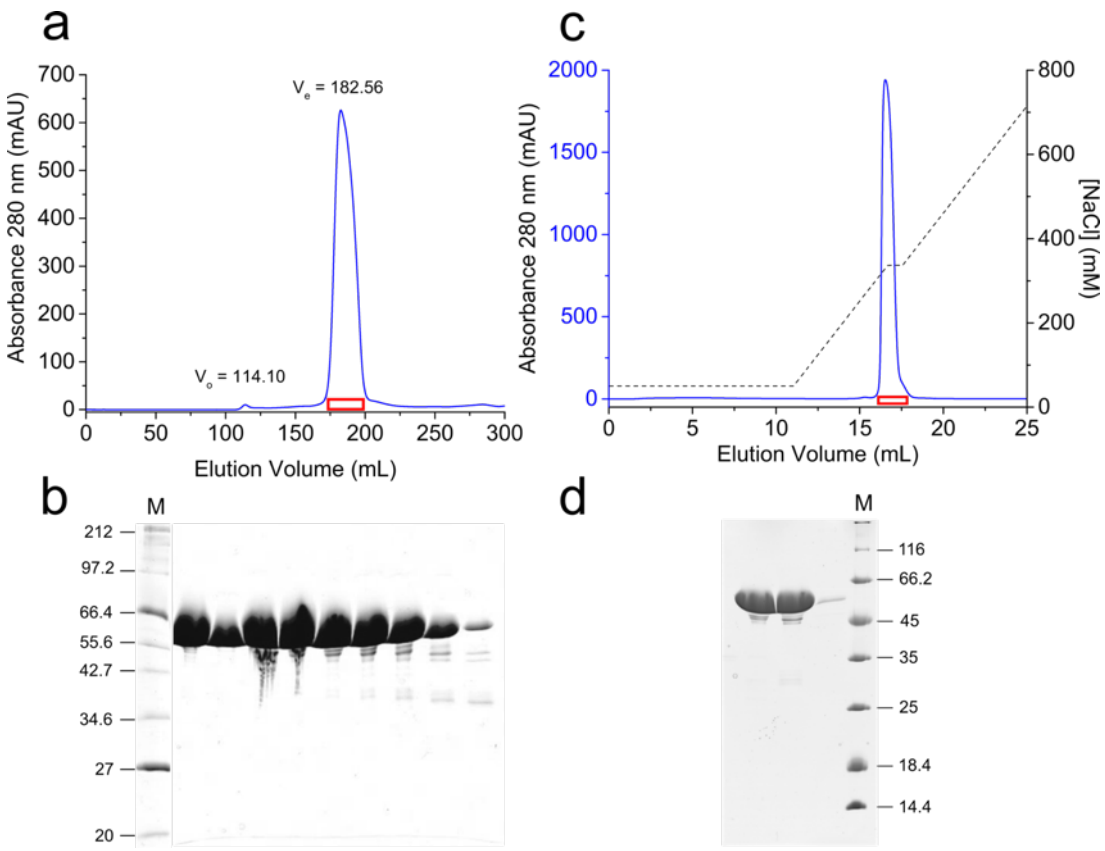


**Figure 21. Purification of $Z_{1212}^{Fn}$.** (a) Size-exclusion chromatogram from a Superdex 200 26/60 column. The void ($V_o$) and exclusion ($V_e$) volumes are indicated on the graph and the inset SDS-PAGE gel (b) shows samples taken from the boxed area (*red*) of the peak. (c) Anion-exchange chromatogram from a MonoQ 5/50 GL column with inset SDS-PAGE gel (d) of peak fractions from the boxed area (*red*). A molecular mass marker (M) in kDa is shown on each gel.

As $Z_{1212}^{Fn}$ contains an FnIII domain previously uncharted in the ZT nanofibre scheme, the effects of FnIII 10 fusion to $Z_{1212}$ were investigated further. As predicted, $Z_{1212}^{Fn}$ eluted as a larger species compared to *wt* $Z_{1212}$ (Figure 22a) and SEC-MALLS measurements confirmed the preservation of the monomeric nature of

$Z_{1212}$ when fused to FnIII 10 (Figure 22b).

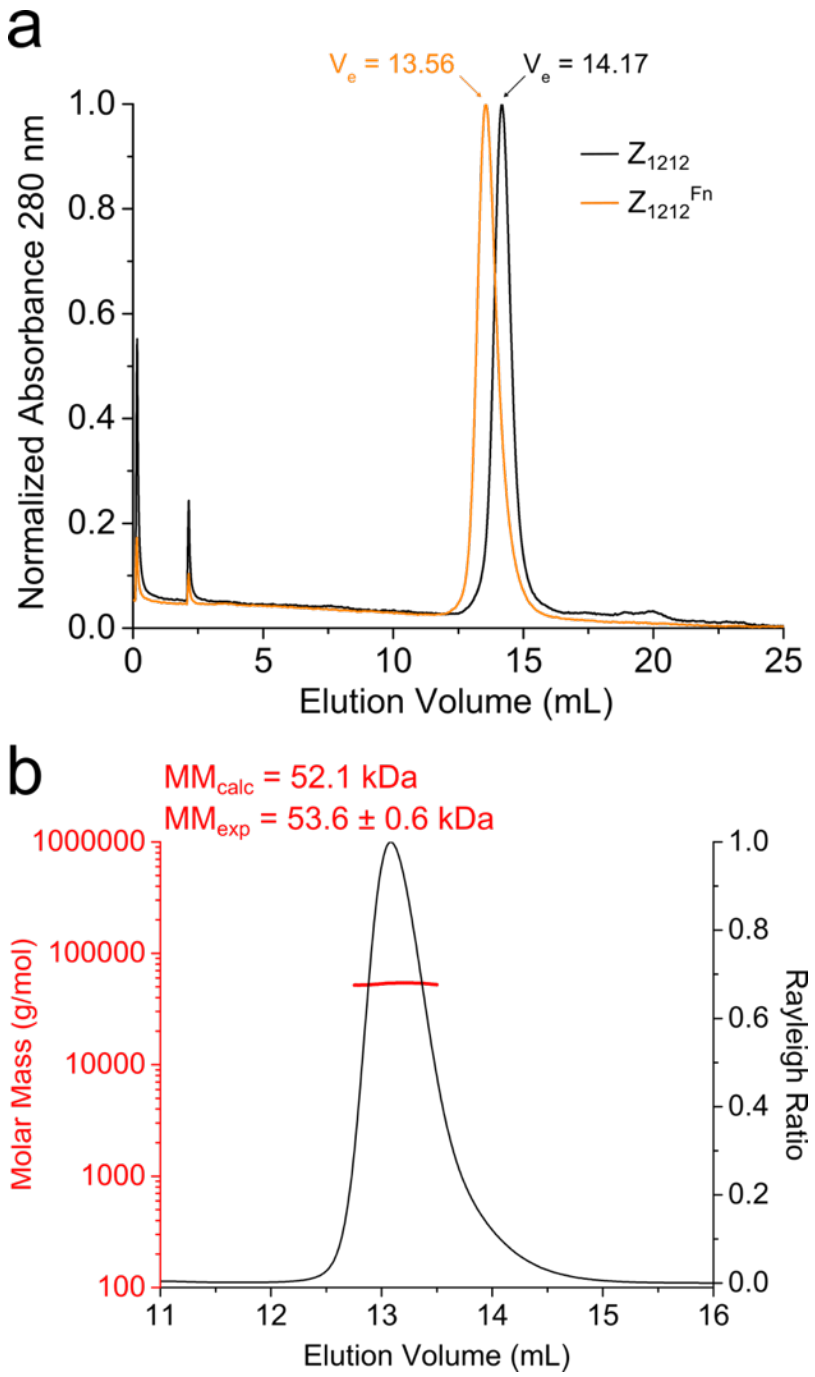


**Figure 22. Characterisation of $Z_{1212}^{Fn}$.** (a) Size-exclusion chromatogram overlays of $Z_{1212}$ (*black trace*) and $Z_{1212}^{Fn}$ (*orange trace*) on a Superdex 200 10/300 Tricorn column. The exclusion volume ($V_e$) of each protein is indicated. (b) SEC-MALLS analysis of $Z_{1212}^{Fn}$. Normalised refractive index (*black line*) is plotted against retention volume. The experimentally determined molecular mass ($MM_{exp}$) of the eluting material, calculated from the refractive index and light scattering measurements, is plotted as a *red line*. Values for both experimental and calculated ($MM_{calc}$) molecular masses are given above.

### *3.2.3.4 Polymerisation capacity of $Z_{1212}^{Fn}$*

Upon mixing, $Z_{1212}^{Fn}$ was found to interact propagatively with Tel to generate supramolecular assemblies observed by native PAGE (Figure 23a). In this case, the electrophoretic mobility profile of assemblies generated from $Z_{1212}^{Fn}$ ($ZT^{Fn}$) was different from *wt* ZT and a band that may correspond to the "blunt" species was again present (Figure 23b). However, despite repeated attempts to characterise the assemblies by TEM, supramolecular structures were not observed on the grids, nor were proteinaceous deposits immediately evident from background staining. The latter would have been observed if $ZT^{Fn}$ would have yielded amorphous assemblies instead of fibres. Although assembly was confirmed by native PAGE and the deposition of insoluble material post-mixing, the absence of an observation by TEM does not permit concluding on the assembly mode of this variant. Thus, it is unclear whether FnIII 10 occludes or allows both parallel and longitudinal assembly pathways.

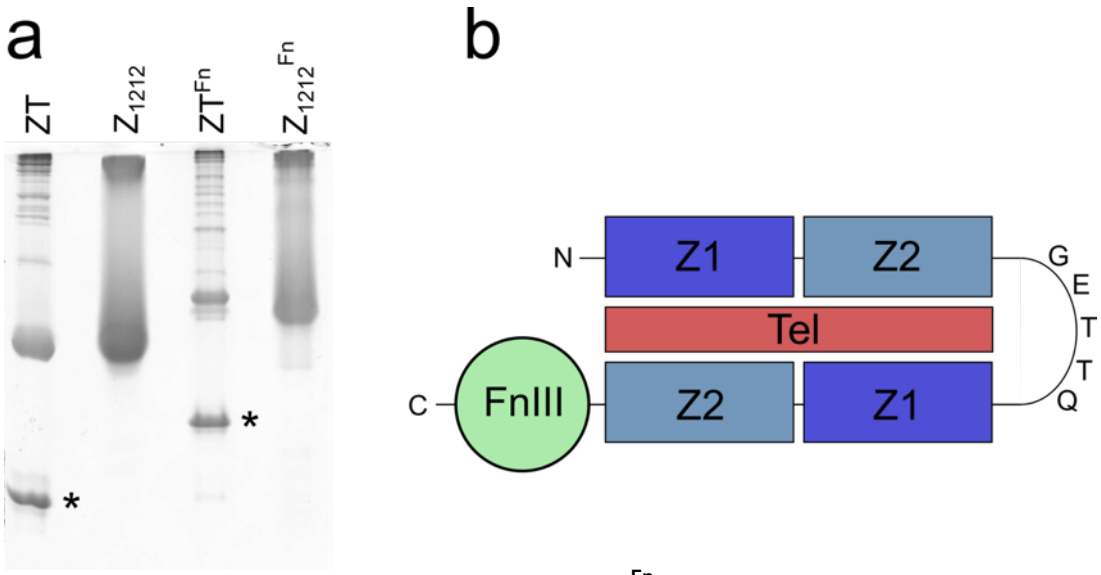


**Figure 23. Polymerisation capacity of $Z_{1212}^{Fn}$.** Native PAGE gel of $Z_{1212}$ and $Z_{1212}^{Fn}$ and their corresponding assemblies in the presence of Tel (samples at 5 mg/mL) 24 hours post-mixing. Hypothetical "blunt" products are marked with asterisks (*). (b) Schematic representation of a non-propagative $Z_{1212}^{Fn}$-Tel interaction.

## 3.3 Discussion

Many previous studies have utilised the scaffolding properties of (V)-type Ig domains to achieve molecular recognition, most notably antibody derivatives in the form of fragments, chimeric fusions or single domains (Holliger and Hudson, 2005). To the best of our knowledge, the results herein described are the first instance of non-native RGD motif exhibition in an (I)-type Ig fold. Also, the genetic encoding and display of FnIII 10 from fibronectin has not previously been explored in a self-assembling system.

The generation of Tel mutants displaying dual RGD motifs at the N- or C-termini resulted in reduced protein yield. The reason for this is unclear, since the addition of small polypeptides is unlikely to imbue toxic characteristics on the proteins, nor dramatically increase demand on the translational machinery of host cells. It seemed most likely that changing from the pETM-11 to pETM-13 expression vector was responsible for the decrease in protein yield. Therefore, a second generation of RGD-modified constructs were encoded in the pETM-11 vector. However, the issue of decreased protein yield persisted and in this case the problem was confounded by the presence of an expression artefact. It is plausible that the unknown species was the product of inefficient termination of transcription, meaning that additional sequence was transcribed after the stop codon and subsequently translated into a $His_6$-tagged recombinant protein of higher residue number and composition than intended. This problem may be resolvable by the incorporation of multiple stop codons at the 3'-end of constructs, resulting in accurate termination of transcription and increased yield of $Tel^{C\text{-}RGD}11$ and $Tel^{C\text{-}RGE}11$. The reduced yield of constructs encoded in the pETM-13 vector may be due

to the chance incorporation of rare codons during mutagenesis, which can cause mRNA instability and inhibition of heterologous protein synthesis (Gustafsson *et al.*, 2004). Taken together, the issues encountered when modifying the N- and C-termini of Tel were surprising, since it was envisioned that these sites were the most likely to support ZT functionalisation due to their accessibility within the Z1Z2-Tel building block, and lack of contribution to protein-protein interfaces. Since other constructs were generated in parallel that showed greater promise, the insertion of additional stop codons or screening for rare codons from *E. coli* were not accomplished. However, the constructs that were successfully fabricated and expressed could be optimised for utilisation in future endeavours.

Insertion of an exogenous RGD sequence in the Z1 CD-loop was well tolerated; $Z_{1212}^{RGD}$ was expressed at high yield, an important factor when evaluating the applicability of recombinant proteins for biotechnological applications. As demonstrated by analytical SEC and SAXS analysis, CD-loop grafted chimeras were structurally stable and capable of cooperative interaction with Tel. By inducing nanofibre formation with $Z_{1212}^{RGD}$, a novel supramolecular assembly was generated with defined nanotopographical distribution of a bioactive moiety, termed $ZT^{RGD}$. It was envisioned that RGD display in the flexible and exposed CD loop, as opposed to a linear conformation at the termini of Tel, would increase the avidity of the motif for cell surface integrin recognition.

Fusion of FnIII 10 at the C-terminus of Z2 did not inhibit the association of $Z1Z2^{Fn}$ with Tel to generate a palindromic complex. In the context of $Z_{1212}^{Fn}$, the additional domain did not decrease protein yield and the monomeric nature of the tandem was retained. Indeed, the titin filament is composed of both Ig and FnIII domains that share structural homology (Labeit and Kolmerer, 1995), thus structural

tolerance and correct folding might be expected for titin-fibronectin chimeras. Encouraged by the retention of the Z1Z2-Tel interface when FnIII 10 is fused, $Z_{1212}^{Fn}$ was induced to interact propagatively with Tel. Native PAGE of the assembly mixture suggests that supramolecular structures are formed, confirming that C-terminal fusion of a globular domain does not block the interaction of $Z_{1212}$ with Tel. These observations were highly encouraging since the exhibition of folded protein modules in the ZT system is a tantalising prospect that may allow for the incorporation of functionalities previously unobtainable with peptidomimetics.

An obvious limitation of the findings described herein was the inability to consistently observe nanofibre morphology by TEM. Although *wt* ZT, $ZT^{RGD}$ and $ZT^{RGE}$ were successfully visualised on occasion, the results were not reproducible for different batches of nanofibre preparations despite employing a consistent assembly protocol. Indeed, each new preparation was routinely assessed by native PAGE to verify the formation of supramolecular assemblies. It could be that larger nanofibres were not always formed and that prematurely-terminated assemblies, which might be indistinguishable from larger assemblies by native PAGE, were not easily discernible on TEM grids. The reason for a potential premature termination of nanofibre polymerisation is unclear. One hypothesis is that the assembly process is highly sensitive to environmental factors, such as temperature and agitation, which were not rigorously controlled batch-to-batch. Future undertakings will aim to control such factors more carefully to observe their effects on nanofibre morphology.

# Chapter 4

# Evaluating the effectiveness of integrin-binding sites in ZT variants and their ability to induce mesenchymal stem cell chondrogenesis

## 4.1 Introduction

### *4.1.1 Osteoarthritis*

The pathophysiology of osteoarthritis (OA) is typified by loss of hyaline articular cartilage in joints causing synovial inflammation, chronic pain and debilitation. Joint degeneration progressively worsens due to the limited regenerative potential of articular cartilage, a bradytrophic tissue, thus accelerating disease progression (Buckwalter and Mankin, 1998). As the most common joint-based affliction, affecting an estimated 10% of over 60s worldwide, OA contributes significantly to the global health burden (Pereira *et al.*, 2011). Prevalence of OA is predicted to increase due to the ageing population and obesity epidemic, which are leading causation factors of OA. Although anti-inflammatory drugs are available to treat the symptoms of OA they do not prevent disease progression(Csaki *et al.*, 2008). Total joint replacement and autologous chondrocyte implantation (ACI) are the most successful treatments for severe OA. However, increased prevalence of the disease and morbidities associated with invasive surgical procedures required by current therapies has highlighted the need for alternative, cell-based approaches (Diekman and Guilak, 2013).

### *4.1.2 Mesenchymal stem cells in cartilage tissue engineering*

The *in vitro* propagation of autologously-derived chondrocytes for cartilage regeneration is an attractive strategy. However, chondrocytes explanted from OA sufferers often have a limited proliferative capacity and poor functional competence. Additionally, chondrocytes from healthy joints grown in high-density cultures are prone to redifferentiation after several passages, subsequent to which the cells do not produce high quality articular cartilage (Schulze-Tanzil *et al.*, 2002). Due to their chondrogenic potential, MSCs have been utilised extensively in cartilage tissue engineering strategies (Song *et al.*, 2004; Vinatier *et al.*, 2009). However, the use of autologously-derived MSCs for cartilage repair is fraught with challenges, such as the limited proliferative capacity of MSCs obtained from OA sufferers (Murphy *et al.*, 2002), production of a lasting hyaline chondrocyte-like phenotype *in vitro* and promoting the deposition of mechanically sound neocartilage (Diekman and Guilak, 2013). A pivotal problem in both *in vitro* and *in vivo* differentiation of MSCs to hyaline chondrocytes is their tendency to redifferentiate to a fibrocartilage or hypertrophic phenotype reminiscent of bone formation (Vinardell *et al.*, 2012). The fact that previous culture conditions and inductive agents did not cater specifically for permanent hyaline differentiation may be to blame for these shortcomings. For example, relying solely on the powerful chondroinductive mediator TGF-β3 can facilitate hypertrophic differentiation of MSCs (Dickhut *et al.*, 2009).

Significant progress has been made in the development of engineered constructs for regeneration of damaged cartilage using MSCs. This next generation approach to ACI attempts to create an implantable scaffold containing newly differentiated chondrocytes from autologous bone marrow-derived MSCs (Csaki *et al.*, 2008). Previous methods of cartilage tissue engineering using MSCs have

employed the use of recombinant growth factors, such as TGF-β family members, incorporated into (Bian *et al.*, 2011) or immobilised onto scaffolds (Re'em *et al.*, 2012). Similar initiatives have tested the potential of a multitude of scaffolds to induce chondrogenesis, the success of which is often attributed to the functionalisation of platforms with short mimetic peptides, collagens and glycosaminoglycans (Table 8). Popular choices of scaffold to create a three-dimensional microenvironment for cell culture are self-assembling polymer and peptide hydrogels. Whilst polymer hydrogels have been successfully utilised for cartilage tissue engineering (Salinas and Anseth, 2009; Ogawa *et al.*, 2012; Re'em *et al.*, 2012), peptide hydrogels offer distinct advantages. These include greater biocompatibility and degradability for *in vivo* use due to the nature of the components. Also, the nanomechanical properties of the gels can be tuned by varying the methods of gelation, a process which does not necessitate the use of photopolymerisation or redox reactions required for the cross-linking of many polymer-based hydrogels (Adams and Topham, 2010). Indeed, hydrogels formed from glycine-containing and phenylalanine-containing dipeptides linked to fluorenylmethoxycarbonyl at physiological pH have been shown to support the proliferation of bovine chondrocytes in two and three dimensions (Jayawarna *et al.*, 2006). Similarly, peptide hydrogels have been utilised to support the chondrogenic differentiation of bone marrow stromal cells by TGF-β1 induction (Kopesky *et al.*, 2011).

**Table 8.** Example materials and functionalities used to promote chondrogenic differentiation of MSCs *in vitro*

| Scaffold | Functional moieties | Reference |
|---|---|---|
| Poly(ethylene glycol) (PEG) | Decorin motif (KLER) | (Salinas and Anseth, 2009) |
| None – added directly to medium | Bone morphogenetic protein 2 peptide | (Renner *et al.*, 2012) |
| Macroporous alginate | Fibronectin RGD motif | (Re'em *et al.*, 2010)<br>(Xu *et al.*, 2008) |
| PEG hydrogels | Fibronectin RGD motif | (Salinas and Anseth, 2008) |
| Polyhydroxyalkanoate (PHA) | PHA granule binding protein fused with fibronectin RGD peptide | (You *et al.*, 2011) |
| Polystyrene | Photoreactive polymer derivatives | (Guo *et al.*, 2008) |
| Poly(ethylene oxide) diacrylate (PEODA) | Collagen mimetic peptides | (Lee *et al.*, 2008) |
| Peptide-based hydrogels | Peptides with varying electrostatic charges | (Sinthuvanich *et al.*, 2012) |
| Hyaluronic acid hydrogel | Hyaluronic acid density | (Bian *et al.*, 2013)<br>(Chung and Burdick, 2009) |
| Porous poly(ε-caprolactone) (PCL) scaffold | None – provides a permeable and mechanically favourable three-dimensional matrix | (Li *et al.*, 2005) |
| Poly(l-lactic acid) nanofibres in bioreactors | Favourable three-dimensional matrix – mimics ECM | (Janjanin *et al.*, 2008) |
| Silk protein/fibroin scaffolds | Silk fibres ± fibronectin RGD motif | (Meinel *et al.*, 2004) |
| Poly(vinyl alcohol)-methacrylate nanofibres | Chondroitin sulphate polysaccharides | (Coburn *et al.*, 2012) |
| Injectable hydrogels | Dextran-tyramine and heparin-tyramine conjugates | (Jin *et al.*, 2011) |
| Chitosan scaffold | Collagen type II | (Ragetly *et al.*, 2010) |

Whilst such constructs can induce the differentiation of MSCs to a chondrocyte-like phenotype, there are considerable limitations to be overcome. For example, the mechanical properties of cartilage formed in such constructs are different from those of natural or *in vitro* chondrocyte-derived cartilage. The

compressive modulus of MSC-derived cartilage from engineered scaffolds is significantly less than that of natural origin (Huang *et al.*, 2009, 2010). Also, explanted hyaline chondrocytes incorporated into a hydrogel matrix form more high quality cartilage compared to MSC-derived chondrocytes (Erickson *et al.*, 2009). As mentioned previously, a major inadequacy of many culture systems is their inability to promote MSC differentiation to articular chondrocytes and a tendency for implanted cells to dedifferentiate *in vivo*. This may be because the amount of inductive factor is critical for correct differentiation. For example, it has been show that increasing the RGD motif density of agarose hydrogels negatively affects articular differentiation of chondrocytes, as demonstrated by a decrease in collagen type II, and promotes dedifferentiation (Schuh *et al.*, 2012). However, it is challenging to control top-down functionalisation at the molecular level by saturating, coating, or mixing substrates with compounds/motifs, as the density and nanotopographical distribution of functional moieties are difficult to assess and reproduce.

### *4.1.3 Aims*

Herein, the accessibility and bioactivity of integrin-binding motifs in $ZT^{RGD}$ and $ZT^{Fn}$ were tested *in vitro* using the murine MSC (mMSC) D1 line. The ability of functionalised nanofibres to promote mMSC adhesion was investigated and cell morphology characterised. Further, the chondroinductive potential of $ZT^{RGD}$ was explored under serum-free culture conditions.

## 4.2 Results

### *4.2.1 Effect of functionalised nanofibres on murine MSC adhesion and spreading*

Since $Z_{1212}$ and Tel were produced in *E. coli*, the presence of bacteriotoxins and contaminant proteins in the assembly mixture could not be discounted. Also, it was hypothesised that a small pool of unpolymerised $Z_{1212}$ would remain following nanofibre assembly and that these molecules may cross cell membranes. To ensure that $Z_{1212}$ was not cytotoxic, mMSCs were cultured for two days in the presence of $Z_{1212}$ at concentrations ranging from 0.01 – 1 mg/mL. A colorimetric assay was used to assess metabolic activity and infer cell viability. $Z_{1212}$ did not cause a significant change in cell viability at any of the tested concentrations (Figure 24).

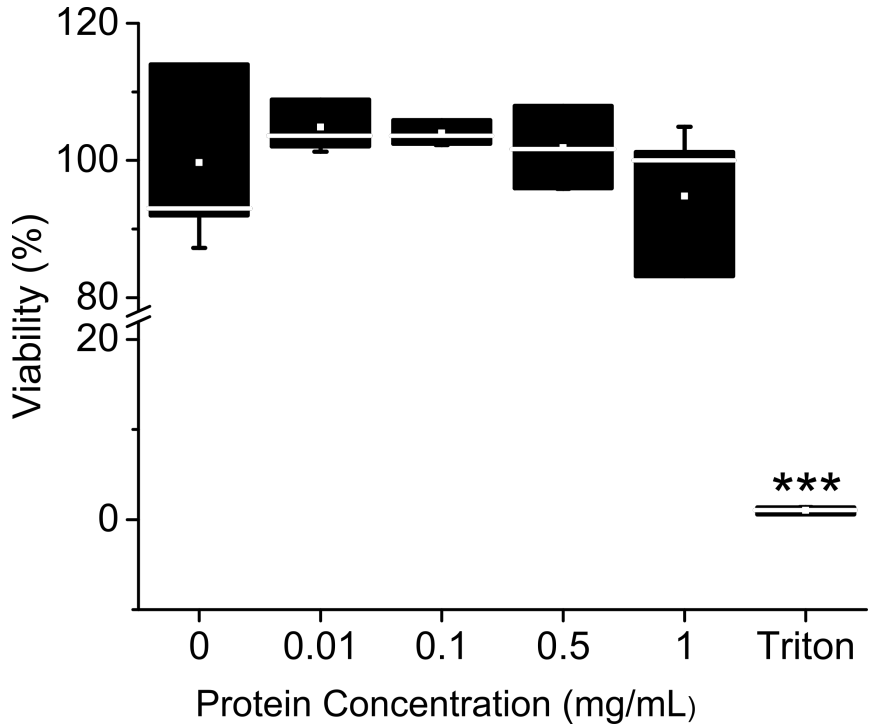


**Figure 24. Evaluation of $Z_{1212}$ cytotoxicity on murine MSCs.** The effect of unpolymerised $Z_{1212}$ at concentrations ranging from 0.01-1 mg/mL was assessed after 3 days of exposure to MSCs in monolayer culture. Viability was measured as described (Section 2.8) and is expressed relative to the untreated control (100%) and 0.1% [v/v] Triton X-100 was included as a positive control. Statistically significant differences were determined by two sample t-tests. Box plots indicate the median (*horizontal line*), mean (*square*), 25$^{th}$ and 75$^{th}$ percentile values (*box ends*) and ± SD (*error bars*; *n* = 3).

To validate the bioactivity of the grafted RGD motif in the context of the Z1 CD-loop and its accessibility for cell-surface integrin binding, mMSCs were seeded on a non-tissue culture treated (TCT) polystyrene surface coated with $ZT^{RGD}$ and control $ZT^{RGE}$ under serum-free conditions. Cells were maintained in TCT vessels before being serum-starved for 24 hours post-seeding (Figure 25a). Cells were maintained in serum-free medium to discount the potential adhesive effects of serum components that may passively adsorb to the hydrophobic polystyrene surface and mask the contribution of ZT nanofibres to cell attachment. $ZT^{Fn}$ was also tested as a comparison between the engineered and FnIII 10-native RGD motifs in the context of the ZT system. A clear adhesive effect of $ZT^{RGD}$ and $ZT^{Fn}$ on mMSCs could be observed 2 hours post-seeding compared to control $ZT^{RGE}$ (Figure 25b).

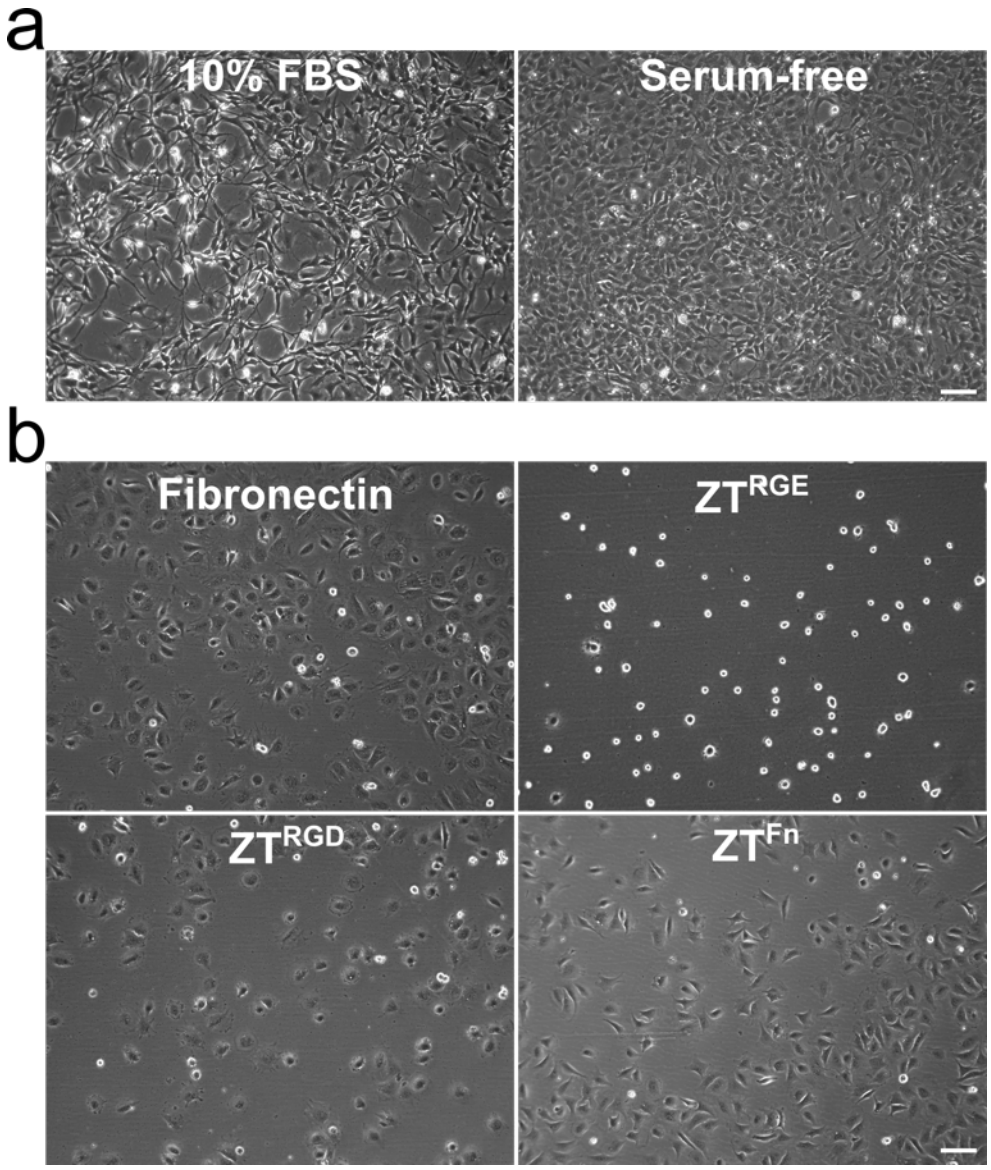


**Figure 25. Murine MSC adhesion to functionalised nanofibres.** (a) Typical morphology of cells plated on TCT plastic in 10% FBS (*left*) and following 24 hours under serum-free conditions. (b) Representative phase contrast micrographs of mMSCs 2 hours post-seeding on control fibronectin and nanofibre variants adsorbed at 10 µg/mL on non-TCT polystyrene. Scale bars = 100 µm.

mMSC attachment and spreading on $ZT^{RGE}$, $ZT^{RGD}$ and $ZT^{Fn}$ was quantified at a range of coating concentrations. Cell attachment was expressed as a percentage of adherence to control human plasma fibronectin (Figure 26a). Compared to non-TCT polystyrene surfaces, both $ZT^{RGD}$ and $ZT^{Fn}$ promoted cell adhesion in a concentration-dependent manner. Control $ZT^{RGE}$ neither promoted nor inhibited cell

attachment. The average cell area was quantified for all conditions tested and was again found to increase relative to the coating concentration of $ZT^{RGD}$ and $ZT^{Fn}$ (Figure 26b). Cell area was significantly increased when cells were cultured on $ZT^{RGD}$ or $ZT^{Fn}$ adsorbed at 1 and 10 μg/mL compared to untreated polystyrene.

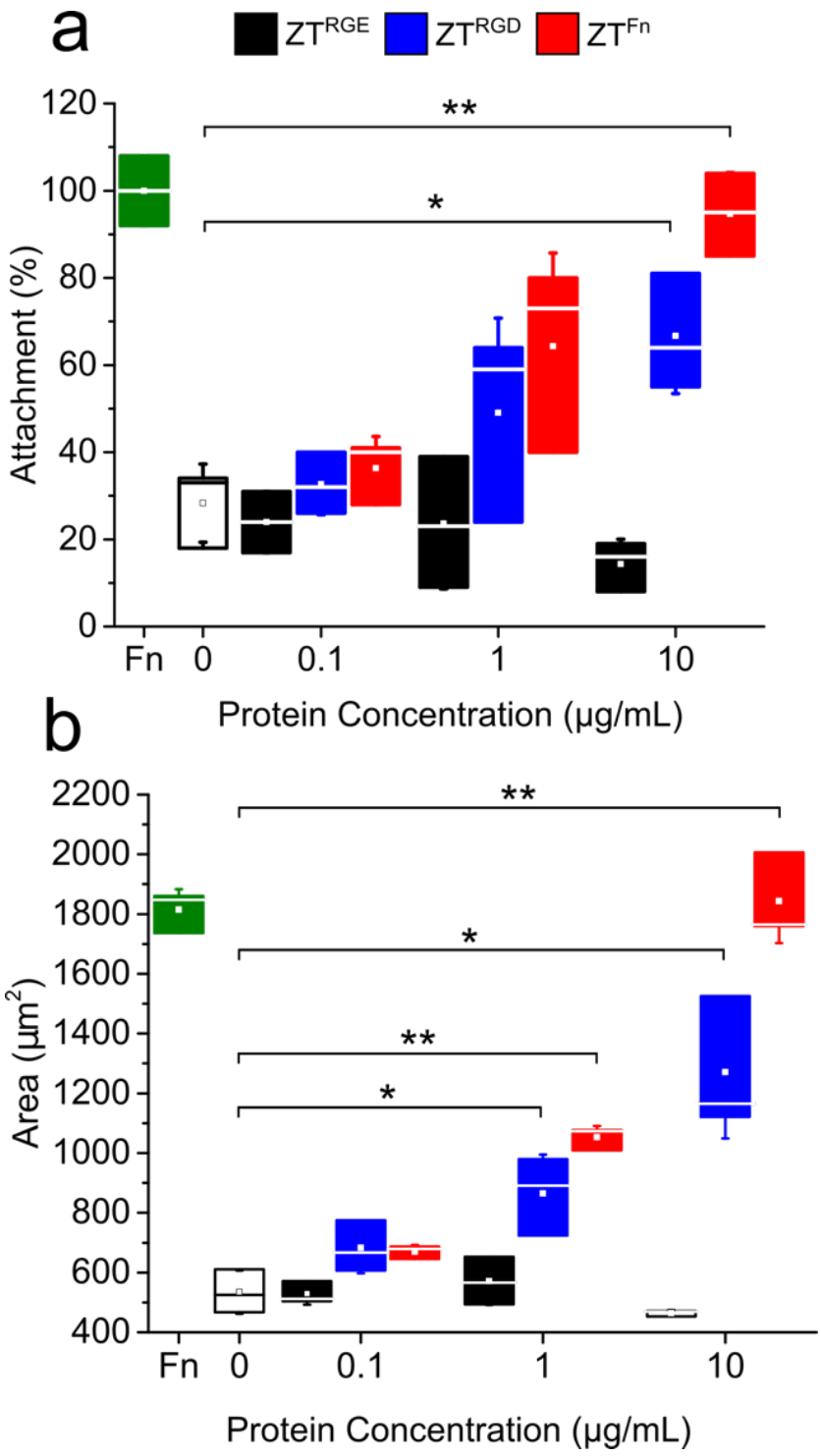


**Figure 26. Effect of functionalised ZT nanofibres on murine MSC adhesion and spreading.** Box plots show the effects of $ZT^{RGE}$, $ZT^{RGD}$ and $ZT^{Fn}$ at coating concentrations ranging from 0.1-10 µg/mL on mMSC attachment (a) and spreading (b) 2 hours post-seeding at a density of $1 \times 10^4$ cells/cm$^2$. Cell attachment is expressed as a percentage of the positive control (fibronectin at 10 µg/mL; *green boxes*) that was taken as 100%. Statistical significance (two sample t-test) is in reference to a non-treated surface (*white*). Box plots indicate the median (*horizontal line*), mean (*square*), 25$^{th}$ and 75$^{th}$ percentile values (*box ends*) and ± SD (*error bars*; $n$ = 3).

In order to explore the specificity of the grafted motif in $ZT^{RGD}$, a competitive inhibition assay was conducted using a linear integrin-binding pentapeptide (GRGDS). mMSCs were pre-incubated with peptide at increasing concentrations and seeded on $ZT^{RGD}$, $ZT^{Fn}$ or control human plasma fibronectin adsorbed at 10 μg/mL. An inactive GRGES peptide at the highest tested concentration was used as a negative control and cell attachment and spreading were quantified (Figure 27). The addition of GRGDS peptide resulted in a dose-dependent decrease in cell adhesion to both $ZT^{RGD}$ and $ZT^{Fn}$ (Figure 27b,c). However, peptide inhibition had a more pronounced effect on cell adhesion to $ZT^{RGD}$ compared to $ZT^{Fn}$, where attachment was less affected at the maximum concentration of 250 μM. Cell spreading followed the same trend as attachment, with average cell area decreasing more on $ZT^{RGD}$ than $ZT^{Fn}$ with increasing peptide concentration (Figure 27b,c). Interestingly, the GRGDS peptide did not significantly decrease cell attachment or spreading on fibronectin at the concentrations tested (Figure 27a,d).

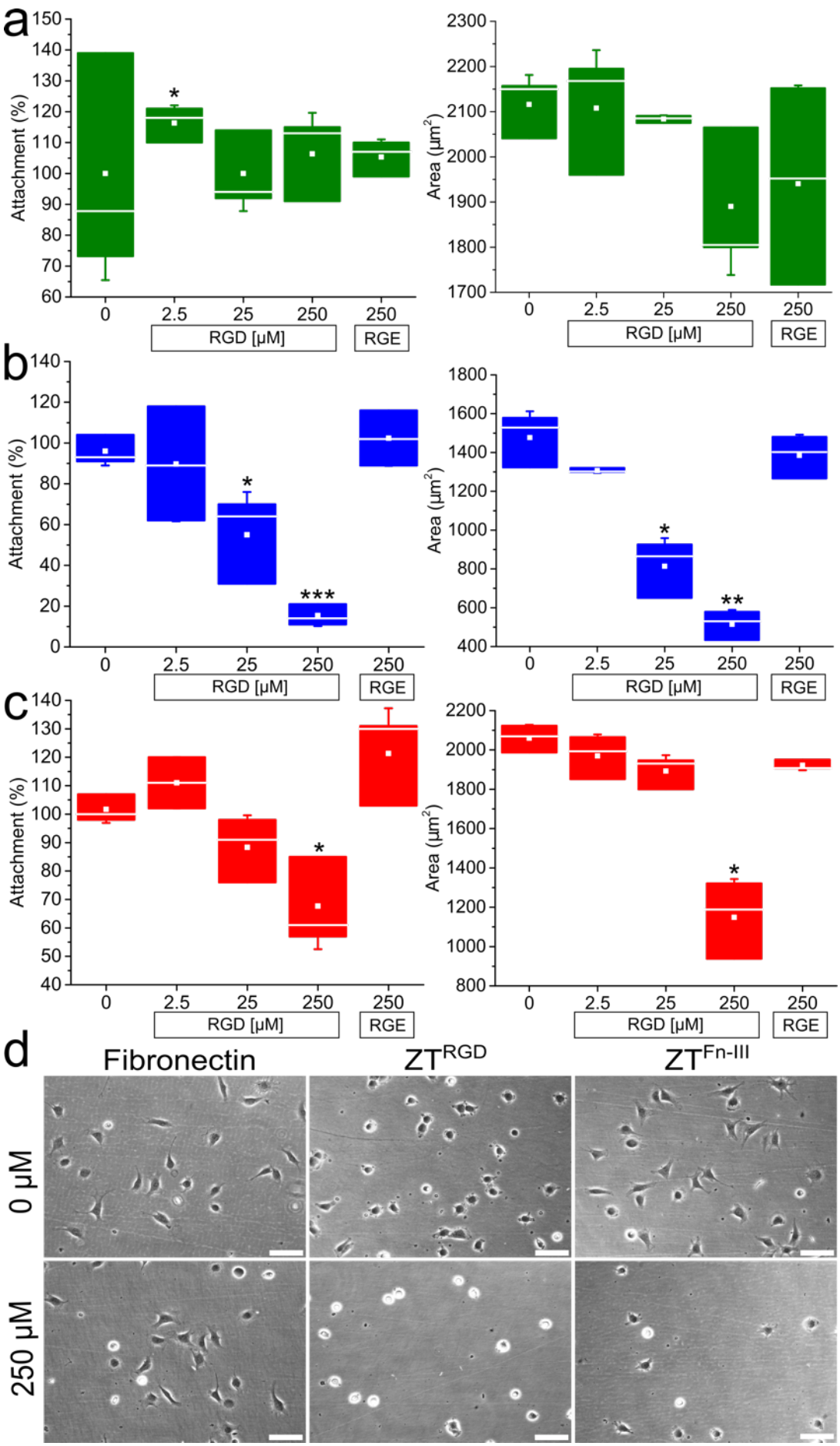
a
Attachment (%)
Area (μm²)
RGD [μM]
RGE
b
Attachment (%)
Area (μm²)
RGD [μM]
RGE
c
Attachment (%)
Area (μm²)
RGD [μM]
RGE
d
Fibronectin
ZT^RGD
ZT^Fn-III
0 μM
250 μM

**Figure 27. Effect of integrin-blocking RGD pentapeptide on murine MSC attachment to functionalised ZT nanofibres.** Box plots show cell attachment and spreading 2 hours post-seeding in the presence of GRGDS peptide at concentrations ranging from 2.5-250 μM. Control GRGES peptide was used at a concentration of 250 μM. mMSCs were seeded at a density of $1 \times 10^4$ cells/cm$^2$ on non-TCT polystyrene precoated with fibronectin (a), $ZT^{RGD}$ (b) or $ZT^{Fn}$ (c) at 10 μg/mL. Cell attachment is expressed as a percentage of the positive control (fibronectin at 10 μg/mL in the absence of peptide), which was taken as 100%. Statistical significance (two sample t-test) is in reference to untreated (0 μM) groups. Box plots indicate the median (*horizontal line*), mean (*square*), 25$^{th}$ and 75$^{th}$ percentile values (*box ends*) and ± SD (*error bars*; *n* = 3). (d) Representative phase contrast micrographs of cells on different substrates at 0 μM and 250 μM GRGDS peptide. Scale bars = 100 μm.

### *4.2.2 Influence of the substratum on murine MSC morphology*

Quantitative shape descriptors can offer important information on how cells engage with a substrate and the phenotypic changes this may induce. However, subtle differences in cell morphology may remain ambiguous by visual inspection alone, prompting the need for quantitative analysis. In this study, cell area, circularity, aspect ratio (AR) and solidity were investigated on different substrates. Surface area affords an unambiguous gauge on the degree of cell spreading on a given substrate. The area to perimeter ratio, termed circularity, provides a measure of divergence from a circular shape (where a perfect circle = 1) and is thus strongly influenced by cellular projections that increase the perimeter (Figure 28a,b). The AR is defined as the ratio of the height to the width of a profiles' fitted ellipse, thus both a square and a circle would have an AR of 1 (Figure 28c). Solidity describes the semblance of a shapes' area with its convex area. The convex area is defined as the area of the convex hull of a shape, meaning that circular shapes will have higher solidity (Figure 28d). Since circularity describes the local shape of a cell, AR and solidity are important parameters for the assessment of global shape in terms of symmetric or asymmetric cell spreading (Siani *et al.*, 2012; Li *et al.*, 2015). Thus, a

combination of shape descriptors can provide a more complete understanding of the effect of a substrate on cell morphology.

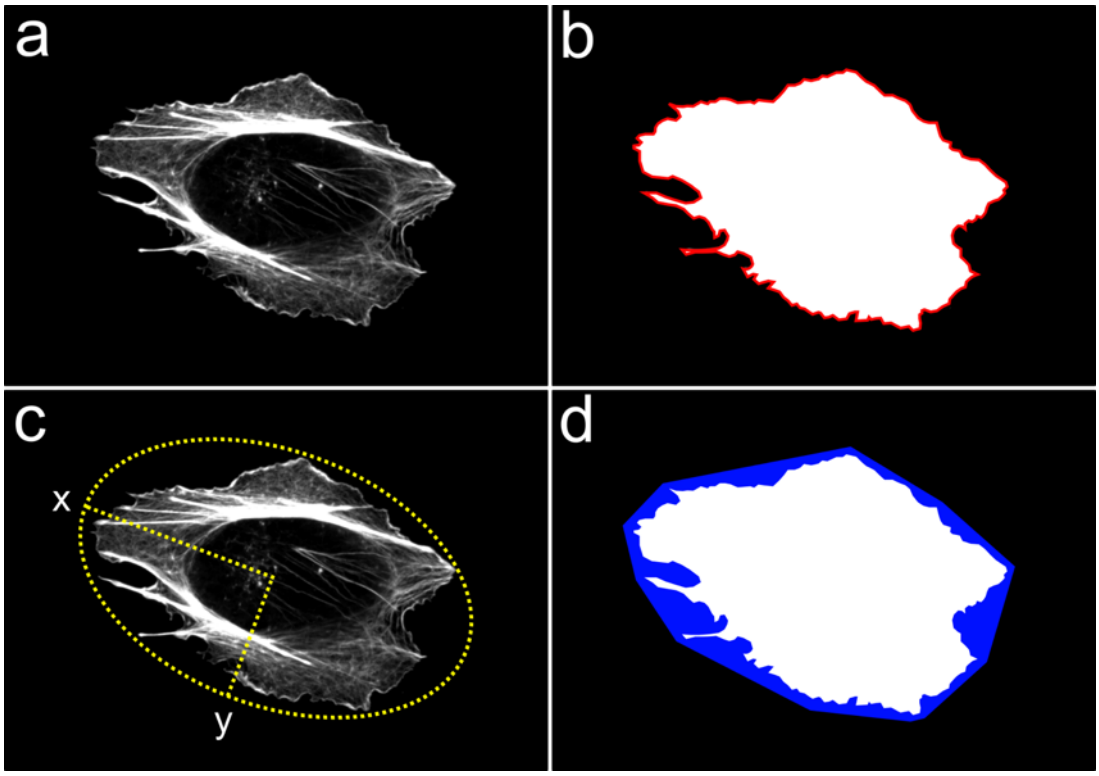


**Figure 28. Quantitative shape descriptors.** The panels show how different parameters are calculated from cell profiles. (a) Immunofluorescence micrograph of a cell stained for F-actin. (b) The cell perimeter (*red line*) can be used to calculate surface area (*white*) and both values are used to calculate circularity. (c) The aspect ratio is defined as the ratio of the major (*x*) and minor (*y*) axis of a shapes best fitted ellipse (*yellow dashed line*). (d) Solidity is defined as the ratio of a shape's area (*white*) and convex hull area (*blue*).

The area, circularity, AR and solidity of mMSCs cultured on $ZT^{RGD}$, $ZT^{Fn}$ or fibronectin were quantified following two hours of attachment. Here, all shape descriptors were calculated using ImageJ software from manually rendered cell profiles. Average cell area was found to be significantly decreased on $ZT^{RGD}$ compared to $ZT^{Fn}$ (Figure 29a). Circularity, AR and solidity were also significantly different for cells attached to $ZT^{RGD}$ compared to $ZT^{Fn}$ and fibronectin (Figure 29b,c,d). However, no significant differences were observed between cells cultured on $ZT^{Fn}$ or fibronectin for any of the parameters investigated.

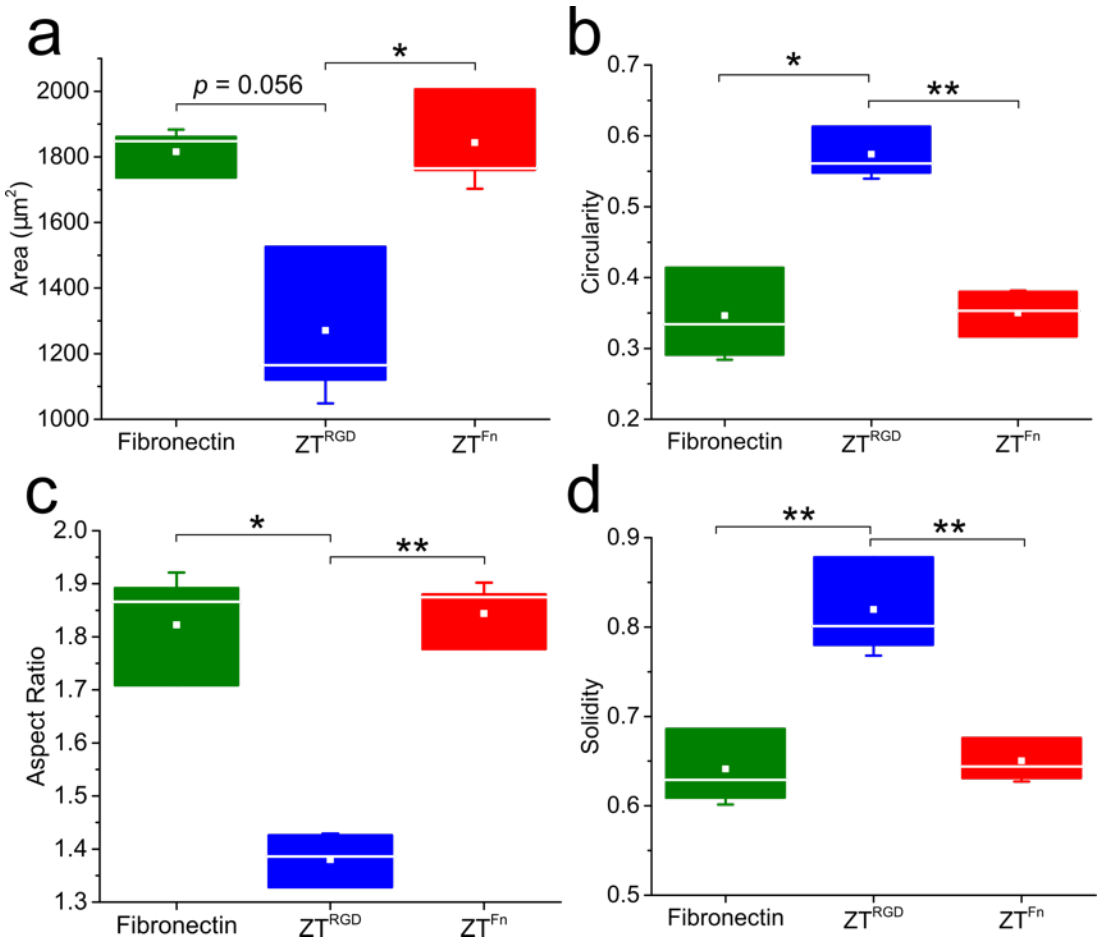


**Figure 29. Effect of functionalised ZT nanofibres on murine MSC shape.** Cell shape was quantified in terms of average cell area (a), circularity (b), aspect ratio (c) and solidity (d) when cultured for 2 hours on fibronectin, $ZT^{RGD}$ or $ZT^{Fn}$ at coating concentrations of 10 μg/mL. Statistically significant differences were determined by two sample t-tests. Box plots indicate the median (*horizontal line*), mean (*square*), 25$^{th}$ and 75$^{th}$ percentile values (*box ends*) and ± SD (*error bars*; *n* = 3).

The higher circularity and solidity of mMSCs cultured on $ZT^{RGD}$, combined with an average AR closer to 1 than cells cultured on fibronectin or $ZT^{Fn}$, were consistent with an approximately symmetric cell spreading and circular shape. The higher than average AR and lower solidity of mMSCs cultured on $ZT^{Fn}$ or fibronectin indicated anisotropic cell spreading on these substrates. Frequency distributions of shape descriptors from all conditions tested and individual cells analysed are show in Figure 30. Parameters derived from the distributions are detailed in Table 9. It was noted that almost all distributions were skewed to a

greater or lesser extent, suggesting that culture on fibronectin, $ZT^{RGD}$ and $ZT^{Fn}$ directly influenced cell morphology.

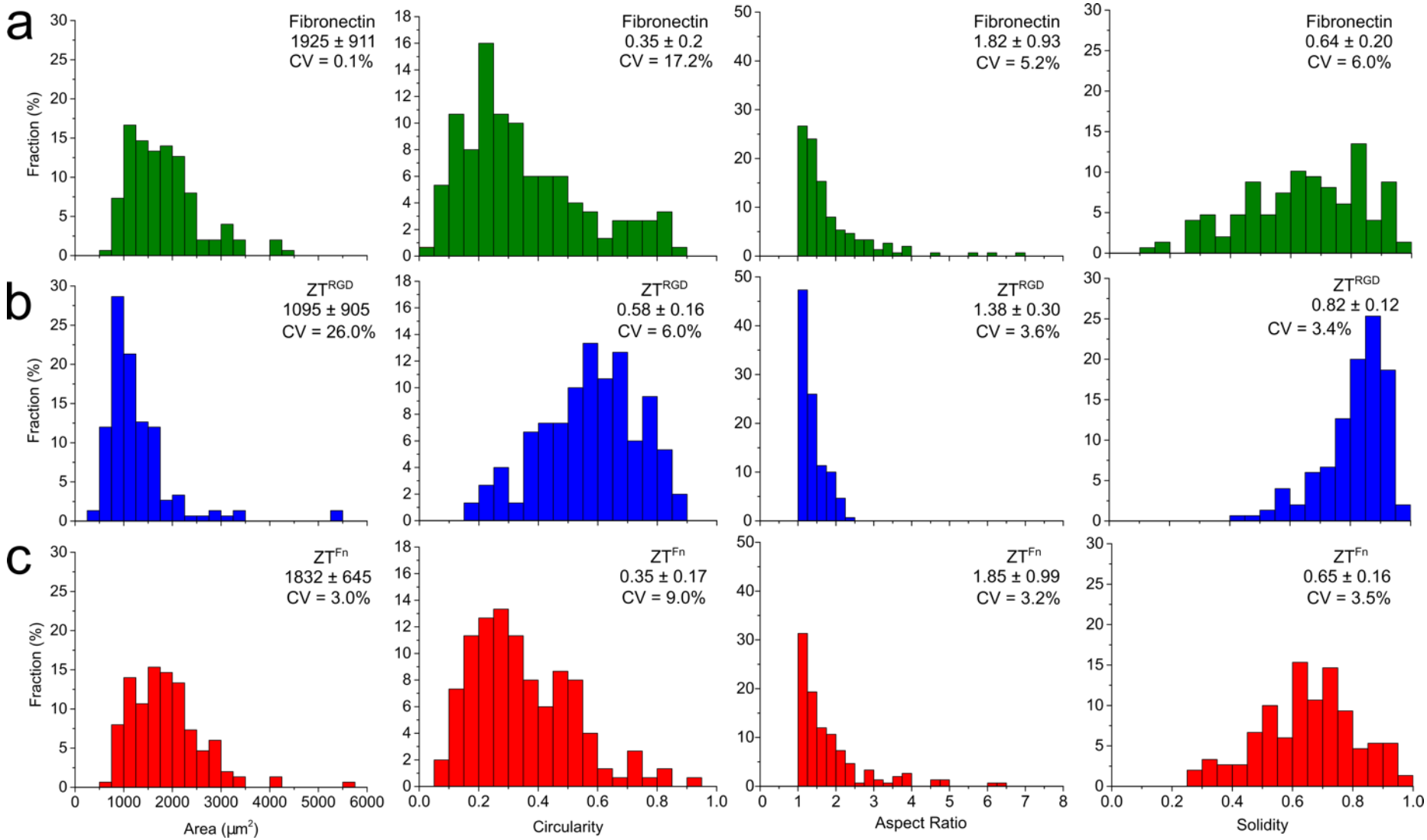
a
Fibronectin
1925 ± 911
CV = 0.1%
Fibronectin
0.35 ± 0.2
CV = 17.2%
Fibronectin
1.82 ± 0.93
CV = 5.2%
Fibronectin
0.64 ± 0.20
CV = 6.0%
b
ZT^RGD
1095 ± 905
CV = 26.0%
ZT^RGD
0.58 ± 0.16
CV = 6.0%
ZT^RGD
1.38 ± 0.30
CV = 3.6%
ZT^RGD
0.82 ± 0.12
CV = 3.4%
c
ZT^Fn
1832 ± 645
CV = 3.0%
ZT^Fn
0.35 ± 0.17
CV = 9.0%
ZT^Fn
1.85 ± 0.99
CV = 3.2%
ZT^Fn
0.65 ± 0.16
CV = 3.5%
Fraction (%)
Area (μm²)
Circularity
Aspect Ratio
Solidity

**Figure 30. Frequency distributions of murine MSC shape parameters for different substrates.** Histograms show the distribution of cell area, circularity, aspect ratio and solidity when cultured on fibronectin (a), $ZT^{RGD}$ (b) and $ZT^{Fn}$ (c). The mean values are indicated with standard deviations (*n* = 150). The coefficient of variation (CV) between biological replicates (*n* = 3) is also stated.

**Table 9.** Morphological parameters for murine MSCs cultured on different substrates derived from all cells analysed.

| | **Median** | **Mean (SD)** | **Skewness** |
|---|---|---|---|
| Area ($\mu m^2$) | | | |
| Fibronectin | 1762 | 1925 (911) | 1.30 |
| $ZT^{RGD}$ | 907 | 1095 (905) | 4.59 |
| $ZT^{Fn}$ | 1763 | 1832 (645) | 1.16 |
| Circularity | | | |
| Fibronectin | 0.30 | 0.35 (0.20) | 0.83 |
| $ZT^{RGD}$ | 0.59 | 0.58 (0.16) | -0.36 |
| $ZT^{Fn}$ | 0.32 | 0.35 (0.17) | 0.82 |
| Aspect ratio | | | |
| Fibronectin | 1.50 | 1.82 (0.93) | 2.67 |
| $ZT^{RGD}$ | 1.26 | 1.38 (0.30) | 1.15 |
| $ZT^{Fn}$ | 1.48 | 1.85 (0.99) | 2.27 |
| Solidity | | | |
| Fibronectin | 0.66 | 0.64 (0.20) | -0.41 |
| $ZT^{RGD}$ | 0.84 | 0.82 (0.12) | -1.19 |
| $ZT^{Fn}$ | 0.66 | 0.65 (0.16) | -0.23 |

### *4.2.3 Influence of the substratum on focal adhesion formation and cytoskeletal organisation*

To further investigate mMSC attachment to functionalised ZT nanofibres, cells were stained for filamentous actin and paxillin (Figure 31). Paxillin is a scaffolding component of focal adhesion complexes, interacting with multiple binding partners to transduce integrin-mediated signalling events to changes in cytoskeletal organisation (Turner, 2000). Interestingly, cells grown on fibronectin, $ZT^{RGD}$ and $ZT^{Fn}$ all contained focal adhesions, but exhibited a distinctive morphology when cultured on $ZT^{RGD}$. mMSC adhesion to fibronectin and $ZT^{Fn}$ typically resulted in a heterogeneous assortment of morphologies with distinct stress fibre networks. Cells cultured on $ZT^{RGD}$ rarely displayed defined stress fibres and the majority of phalloidin staining was at the cell periphery, highlighting a rounded phenotype defined by lamellipodia-like projections. Cells were also stained for zyxin, a zinc-binding phosphoprotein recruited to focal plaques upon integrin engagement to interact with α-actinin and other components of the focal adhesion complex (Wang and Gilmore, 2003). Zyxin is a marker of mature focal adhesions and is not observed in nascent focal plaques (Zaidel-Bar *et al.*, 2003). Analysis by immunofluorescence revealed that mMSCs on all substrates possessed focal complexes containing zyxin (Figure 32), thus the engineered motif of $ZT^{RGD}$ is capable of supporting focal adhesion maturation. However, cell morphology and cytoskeletal arrangement was uniquely influenced by $ZT^{RGD}$, therefore, mMSCs were stained for integrins to discern alterations in heterodimer expression on this substrate.

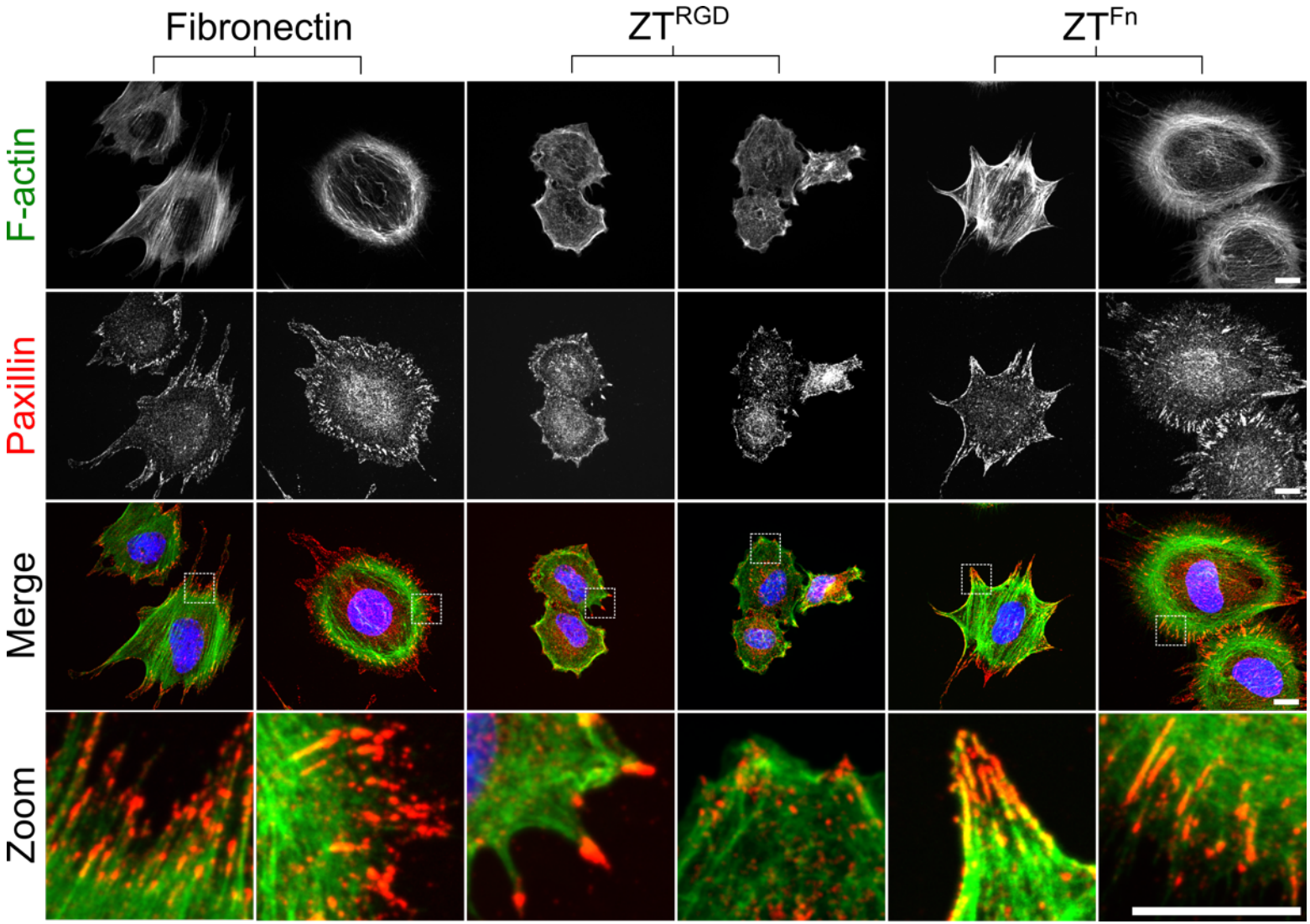


**Figure 31. Focal adhesion formation and cytoskeletal organisation in murine MSCs cultured on different substrates.** Immunofluorescence micrographs show representative z-series projections of cells 2 hours post-seeding on fibronectin, $ZT^{Fn}$ or $ZT^{RGD}$. Cells were stained for F-actin (*green*), paxillin (*red*) and DAPI (*blue*). Zoomed views of the boxed areas in the upper panels are shown below to highlight focal adhesions and cytoskeletal structures. Scale bars = 10 μm.

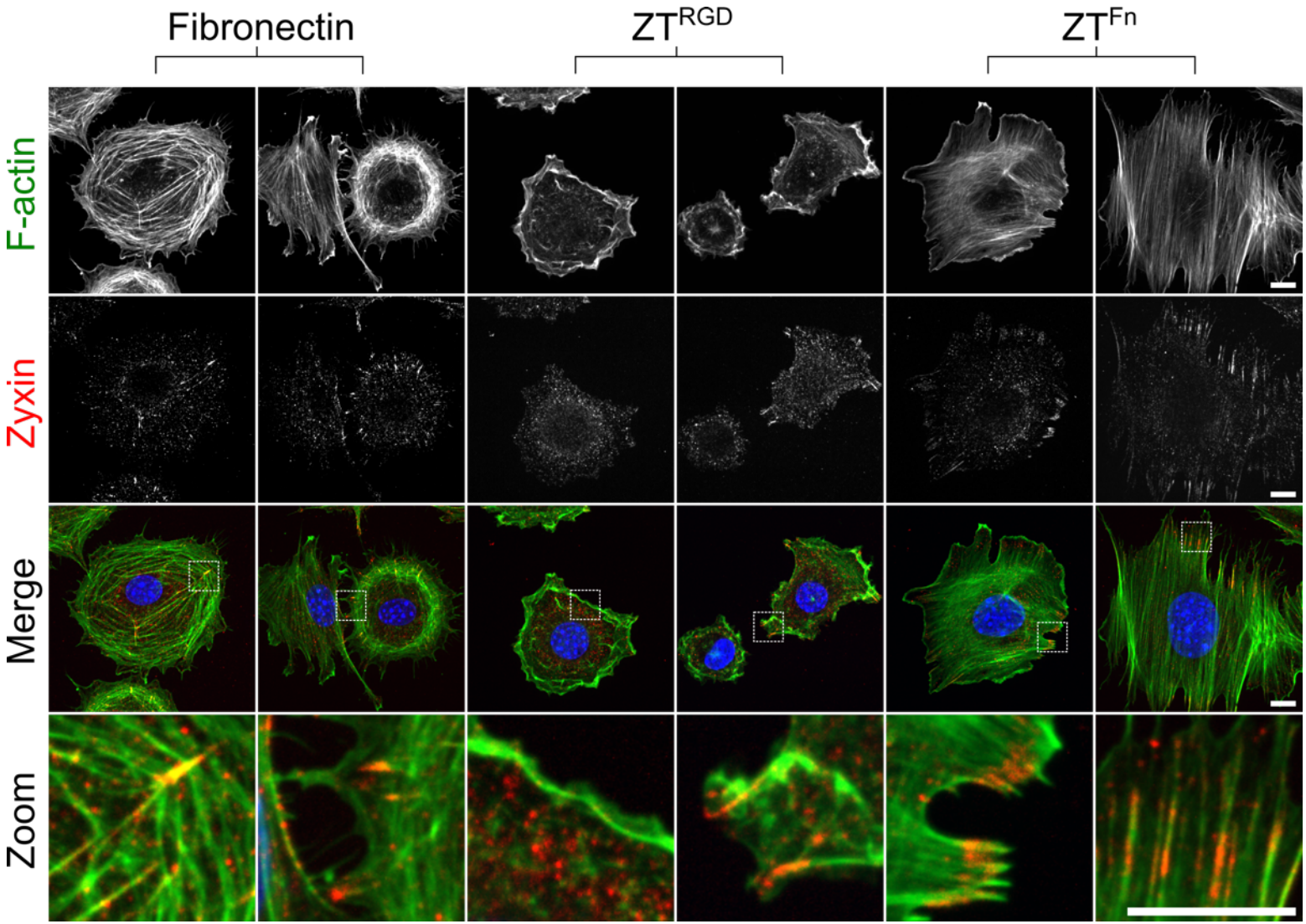


**Figure 32. Zyxin recruitment to focal adhesions in murine MSCs cultured on different substrates.** Immunofluorescence micrographs show representative z-series projections of cells 2 hours post-seeding on fibronectin, $ZT^{Fn}$ or $ZT^{RGD}$. Cells were stained for F-actin (*green*), zyxin (*red*) and DAPI (*blue*). Zoomed views of the boxed areas in the upper panels are shown below to highlight focal adhesions and cytoskeletal structures. Scale bars = 10 μm.

As the RGD motif was the adhesive moiety in each substrate, cells were stained first for the well-characterised fibronectin receptors α5β1 and αVβ3. However, monoclonal antibodies targeting the unique α5 subunit, β1 subunit, αV subunit or β3 subunit did not generate specific staining (data not show). Despite clear differences in morphology following a two-hour culture period on $ZT^{RGD}$, cells on all substrates obtained a typical fibroblastic morphology after one day and formed focal adhesions expressing paxillin and zyxin (Figure 33).

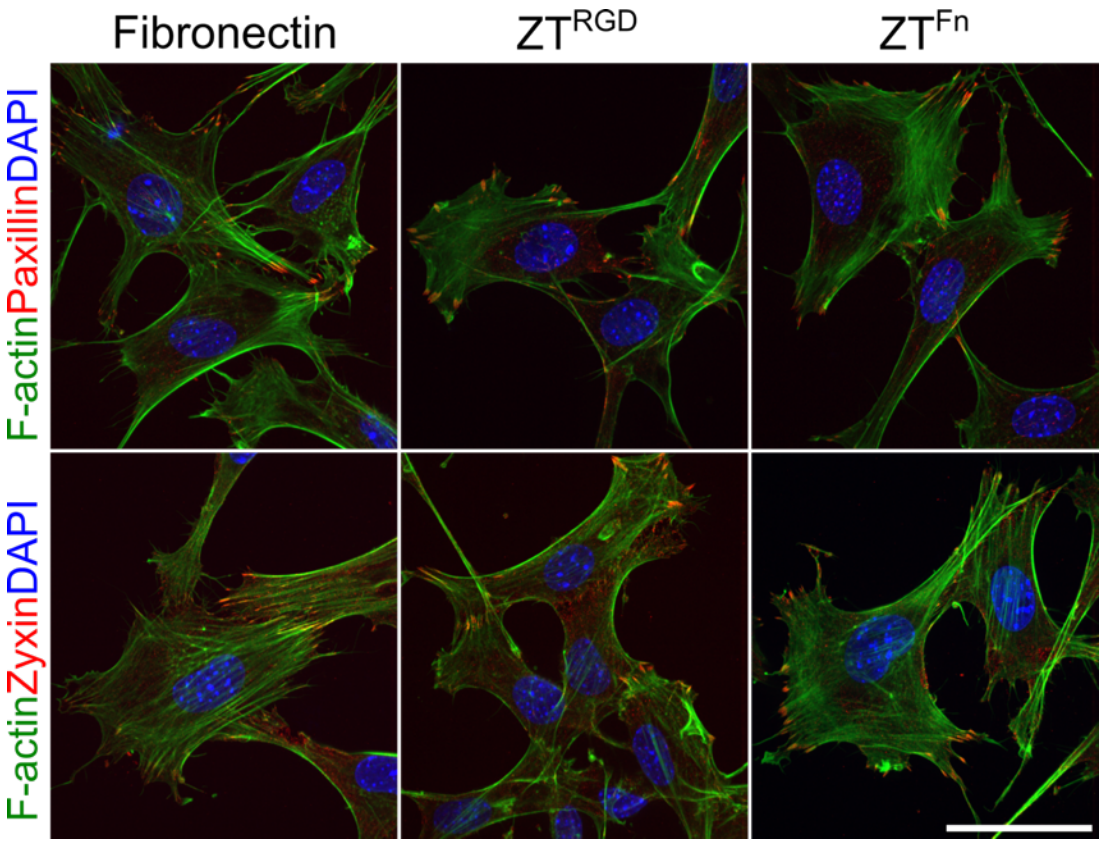


**Figure 33. Murine MSC morphology following prolonged culture on different substratum.** Immunofluorescence micrographs show representative z-series projections of cells on fibronectin, $ZT^{RGD}$ or $ZT^{Fn}$ 24 hours post-seeding. Cells were stained for F-actin (*green*), paxillin/zyxin (*red*) and DAPI (*blue*). Scale bar = 50 μm.

### *4.2.4 Structural analysis of $Z_{1212}^{RGD}$*

The rational for inserting the RGD motif in the CD-loop of Z1 was to better mimic the native environment of the motif for enhanced integrin binding. However, reduced mMSC adhesion and spreading area when cultured on $ZT^{RGD}$ compared to $ZT^{Fn}$ or fibronectin suggested that the grafted motif was not as active and/or accessible in the context of the Z1 domain. Therefore, $Z_{1212}^{RGD}$ was screened for crystallogenesis in an attempt to observe the grafted motif at atomic detail, thus permitting the comprehensive analysis of the modified CD-loop environment. Furthermore, structural characterisation of the engineered linker between the fused Z1Z2 doublets of $Z_{1212}$ may prove useful in the future design of new nanofibre phenotypes. Screening of $Z_{1212}$ and $Z_{1212}^{RGD}$ was carried out using commercial crystallisation matrices, from which several conditions were identified that induced crystallogenesis. The diffraction potential of initial hits was tested and one crystal type corresponding to $Z_{1212}^{RGD}$ was found to show the greatest promise (Figure 34a). Attempts to optimise these crystals by varying pH and PEG concentration were successful in reproducing the original crystals but failed to improve resolution (Figure 34b). Instead, these crystals were used for microseed screening against commercial crystallisation matrices, which generated multiple crystal hits. Diffraction experiments identified one crystal type as superior (Figure 34c) and the best diffraction data set was collected to 2.4 Å resolution (Figure 34d). The crystals belong to the centred trigonal space group H3 with unit cell dimensions $a$ = 133.23, $b$ = 133.23 and $c$ = 135.58 Å. The data were processed at 2.5 Å and the partial structure of $Z_{1212}^{RGD}$ was solved by molecular replacement with Phaser (McCoy *et al.*, 2007), using Z1 and Z2 domains (PDB: 2A38) as search models. Structure building and refinement was conducted by Dr. Jennifer Fleming (Universität

Konstanz). Data collection and refinement statistics are given in Table 10.

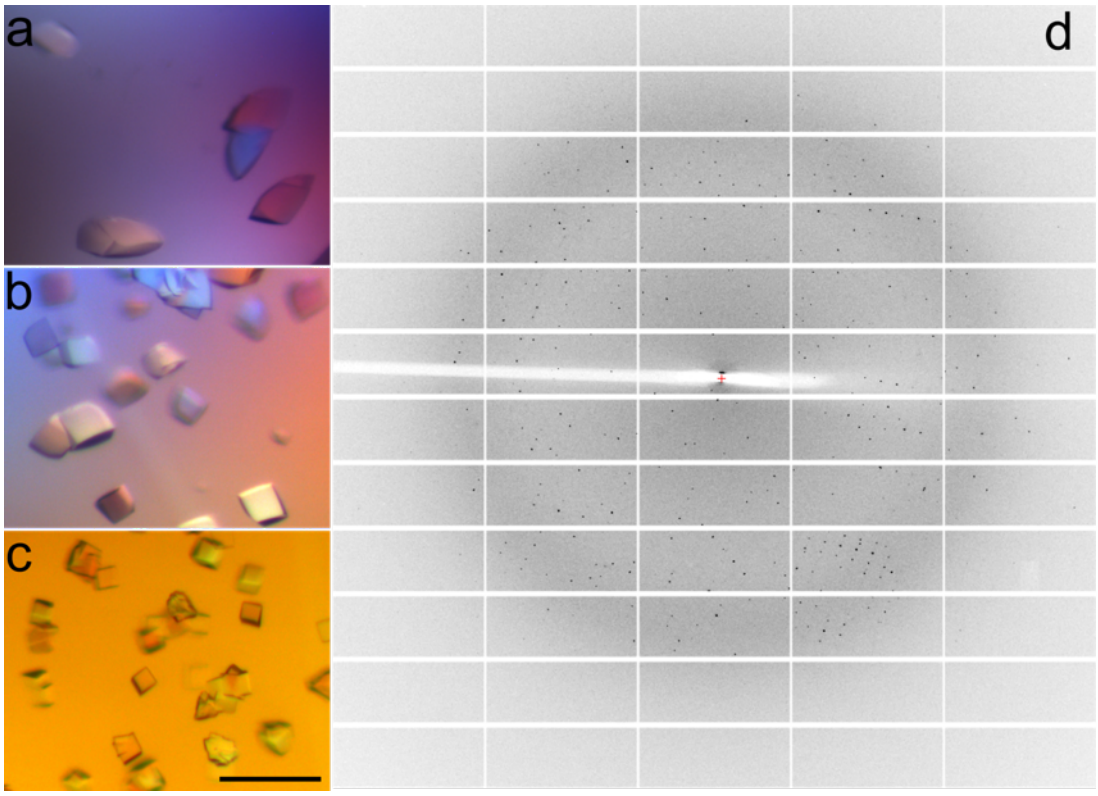


**Figure 34. $Z_{1212}^{RGD}$ crystals and X-ray diffraction pattern.** (a) Crystals from the initial screening were grown in 10% [w/v] 8000 kDa polyethylene glycol, 100 mM Tris HCl pH 7.0, 200 mM $MgCl_2$. (b) The original crystallisation conditions were varied in an attempt to improve quality and crystals were regrown in 7% [w/v] 8000 kDa polyethylene glycol, 100 mM Tris HCl pH 7.0, 350 mM $MgCl_2$. Crystals in panels (a) and (b) were obtained from 200 nL drops using a 1:1 ratio of protein solution to crystallisation media. (c) Crystals from microseed screening were grown in 10% [v/v] isopropanol, 100 mM $Na_2HPO_4$ pH 4.2, 200 mM $LiSO_4$ in 200 nL drops using a 1:1:2 ratio of protein solution to seed stock to crystallisation media. All crystals were grown at 22°C using the sitting drop vapour diffusion method and images were acquired under cross-polarised light. Scale bar = 250 µm. (d) Representative diffraction pattern of crystals from microseed screening extending to 2.4 Å resolution.

**Table 10.** X-ray data collection parameters and structure refinement statistics.

| **Diffraction data** | **$Z_{1212}^{RGD}$** |
|---|---|
| Beamline | I03 (Diamond Light Source) |
| Detector | Pilatus3 6M |
| Wavelength (Å) | 0.97 |
| Resolution (Å) | 29.30 – 2.50 (2.59 – 2.50) |
| Space group | H3 |
| Cell dimensions | |
| *a*, *b*, *c* (Å) | 133.23, 133.23, 135.58 |
| $\alpha$, $\beta$, $\gamma$ (º) | 90.00, 90.00, 120.00 |
| Total observations | 124792 (10896) |
| Unique reflections | 30971 (2968) |
| $R_{merge}$ | 0.064 (0.599) |
| Multiplicity | 4.1 (3.7) |
| Completeness (%) | 99.00 (96.00) |
| I/$\sigma$ (I) | 15.11 (2.35) |
| **Refinement** | |
| Reflections in working/free set | 30780/1488 |
| Number of protein residues | 379 |
| R-factor/R-free (%) | 20.95/22.67 |
| RMSD bond length (Å)/bond angle (°) | 0.009/1.17 |
| **Validation statistics** | |
| Ramachandran favoured/allowed/outliers (%) | 97.05/2.41/0.54 |

Values in parenthesis are for the outermost resolution shell

The asymmetric unit of the crystal formed contained two molecular copies of $Z_{1212}^{RGD}$. However, the lattice suffered from partial disorder and only two of four domains could be observed for any given $Z_{1212}^{RGD}$ molecule (Figure 35). The packing arrangement of $Z_{1212}^{RGD}$ resulted in two different conformations of the Ig doublets that could be resolved. These were an extended arrangement composed of the first Z1 and Z2 domains and a compact, V-shaped conformation of the first Z2 and second Z1 domains (Figure 35a). The V-shaped conformation encompassed both the engineered linker and grafted RGD motif. The engineered linker was well defined in the electron density map (Figure 35b) and the threonine residues hypothesised to act as a mechanical hinge (Bruning *et al*., 2010) were indeed free from interaction with the flanking domains. Further, the V-shaped conformation highlighted the flexibility of the linker. However, the grafted CD-loop could not be resolved because this region was characterised by low electron density, most likely due to loop flexibility (Figure 35c).

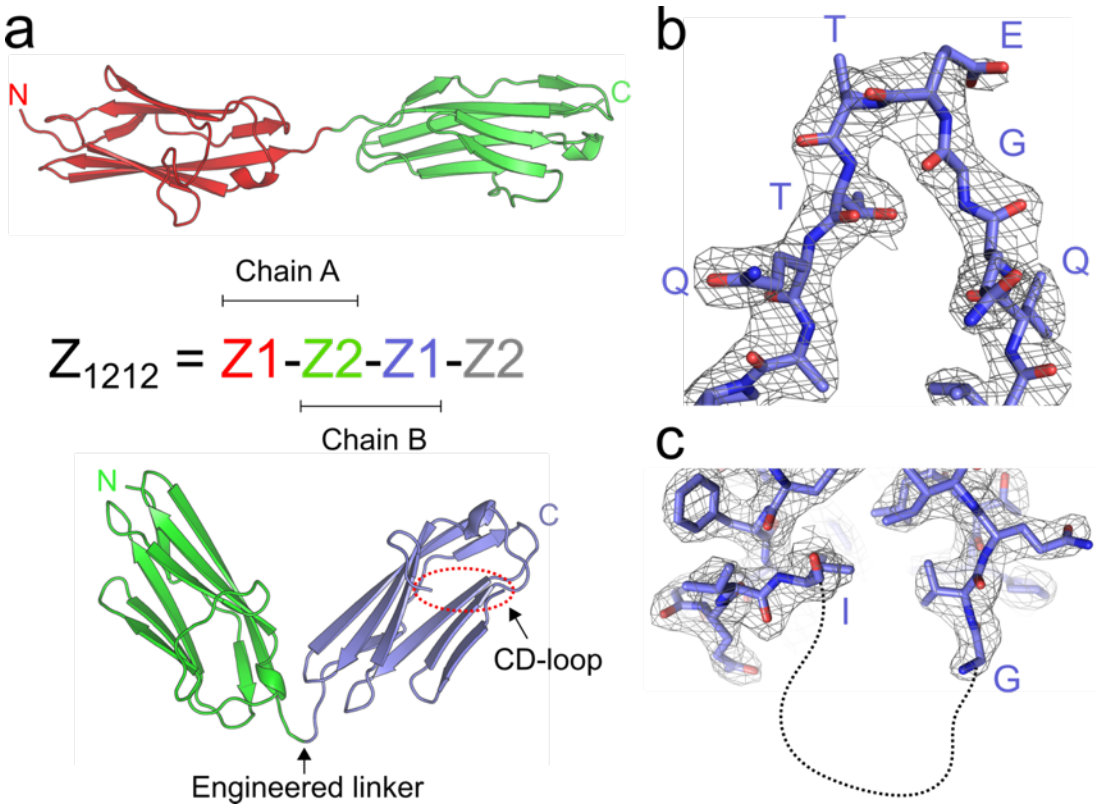


**Figure 35. Crystal structure of $Z_{1212}^{RGD}$.** (a) Ribbon diagrams of the elongated (*top*) and compacted (*bottom*) conformations of resolved modules. The domain architecture of $Z_{1212}$ (*middle*) is colour-coded to match the ribbon diagrams. The engineered linker and position of the modified CD-loop (*red oval*) in chain B are labelled. (b) Structure of the engineered linker with associated electron density (*grey mesh*). Amino acid residues are labelled and represented as sticks coloured according to atom type: carbon (*purple*), nitrogen (*blue*) and oxygen (*red*). (c) Position of the CD-loop containing the RGD motif. The unbuilt region between isoleucine and glycine is represented by a dotted line (not based on experimental observations). $2F_o$-$F_c$ electron density maps are contoured at 1 σ.

### *4.2.5 Effects of $ZT^{RGD}$ on murine MSC phenotype*

Following 7 days of culture on $ZT^{RGD}$ under serum-free conditions, mMSCs were observed to form multi-layered aggregates of 200 to 500 μm in diameter (Figure 36). Live cell imaging revealed that aggregate formation was through cellular condensation, rather than monolayer detachment and consequent aggregation. Cells cultured on non-TCT polystyrene did not form aggregates (Figure 36), and were visually indistinguishable from cells cultured on $ZT^{RGE}$ (data not shown).

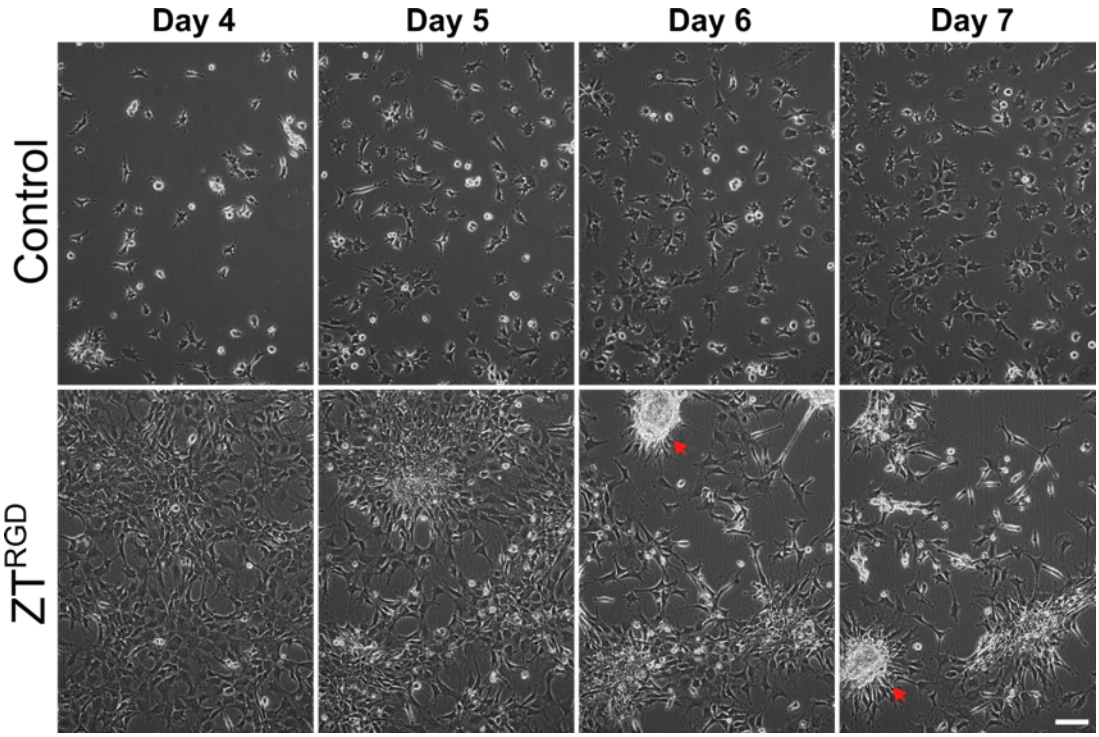


**Figure 36. Aggregation of murine MSCs following culture on $ZT^{RGD}$.** Phase contrast micrographs show a time lapse series of the same area within the cultures at days 4-7 post-seeding. Cells were seeded at a density of $2 \times 10^4$ cells/cm$^2$ on non-TCT plastic (*control, top panels*) or $ZT^{RGD}$ (*bottom panels*). $ZT^{RGD}$ was adsorbed at a concentration of 10 µg/mL. Cell aggregates are indicated (*red arrows*) and the scale bar = 100 µm.

Since a process of cellular condensation precedes chondrogenic commitment of progenitor cells in the developing limb bud, mMSC aggregates were investigated for chondrogenic differentiation. The chondrogenic potential of the D1 mMSC line was first verified *in vitro* using the conventional pellet culture method (Johnstone *et al*., 1998). Following 21 days of culture in serum-free medium supplemented with TGFβ-3 and BMP7, cell pellets stained positive for sulphated glycosaminoglycans compared to control pellets (Figure 37a), which indicated that chondrogenic differentiation had occurred. However, mMSC aggregates formed on $ZT^{RGD}$ did not stain positive for collagen type II but did express osteocalcin, which localised predominantly to cells at the periphery (Figure 37b). Since expression of osteocalcin at day 7 suggested that mMSCs were undergoing osteogenic differentiation, cells

from day 4 of culture were analysed to determine whether chondrogenic differentiation preceded aggregate formation and ensuing hypertrophy. Gene expression analysis at this time point showed that expression of chondrogenic markers *Col2a1* (collagen type II) and *Sox9* were not notably elevated in cells cultured on either non-TCT plastic or $ZT^{RGD}$ in comparison to mMSCs cultured under standard conditions (TCT plastic and serum) (Figure 37c). However, *Bglap* (osteocalcin) gene expression was highly elevated in both groups (100-fold and 44-fold for non-TCT plastic and $ZT^{RGD}$, respectively) (Figure 37c). It should be noted that RT-qPCR analysis was performed on 2 biological replicates only, since undesired osteogenic differentiation was clearly occurring.

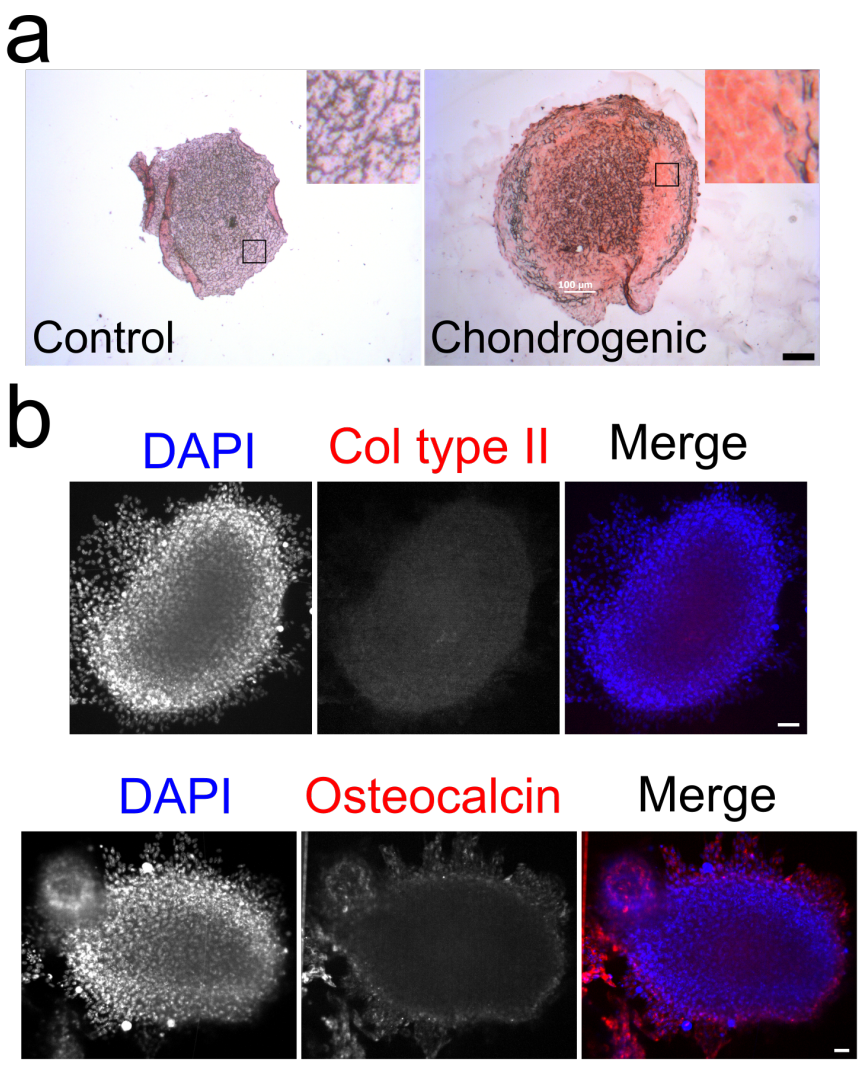
a
Control
Chondrogenic
b
DAPI
Col type II
Merge
DAPI
Osteocalcin
Merge
c
Relative Gene Expression
180
160
140
120
100
80
60
40
4
2
0
-2
-4
-6
Col2a1
Sox9
Bglap
Control
ZTRGD

**Figure 37. Osteogenic differentiation of murine MSCs.** (a) Representative images of *in vitro* pellet culture sections. Aggregates were cultured for 21 days in control (*left*) or chondroinductive (*right*) medium followed by fixation, cryoembedding, sectioning and Safranin-O staining. Zooms of boxed areas are show in the upper right of the respective image. Scale bar = 100 μm. (b) Immunostaining of multi-layered mMSC aggregates formed on $ZT^{RGD}$ following 7 days of culture. Aggregates were stained for collagen type II or osteocalcin (*red*) and counterstained with DAPI (*blue*). (c) RT-qPCR analysis of *Col2a1* (collagen type II), *Sox9* (Sox9) and *Bglap* (osteocalcin) gene expression in mMSCs cultured for 4 days on non-TCT polystyrene (control) or $ZT^{RGD}$ in serum-free medium. Expression values are normalised to cells grown on TCT plastic in the presence of serum (*dashed horizontal line*) using *Actb* (β-actin) as a reference gene. Error bars represent SD (*n* = 2*).

## 4.3 Discussion

For *in vitro* cell culture and tissue engineering strategies, it is often desirable to mimic the natural ECM for enhanced cell propagation or to induce differentiation to a desired phenotype. This chapter describes the assessment of functionalised ZT nanofibre bioactivity using mMSCs, along with their ability to induce chondrogenic differentiation for cartilage tissue engineering.

mMSCs attached and spread on $ZT^{Fn}$ at rates comparable to adsorbed fibronectin and exhibited heterogeneous morphologies on both substrates. Since mMSCs attached to $ZT^{RGD}$, the successful grafting of the active motif in Z1 was confirmed. However, a notable reduction in cell spreading, lack of matured cytoskeletal features and a rounded morphology implied that the motif was less effective in the context of the CD-loop. The average circularity of cells was higher for those cultured on $ZT^{RGD}$, an unsurprising result given the rounded morphology observed on this substrate. Lower circularity can be attributed to more robust adhesion due to the development of focal adhesions and subsequent cell spreading. However, cells grown on $ZT^{Fn}$ and fibronectin typically had more filopodia, a feature that increases the perimeter and may significantly influence circularity.

Therefore, other parameters were investigated to validate the observed influences of the substrates on cell shape. The AR of cells cultured on $ZT^{Fn}$ and fibronectin was higher than those grown on $ZT^{RGD}$, which is consistent with the anisotropic cell spreading induced by the former two substrates. Finally, solidity was highest in cells grown on $ZT^{RGD}$, which taken together with AR confirms the results from circularity measurements and shows that mMSCs spread isotropically on this substrate during the initial stages of attachment. Therefore, mMSCs exhibit a morphogenetic reaction to culture on $ZT^{RGD}$ that is mitigated following longer culture periods, since at later stages of adhesion the cells will have begun to secrete their own ECM.

Cell adhesion and spreading on $ZT^{Fn}$ and $ZT^{RGD}$ could be inhibited by a linear GRGDS peptide in a dose-dependent manner, confirming the specificity of the RGD motifs in these variants for cell surface integrin binding. Interestingly, the peptide had no effect on cell adhesion to fibronectin, suggesting that other regions of the protein could support cell attachment. It seemed most likely that mMSCs express integrins that recognise the LVD motif in the V region of fibronectin (Humphries *et al.*, 2006) or cell surface proteoglycans that interact with the heparan binding region (Dalton *et al*., 1995). mMSCs cultured on all substrates formed focal adhesions, and cells were immunostained for specific heterodimers in an attempt to discern any variance in integrin engagement induced by the different RGD contexts. However, no specific staining was observed for the established fibronectin receptors $\alpha5\beta1$, $\alpha V\beta3$ or $\alpha V\beta1$ (Mao and Schwarzbauer, 2005; Humphries *et al.*, 2006). These findings were unexpected since human MSC (hMSC) migration on fibronectin is mediated through $\alpha5\beta1$ (Veevers-Lowe *et al.*, 2011). Furthermore, focal adhesion complexes isolated from hMSCs cultured on fibronectin were found to contain $\alpha5\beta1$, $\alpha V\beta3$ and $\alpha V\beta1$ integrins by proteomic analysis (Ajeian *et al.*, 2016). It may

be that integrin epitopes were destroyed during the fixation procedure, although this scenario seems unlikely, since specific staining was observed for paxillin and zyxin. Integrin expression on different substrates could be further probed by flow cytometry or proteomic analysis of isolated adhesion complexes. However, integrin expression in the murine MSC line used in this study remains unclear.

By solving the partial crystal structure of $Z_{1212}^{RGD}$, several important features of the molecule were determined. Firstly, the engineered linker designed to join the Z1Z2 Ig doublet could be observed in atomic detail. The structure shows that the linker permits a high degree of flexibility as demonstrated by the compacted V-shape conformation of the Ig domains. These findings are in good agreement with predictions made by Bruning *et al*. (2010), who hypothesised that the small, polar threonine residues incorporated in the engineered linker could act as a mechanical hinge. Furthermore, polar amino acids are common in natural protein linkers and are thought to aid in the stability of the structure by forming hydrogen bonds with water molecules (Argos, 1990; George and Heringa, 2002). It is reasonable to predict that by altering the flexibility of the engineered linker, the morphology of ensuing nanofibres would also be altered. For example, a more ridged linker may influence the morphology of longitudinally assembled nanofibres by decreasing intermodular motion, thereby limiting kinking and producing straighter fibres. To achieve this, prolines could be incorporated into the linker since the cyclic side chain of this residue restricts its conformation (Williamson, 1994). Additionally, the lack of an amide hydrogen in the side chain limits the hydrogen bonding potential of proline, thus it is less likely to interact with flanking protein domains (Chen *et al.*, 2013). Alternatively, a rigid α-helical linker such as the sequence $(EAAAK)_n$ could be incorporated to the same effect (Amet *et al.*, 2009).

The second purpose for $Z_{1212}^{RGD}$ crystallisation was to interrogate the functionalised CD-loop environment, since $ZT^{RGD}$ appeared to be less potent than fibronectin or $ZT^{Fn}$ in promoting mMSC attachment and spreading. However, the grafted CD-loop could not be resolved using the X-ray data currently available. This indicated that the loop exhibits high flexibility, which was a specific goal of the design process to permit integrin engagement. Indeed, the RGD motif of fibronectin has only been resolved when taking part in crystal lattice contacts, as the solvent-exposed loop is disordered and may adopt multiple conformations (Main *et al.*, 1992). Since the grafted RGD motif could not be resolved in atomic detail, the exact reason for less robust integrin engagement can only be hypothesised. It is plausible that the distorted β-hairpin conformation of the RGD loop in fibronectin was not successfully mimicked in Z1, as only five native fibronectin residues were inserted. Therefore, it may be possible to improve $ZT^{RGD}$ integrin avidity by inclusion of more native flanking residues from fibronectin (Pierschbacher and Ruoslahti, 1987; Hautanen *et al.*, 1989). Alternatively, the synergistic effect of the PHSRN motif native to FnIII 9 may be responsible for the enhanced cell adhesion observed on fibronectin.

Attempts to utilise $ZT^{RGD}$ for cartilage tissue engineering proved unsuccessful in its tested context. The formation of mMSC aggregates by cellular condensation when cultured on $ZT^{RGD}$ was considered promising, due to its parallels with early chondrogenic differentiation during skeletogenesis (Goldring *et al.*, 2006; Djouad *et al.*, 2007). Furthermore, polyacrylate substrates that mimic the RGD motif, in terms of functional group composition and stereochemistry, have been shown to induce mMSC aggregation and chondrogenic differentiation (Glennon-Alty *et al.*, 2013). However, protein and gene expression analysis revealed that

mMSCs cultured either on non-TCT plastic or $ZT^{RGD}$ expressed high levels of osteocalcin, a specific marker of osteoblasts (Lee *et al.*, 2007), relative to cells maintained under standard conditions. Further, the chondrogenic markers collagen type II and Sox9 were not notably different between control and treated cells. It can, therefore, be concluded that osteogenic differentiation of mMSCs was a direct result of the change in culture environment (serum-free medium and non-TCT plastic) rather than an effect of $ZT^{RGD}$. It should be noted that although *in vitro* chondrogenesis assays were consistent with successful chondrogenic differentiation, the D1 mMSC line used in this study has been shown to form bone-like structures when subcutaneously implanted in mice (Juffroy *et al.*, 2009). Therefore, D1 mMSCs may be predisposed to osteogenic differentiation and other cell lines should be tested to verify the osteoinductive effects of the culture conditions. FCS was not included in the assays for several reasons. Firstly, some studies have reported an inhibitory effect of serum on chondrogenesis (Bilgen *et al.*, 2007; Lee *et al.*, 2009). FCS is also undefined and xenogeneic, thus issues exist for its use in the *in vitro* propagation or differentiation of stem cells for clinical application (Tuschong *et al.*, 2002). Non-adhesive culture vessels were utilised primarily to observe the effects of the engineered integrin-binding motif of $ZT^{RGD}$ on mMSC phenotype, without the additional contribution of hydrophilic TCT polystyrene. However, it would appear that a combination of serum-free medium and a hydrophobic culture substrate induced mMSC osteogenesis. Therefore, the ability of $ZT^{Fn}$ to induce mMSC chondrogenesis was not pursued using the present methodologies.

# Chapter 5

# Generation of N-cadherin and Decorin Chimeras

## 5.1 Introduction

### *5.1.1 Cadherins and their roles in cell-cell adhesion*

Cadherins are a family of transmembrane proteins with roles in cell-cell adhesion. The cadherin superfamily is vast, comprising a plethora of highly diverse members. Of these, the classical cadherins have a conserved ectodomain containing five calcium-binding domains with structural homology to the immunoglobulin fold (Angst *et al.*, 2001). The classical cadherins, such as N-, E- and T-cadherin, are present at adherens junctions between cells where they mediate cell-cell interactions by the homophilic association of ectodomains in opposing membranes. Homodimerisation occurs in either a *trans* or *cis* conformation (Figure 38a). *Trans* dimerisation arises from the homophilic interaction of the extracellular 1 domains (EC1) of cadherins on adjacent cells. At the molecular level, this interaction is governed by a conserved tryptophan that anchors into a hydrophobic pocket on the opposing EC1 of the partner molecule to create a so called β-strand-swapped interface (Boggon *et al.*, 2002). *Cis* dimerisation occurs between EC1 and EC2 of cadherin ectodomains on the same cell membrane (Figure 38a). A highly conserved tripeptide sequence, HAV, is present in β-strand F of EC1 in all classical cadherins (Figure 38b), and was shown to be essential for cell-cell adhesion since peptides containing the sequence could inhibit the aggregation of mouse blastocysts and prevent neurite outgrowth from dorsal root ganglia over astrocytes (Blaschuk *et al.*,

1990). Furthermore, Williams *et al.* (2000) showed that HAV peptides in a cyclic conformation were more effective in preventing neurite outgrowth over cells expressing N-cadherin. Interestingly, the residues flanking the HAV motif were important for both potency and specificity of the cyclic peptides. Addition of a conserved aspartic acid residue (Figure 38c) native to N-cadherin (HAVD motif) increased the inhibitory activity of the peptide, whilst a serine residue native to E-cadherin (HAVS) did not. Elucidation of the first crystal structure of N-cadherin EC1 was not particularly informative on HAV-mediated homophilic interactions, since the tripeptide was partially buried and did not relate to observed dimer interfaces. However, the hydrophobic pocket into which the conserved tryptophan docks in *trans* dimerisation was partially formed by alanine from the HAV motif (Shapiro *et al.*, 1995). Crystal structures of the ectodomains from C-, E- and N-cadherin showed that β-strand F of EC1 forms a major portion of the *cis* dimer interface with EC2, with the valine residue of HAV contributing to the formation of a hydrophobic core between the domains. Mutation of the valine residue abolishes *cis* dimerisation of E-cadherin in crystal lattices and destabilises adherens junctions between cells (Harrison *et al.*, 2011). Bunse *et al.* (2013) show that the same mutation in EC1 of N-cadherin decreases the lifetime of adherens junctions, highlighting the cooperative roles of both *trans* and *cis* dimerisation in cadherin-mediated cell-cell adhesion. Thus, the HAV motif clearly plays an important role in homotypic association of classical cadherins but the precise mechanisms of action are poorly understood (Perez and Nelson, 2004).

Alongside homophilic interactions resulting in cell-cell adhesion, cadherins can also bind cell surface receptors and activate downstream signalling cascades. N-cadherin has been shown to interact with fibroblast growth factor receptors (FGFRs)

via the acid box region located in the extracellular D2 domain of FGFR1 (Williams *et al*., 1994). Furthermore, FGF signalling is permitted in the absence of the acid box region, which is supportive of FGF-independent activation of FGFRs by cell adhesion molecules (Shimizu *et al*., 2001; Sanchez-Heras *et al*., 2006). The interaction of N-cadherin with FGFR1 has been shown to stimulate neurite outgrowth (Williams *et al*., 1994), but also to exacerbate the metastatic potential of tumour cells by blocking FGF2-mediated receptor internalisation, inducing prolonged MAPK-ERK signalling and subsequent upregulation of matrix metalloproteases (Suyama *et al*., 2002). Since FGF signalling plays a fundamental role in skeletogenesis (Su *et al*., 2014), it is possible that synergistic interactions between N-cadherin and FGFRs could contribute to chondrogenic differentiation of precursor cells. However, evidence for such associations during development and cartilogenesis remains unexplored.

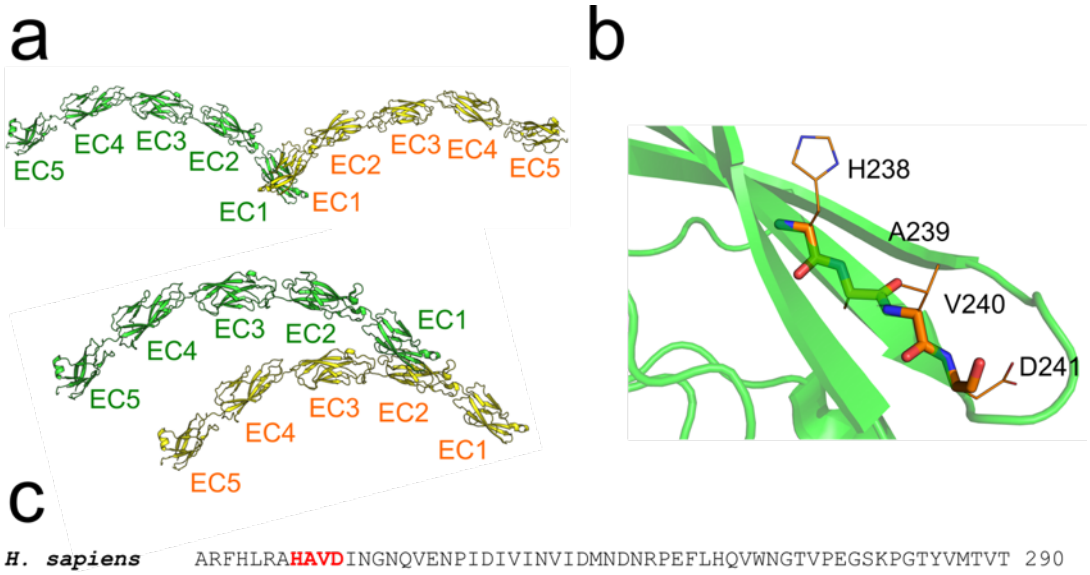

**Figure 38. N-cadherin structure and homophilic interactions.** (a) Crystal structure of the mouse N-cadherin ectodomain comprising extracellular domains (EC) 1 to 5 (PDB: 3Q2W, Harrison *et al*., 2011). The ectodomain is observed to form dimers in both the *trans* (upper structure) and *cis* (lower structure) conformations within the crystal lattice. (b) Position of the HAVD motif within EC1, which is required for *cis* dimerisation. Residues encompassing the motif are shown as main chain sticks with side chain lines (*orange*). (c) Multiple sequence alignment of N-cadherin orthologs demonstrating conservation of the HAVD motif (*red*). Species acronyms are as follows: *H. sapiens*; human, *M. musculus*; mouse, *G. gallus*; chicken and *D. rerio*; zebrafish.

N-cadherin is known to play a critical role in the condensation of progenitor cells during the early stages of cartilogenesis, since inhibition of homotypic interactions results in failed cellular aggregation and subsequent chondrogenic differentiation. Furthermore, both the ectodomain and cytoplasmic domain of N-cadherin are required for *in vitro* condensation and chondrogenic differentiation of chick limb bud micromass cultures (Oberlender and Tuan, 1994a; Oberlender and Tuan, 1994b). These findings suggest that not only are homotypic interactions required for cellular condensation, but also that activation of the catenin-signalling pathway is necessary for chondrogenesis to occur (Delise and Tuan, 2002). These discoveries have recently been utilised in the design of biomaterials for cartilage tissue engineering. Bian *et al.* (2013) showed that incorporation of a peptide derived from the HAVD motif of N-cadherin into hyaluronic acid-methacrylate (HA-Me) hydrogels resulted in enhanced chondrogenic differentiation of hMSCs in the presence of TGF-β3. The same HA-Me hydrogel functionalised with both the N-cadherin mimetic and an RGD peptide was shown to improve the osteogenic differentiation of hMSCs in the presence of osteoinductive factors (Zhu *et al.*, 2016).

### *5.1.2 Structure and function of decorin*

Decorin is a member of the small leucine-rich proteoglycan (SLRP) family

and has roles in ECM organisation and growth factor signalling. The tertiary structure of decorin is composed of leucine-rich repeats (LRRs) flanked by β-hairpins, producing a curved solenoid shape characteristic of SLRPs (Figure 39a) (Scott *et al.*, 2004). Decorin binds to collagens and plays a role in fibril stability, organisation and fibrillogenesis (Iozzo, 1998). It was proposed that the orthogonal positioning of decorin on collagen triple helices is responsible for correct spacing of fibrils by preventing lateral fusion (Scott, 1991). Decorin has been observed to localise at specific sites on collagen fibrils that contain a conserved motif of 11 residues. Complementarily-charged peptides exist on the concave inner surface of the decorin monomer, namely the RELH and KLER motifs (Scott, 1996). The conserved KLER motif is located at the boundary between LRRs 3 and 4 (Figure 39b,c), the region determined to interact most closely with collagen (Weber *et al.*, 1996; Orgel *et al.*, 2009).

A number of SLRPs, including decorin and biglycan, are found in cartilage and tendons where they play key roles in tissue homeostasis (Elliott *et al.*, 2003; Zhang *et al.*, 2006). Hyaline articular cartilage is rich in collagen type II and proteoglycans, which impart the physical resilience and load-bearing properties of the tissue. In osteoarthritic cartilage there is a reduction in decorin and biglycan expression that can be correlated with increased ECM destruction as the disease progresses (Poole *et al.*, 1996; Cs-Szabó *et al.*, 1997). Furthermore, analysis of single chondrocytes from late-stage OA patients has revealed that diseased cells produce less decorin and biglycan than cells from healthy cartilage (Bock *et al.*, 2001). Decorin also interacts with members of the TGF-β family and modulates their activity by inhibiting the activation of cognate receptors (Droguett *et al.*, 2006). TGF-β signalling is fundamental to cartilage formation during skeletogenesis

(section 1.1.2) and has been implicated in OA pathogenesis. Patients with early-onset OA have been found to harbour mutations in SMAD3, an essential component of the TGF-β signalling pathway (Valdes *et al.*, 2010). Decorin may also play a protective role in the cartilage matrix since its binding to collagen type II has been shown to prevent proteolysis by matrix metalloprotease (MMP) 1 and 13, hypothetically to prevent excessive ECM degradation under physiological conditions (Geng *et al.*, 2006). Indeed, both MMP1 and MMP13 were found to be upregulated in osteoarthritic joints (Vincenti and Brinckerhoff, 2002). Furthermore, both decorin and biglycan can act as damage-associated molecular patterns (DAMPs) in response to tissue injury, orchestrating the activation of proinflammatory signalling cascades (Moreth *et al*., 2012). Decorin can also act as a ligand for receptor tyrosine kinases, including the epidermal growth factor receptor and insulin-like growth factor 1 receptor, which in the latter case regulates the synthesis of fibrillin-1 for maintained kidney homeostasis (Schaefer *et al*., 2007).

The association of decorin with cartilage homeostasis has inspired the development of a biomaterial that mimics the collagen-binding function of the protein. Salinas and Anseth (2009) reported on the incorporation of a peptide containing the decorin KLER motif in PEG hydrogels co-functionalised with an RGD peptide. Encapsulation of hMSCs in hydrogels containing both motifs resulted in enhanced chondrogenic differentiation and cartilaginous ECM deposition compared to the RGD motif alone. Thus, the non-adhesive KLER motif is effective in promoting the chondrogenic differentiation of hMSCs, possibly by modulating ECM organisation to better emulate the cartilage niche (Salinas and Anseth, 2009).

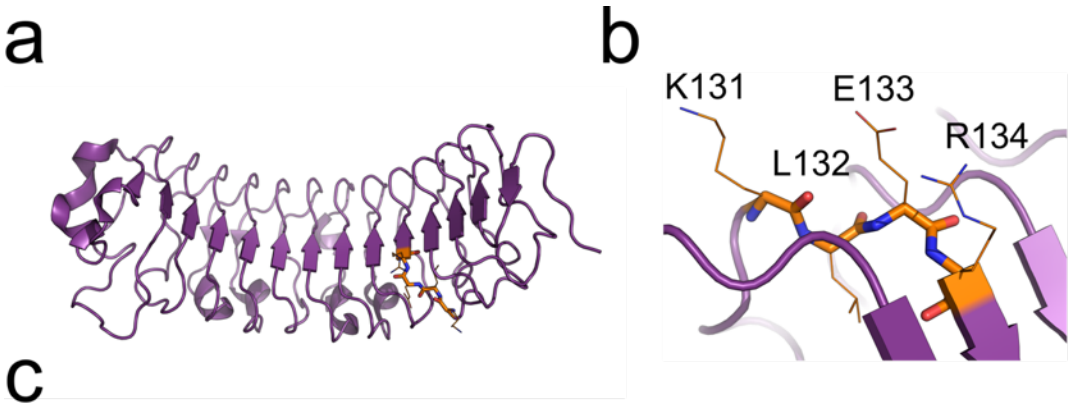


```
H. sapiens      ALILVNNKISKVSPGAFTPLVKLERLYLSKNQLKELPEKMPKTLQELRAHENEITKVRKV 168
M. musculus     TLILVNNKISKISPEAFKPLVKLERLYLSKNQLKELPEKMPRTLQELRVHENEITKLRKS 163
G. gallus       ALILVNNKISKISPAAFAPLKKLERLYLSKNNLKELPENMPKSLQEIRAHENEISKLRKA 166
B. taurus       TLILINNKISKISPGAFAPLVKLERLYLSKNQLKELPEKMPKTLQELRVHENEITKVRKS 169
D. rerio        TLILVNNKITIIHAKAFSSLINLERLYLSKNLLKEVPANIPKSLQELRIHENQINKIKKS 180
                 ********     **  *  ********* *** *   *  *** * *** * *  *
```

**Figure 39. Decorin structure and collagen binding motif.** (a) Crystal structure of bovine decorin (PDB: 1XKU, Scott *et al*., 2004). (b) Position of the KLER motif within LRR 3 (leucine-rich repeat). Residues encompassing the motif are shown as main chain sticks with side chain lines (*orange*). (c) Multiple sequence alignment of decorin orthologs demonstrating conservation of the KLER motif (*red*). Species acronyms are as follows: *H. sapiens*; human, *M. musculus*; mouse, *G. gallus*; chicken, *B. taurus*; cattle and *D. rerio*; zebrafish.

### *5.1.3 Aims*

In this chapter, the ZT system is functionalised with amino acid sequences derived from N-cadherin or decorin in an attempt to impart chondroinductive properties on the resulting nanofibres. Further, these variants were created to complement those inspired by fibronectin so as to broaden the repertoire of functionalities to encompass cell-matrix, cell-cell and matrix-matrix interactions. To achieve this, the HAVD or KLER motifs were grafted in the Z1 Ig domain and the resulting chimeras were recombinantly expressed and characterised.

## 5.2 Results

### *5.2.1 Protein construct design*

To functionalise the ZT system with chondroinductive moieties, motifs from N-cadherin and decorin were grafted within the first Z1 domain of $Z_{1212}$ ($Z_{1212}^{HAVD}$ and $Z_{1212}^{KLER}$, respectively). As the HAVD motif from N-cadherin is located within a β-strand, a similar site was chosen in the Z1 domain. A single native histidine (H27) residue is present in β-strand B of Z1, from which the subsequent three residues were mutated to form the HAVD motif (Figure 40a). By chance, H27 of Z1 is flanked N-terminally by an alanine residue conserved in N-cadherin (Figure 38c). The decorin KLER motif is located within a loop of LRR 3, thus the Z1 CD loop was chosen to incorporate the motif. Specifically, the KLER peptide replaced five native residues so as to position the motif between a valine and leucine (Figure 40b). Leucine was conserved between the decorin orthologs compared herein and the amino-flanking residue was hydrophobic in all but one case (*G. gallus*) (Figure 39c).

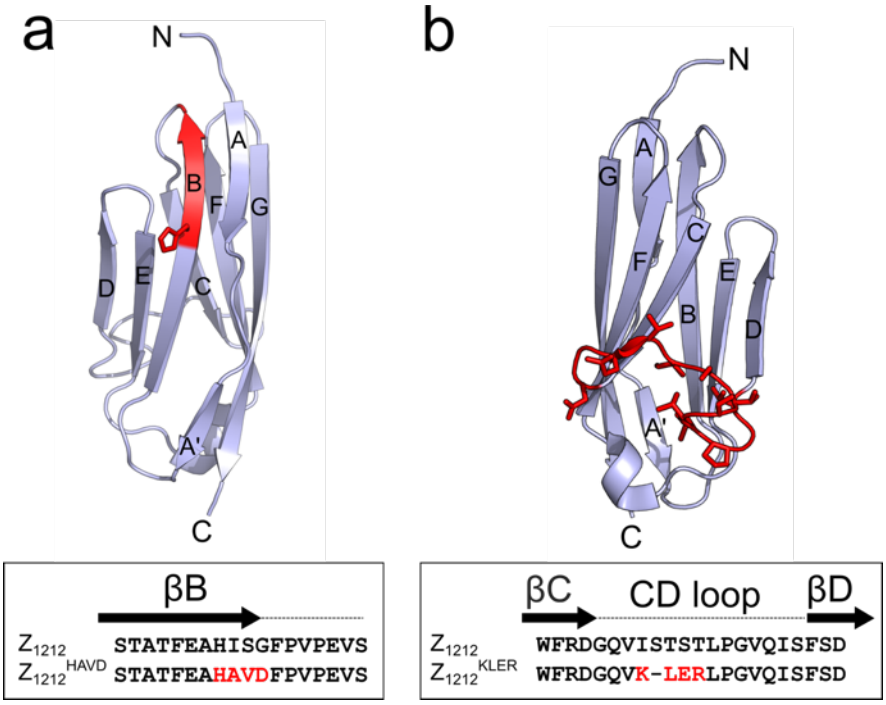


**Figure 40. Z1 domain diversification with N-cadherin and decorin functional motifs.** Cartoon renderings show the crystal structure of the titin Z1 Ig domain (PDB: 2A38, Marino *et al.*, 2006) with secondary structural elements labelled. (a) N-cadherin chimera: β-strand B is highlighted (*red*) and the side chain of histidine 27 is shown. The amino acid sequences of β-strand B in *wt* $Z_{1212}$ and $Z_{1212}^{HAVD}$ are shown below with non-native residues highlighted (*red*). (b) Decorin chimera: the side chains of residues comprising the CD-loop are shown as sticks (*red*). The amino acid sequences of the CD-loop in *wt* $Z_{1212}$ and $Z_{1212}^{KLER}$ are shown below with non-native residues highlighted (*red*).

### *5.2.2 Purification and characterisation of Z1Z2$^{HAVD}$ and Z1Z2$^{KLER}$*

Due to the unexplored nature of Z1 diversification to generate N-cadherin and decorin chimeras (β-strand modification and CD-loop shortening) it was unknown whether the changes would be structurally tolerated. Therefore, the simpler Z1Z2$^{HAVD}$ and Z1Z2$^{KLER}$ chimeric Ig doublets were first produced and characterised. Both proteins could be successfully overexpressed in *E. coli*, with Z1Z2$^{KLER}$ produced at yields comparable to *wt* Z1Z2. However, a large proportion (~70%) of Z1Z2$^{HAVD}$ was retained in the insoluble fraction following lysate clarification (data not shown), suggesting that the protein was prone to misfolding or aggregation *in vivo*. The proteins were purified, as previously described for fibronectin chimeras

(section 3.2.2.2). Despite exhibiting insolubility when expressed heterologously, Z1Z2$^{HAVD}$ eluted as a single species by SEC (Figure 41a) without signs of degradation or aggregation (Figure 41b). Fractions from the main exclusion peak ($V_e$ = 86.99 mL) were further purified by AEC (Figure 41c), which removed an unknown contaminant (~28 kDa) observed in all Z1Z2 preparations throughout this study (Figure 41d).

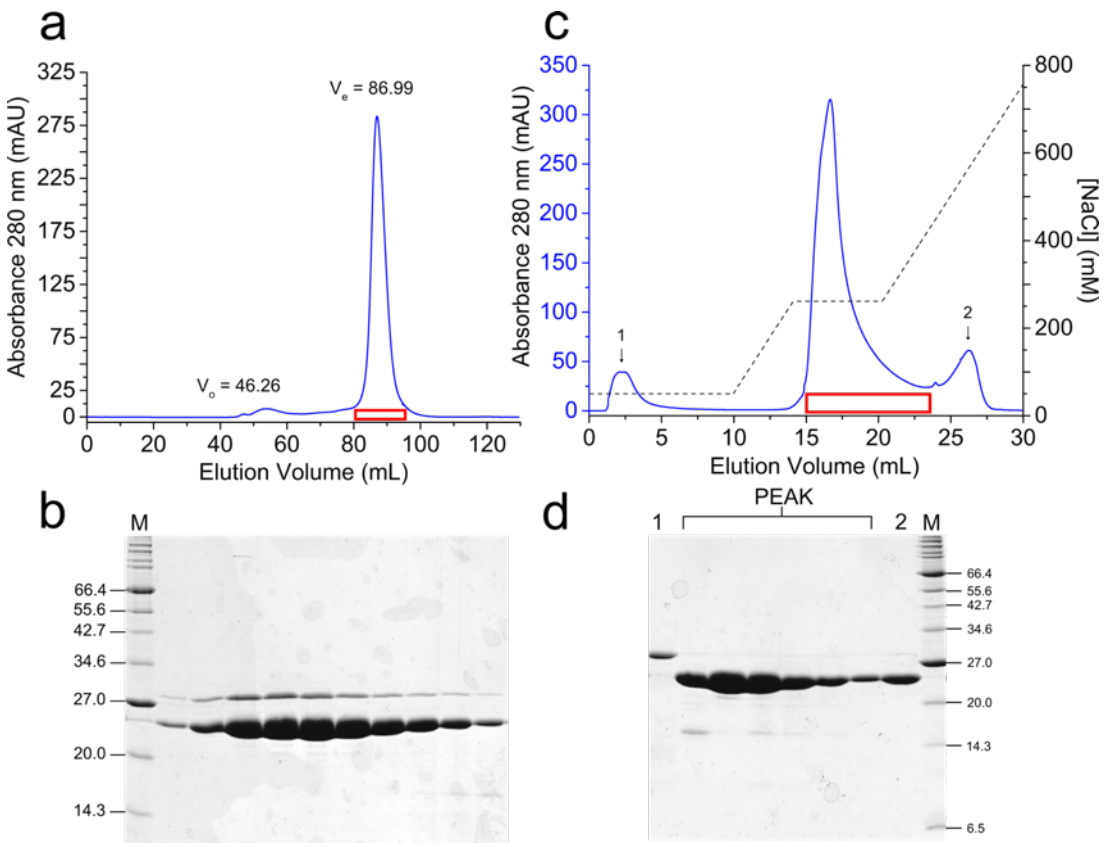


**Figure 41. Purification of Z1Z2$^{HAVD}$.** (a) Size-exclusion chromatogram from a Superdex 200 16/60 column. The void ($V_o$) and exclusion ($V_e$) volumes are indicated on the graph and the inset SDS-PAGE gel (b) shows samples taken from the boxed area (*red*) of the peak. (c) Anion-exchange chromatogram from a MonoQ 5/50 GL column with inset SDS-PAGE gel (d) of fractions taken from individual peaks (*numbers*) or the boxed area (*red*). Molecular mass markers (M) in kDa are shown on each gel.

Z1Z2$^{KLER}$ was poorly resolved by SEC, as demonstrated by the presence of shoulders in the main peak ($V_e$ = 89.82 mL) (Figure 42a). Importantly, the protein did not show a propensity to aggregate or degrade and lack of a symmetrical peak

appeared to be caused by contaminants in the latter half of the elution (Figure 42b). As with Z1Z2$^{HAVD}$, an unknown contaminant was removed by AEC (Figure 42c) and Z1Z2$^{KLER}$ was purified to a high level of homogeneity for further analysis (Figure 42d).

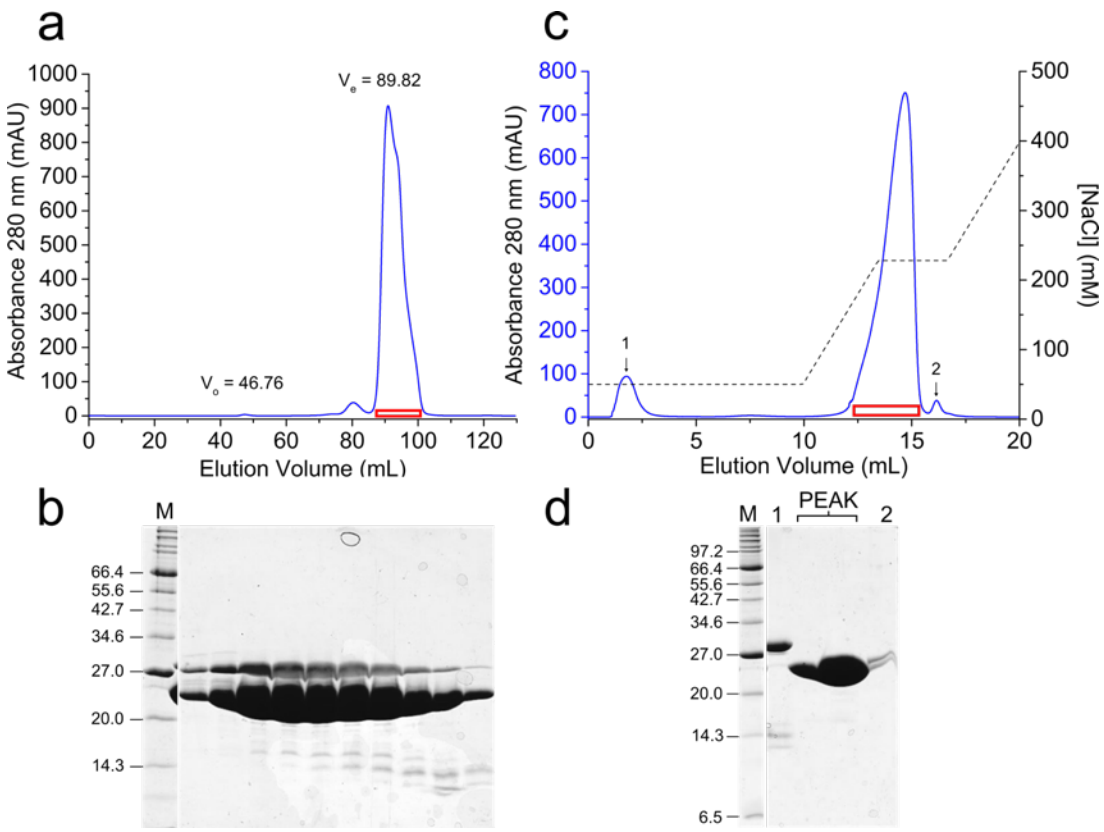


**Figure 42. Purification of Z1Z2$^{KLER}$.** (a) Size-exclusion chromatogram from a Superdex 200 16/60 column. The void ($V_o$) and exclusion ($V_e$) volumes are indicated on the graph and the inset SDS-PAGE gel (b) shows samples taken from the boxed area (*red*) of the peak. (b) Anion-exchange chromatogram from a MonoQ 5/50 GL column with inset SDS-PAGE gel (d) of fractions taken from individual peaks (*numbers*) or the boxed area (*red*). Molecular mass markers (M) in kDa are shown on each gel.

### *5.2.3 Z1Z2$^{HAVD}$ and Z1Z2$^{KLER}$ crystallogenesis*

In an attempt to observe the grafted HAVD and KLER motifs at atomic detail, Z1Z2$^{HAVD}$ and Z1Z2$^{KLER}$ were screened for crystallogenesis. Unlike the RGD-grafted Z1 domain, which was crystallised as a module of the $Z_{1212}$ tandem, N-

cadherin and decorin chimeras were screened as Z1Z2 Ig doublets for two reasons; firstly, Z1Z2 has one interdomain linker whilst $Z_{1212}$ has three. Hypothetically, interdomain linkers have a negative impact on crystallogenesis because they increase conformational flexibility. Secondly, both *wt* $Z_{1212}$ and $Z_{1212}^{RGD}$ crystallised in space group H3 only, an arrangement which produced disorder within the lattice. Therefore, $Z1Z2^{HAVD}$ and $Z1Z2^{KLER}$, rather than $Z_{1212}^{HAVD}$ and $Z_{1212}^{KLER}$, were screened in an attempt to improve crystallisation success and avoid lattice disorder associated with the four Ig tandem.

As described in Chapter 2 (section 2.5.2), screening of $Z1Z2^{HAVD}$ and $Z1Z2^{KLER}$ was carried out against commercial crystallisation matrices. No hits were identified for $Z1Z2^{HAVD}$ and only a single condition induced crystallisation of $Z1Z2^{KLER}$ (Figure 43a), from which the best X-ray diffraction data set was collected to 2.6 Å resolution (Figure 43b). The crystal had the symmetry of the hexagonal point group 6 with unit cell dimensions $a$ = 149.90 $b$ = 149.90 $c$ = 150.60 Å. Attempts to recreate the initial hit for optimisation were unsuccessful. Data collection statistics are given in Table 11.

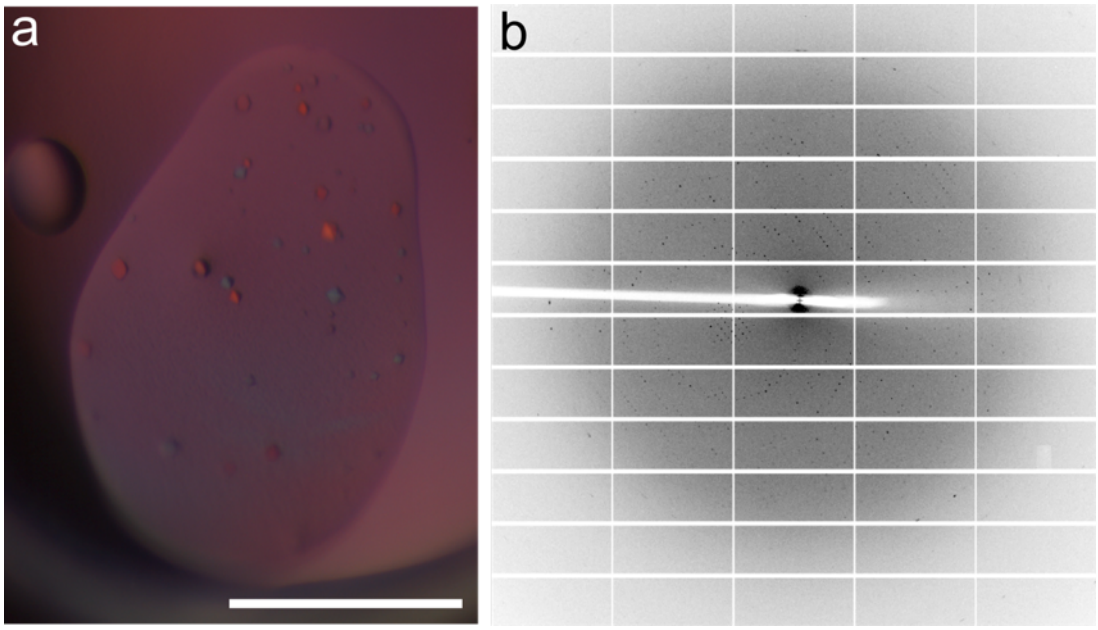


**Figure 43. Z1Z2$^{KLER}$ crystals and X-ray diffraction pattern.** (a) Crystals were grown in 1 M $NH_4H_2PO_4$ pH 4.6, 100 mM sodium acetate at 22°C using the sitting drop vapour diffusion method. The image shows crystals exhibiting birefringence under cross-polarised light. Scale bar = 500 μm. (b) Representative diffraction pattern of a Z1Z2$^{KLER}$ crystal extending to 2.6 Å resolution.

**Table 11.** Crystallographic data collection parameters and statistics.

| | **Z1Z2$^{KLER}$** |
|---|---|
| Beamline | I03 (Diamond Light Source) |
| Detector | Pilatus3 6M |
| Wavelength (Å) | 0.97 |
| Resolution (Å) | 29.87 – 3.30 (3.42 – 3.30) |
| Point group | P6 |
| Unit cell dimensions | |
| *a*, *b*, *c* (Å) | 149.90, 149.90, 150.60 |
| $\alpha$, $\beta$, $\gamma$ (°) | 90.00, 90.00, 120.00 |
| Total observations | 299922 |
| Unique reflections | 28921 |
| Completeness (%) | 100.0 (100.0) |
| Multiplicity | 10.4 (10.0) |
| $R_{merge}$ | 0.23 (0.94) |
| Mean I/$\sigma$(*I*) | 12.68 (3.16) |

Statistics for the highest resolution shell are shown in parenthesis

Diffraction data was indexed, integrated and scaled to 3.3 Å resolution using the program XDS (Kabsch, 2010). The asymmetric unit was estimated to contain between 8 and 13 Ig domains by calculation of Matthews coefficients ($V_M$) (Matthews, 1968) using the CCP4 software suite (Winn *et al.*, 2011) (Table 12). Model building by molecular replacement is currently underway using the the Z1 and Z2 Ig domains (PDB: 2A38) as individual search models. Although Z1 and Z2 share relatively low sequence identity (41%) they are structurally highly similar, with a rmsd of approximately 1.02 Å between their Cα backbones (Marino *et al.*, 2006). Therefore, molecular replacement using the low resolution data available may be challenging.

**Table 12. Estimation of Z1Z2$^{KLER}$ asymmetric unit content.** Matthews coefficient ($V_M$) and solvent content values within the expected range for protein molecules are shown.

| Number of molecules per asymmetric unit | $V_M$ (Å$^3$/Da) | Solvent content (%) |
|---|---|---|
| 8 | 3.05 | 59.73 |
| 9 | 2.71 | 54.70 |
| 10 | 2.44 | 49.67 |
| 11 | 2.22 | 44.63 |
| 12 | 2.04 | 39.60 |
| 13 | 1.88 | 34.57 |

### *5.2.4 Analysis of Z1Z2$^{HAVD}$-Tel and Z1Z2$^{KLER}$-Tel complexes*

Since the successful interaction with Tel is of paramount importance for nanofibre assembly, Z1Z2$^{HAVD}$ and Z1Z2$^{KLER}$ were co-expressed with Tel to allow

for *in vivo* complexation (Z1Z2$^{HAVD}$-Tel and Z1Z2$^{KLER}$-Tel, respectively). The expression system comprised His$_6$-tagged Tel and untagged Z1Z2 variants as previously described (section 3.2.2.2). Z1Z2$^{HAVD}$-Tel eluted as a single species by SEC (Figure 44a) and both proteins were present in the main peak (Figure 44b). Fractions from the peak ($V_e$ = 84.43 mL) were further purified by AEC (Figure 44c,d).

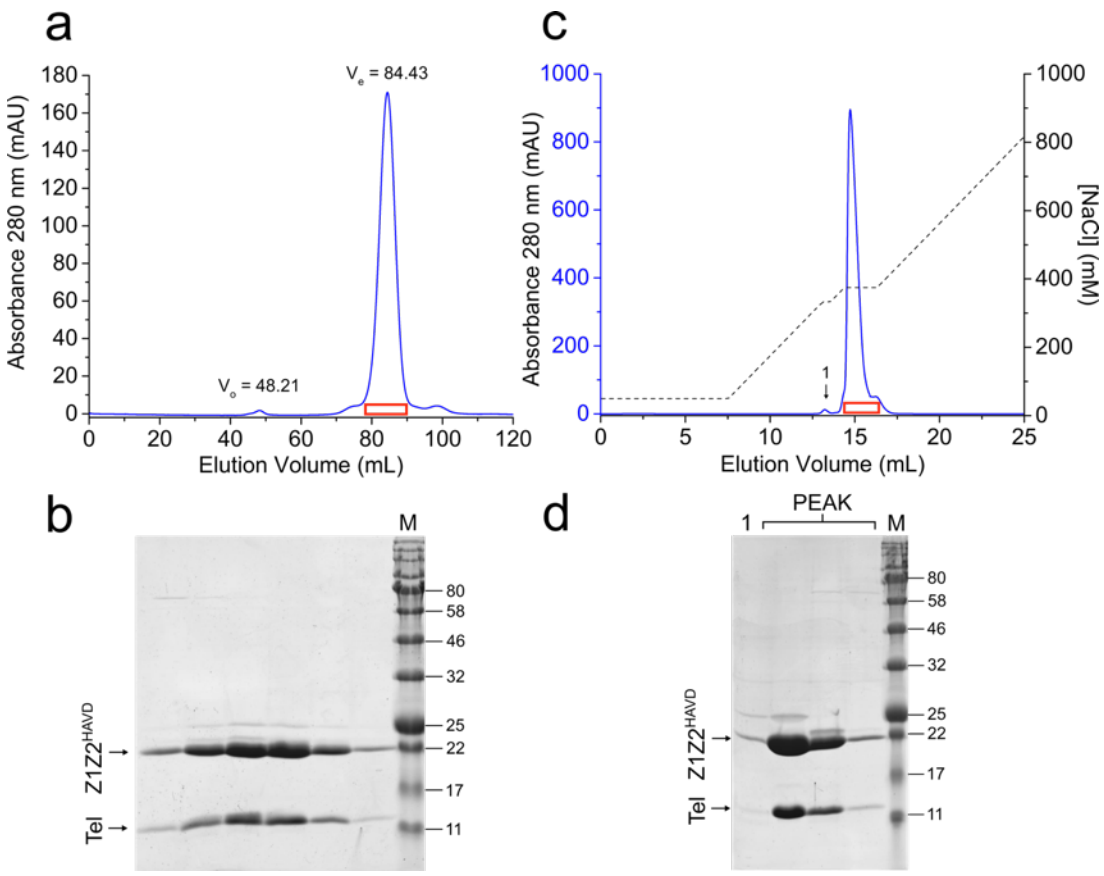


**Figure 44. Purification of the Z1Z2$^{HAVD}$-Tel complex.** (a) Size-exclusion chromatogram from a Superdex 200 16/60 column. The void ($V_o$) and exclusion ($V_e$) volumes are indicated on the graph and the inset SDS-PAGE gel (b) shows fractions taken from the boxed area (*red*). (c) Anion-exchange chromatogram from a MonoQ 5/50 GL column with inset SDS-PAGE gel (d) of fractions taken from individual peaks (*numbers*) or the boxed area (*red*). A molecular mass marker (M) in kDa is shown on each gel and individual protein components of the complex are indicated.

Z1Z2$^{KLER}$-Tel also eluted as a single species by SEC (Figure 45a) and co-elution of each protein was observed without signs of degradation or aggregation

(Figure 45b). Fractions from the main peak ($V_e$ = 84.51 mL) were purified by AEC (Figure 45c,d) for comparison to the *wt* complex.

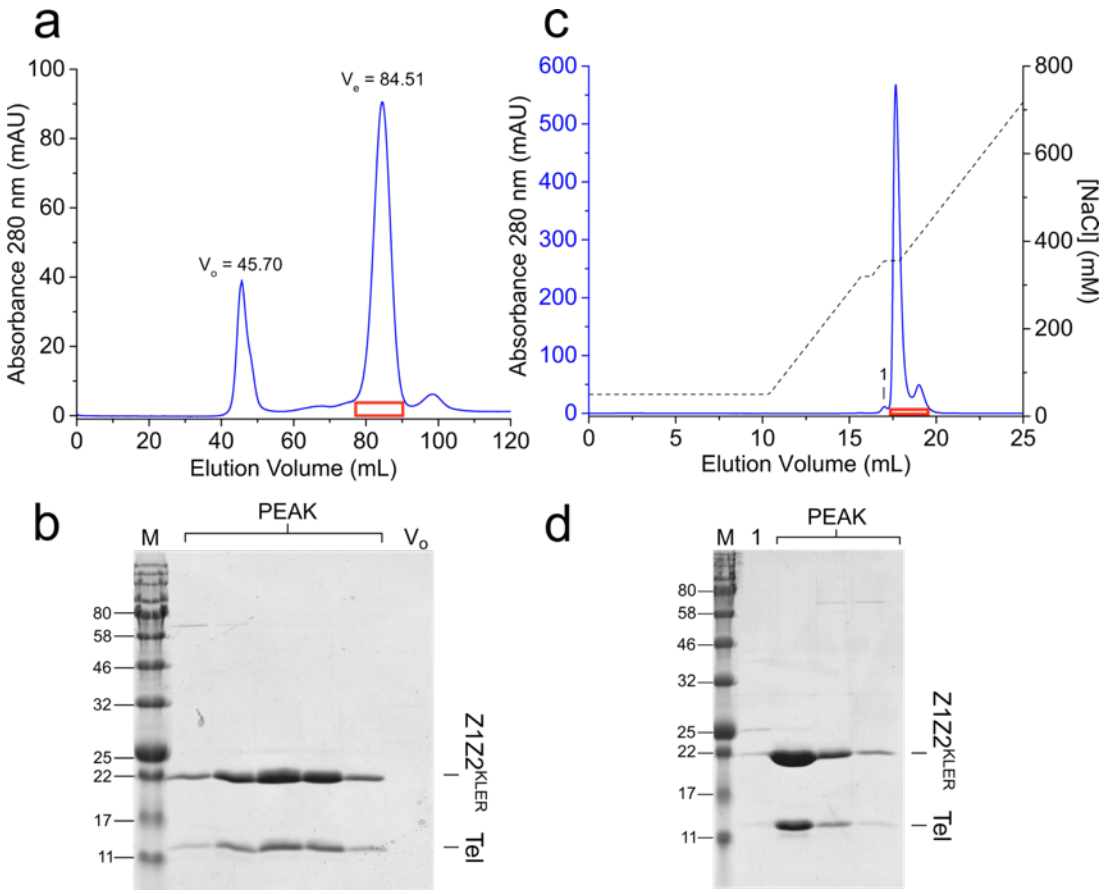


**Figure 45. Purification of the Z1Z2$^{KLER}$-Tel complex.** (a) Size-exclusion chromatogram from a Superdex 200 16/60 column. The void ($V_o$) and exclusion ($V_e$) volumes are indicated on the graph and the inset SDS-PAGE gel (b) shows fractions taken the boxed area (*red*). (c) Anion-exchange chromatogram from a MonoQ 5/50 GL column with inset SDS-PAGE gel (d) of fractions taken from individual peaks (*numbers*) or the boxed area (*red*). A molecular mass marker (M) in kDa is shown on each gel and individual protein components of the complex are indicated.

Following the observations of successful interaction between Z1Z2 N-cadherin and decorin chimeras with Tel, the complexes were analysed by SEC to verify the correct stoichiometric ratios of components. Z1Z2$^{HAVD}$-Tel eluted at 14.38 mL (Figure 46a) and Z1Z2$^{KLER}$-Tel at 14.44 mL (Figure 46b), both of which were comparable to the *wt* complex ($V_e$ = 14.49). Therefore, it can be assumed that diversification of β-strand B or the CD-loop with peptides from N-cadherin and

decorin, respectively, does not induce confounding structural perturbations that prevent Tel binding or induce unwanted self-association.

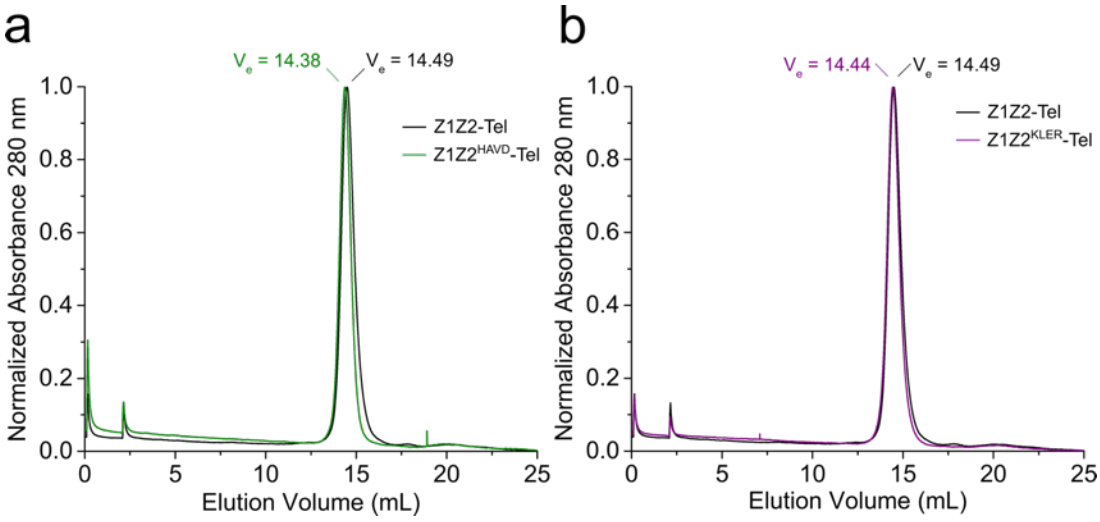


**Figure 46. Characterisation of Z1Z2$^{HAVD}$-Tel and Z1Z2$^{KLER}$-Tel complexes.** Size-exclusion chromatograms of *wt* Z1Z2-Tel (*black traces*) overlaid with (a) Z1Z2$^{HAVD}$-Tel (*green trace*) or (b) Z1Z2$^{KLER}$-Tel (*purple trace*) complexes on a Superdex 200 10/300 column. The exclusion volumes ($V_e$) are indicated.

### *5.2.5 Purification, characterisation and polymerisation capacity of $Z_{1212}^{HAVD}$ and $Z_{1212}^{KLER}$*

As with Z1Z2 N-cadherin and decorin chimeras, $Z_{1212}^{HAVD}$ and $Z_{1212}^{KLER}$ could be recombinantly expressed at yields comparable to *wt* $Z_{1212}$. However, modification of β-strand B in $Z_{1212}^{HAVD}$ once again resulted in a significant proportion of the protein becoming insoluble following heterologous expression (data not shown). The soluble fraction of $Z_{1212}^{HAVD}$ eluted as multiple peaks by SEC (Figure 47a), suggesting that the protein is prone to aggregation. Despite this, the majority of the sample eluted as a single peak ($V_e$ = 81.12 mL) and did not appear to degrade (Figure 47b). $Z_{1212}^{HAVD}$ was purified by AEC (Figure 47c,d) prior to analytical SEC and assembly analysis.

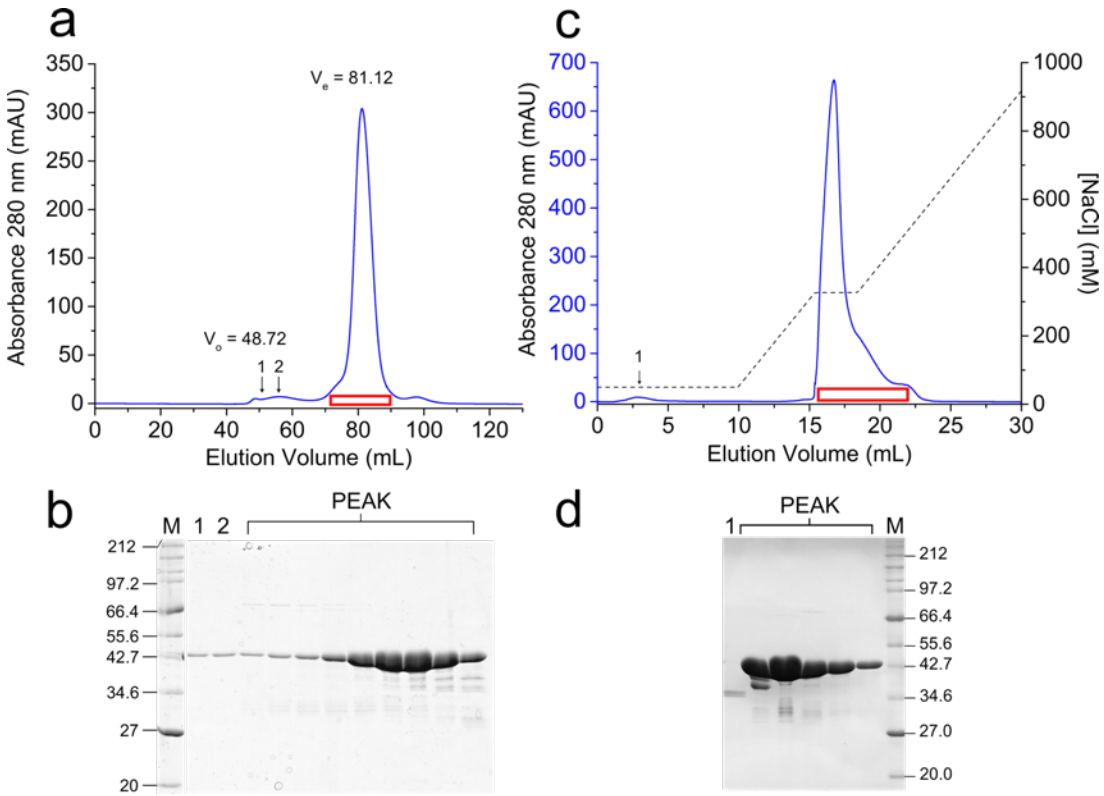


**Figure 47. Purification of $Z_{1212}^{HAVD}$.** (a) Size-exclusion chromatogram from a Superdex 200 16/60 column. The void ($V_o$) and exclusion ($V_e$) volumes are indicated on the graph and the inset SDS-PAGE gel (b) shows fractions taken from individual peaks (*numbers*) or the boxed area (*red*). (c) Anion-exchange chromatogram from a MonoQ 5/50 GL column with inset SDS-PAGE gel (d) of fractions taken from individual peaks (*numbers*) or the boxed area (*red*). Molecular mass markers (M) in kDa are shown on each gel.

Following purification, the oligomeric state of $Z_{1212}^{HAVD}$ was estimated; the protein eluted at 14.03 mL by analytical SEC, which was comparable to that of *wt* $Z_{1212}$ ($V_e$ = 14.17) and confirms the monomeric nature of this variant (Figure 48a). It is interesting to note that the presence of higher order oligomers was not observed post-purification. This may indicate that a fraction of the protein had oligomerised *in vivo* due to misfolding but that the monomeric fraction is not prone to further self-association. In the presence of Tel, $Z_{1212}^{HAVD}$ was shown to assemble into supramolecular species ($ZT^{HAVD}$) by native PAGE (Figure 48b). However, the electrophoretic mobility profile was markedly different from *wt* ZT in that the

amount of unpolymerised $Z_{1212}^{HAVD}$ appeared to be less than $Z_{1212}$ and the "blunt" assembly artefact was not present. These data would suggest that assembly is more efficient for $Z_{1212}^{HAVD}$ and that the nature of structural changes to β-strand B precludes "blunt" assembly by an unknown mechanism.

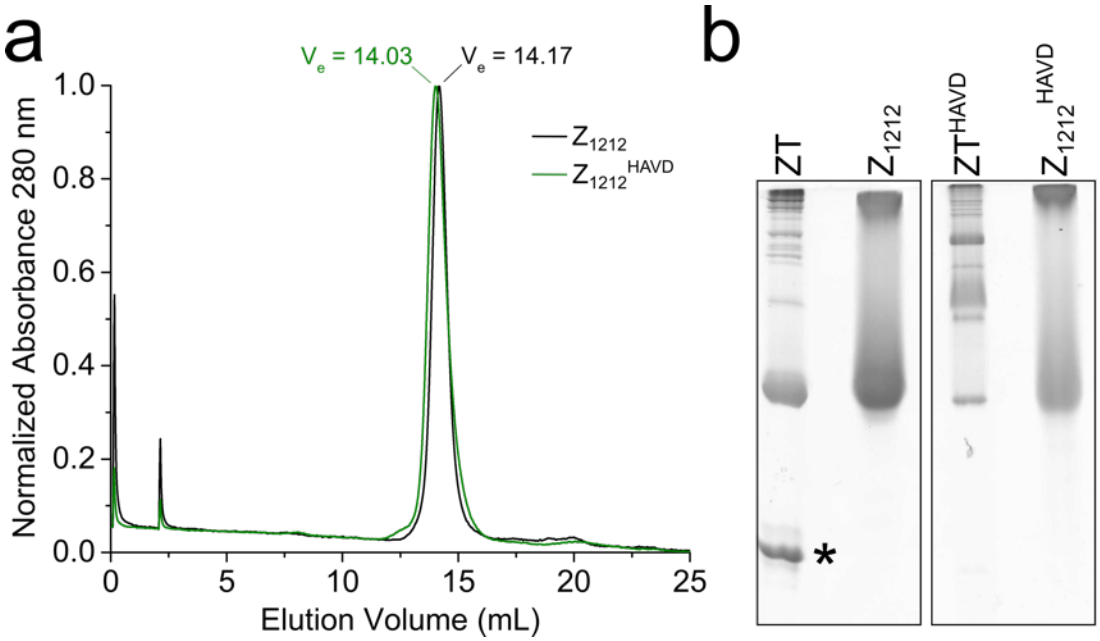


**Figure 48. Characterisation and polymerisation capacity of $Z_{1212}^{HAVD}$.** (a) Size-exclusion chromatogram overlays of *wt* $Z_{1212}$ (*black trace*) and $Z_{1212}^{HAVD}$ (*green trace*) on a Superdex 200 10/300 column. The exclusion volumes ($V_e$) are indicated. (b) Native PAGE of $Z_{1212}$ and $Z_{1212}^{HAVD}$ and their corresponding assemblies in the presence of TeI (samples at 5 mg/mL) 24 hours post-mixing. Hypothetical "blunt" products are marked with asterisks (*).

$Z_{1212}^{KLER}$ was excluded in an unusual mixture of unresolved species by SEC (Figure 49a). As with $Z1Z2^{KLER}$, this could be an effect of contaminant co-elution or heterogeneity in the global conformation of the protein, since the first exclusion peak ($V_e$ = 83.26 mL) corresponds to monomeric $Z_{1212}$ and no evidence of degradation was observed by SDS-PAGE (Figure 49b). Fractions from both main peaks were pooled and purified by AEC, which removed some smaller MM contaminants

(Figure 49c,d).

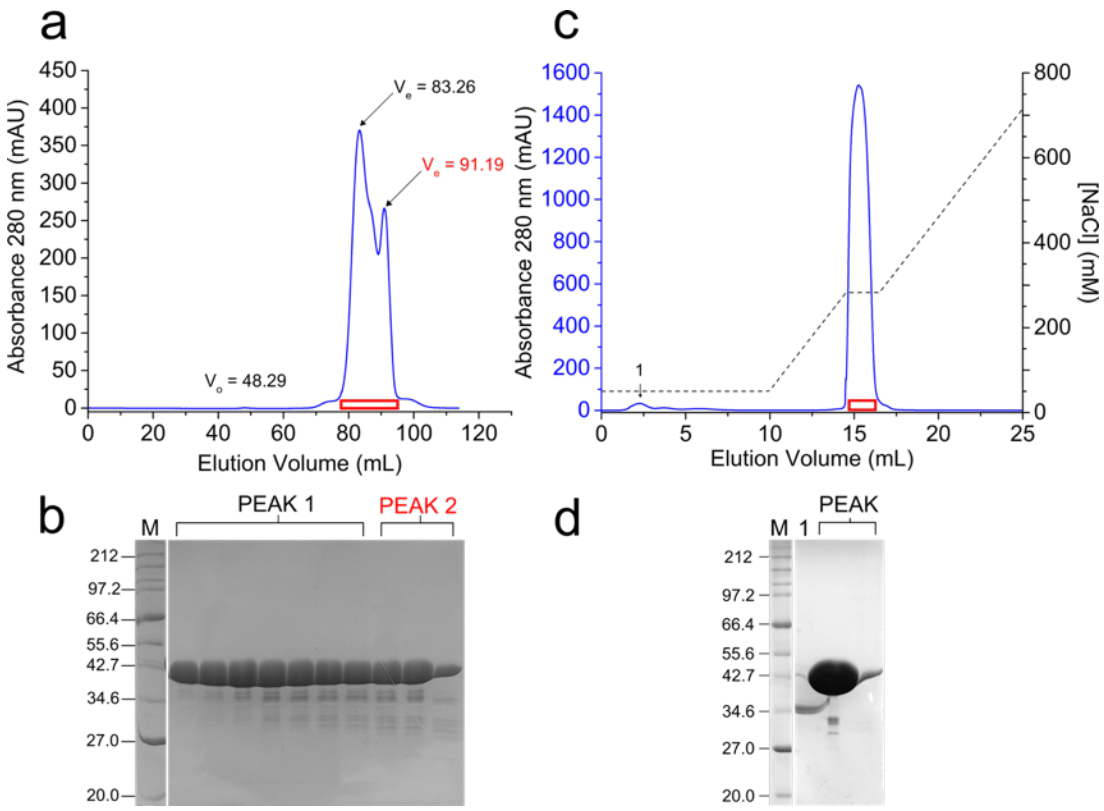


**Figure 49. Purification of $Z_{1212}^{KLER}$.** (a) Size-exclusion chromatogram from a Superdex 200 16/60 column. The void ($V_o$) and exclusion ($V_e$) volumes are indicated on the graph and the inset SDS-PAGE gel (b) shows samples taken from the boxed area (*red*) of the peak. (c) Anion-exchange chromatogram from a MonoQ 5/50 GL column with inset SDS-PAGE gel (d) of fractions taken from individual peaks (*numbers*) or the boxed area (*red*). Molecular mass markers (M) in kDa are shown on each gel.

Analytical SEC of purified $Z_{1212}^{KLER}$ yielded a single symmetrical peak ($V_e$ = 14.22) comparable to *wt* $Z_{1212}$ ($V_e$ = 14.17), thus confirming the monomeric state of this variant (Figure 50a). The generation of a single peak elution profile post-purification suggested that the double peak observed prior to AEC was caused by the co-elution of contaminants that may have bound to $Z_{1212}^{KLER}$ and altered its conformation, thereby retarding the progress of some molecules through the column bed. In the presence of Tel, $Z_{1212}^{KLER}$ was found to form supramolecular species ($ZT^{KLER}$) by native PAGE (Figure 50b). Unlike $ZT^{HAVD}$, the electrophoretic mobility

profile of $ZT^{KLER}$ was near identical to *wt* ZT and the "blunt" assembly product could be observed.

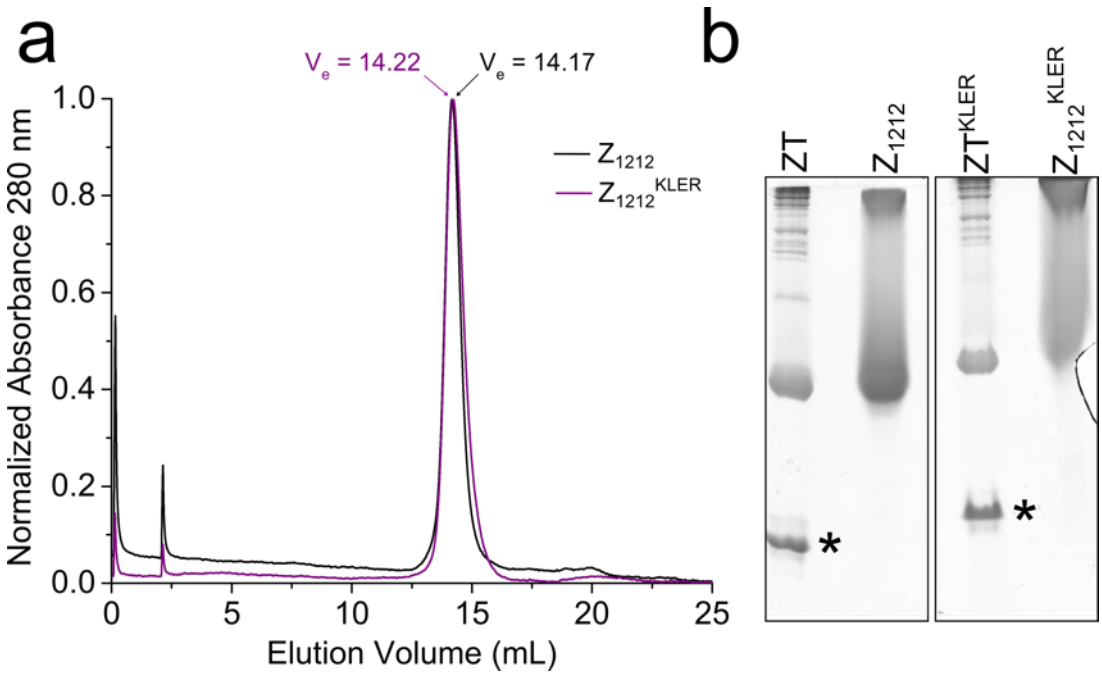


**Figure 50. Characterisation and polymerisation capacity of $Z_{1212}^{KLER}$.** (a) Size exclusion chromatogram overlays of *wt* $Z_{1212}$ (*black trace*) and $Z_{1212}^{KLER}$ (*purple trace*) on a Superdex 200 10/300 column. The exclusion volumes ($V_e$) are indicated. (b) Native PAGE of $Z_{1212}$ and $Z_{1212}^{KLER}$ and their corresponding assemblies in the presence of Tel (samples at 5 mg/mL) 24 hours post-mixing. Hypothetical "blunt" products are marked with asterisks (*).

Unfortunately, more detailed analysis of $ZT^{HAVD}$ and $ZT^{KLER}$ was not possible due to the inability to observe the assemblies by TEM, for reasons discussed previously (section 3.2.2.6). However, retention of Tel binding capacity in grafted chimeras, along with native PAGE analysis and visual inspection, were highly supportive of nanofibre formation.

### *5.2.6 Preliminary study with murine MSCs*

Due to the non-adherent nature of the decorin motif, $ZT^{KLER}$ was not hypothesised to support cell adhesion. However, $ZT^{HAVD}$ might be expected to

enhance cell attachment if the inserted HAVD motif is capable of interacting with N-cadherin ectodomains on the cell surface. Therefore, the interaction of mMSCs with $ZT^{KLER}$ and $ZT^{HAVD}$ was investigated. As with other nanofibre variants, $ZT^{HAVD}$ and $ZT^{KLER}$ were adsorbed to non-TCT polystyrene followed by seeding of mMSCs in serum-free medium. As predicted, the variants did not promote cell adhesion, nor were obvious changes in cell morphology observed (Figure 51).

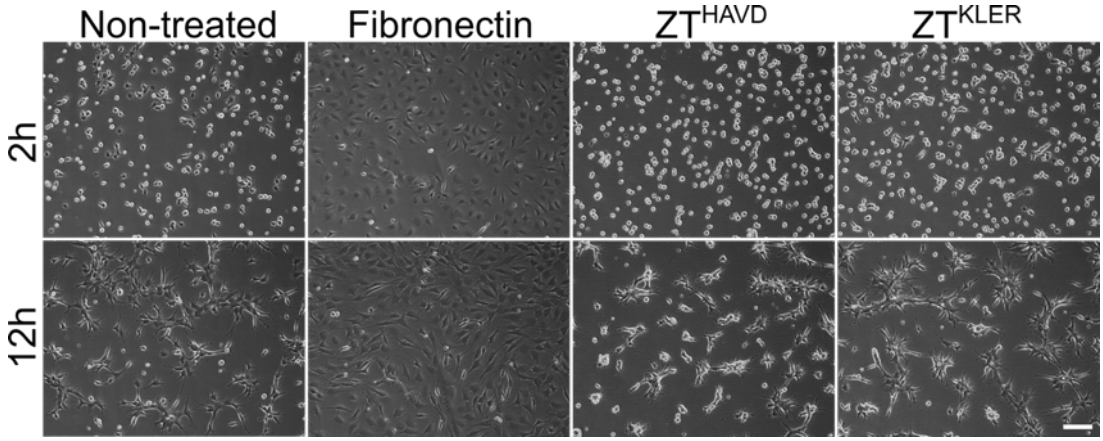


**Figure 51. Murine MSCs cultured on $ZT^{HAVD}$ and $ZT^{KLER}$.** Phase contrast micrographs show a time lapse series of the same areas within the cultures at 2 hours (*top panels*) and 12 hours (*bottom panels*) post-seeding. Fibronectin, $ZT^{HAVD}$ and $ZT^{KLER}$ were adsorbed to non-TCT plastic at a concentration of 10 µg/mL and cells were seeded at a density of $2 \cdot 10^4$ cells/cm$^2$. Scale bar = 100 µm.

## 5.3 Discussion

As observed in $Z_{1212}{}^{RGD}$, diversification of the Z1 CD-loop in $Z_{1212}{}^{KLER}$ was well tolerated and did not result in unfavourable overall structural perturbations. The evidence for this conclusion came in part from $Z1Z2^{KLER}$ crystallogenesis, which necessitates a high level of stability and uniformity in the protein. Further, the cooperative interaction of $Z1Z2^{KLER}$ with Tel and retention of a monomeric state in $Z_{1212}{}^{KLER}$ are supportive of this conclusion. The completed crystal structure of $Z1Z2^{KLER}$ may provide important insights into the precise orientation of the motif

within the CD-loop, allowing for the rational modification of the loop to more precisely mimic that of decorin.

In the case of the N-cadherin chimera, $Z_{1212}^{HAVD}$, modification of β-strand B caused a significant amount of the expressed protein to become insoluble. However, the soluble fraction of both $Z1Z2^{HAVD}$ and $Z_{1212}^{HAVD}$ behaved normally during purification and were comparable to fibronectin and decorin chimeras in terms of Tel binding and oligomeric state. During construct design, it was noted that the distal flanking residue of His28 in Z1 is an isoleucine (Ile23), the side chain of which is buried in the hydrophobic core. To incorporate the N-cadherin HAVD motif at this position, Ile23 was replaced with an alanine. In EC1 of N-cadherin, the side chain of Ala239 is also orientated towards the protein core, as is expected for hydrophobic residues (Figure 38b). Thus, the positioning of the HAVD motif in β-strand B of Z1 was not predicted to be problematic in terms of destabilising the domain. However, expression of insoluble $Z1Z2^{HAVD}$/$Z_{1212}^{HAVD}$ in *E. coli* indicated that these alterations in sequence composition were indeed problematic. This is most likely due to protein misfolding caused by β-hairpin destabilisation through mutation of Gly25. Surprisingly, a fraction of N-cadherin chimeras remained soluble and stable throughout the purification process. This would indicate that insertion of the HAVD motif in β-strand B is not innately intolerable for successful folding, but rather that the process is somewhat perturbed. The use of genetically-engineered bacterial cell lines that co-express chaperonins or are amenable to low temperature expression may improve the yield of this construct.

In the presence of Tel, $Z_{1212}^{KLER}$ and $Z_{1212}^{HAVD}$ were shown to generate supramolecular structures by native PAGE and the resulting assemblies, $ZT^{KLER}$ and $ZT^{HAVD}$, may represent novel chondroinductive nanomaterials. As expected, $ZT^{KLER}$

did not have an adhesive effect on mMSCs, thus the bioactivity of the KLER motif has not been proven experimentally. The KLER motif might be expected to illicit a chondroinductive effect due to its positioning in the CD-loop, a site demonstrated herein to be both bio-functionalisable and accessible in the context of the ZT system. This hypothesis is supported by the positive effects of a linear KLER peptide on the chondrogenic differentiation of hMSCs observed by Salinas and Anseth (2009). β-strand B of Z1 was previously uncharacterised as a diversifiable site, thus incorporation of the HAVD motif will allow for the assessment of a secondary structural element to support functionalisation. HAV peptides derived from E-cadherin have been shown to block E-cadherin mediated cellular processes including aggregation (Noë *et al.*, 1999), whilst overexpression of N-cadherin can induce cell aggregation (Tamura *et al.*, 1998). Therefore, an assay could be established wherein a cell line expressing N-cadherin are dosed with $Z_{1212}^{HAVD}$ or $ZT^{HAVD}$ to investigate their ability to block N-cadherin mediated processes, thus confirming or revoking HAVD motif bioactivity in its current context.

# Chapter 6

# ZT nanofibres as substrates for human embryonic stem cell self-renewal

## 6.1 Introduction

### *6.1.1 Substrates for pluripotent stem cell culture*

PSCs, such as ESCs and iPSCs, can generate all adult cell types and thus have huge potential for treating a range of human diseases. However, traditional PSC culture protocols typically involve growing cells on murine fibroblast feeder layers or animal cell-derived substrates such as Matrigel and Geltrex, in culture medium containing foetal calf serum. The use of xenogeneic materials is a cause for concern when the ultimate aim is therapeutic application of stem cells due to the risk of pathogenic infection or adverse immunogenic reaction. For example, mouse fibroblasts are a source of the non-human sialic acid Neu5Gc that ESCs metabolically incorporate (Martin *et al.*, 2005). Potential pathogenic transmissions from murine fibroblasts include lactate dehydrogenase-elevating virus (LDV) and retroviruses (Cobo *et al.*, 2008; Carlson Scholz *et al.*, 2011). Therefore, culture systems have been established to replace traditional components with xeno-free, chemically defined alternatives for the maintenance and propagation of clinical grade PSCs. To this end, xeno-free media have been developed such as Essential 8™ Medium (marketed by Thermo Fisher Scientific) and TeSR™2 (marketed by Stem Cell Technologies). However, the choice of xeno-free substrates currently available is wider and can be broadly split into four categories: peptides, polymers, hydrogels

and ECM proteins (Sanjar and Jin, 2015).

Peptide-based substrates are attractive due to their scalability under good manufacturing practice (GMP) conditions and synthetic nature. Most often, peptides exhibiting cell binding motifs derived from ECM proteins are covalently attached to glass or polystyrene surfaces to create adhesive substrates for PSC self-renewal. Examples include laminin-derived peptides (Derda *et al.*, 2007) and cyclic RGD peptides (Kolhar *et al.*, 2010). A peptide-acrylate composite, marketed as Synthemax by Corning, was developed by first depositing a carboxylic acid-containing acrylate on culture surfaces and subsequent conjugation of a peptide containing the vitronectin RGD motif. Synthemax was successful in preserving both hESCs (Fadeev *et al.*, 2010) and hiPSCs (Jin *et al.*, 2012) in an undifferentiated state over more than ten passages. However, a drawback of peptide substrates is the high production cost, making them less attractive when large numbers of cells must be propagated for clinical application (Sanjar and Jin, 2015).

Polymer-derived substrates are typically cheaper to synthesise than those composed of peptides, making them a potential alternative. Poly(methyl vinyl ether-alt-maleic anhydride) was found to preserve the phenotype of hESCs and hiPSCs following the screening of 90 different polymers (Brafman *et al.*, 2010). Celiz *et al.* (2015) employed a similar microarray screening approach to identify a polymer composed of 5 (*N*-(4-hydroxyphenyl)methacrylamide) as suitable for PSC culture and demonstrated both pluripotent expansion and lineage specific differentiation of hESCs and hiPSCs on the substrate. Another polymer, aminopropyl methacrylamide, was capable of supporting hESCs, but only in the presence of BSA (Irwin *et al.*, 2011).

Hydrogels offer the opportunity to culture cells in 3D and thus better imitate

the *in vivo* environment. Hyaluronic acid has been utilised as a hydrogel to culture hESCs (Gerecht *et al.*, 2007). Recently, Higuchi *et al.* (2015) demonstrated that hESCs and hiPSCs could be cultured on polyvinylalcohol-co-itaconic acid hydrogels containing a vitronectin-derived peptide and explored the effects of substrate elasticity on self-renewal. They found that the stiffest hydrogel induced differentiation after five days of culture, whereas the more elastic hydrogels promoted self-renewal.

Protein-based substrates can be either naturally derived or recombinantly produced. ECM proteins such as vitronectin and fibronectin can be purified from human or animal plasma and both have been utilised as substrates for PSCs. Plasma-derived vitronectin was first used in combination with other ECM proteins including laminin and collagen IV to support hESC culture (Ludwig *et al.*, 2006). Braam *et al.* (2008) demonstrated the self-renewal of three hESC lines on full-length recombinant vitronectin following prolonged culture. However, in this study, the recombinant vitronectin was expressed in a mouse myeloma cell line and was thus xenogeneic. Similarly, a recombinant fragment of vitronectin encompassing only the Somatomedin-B domain was capable of supporting hESCs in an undifferentiated state (Prowse *et al.*, 2010). In this case, recombinant Somatomedin-B domain was produced heterologously in *E. coli* but adsorption to a surface required the use of nickel-coated culture plates that the protein attached to via a C-terminal $His_6$-tag, thus increasing the complexity and cost of the coating procedure. hiPSCs have also been investigated; Rowland *et al.* (2010) reported attachment and expansion of three iPSC lines on human plasma vitronectin. Fibronectin is somewhat underrepresented as a substrate for PSC culture but is nonetheless effective; Baxter *et al.* (2009) showed that human plasma fibronectin can support the self-renewal of three hESC

lines under defined conditions. Furthermore, hESC attachment to fibronectin requires only the proteolytic 120 kDa central binding domain containing the RGD motif and synergy site (Kalaskar *et al.*, 2013). As a primary component of Matrigel, many laminin isoforms have been explored for their ability to promote PSC attachment and self-renewal. Laminins are heterotrimeric glycoproteins comprising an α, β, and γ chain. Thus far, 12 chains have been discovered (5 α, 4 β, and 3 γ), which associate to form 16 unique laminin isoforms found predominantly in basement membranes (Hallmann *et al.*, 2005). Isoform nomenclature is such that laminin 511 (LN-511) is composed of chains α5, β1, and γ1. LN-511 is expressed ubiquitously in most tissues and has been shown to support human PSC self-renewal (Rodin *et al.*, 2010). Miyazaki *et al.* (2012) found that N-terminal truncated fragments of recombinant LN-332 and LN-511, which contain the integrin binding site, stimulated hESC and hiPSC attachment and maintained pluripotency. Recombinant LN-521 had the same effect on human PSCs as LN-511, and when combined with an E-cadherin fragment cloning efficacy was significantly increased over LN-521 alone (Rodin *et al.*, 2014). However, like recombinant vitronectin substrates, the above described laminin derivatives were produced in mammalian expression systems, thus the high production cost and risk of pathogenic/immunogenic contamination remains.

In summary, much research has been devoted to the development of defined and/or xeno-free substrates for PSC culture. Protein-based substrates may be advantageous, since they represent the natural ECM and are typically biocompatible; however, almost all are derived from mammalian expression systems. This is because prokaryotes lack the required eukaryotic translation machinery for correct folding and modification of some human proteins, such as vitronectin and

fibronectin, meaning that they cannot be easily produced in bacteria. Large-scale mammalian cell culture is also inherently more expensive than bacterial culture due to the increased cost of the media. High yield protein expression is most credible under GMP conditions when produced in *E. coli*, which can be easily scaled to high volume fermentation vessels (Gomes *et al.*, 2012).Thus, there is a niche market for bacterially-expressed proteins that has yet to be exploited for PSC substrates.

### *6.1.2 Integrins and their role in cell adhesion*

Integrins are a family of cell adhesion receptors consisting of one α and one β subunit. Mammals have 18 α and 8 β subunits that combine in a non-covalent fashion upon activation to produce 24 unique heterodimers. Each subunit is a single-pass transmembrane glycoprotein composed of multiple modules, of which the αA and βA domains represent the major ligand interaction sites in the α and β subunits, respectively (Arnaout *et al.*, 2005) (Figure 52a). The binding of a ligand, such as a protein containing the RGD motif, induces both tertiary and quaternary alterations in integrin structure that initiate focal adhesion formation and downstream signalling cascades (Humphries *et al.*, 2006). At the molecular level, focal adhesions are composed primarily of focal adhesion kinase (FAK), paxillin, talin and vinculin (Figure 52b). However, focal adhesions are highly dynamic and complex assemblies, the mechanistic actions of which may require a myriad of additional components depending on cell type, integrin engagement and nature of the extracellular stimuli. Following recruitment of focal plaque components, talin binds actin microfilaments comprising two polymers of actin subunits in a helical arrangement. These structures are termed nascent adhesions and may disassemble or mature into focal adhesions that generate stress fibres. The maturation process is mechanically stimulated by

actomyosin force generation, which is in turn induced by the small GTPases Rac1 and RhoA (Chrzanowska-Wodnicka and Burridge, 1996; Burridge and Wennerberg, 2004). Stress fibres are formed when individual actin microfilaments are cross-linked by α-actinin and myosin II and may be classed as dorsal, ventral or transverse arcs depending upon their position in the cell. Actin filamentation induces projection of the plasma membrane, resulting in the formation of protrusions called lamellipodia and filopodia (Figure 52c). It is through a combination of nascent adhesion formation/dissociation, focal adhesion maturation and stress fibre contraction that cells migrate (Ciobanasu *et al.*, 2012).

Several studies have shown the dependence of focal adhesion maturation on Rho-mediated myosin II contractility (Ridley and Hall, 1992; Chrzanowska-Wodnicka and Burridge, 1996; Even-Ram *et al.*, 2007; Pasapera *et al.*, 2010; Burridge and Wittchen, 2013). However, it has long been noted that cells cultured on rigid substrates develop focal adhesions and stress fibres whilst those on soft substrates do not. It has been demonstrated that cells growing on rigid substrates have higher RhoA activity, thus the extracellular environment can stimulate focal adhesion and stress fibre formation by activating RhoA (Wozniak *et al.*, 2003; Paszek *et al.*, 2005). Further, RhoA activates the formin mDia1 to promote actin polymerisation. There is also a relationship between integrin engagement and focal adhesion formation through heterodimer-specific signalling. An example is the spatial and temporal expression of integrins α5β1 and αVβ3 during adhesion. α5β1 is found in mature focal adhesions whilst αVβ3 expression is characteristic of nascent adhesions. This is because engagement of α5β1 reactivates RhoA signalling whilst αVβ3 does not (Danen *et al.*, 2002). These differences in signalling manifest as distinctive morphologies in cells expressing specific heterodimers; cells

expressing α5β1 develop stress fibres whilst αVβ3-expressing cells typically have broad lamellipodia (Morgan *et al.*, 2009). Similarly, Schiller *et al.* (2013) demonstrated distinctive roles of αV and β1-containing integrins during cell attachment to fibronectin; both subtypes activate RhoA in a cooperative manner but engagement of β1integrins was required for Rho-associated protein kinase (ROCK) signalling to activate myosin II. Conversely, αV integrin engagement promoted the activation of mDia1 and subsequent actin assembly.

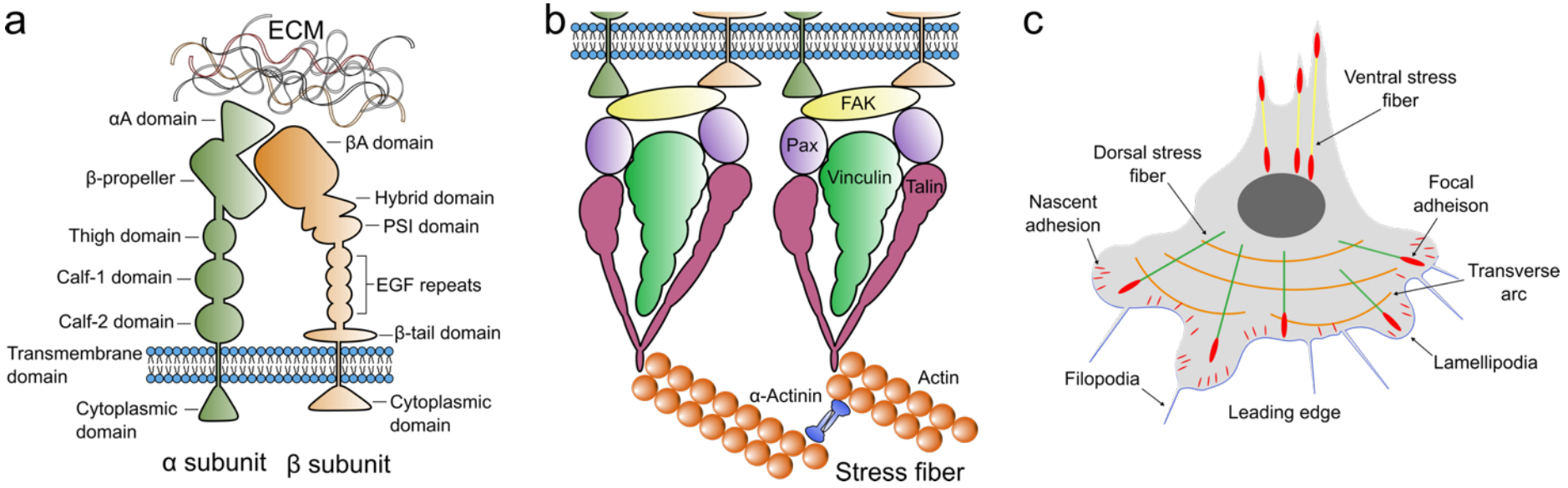


**Figure 52. Integrins, cell adhesion and cytoskeletal organisation.** (a) Schematic representation of integrin α and β subunits; each contains an extracellular, transmembrane and cytoplasmic region. The extracellular segments are composed of multiple domains with distinct functions. It should be noted that not all α subunits contain an αA domain. Schematic adapted in part from Humphries *et al.* (2006). (b) Focal adhesion organisation; major components of the complex are depicted which includes focal adhesion kinase (FAK), paxillin (Pax), vinculin, talin and the actin crosslinker α-actinin. Myosin II is not included for simplicity but would be sandwiched between actin polymers as bipolar filaments. The organisation of components in the schematic is based on observations by Kanchanawong *et al.* (2010). (c) Cytoskeletal organisation and structures in migrating cells; actin structures (stress fibres and transverse arcs) form as the cell moves forward. As integrins interact with the substrate, dynamic nascent adhesions and robust focal adhesions are assembled which induce characteristic lamellipodia and filopodia at the leading edge. Schematic adapted from Ciobanasu *et al.* (2012).

### *6.1.3 Aims*

Due to the inherently higher cost of recombinant protein production in eukaryotic expression systems and risk of contamination from immunogens or viruses, equivalents are needed for the propagation of clinical grade PSCs. Although human plasma-derived ECM proteins are an alternative, heterogeneous sampling techniques are known to cause batch to batch variability and the risk of pathogenic transmission remains (Gomes *et al.*, 2012). Kalaskar *et al*. (2013) have previously shown that hESC lines HUES1 and HUES7 could attach to and proliferate on TCT polystyrene coated with human plasma fibronectin or the 120 kDa proteolytic fragment. The 120 kDa proteolytic fragment encompasses FnIII domains 1-10, thus it includes the integrin-binding RGD motif in FnIII 10. Interestingly, HUES7 cells did not attach to modified glass coverslips functionalised with a linear RGD hexapeptide (HUES1 cells were not tested). Therefore, HUES7 cells are either sensitive to the presentation of the RGD motif or they require additional interactions with the 120 kDa fibronectin fragment in conjunction with RGD for attachment and proliferation. However, the fact that the RGD hexapeptide in solution could partially inhibit HUES7 adhesion to both fibronectin and the 120 kDa fragment was indicative of a crucial role for the RGD motif in cell attachment (Kalaskar *et al.*, 2013).

Here, the use of cell-adhesive ZT nanofibre variants as substrates for hESC culture is explored. It was hypothesised that by mimicking the fibronectin RGD motif in $ZT^{RGD}$ or by presenting the motif in its native form in $ZT^{Fn}$, we could promote attachment and proliferation of a hESC line. Both $ZT^{RGD}$ and $ZT^{Fn}$ were tested for their ability to promote adhesion of HUES7 cells. Further, the specific integrin receptors involved in attachment to the recombinant substrates were

characterised and the self-renewal of HUES7 cells was investigated over multiple passages.

## 6.2 Results

### *6.2.1 Effect of functionalised nanofibres on hESC adhesion and spreading*

To explore the usefulness of ZT nanofibre variants as recombinant substrates for hESC culture, the ability of $ZT^{RGD}$ and $ZT^{Fn}$ to promote HUES7 cell adhesion and spreading was investigated. Cells cultured on Matrigel in serum-free mTeSR1 medium were seeded on non-TCT polystyrene precoated with $ZT^{RGD}$ or $ZT^{Fn}$ at 10 μg/mL. Matrigel, human fibronectin and $ZT^{RGE}$ were included as control substrates. HUES7 cells did not attach to $ZT^{RGE}$ or $ZT^{RGD}$. However, cells did adhere to $ZT^{Fn}$ after a two-hour incubation and continued to attach and spread after four hours (Figure 53a). Quantification of cell attachment and area revealed that HUES7 cells attach to $ZT^{Fn}$ at a rate comparable to fibronectin following two or four hours of incubation (Figure 53b). Furthermore, cell spreading on $ZT^{Fn}$ was not significantly different from control Matrigel or fibronectin ($p > 0.05$) (Figure 53c).

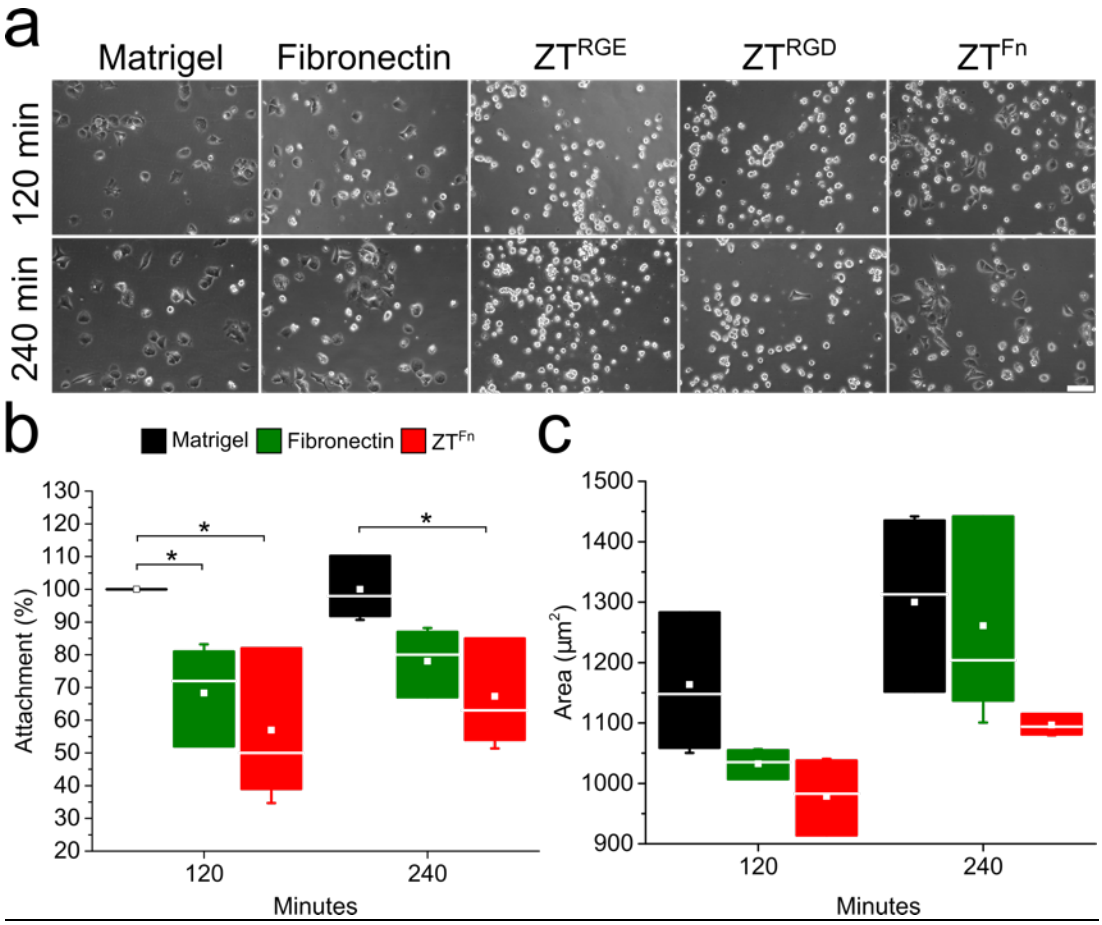


**Figure 53. Effects of functionalised ZT nanofibres and control substrates on hESC attachment and spreading.** (a) Representative phase-contrast micrographs of HUES7 cells on different substrates 2 and 4 hours post-seeding. Scale bar = 100 µm. Box plots show quantification of cell attachment (b) and spreading (c). Cell attachment to fibronectin and $ZT^{Fn}$ is expressed as a percentage of the positive control (Matrigel) taken as 100%. Fibronectin and $ZT^{Fn}$ were adsorbed at concentrations of 10 µg/mL and cells were seeded at a density of $1 \times 10^4$ cells/cm$^2$. Statistically significant differences were determined by two sample t-tests. Box plots indicate the median (*horizontal line*), mean (*square*), 25$^{th}$ and 75$^{th}$ percentile values (*box ends*) and ± SD (*error bars*; *n* = 3)

### *6.2.2 Influence of the substratum on hESC shape*

The average surface area of HUES7 cells cultured on $ZT^{Fn}$ for four hours tended to be smaller than those cultured on Matrigel or fibronectin, but the difference was not significant (Figure 54a). The effects of different substrates on cell shape were interrogated by calculating average circularity, AR and solidity using ImageJ (Figure 54b,c,d). Interestingly, the average AR of cells cultured on $ZT^{Fn}$ was

found to be significantly higher than that of cells cultured on Matrigel, indicating asymmetric cell spreading on the former substrate. Frequency distributions of shape descriptors from all conditions tested and individual cells analysed are shown in Figure 55. Parameters derived from the distributions are detailed in Table 13.

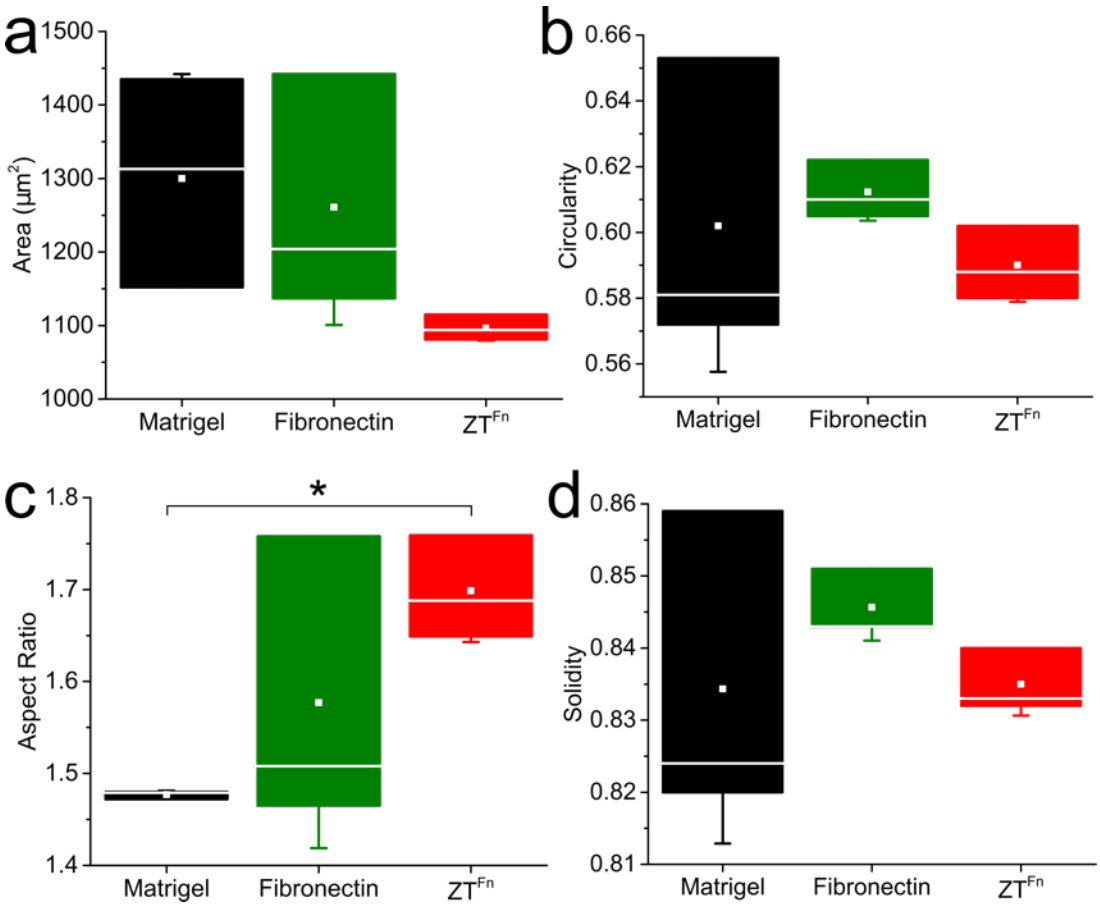


**Figure 54. Effect of functionalised ZT nanofibres on hESC shape 4 hours post-seeding.** HUES7 cell shape was quantified in terms of average cell area (a), circularity (b), aspect ratio (c) and solidity (d) when cultured on Matrigel, fibronectin or $ZT^{Fn}$. Fibronectin and $ZT^{Fn}$ were adsorbed at concentrations of 10 μg/mL. 50 cells were measured per condition for each replicate. Statistically significant differences were determined by two sample t-tests. Box plots indicate the median (*horizontal line*), mean (*square*), 25$^{th}$ and 75$^{th}$ percentile values (*box ends*) and ± SD (*error bars*; *n* = 3).

The circularity of HUES7 cells was approximately normally distributed, but area, circularity and AR were significantly skewed (skewness > 1/-1) across the three substrates, suggesting that these parameters are influenced by Matrigel, fibronectin and $ZT^{Fn}$.

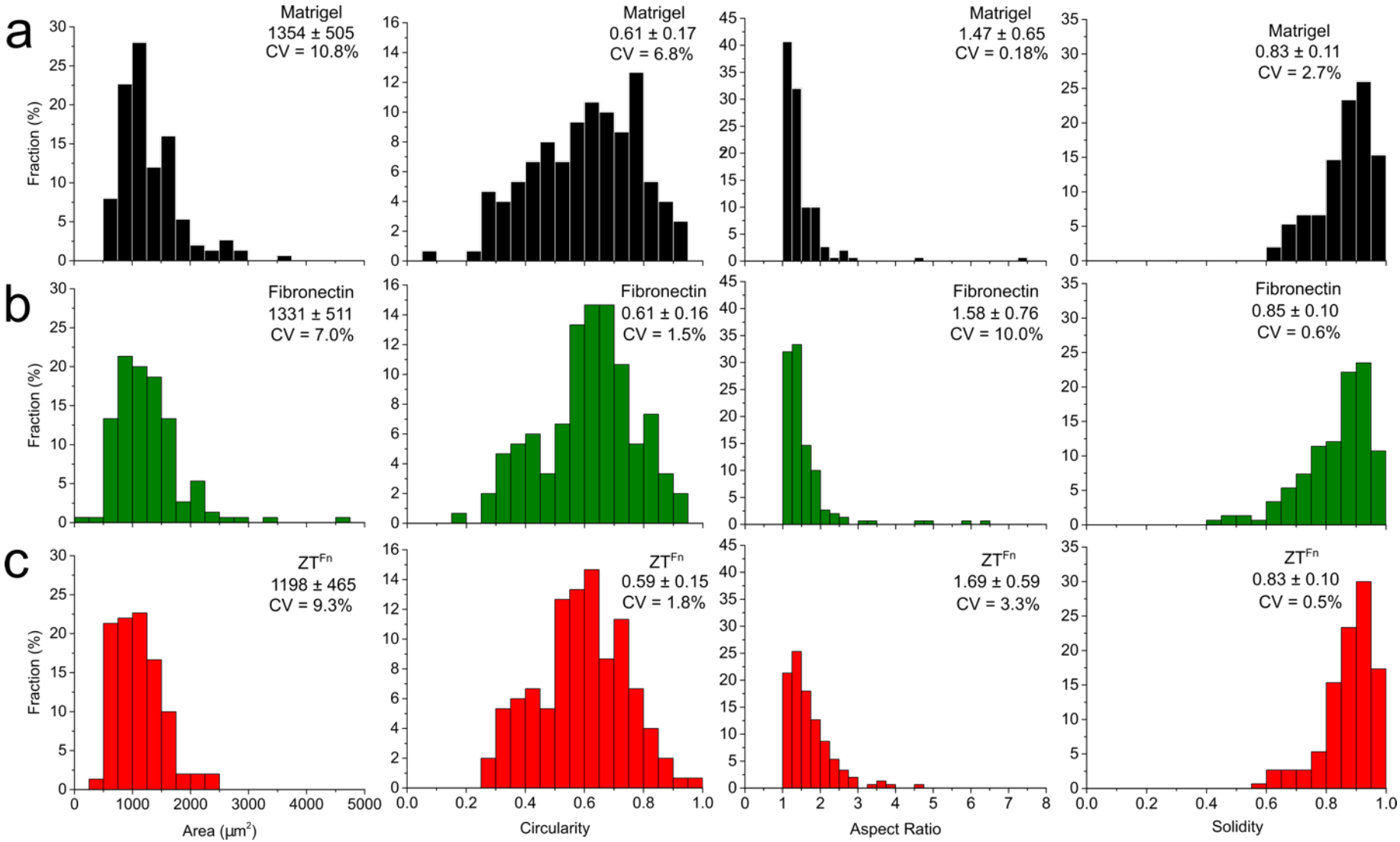
a
Matrigel
1354 ± 505
CV = 10.8%
Matrigel
0.61 ± 0.17
CV = 6.8%
Matrigel
1.47 ± 0.65
CV = 0.18%
Matrigel
0.83 ± 0.11
CV = 2.7%
b
Fibronectin
1331 ± 511
CV = 7.0%
Fibronectin
0.61 ± 0.16
CV = 1.5%
Fibronectin
1.58 ± 0.76
CV = 10.0%
Fibronectin
0.85 ± 0.10
CV = 0.6%
c
ZTFn
1198 ± 465
CV = 9.3%
ZTFn
0.59 ± 0.15
CV = 1.8%
ZTFn
1.69 ± 0.59
CV = 3.3%
ZTFn
0.83 ± 0.10
CV = 0.5%
Fraction (%)
Area (μm²)
Circularity
Aspect Ratio
Solidity

**Figure 55. Frequency distributions of hESC shape parameters on different substrates.** Histograms show the distribution of cell area, circularity, aspect ratio and solidity when cultured on Matrigel (a), fibronectin (b) and $ZT^{Fn}$ (c). The mean values are indicated with standard deviations (*n* = 150). The coefficient of variation (CV) between biological replicates (*n* = 3) is also stated.

**Table 13.** Morphological parameters for hESCs cultured on different substrates derived from all cells analysed.

| | Median | Mean ± SD | Skewness |
|---|---|---|---|
| Area ($\mu m^2$) | | | |
| Matrigel | 1295 | 1354 ± 505 | 1.37 |
| Fibronectin | 1255 | 1331 ± 511 | 2.07 |
| $ZT^{Fn}$ | 1108 | 1198 ± 465 | 1.30 |
| Circularity | | | |
| Matrigel | 0.62 | 0.61 ± 0.17 | -0.24 |
| Fibronectin | 0.64 | 0.61 ± 0.16 | -0.35 |
| $ZT^{Fn}$ | 0.60 | 0.59 ± 0.15 | -0.07 |
| Aspect ratio | | | |
| Matrigel | 1.31 | 1.47 ± 0.65 | 5.87 |
| Fibronectin | 1.37 | 1.58 ± 0.76 | 4.16 |
| $ZT^{Fn}$ | 1.53 | 1.69 ±0.59 | 1.98 |
| Solidity | | | |
| Matrigel | 0.86 | 0.83 ± 0.11 | -1.21 |
| Fibronectin | 0.87 | 0.85 ± 0.10 | -1.55 |
| $ZT^{Fn}$ | 0.86 | 0.83 ± 0.10 | -1.06 |

### *6.2.3 Effects of $ZT^{Fn}$ on focal adhesion formation and cytoskeletal organisation*

Having demonstrated that HUES7 cells adhere to a polystyrene surface coated with $ZT^{Fn}$, we next wanted to investigate the effects of the substrate on focal adhesion formation and actin filamentation. For this, HUES7 cells were fixed after 4 hours incubation on Matrigel, fibronectin or $ZT^{Fn}$ and co-stained for F-actin and paxillin. The results show that cells on all three substrates exhibited actin filamentation and focal adhesion formation; however, marked differences were observed (Figure 56). Cells grown on Matrigel typically displayed abundant filopodia and focal adhesions around the cell periphery. Attachment to fibronectin

induced a similar morphology but focal adhesions appeared smaller and more disperse compared to cells grown on Matrigel. Intriguingly, cells on $ZT^{Fn}$ presented a highly uniform morphology characterised by the absence of filopodia and presence of thick actin stress fibres terminating in large focal adhesions. Following two days of culture on $ZT^{Fn}$, defined stress fibres ending in focal adhesions could still be observed in HUES7 cell colonies, suggesting that the effects of the substrate on morphology are maintained throughout culture (Figure 57).

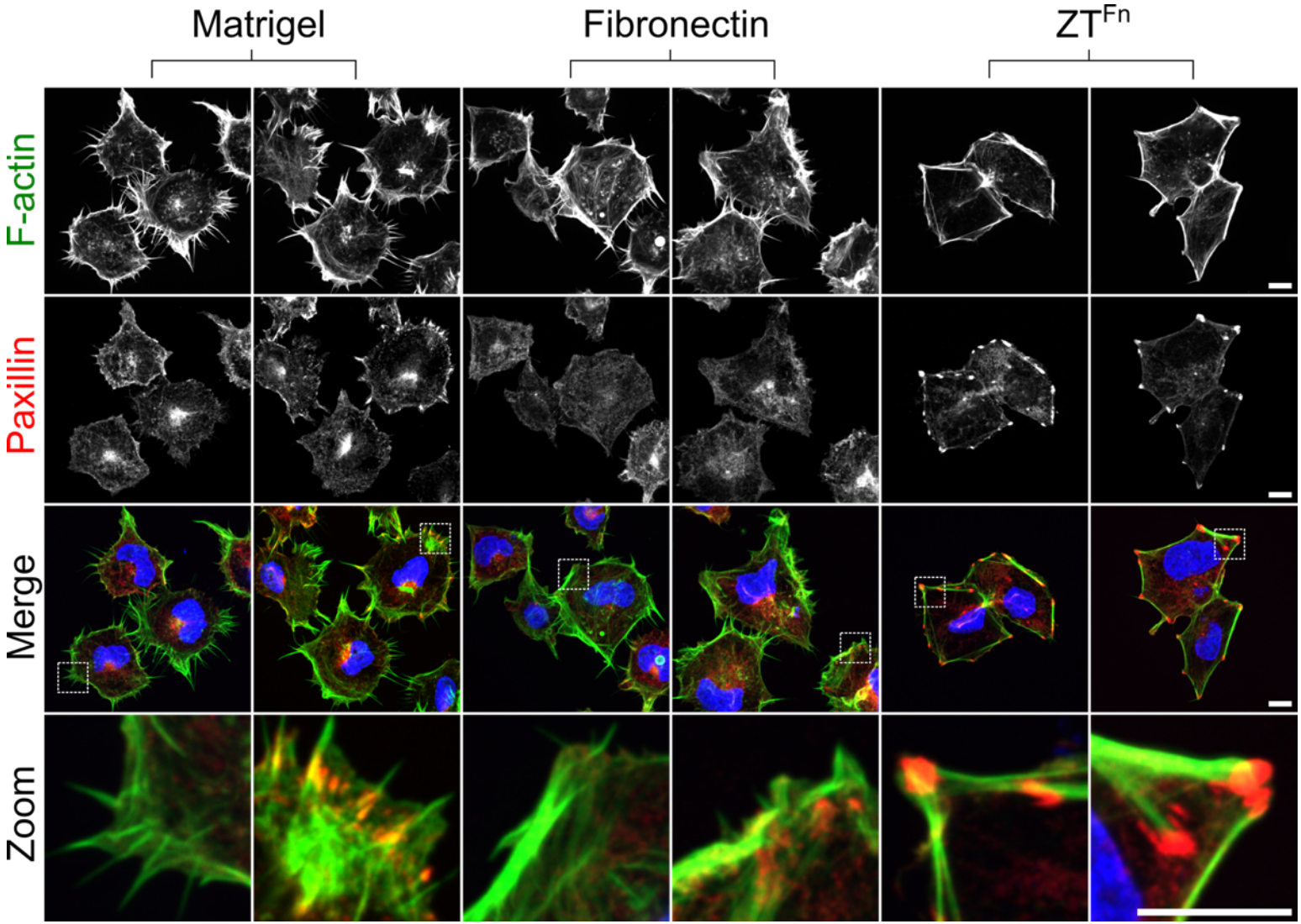


**Figure 56. Focal adhesion formation and cytoskeletal organisation in hESCs cultured on different substrates.** Immunofluorescence micrographs show representative z-series projections of HUES7 cells 4 hours post-seeding on Matrigel, fibronectin or $ZT^{Fn}$. Cells were stained for F-actin (*green*), paxillin (*red*) and DAPI (*blue*). Zoomed views of the boxed areas in the upper panels are shown below to highlight focal adhesions and cytoskeletal structures. Scale bars = 10 μm.

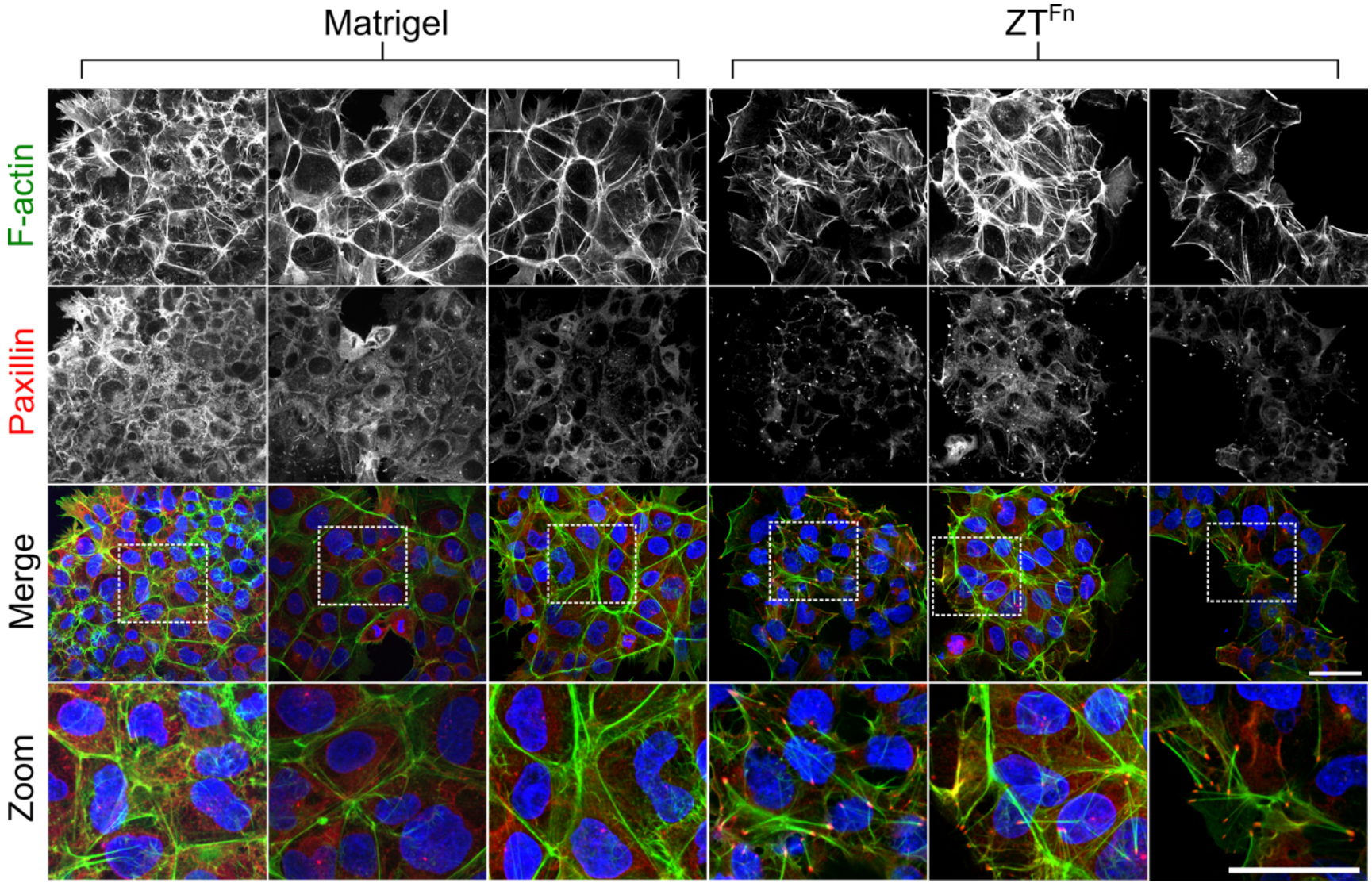
Matrigel
ZT^Fn
F-actin
Paxillin
Merge
Zoom

**Figure 57. Focal adhesion formation and cytoskeletal organisation in hESCs on different substrates following 2 days of culture.** Immunofluorescence micrographs show representative z-series projections of HUES7 cells cultured on Matrigel or $ZT^{Fn}$. Cells were stained for F-actin (*green*) paxillin (*red*) and DAPI (*blue*). The bottom panels show zoomed views of the boxed areas from the merged panels. Scale bars = 50 μm.

Since stress fibre formation is mechanically stimulated by actomyosin contraction on rigid substrata, HUES7 cells were stained for zyxin to observe its distribution. Zyxin is known to relocate from focal adhesions to the actin cytoskeleton upon application of force in the form of cyclic stretching. This translocation is associated with recruitment of vasodilator-stimulated phosphoprotein (VASP) and stress fibre formation, which establishes zyxin as a mechanosensitive factor with a role in cytoskeletal remodelling (Yoshigi *et al.*, 2005). HUES7 cells attached to $ZT^{Fn}$ did express zyxin at focal adhesion sites, but it did not appear to be mobilised to stress fibres (Figure 58). Cells cultured on fibronectin or Matrigel also expressed zyxin in focal adhesions, with a staining pattern comparable to paxillin (Figure 58).

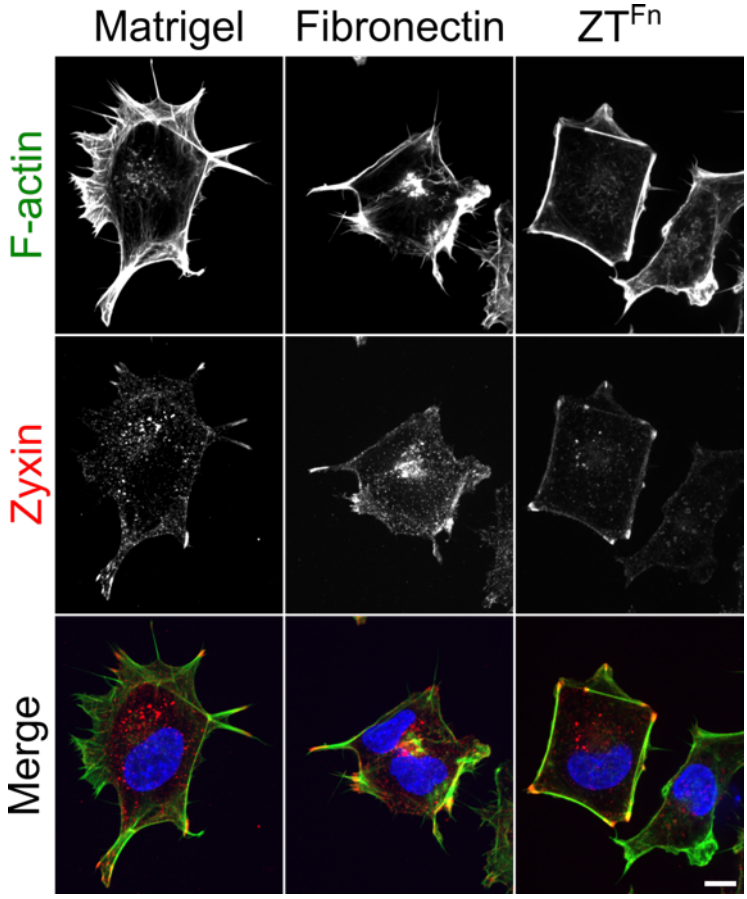


**Figure 58. Zyxin recruitment to focal adhesions in hESCs cultured on different substrates.** Immunofluorescence micrographs show representative z-series projections of HUES7 cells 4 hours post-seeding on Matrigel, fibronectin or $ZT^{Fn}$. Cells were stained for F-actin (*green*), zyxin (*red*) and DAPI (*blue*). Scale bar = 10 μm.

### *6.2.4 Differential integrin engagement on $ZT^{Fn}$*

Due to the notable differences in cell morphology on $ZT^{Fn}$ compared to Matrigel and fibronectin, integzrin engagement was explored by immunofluorescence. In the first instance, the presence of well-characterised fibronectin receptors α5β1 and αVβ3 integrins was tested. For this, antibodies to the unique α5 subunit and αVβ3 heterodimer were used to stain cells on each substrate following four hours of attachment. Analysis revealed that only cells on $ZT^{Fn}$ showed focal adhesion-like staining for α5β1 integrin (Figure 59). Interestingly, a subpopulation of spontaneously differentiated cells showed robust α5 staining on all

substrates. Evidence for the differentiated phenotype of this subpopulation came from the relative infrequency with which they were observed coupled with differences in morphology and focal adhesion characteristics.

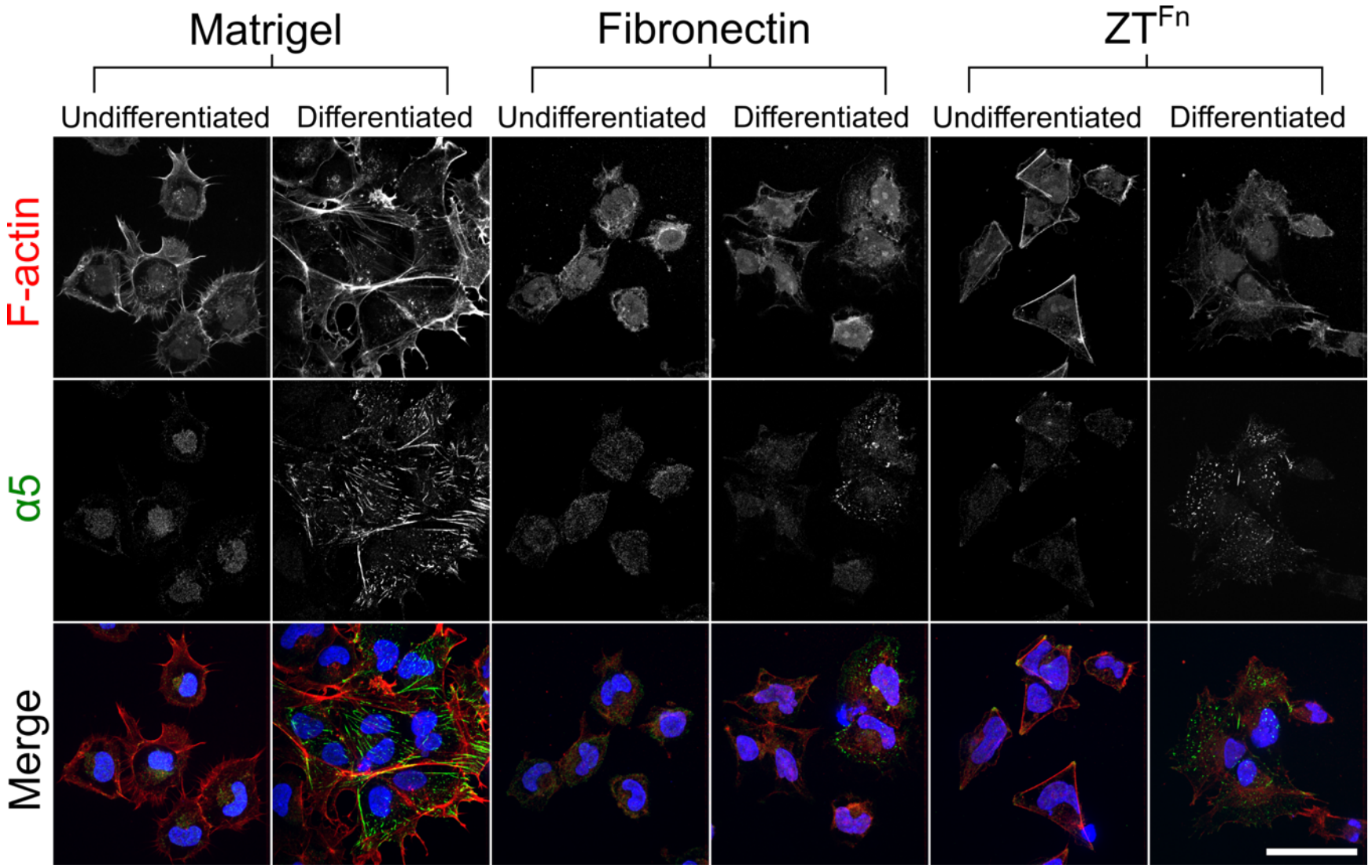
Matrigel
Fibronectin
ZT^Fn
Undifferentiated
Differentiated
Undifferentiated
Differentiated
Undifferentiated
Differentiated
F-actin
α5
Merge

**Figure 59. Staining of hESCs on different substrates for integrin α5 subunit.** Immunofluorescence micrographs show representative z-series projections of undifferentiated and spontaneously differentiated HUES7 cells 4 hours post-seeding on Matrigel, fibronectin or $ZT^{Fn}$. Cells were stained for F-actin (*red*) integrin α5 subunit (*green*) and DAPI (*blue*). Scale bar = 50 μm.

However, the fluorescence was diffuse and difficult to localise precisely to the areas of focal adhesion formation. Therefore, cells cultured on $ZT^{Fn}$ were dual stained for paxillin and the α5 subunit for more precise localisation of the integrin. Despite a diffuse staining pattern for α5, an increased intensity was observed in focal adhesions formed on $ZT^{Fn}$ (Figure 60a). Fluorescence intensity profiles of α5 and paxillin were plotted for cells grown on $ZT^{Fn}$, Matrigel and fibronectin (Figure 60b). Unsurprisingly, the α5 subunit was shown to colocalise strongly with paxillin in focal adhesions formed on $ZT^{Fn}$ but not on Matrigel. Intensity profiles from cells grown on fibronectin gave the impression of α5-paxillin colocalisation, however, cells on this substrate rarely displayed prominent focal adhesions but rather a disperse paxillin expression at the cell periphery. Thus, it may be that α5β1 was mediating adhesion to fibronectin but the association was transient and infrequently resulted in the formation of mature focal adhesions.

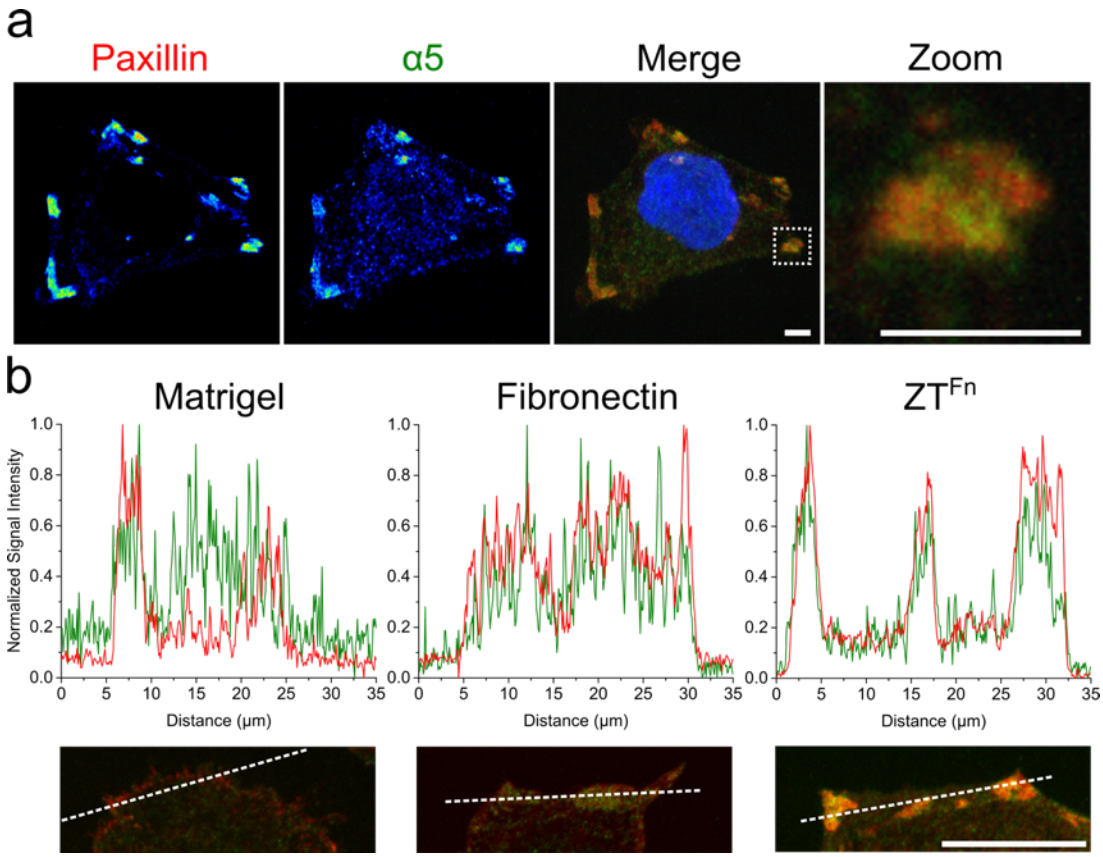


**Figure 60. Colocalisation of integrin α5 subunit with paxillin in hESCs.** (a) Immunofluorescence micrographs show representative z-series projections of HUES7 cells 4 hours post-seeding on $ZT^{Fn}$. Cells were stained for paxillin (*red*), integrin α5 subunit (*green*) and DAPI (*blue*). The right panel shows a zoomed view of the boxed area within the merged panel. 16 colours look up tables were applied to paxillin and α5 micrographs using ImageJ. (b) Fluorescence intensity profiles of α5 (*green line*) and paxillin (*red line*) staining in cells cultured on Matrigel, fibronectin or $ZT^{Fn}$. The profiles from which the plots were generated are shown below (*dashed white line*). Scale bars = 10 μm.

Immunofluorescence staining for the αVβ3 heterodimer did not produce focal adhesion-specific staining on any substrate (data not show). However, using an antibody against the αV subunit alone produced robust staining at the termini of actin filaments in cells cultured on $ZT^{Fn}$, but not on Matrigel or fibronectin (Figure 61). We consequently investigated the presence of the β1 subunit, since αVβ1 is also known to selectively bind fibronectin (Zhang *et al.*, 1993). Once again, no positive staining was observed in cells grown on any of the three substrates (data not shown).

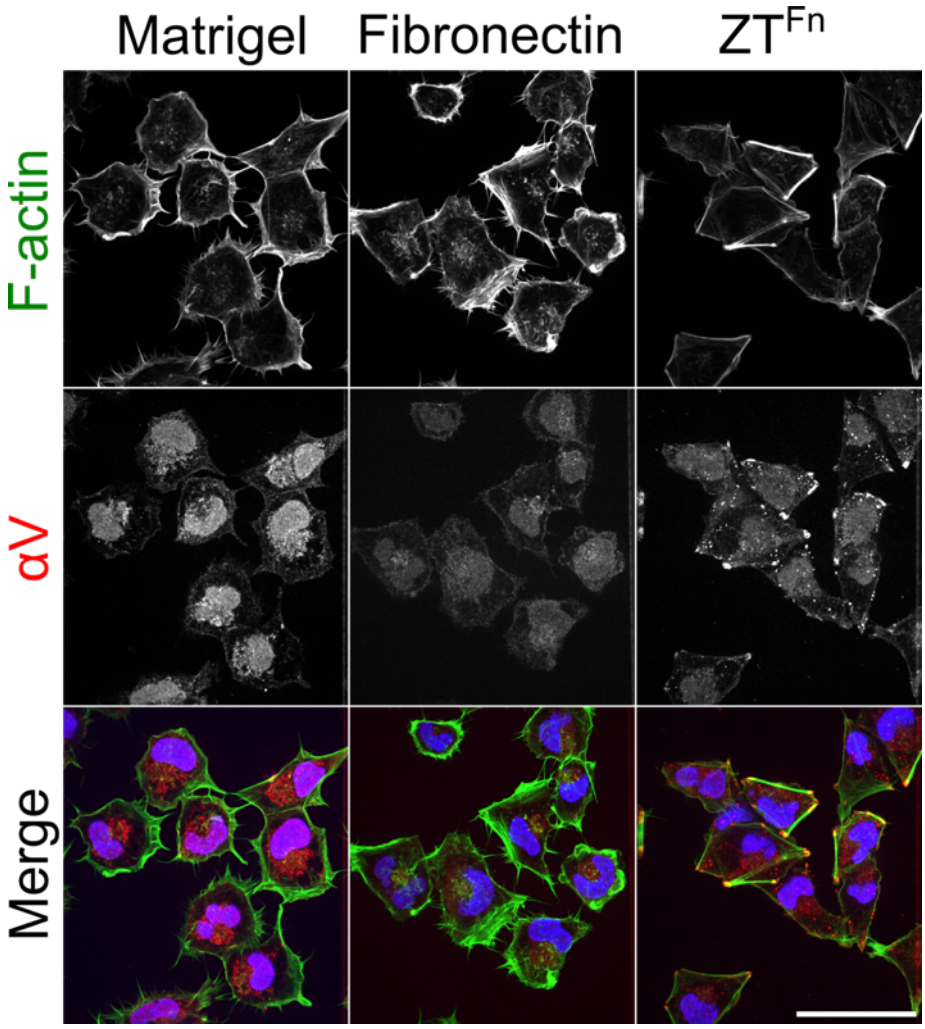


**Figure 61. Staining of hESCs on different substrates for integrin αV subunit.** Representative immunofluorescence z-series projections of HUES7 cells 4 hours post-seeding on Matrigel, fibronectin or $ZT^{Fn}$. Cells were stained for F-actin (*green*) integrin αV subunit (*red*) and DAPI (*blue*). Scale bar = 50 μm.

Intriguingly, cells on $ZT^{Fn}$ contained focal adhesions expressing the unique β5 subunit of the αVβ5 heterodimer, whilst focal adhesions on Matrigel and fibronectin were negative for this integrin (Figure 62). It can therefore be concluded that the initial attachment of HUES7 cells to $ZT^{Fn}$ is facilitated by the combined activation of both α5β1 and αVβ5 integrins, although the potential contribution of other heterodimers not examined cannot be ruled out.

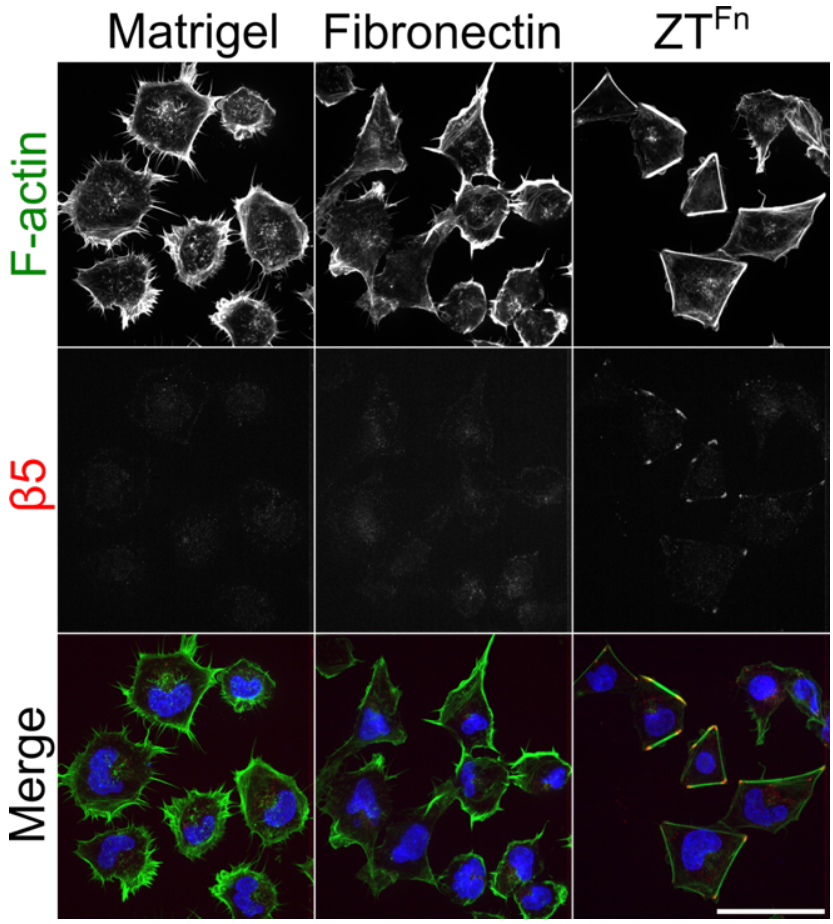


**Figure 62. Staining of hESCs on different substrates for integrin β5 subunit.** Representative immunofluorescence z-series projections of HUES7 cells 4 hours post-seeding on Matrigel, fibronectin or $ZT^{Fn}$. Cells were stained for F-actin (*green*) integrin β5 subunit (*red*) and DAPI (*blue*). Scale bar = 50 μm.

Following two days of culture and early colony formation, HUES7 cells proliferating on $ZT^{Fn}$ continued to express αVβ5 in focal adhesions but α5β1 was absent (Figure 63a,b). On the other hand, cells on Matrigel remained negative for αVβ5 but exhibited definitive staining for α5β1, which appeared more fibrillar than focal in nature (Figure 63a,b). To further explore the appearance of fibrillar adhesion in cells grown on Matrigel, an antibody targeting fibronectin was used since the α5β1 integrin is the primary mediator of fibronectin fibrillogenesis (Ruoslahti and Obrink, 1996). As expected, cells on Matrigel appear to secrete and assemble more soluble fibronectin into insoluble fibrils compared to cells on $ZT^{Fn}$ (Figure 64).

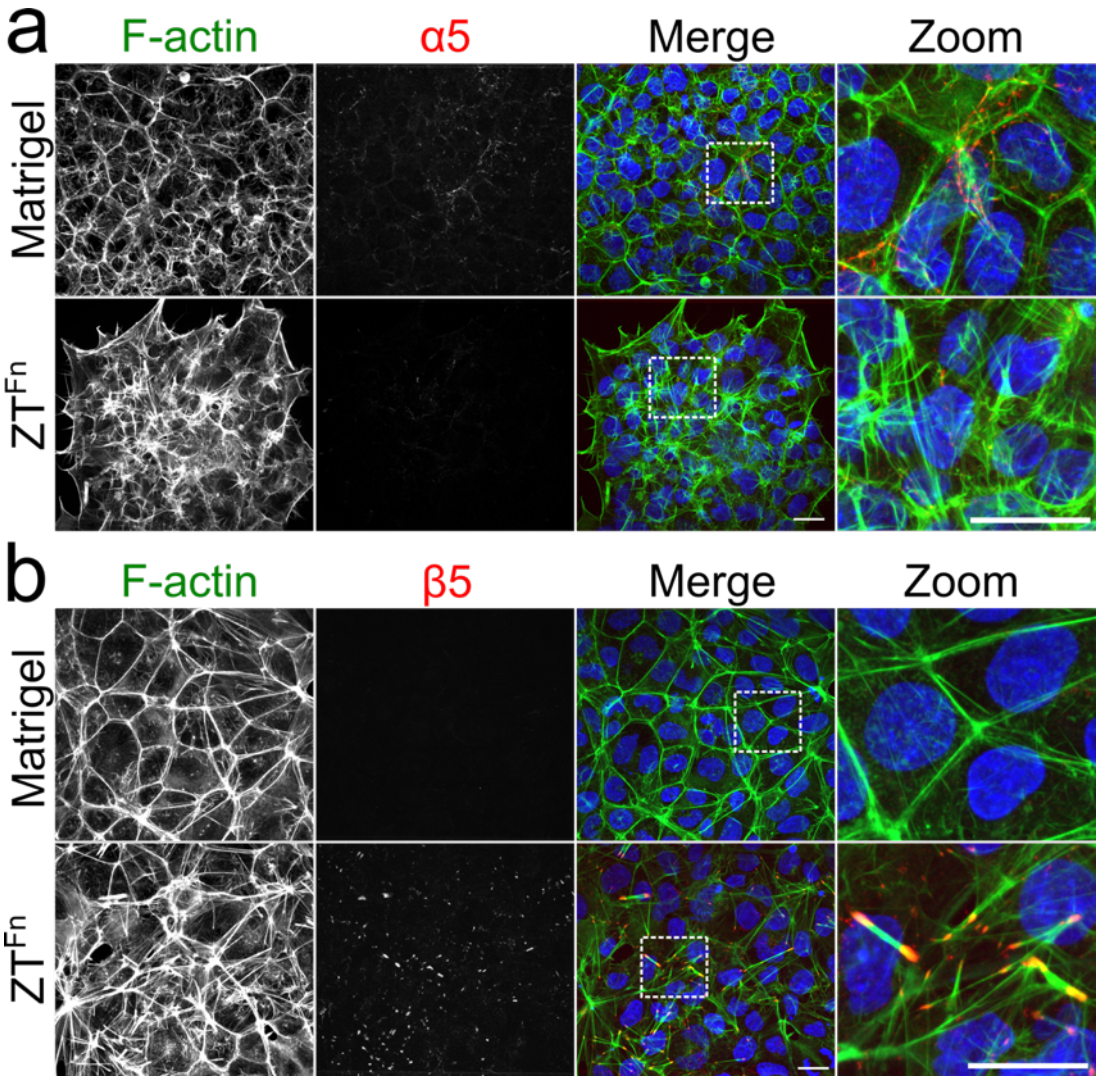


**Figure 63. Integrin engagement by hESCs on different substrates following 2 days of culture.** Immunofluorescence micrographs show representative z-series projections of HUES7 cells cultured on Matrigel or $ZT^{Fn}$. Cells were stained for F-actin (*green*), integrin $\alpha$5 (a) or $\beta$5 (b) subunits (*red*) and DAPI (*blue*). The right panel shows a zoomed view of the boxed area within the merged panel. Scale bars = 25 μm.

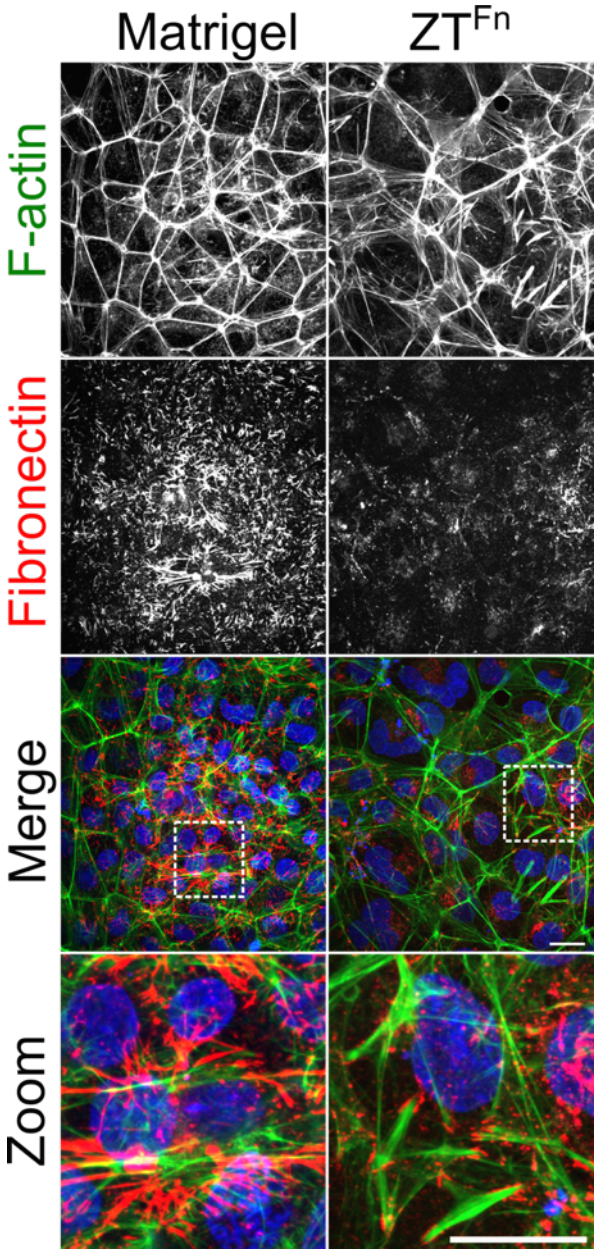


**Figure 64. Staining of hESCs for fibronectin following 2 days of culture on different substrates.** Immunofluorescence micrographs show representative z-series projections of HUES7 cells cultured on Matrigel or $ZT^{Fn}$. Cells were stained for F-actin (*green*), fibronectin (*red*) and DAPI (*blue*). The bottom panel shows a zoomed view of the boxed area within the merged panel. Scale bars = 25 μm.

### *6.2.5 hESC self-renewal on $ZT^{Fn}$*

Following single cell dissociation of HUES7 colonies using an enzymatic reagent (Accutase) and seeding on various substrates for attachment experiments, cells were maintained in culture to investigate survival and morphology. It was found that cells seeded on Matrigel, fibronectin and $ZT^{Fn}$ formed colonies after five days and that most cells exhibited a typical ESC morphology characterised by

prominent nucleoli and a high nuclear to cytoplasmic ratio (Figure 65a). Further, colonies formed on $ZT^{Fn}$ were positive for pluripotency markers octamer-binding transcription factor 4 (OCT4) and NANOG (Figure 65b). Oct4 and NANOG are transcription factors essential for hESC self-renewal (Nichols *et al.*, 1998; Hyslop *et al.*, 2005; Wang *et al.*, 2012). These results suggest that engagement of the αVβ5 integrin via the RGD motif of FnIII 10 is sufficient to promote self-renewal of undifferentiated HUES7 cells in the short term. Therefore, an in-depth study was undertaken to evaluate the prospective use of $ZT^{Fn}$ as a xeno-free substrate for ESC culture.

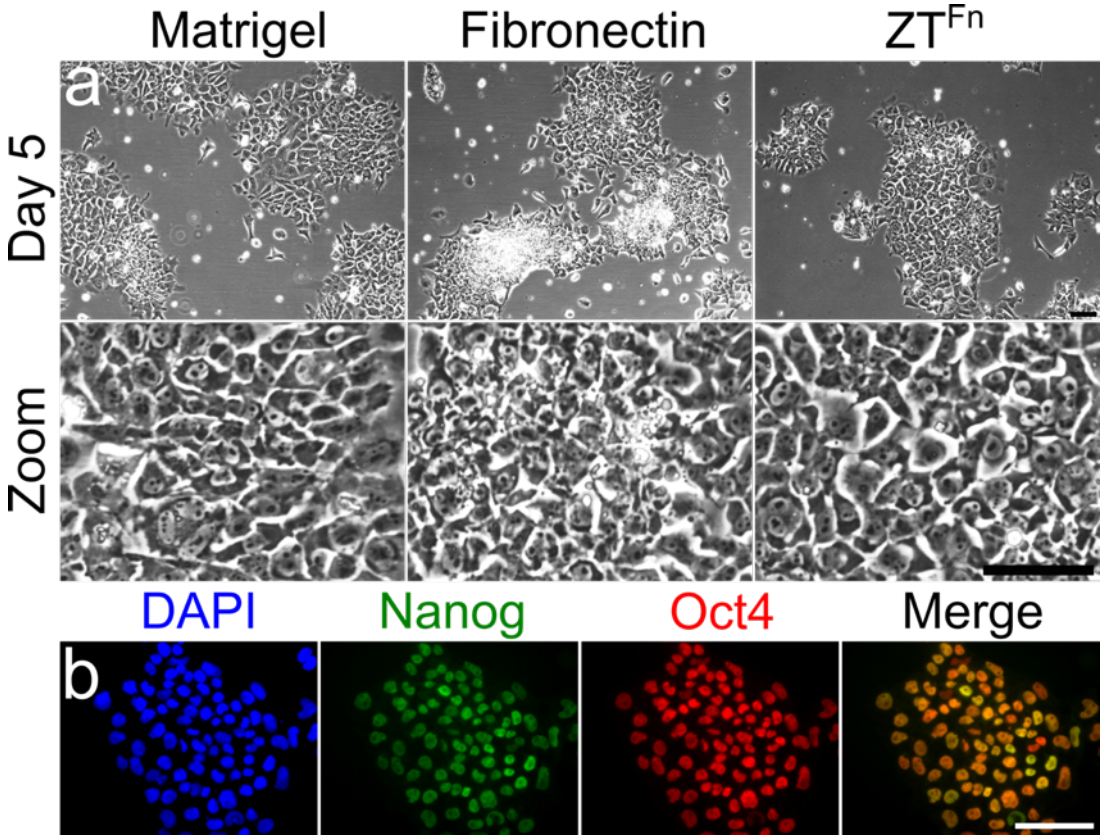


**Figure 65. Colony formation and typical morphology of hESCs cultured on different substrates as a single cell suspension.** (a) Representative phase-contrast micrographs of HUES7 cells grown on Matrigel, fibronectin or $ZT^{Fn}$ after 5 days of culture. The lower panels show zoomed areas to highlight cell morphology. (b) Immunofluorescence images of a colony grown on $ZT^{Fn}$ and stained for pluripotency markers NANOG (*green*) and OCT4 (*red*). Cells were counterstained with DAPI (*blue*) and a merged image of the green and red channels in shown to the right. Scale bars = 100 μm.

Firstly, the ability of $ZT^{Fn}$ to promote clonal survival of HUES7 cells was investigated alongside Matrigel and fibronectin controls (Figure 66a). Clonogenic assays were carried out by Masoumeh Mousavinejad (University of Liverpool). Matrigel supported the most efficient cell survival and colony formation (efficacy of 11.5%), which was significantly higher than fibronectin or $ZT^{Fn}$ ($p < 0.01$). However, $ZT^{Fn}$ did support clonal survival of HUES7 cells at an efficacy comparable to plasma fibronectin ($p = 0.55$). Furthermore, cells on fibronectin appeared to proliferate more quickly than those on $ZT^{Fn}$ as shown by a highly significant ($p < 0.001$) increase in the percentage of well area covered by colonies, despite clonal survival being comparable between the substrates (Figure 66b).

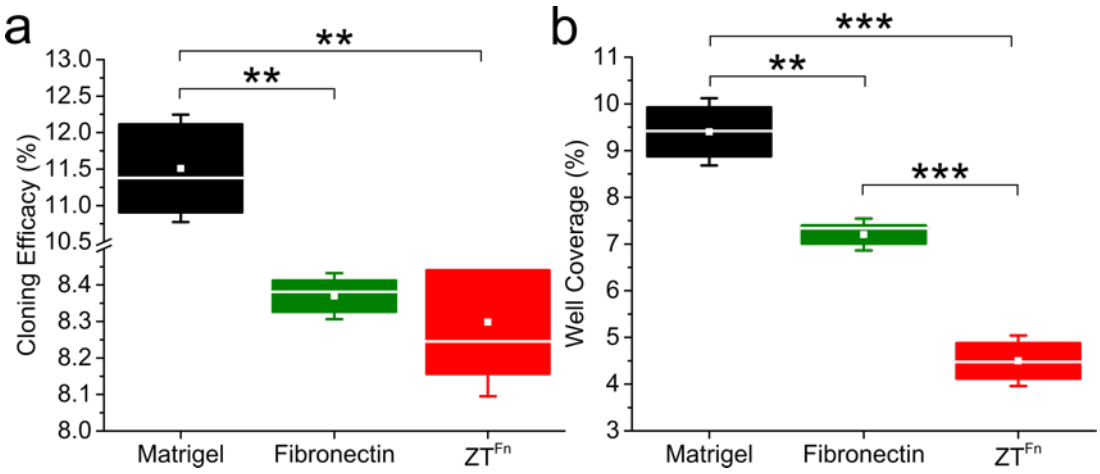


**Figure 66. Clonal survival of hESCs 4 days post-seeding.** (a) Ratios of the number of colonies to the number of cells seeded on Matrigel, fibronectin or $ZT^{Fn}$. (b) Average area of wells covered by colonies. Cells were seeded at a density of 2.5 × $10^3$/$cm^2$. Statistically significant differences were determined by two sample t-tests. Box plots indicate the median (*horizontal line*), mean (*square*), 25$^{th}$ and 75$^{th}$ percentile values (*box ends*) and ± SD (*error bars*; $n = 3$).

The self-renewal of HUES7 cells was evaluated following long-term (18

passages) culture on $ZT^{Fn}$ and control fibronectin. For this, cells previously cultured on Matrigel were seeded on non-TCT polystyrene plates coated with $ZT^{Fn}$ or fibronectin. The cells were passaged by loosening colonies with a non-enzymatic dissociation reagent followed by gentle scraping and trituration to generate aggregates of approximately 50-200 cells. The medium used was mTeSR1 which contains recombinant human fibroblast growth factor 2 (FGF2) and TGF-β 1 for feeder-free maintenance of an undifferentiated phenotype (Ludwig *et al.*, 2006). Figure 67a shows images of HUES7 cells at passages five and ten of culture on $ZT^{Fn}$. The cells were found to adopt a typical morphology and continued to express OCT4 and NANOG (Figure 67b).

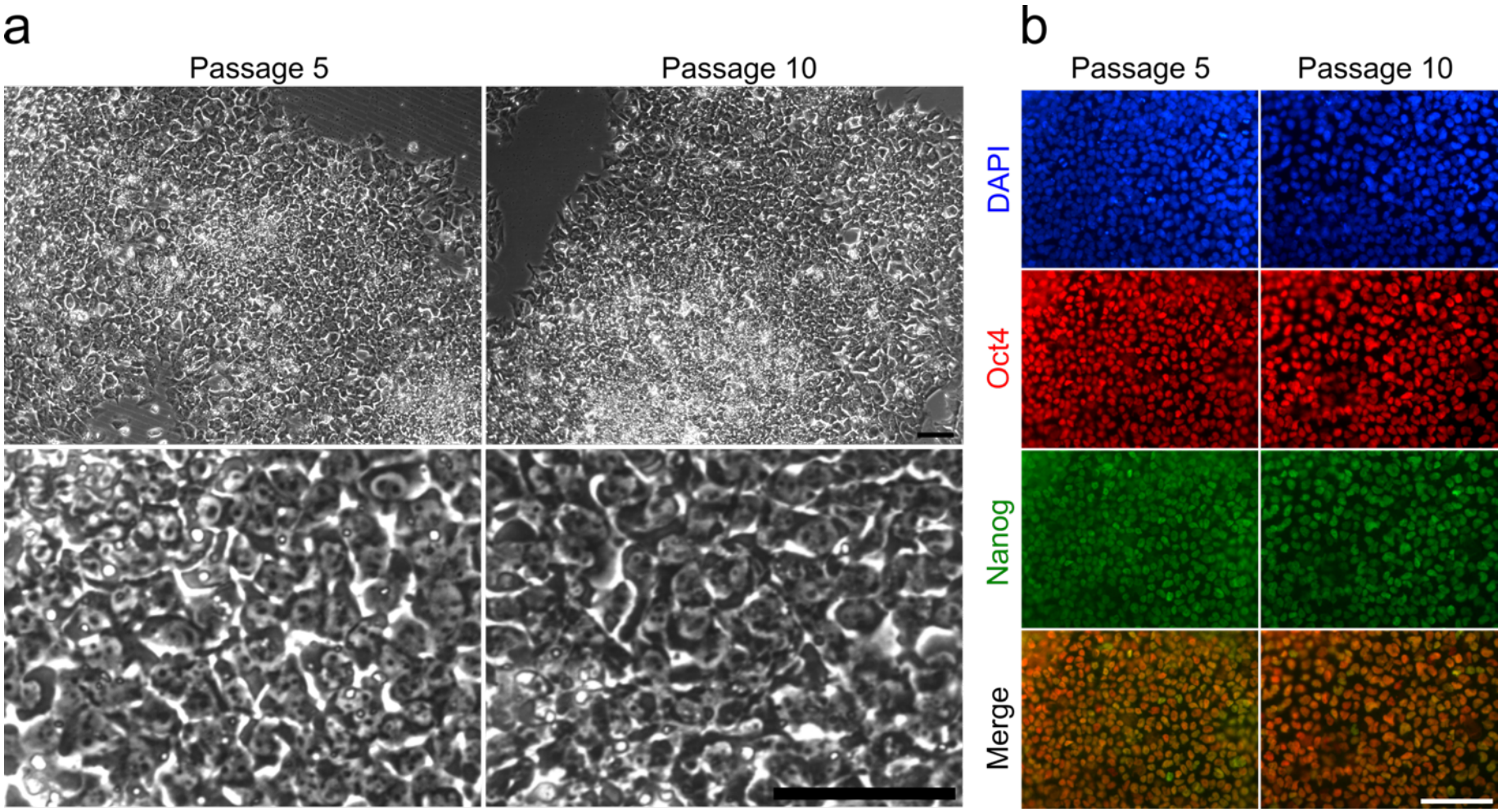


**Figure 67. Long-term culture of hESCs on ZT$^{Fn}$.** (a) Representative phase-contrast micrographs of HUES7 cells cultured for 5 and 10 passages on ZT$^{Fn}$. The lower panels show zoomed areas to highlight cell morphology. (b) Immunofluorescence images of staining for pluripotency markers Oct4 (*red*) and nanog (*green*). Cells were counterstained with DAPI (*blue*) and merged images of the red and green channels are shown in the lower panels. Scale bars = 100 µm.

In order to quantify the level of pluripotency-associated transcription factor gene expression, RT-qPCR analysis was undertaken. Following one or five passages on fibronectin or $ZT^{Fn}$, cultures were assessed for expression levels of *NANOG*, *OCT4* and *SOX2* relative to control cells grown on Matrigel. Like OCT4 and NANOG, sex determining region Y-box 2 (SOX2) is a transcription factor essential for ESC self-renewal (Wang *et al*., 2012). It was found that cells cultured on $ZT^{Fn}$ continue to express all three transcription factors, and no significant differences were observed compared to cells grown on control Matrigel ($p > 0.05$). However, it was noted that expression levels of *SOX2* and *NANOG* were slightly lower in cells cultured on $ZT^{Fn}$ and fibronectin relative to the control (Figure 68).

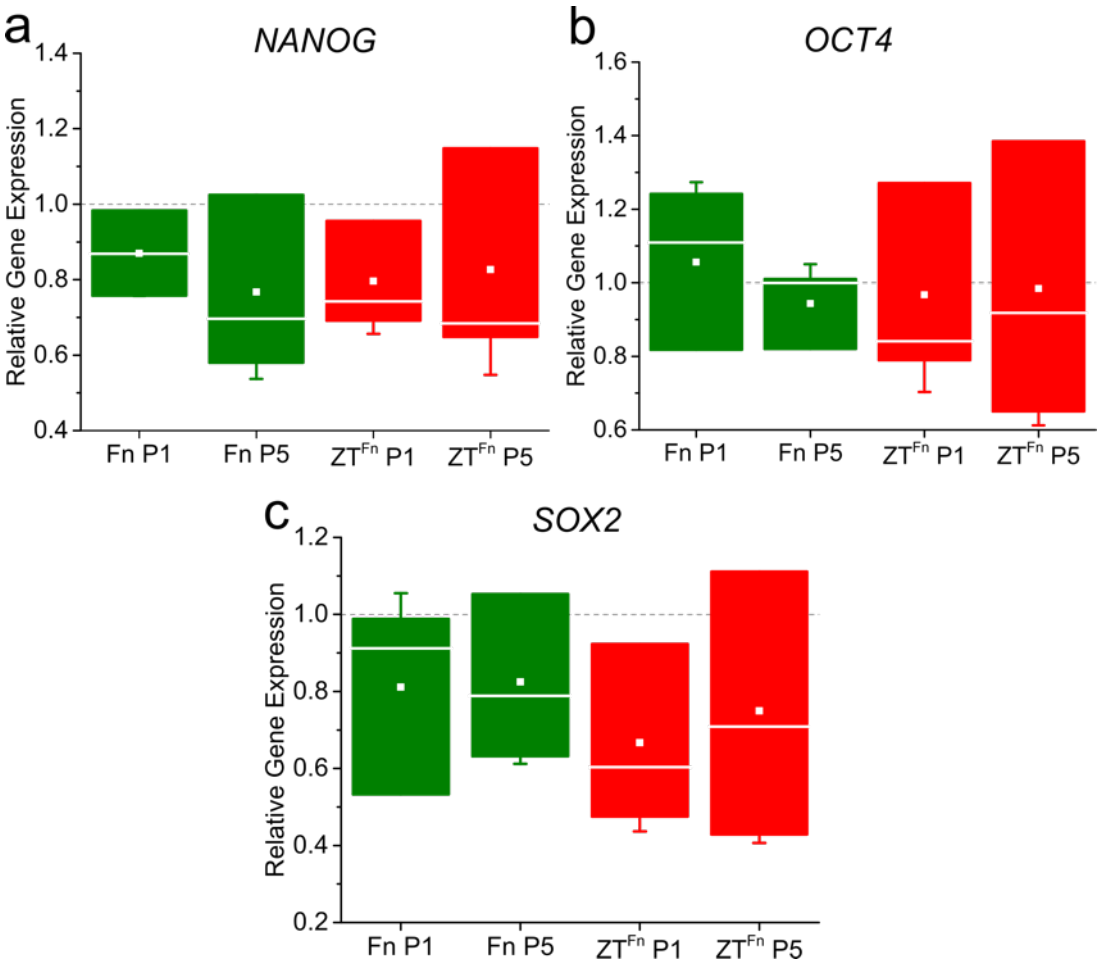


**Figure 68. Relative quantification of pluripotency marker gene expression in hESCs cultured on different substrates for multiple passages.** RT-qPCR analysis of (a) *NANOG*, (b) *OCT4* and (c) *SOX2* gene expression in HUES7 cells passaged 1 (P1) or 5 (P5) times on fibronectin (Fn) or $ZT^{Fn}$. Expression values are normalised to control cells grown on Matrigel (*dashed horizontal line*) using *GAPDH* and *HPRT1* as reference genes. Box plots indicate the median (*horizontal line*), mean (*square*), 25$^{th}$ and 75$^{th}$ percentile values (*box ends*) and ± SD (*error bars*; *n* = 3).

### *6.2.6 Maintenance of hESC pluripotency*

Although HUES7 cells were shown to self-renew on $ZT^{Fn}$ and express key markers of an undifferentiated phenotype, it is also necessary to demonstrate that cells remain pluripotent following culture on novel scaffolds. To this end, HUES7 cells grown on $ZT^{Fn}$ and control fibronectin for thirteen passages were used to generate embryoid bodies (EBs) from single cell suspensions in ultra-low attachment 96 well plates. EB formation and subsequent ESC differentiation was stimulated by

the use of a defined medium called APEL (Albumin Polyvinylalcohol Essential Lipids; Ng *et al.*, 2008). The medium was not supplemented with factors to drive differentiation to a specific germ layer or somatic cell lineage, thus the EBs differentiated under "neutral" conditions. Following seeding and centrifugation to encourage aggregation, EBs were allowed to develop for ten days (Figure 69a) before transferring to a Matrigel-coated dish to promote attachment. After ten days of attachment, cells exhibiting multiple morphologies had begun to grow out from the EBs (Figure 69b) and were subsequently probed for markers of the three embryonic germ layers by immunofluorescence.

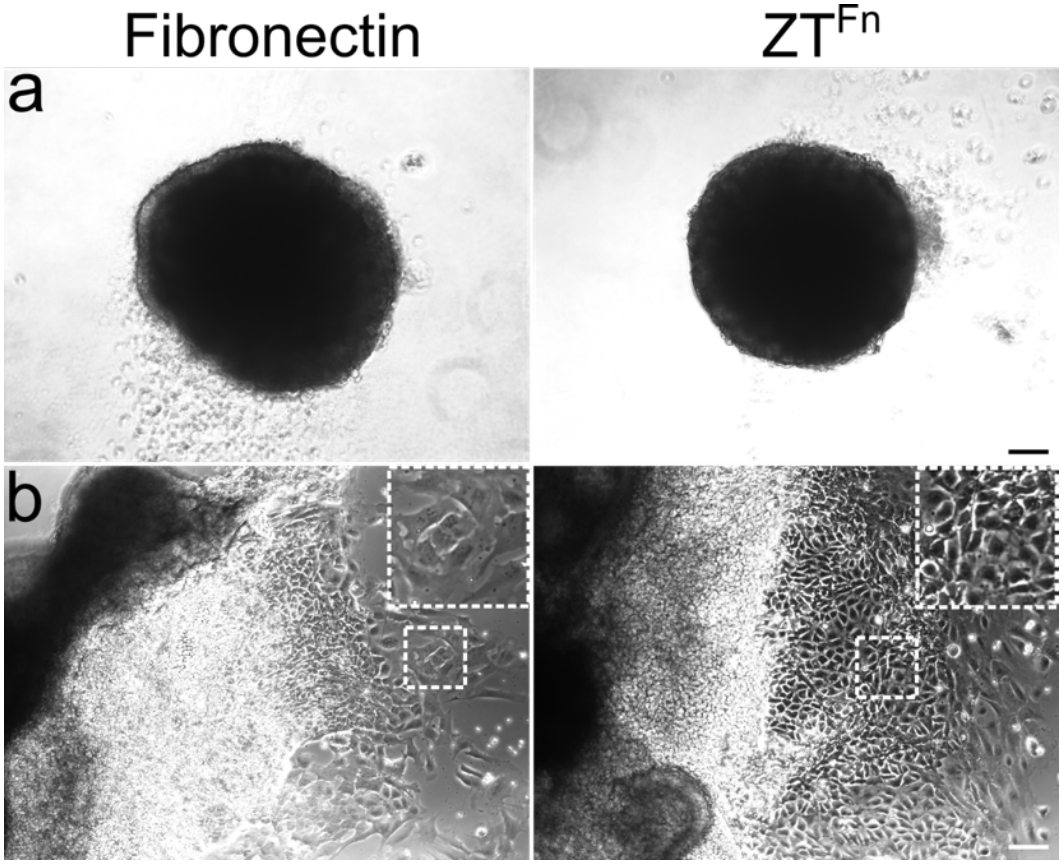


**Figure 69. Derivation of embryoid bodies from hESCs following prolonged cultured on protein substrates.** Representative phase contrast micrographs show EBs differentiated from HUES7 cells cultured on fibronectin or $ZT^{Fn}$ for 13 passages. EBs at day 10 post-aggregation (a) and following a further 10 days of spreading on Matrigel (b) are shown. Zoomed views of the boxed areas are shown in the upper right corners to highlight cell morphology. Scale bar = 100 μm.

The chosen markers were brachyury, GATA-binding transcription factor 6 (GATA6) and nestin to represent mesoderm, endoderm and ectoderm-derived lineages, respectively. Brachyury is a transcription factor with a specific role in mesoderm differentiation during gastrulation (Kavka and Green, 1997). Another transcription factor, GATA6 is a key inducer of both extra-embryonic and definitive endoderm formation (Morrisey *et al.*, 1998; Koutsourakis *et al.*, 1999). Nestin is a class VI intermediate filament protein and marker of neural progenitor cells (Lendahl *et al.*, 1990). Cells derived from both fibronectin (Figure 70a) and $ZT^{Fn}$ (Figure 70b) were found to differentiate to lineages from all three germ layers *in vitro*, confirming the pluripotent nature of ESCs cultured on these substrates.

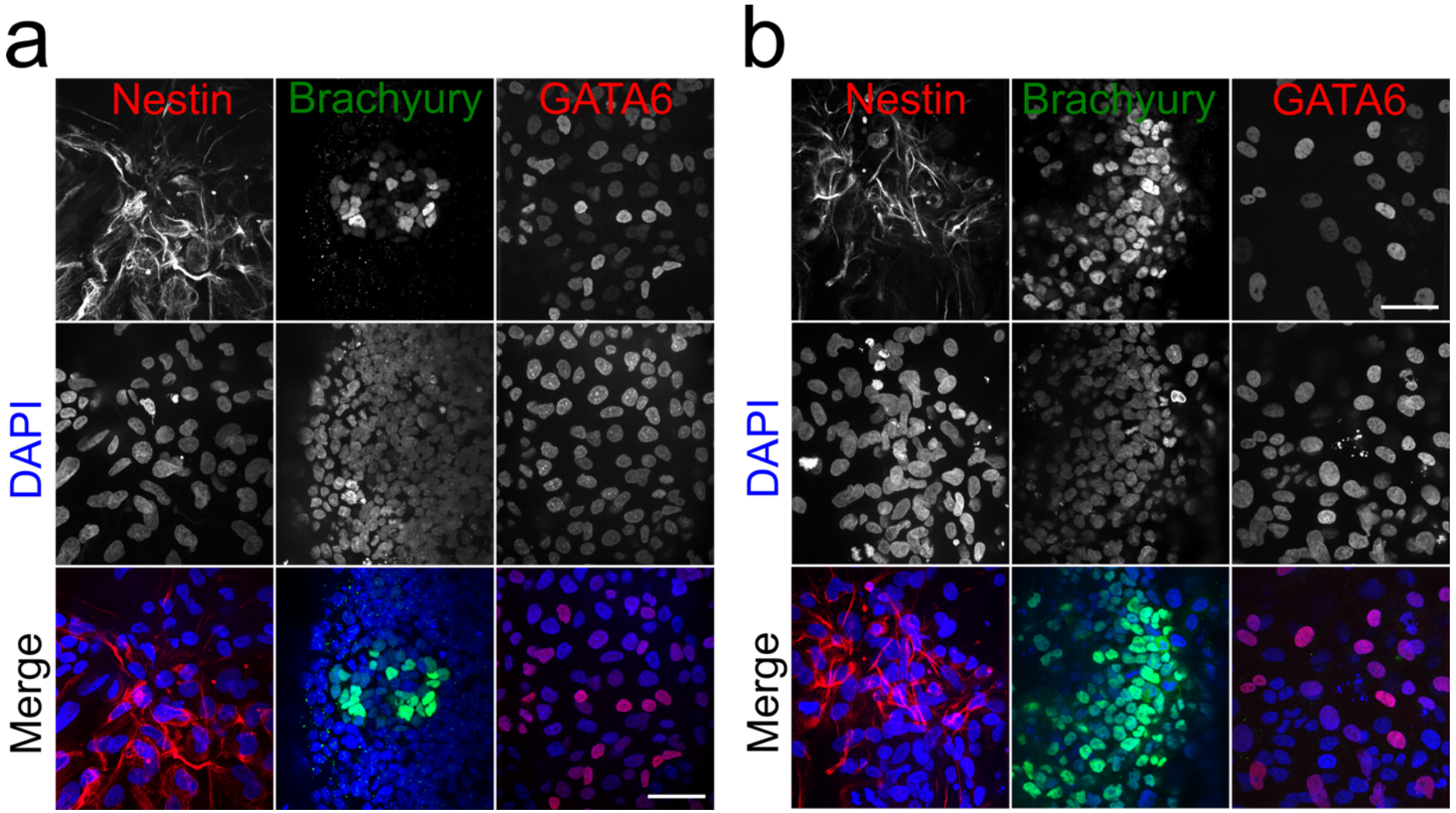
a
Nestin
Brachyury
GATA6
DAPI
Merge
b
Nestin
Brachyury
GATA6
DAPI
Merge

**Figure 70. Characterisation of the differentiation potential of hESCs following prolonged culture on protein substrates.** Immunofluorescence micrographs show representative z-series projections of embryoid body-derived cells stained for markers of the three primary germ layers. HUES7 cells cultured on fibronectin (a) or $ZT^{Fn}$ (b) for 13 passages were used to form embryoid bodies that were subsequently allowed to attach and spread on Matrigel-coated plastic wells. Following 10 days of culture, cells were stained for mesoderm-associated brachyury (*green*), endoderm-associated GATA6 (*red*) or ectoderm-associated nestin (*red*) and counterstained with DAPI (*blue*). Scale bars = 50 μm.

### *6.2.7 Issues with culture on $ZT^{Fn}$*

Despite the successful propagation of pluripotent HUES7 cells on $ZT^{Fn}$, issues with the culture protocol were noted. Firstly, cells on both fibronectin and $ZT^{Fn}$ had a tendency to aggregate when nearing confluency. This resulted in larger than desired clumps of cells when passaging, because excessive shear force and/or non-enzymatic dissociation was required to separate the aggregates, which is undesirable when working with sensitive cell types. Larger aggregates would often attach to the protein substrates (Figure 71a), thus perpetuating the issue upon subsequent passaging. However, cells on Matrigel rarely formed such aggregates. Secondly, cells on both fibronectin and $ZT^{Fn}$ were prone to spontaneous differentiation (Figure 71b). It should be noted that differentiated regions were not manually removed throughout the course of this study, however, replicates were discarded where the proportion of pluripotent cells was less than ~90% of the population. Although spontaneous differentiation was observed on $ZT^{Fn}$ (particularly around the periphery of aggregates), a similar level was noted in cells cultured on fibronectin. Further, a small degree of differentiation is considered normal in ESC cultures (Kent, 2009) and cells on Matrigel also displayed this characteristic.

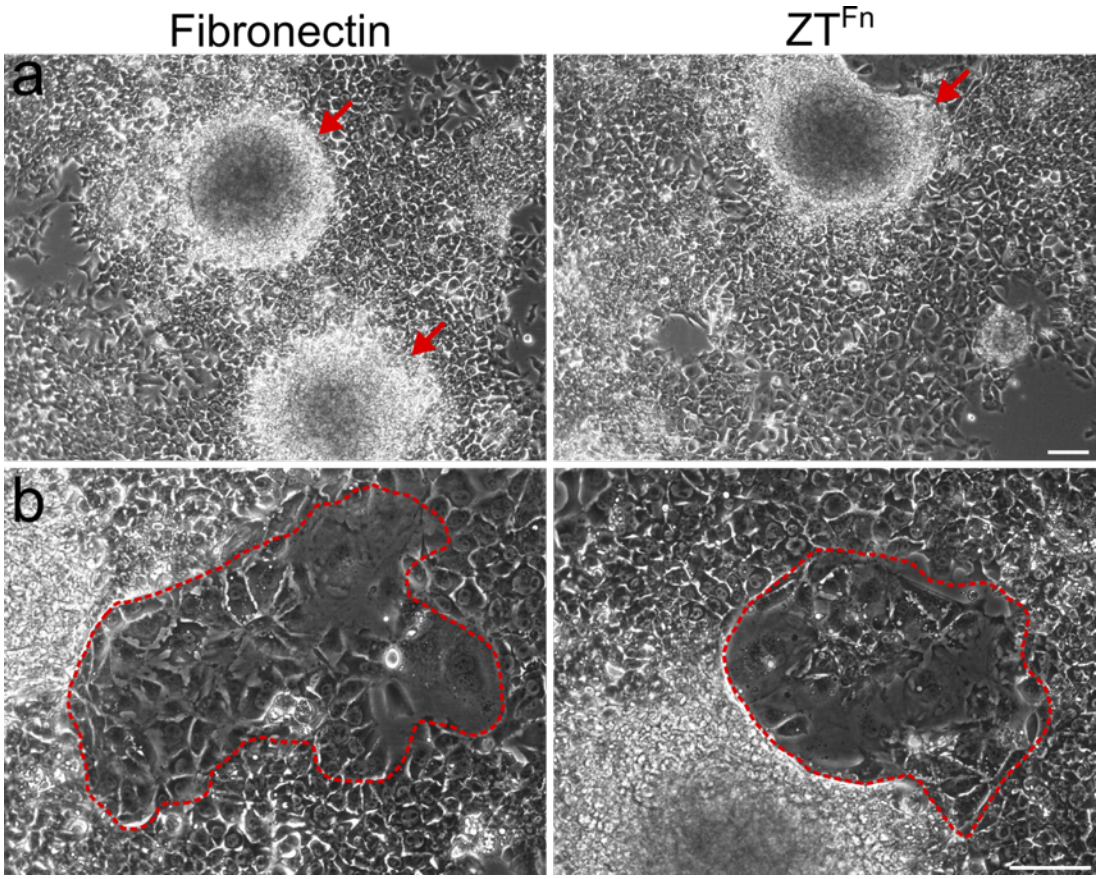


**Figure 71. hESC aggregation and spontaneous differentiation on protein substrates.** Representative phase contrast micrographs show HUES7 cells cultured on fibronectin or $ZT^{Fn}$ for 6 passages. (a) Multilayered aggregates of cells (*red arrows*) were observed to form on both substrates. (b) Areas of spontaneous differentiation (*red dashed lines*) surrounded by pluripotent stem cells. Scale bars = 100 µm.

The cause of cell aggregation when cultured on fibronectin or $ZT^{Fn}$ may be an effect of the non-TCT polystyrene. Indeed, several hESC lines have been cultured successfully on TCT vessels coated with fibronectin without reports of cell detachment or aggregation (Liu *et al.*, 2006; Baxter *et al.*, 2009). Untreated polystyrene is a highly hydrophobic polymer, which does not readily encourage cell attachment, thus culture vessels are treated to introduce a hydrophilic surface chemistry (Ramsey *et al.*, 1984). The hydrophilic surface encourages the adsorption of serum components such as fibronectin and vitronectin to which cells can attach.

## 6.3 Discussion

The attachment of HUES7 cells to $ZT^{Fn}$ was an exciting result because no previous studies (to the best of our knowledge) have investigated the use of a recombinant fibronectin fragment for hESC self-renewal. Although cell attachment to $ZT^{Fn}$ was noticeably lower than Matrigel, it was not significantly different to control full-length human plasma fibronectin. The fact that cells attached to $ZT^{Fn}$, but not $ZT^{RGD}$ is intriguing; it has been shown that HUES7 cells do not attach to linear RGD peptides on silanised surfaces (Kalaskar *et al.*, 2013). It was hypothesised that the lack of adhesion was due to an inaccessible conformation of the peptide induced by the coating protocol or that HUES7 cells require additional peptidic sequences of fibronectin for integrin engagement. The fact that HUES7 cells attached to $ZT^{Fn}$ would suggest that only the RGD-containing FnIII 10 domain is required. Further, the failure of $ZT^{RGD}$ to promote attachment supports the hypothesis that the precise conformation of the RGD motif in FnIII 10 is required for successful integrin engagement in this cell line. It was noted during the attachment assays that cells on $ZT^{Fn}$ presented a distinctive angular morphology when compared to other substrates. The observed difference was supported by an increase in the AR of cells cultured on $ZT^{Fn}$, indicating asymmetric spreading on this substrate. Visualisation of the actin cytoskeleton and focal adhesions revealed that cells on $ZT^{Fn}$ form thick stress fibres terminating in large focal adhesions. However, stress fibre arrangement was not typical of those seen in migrating cells; rather they defined the cell periphery. It was hypothesised that $ZT^{Fn}$ adsorption to polystyrene had created a stiffer substrate than Matrigel or fibronectin, thus influencing cytoskeletal organisation. However, zyxin was not mobilised to stress fibres,

suggesting that external stimulus is not the causative factor (Yoshigi *et al.*, 2005). Therefore, integrin expression on different substrates was investigated to dissect heterodimer-specific engagement by $ZT^{Fn}$.

Cells cultured on $ZT^{Fn}$ were found to engage αVβ5 and, to a lesser extent, α5β1. α5β1 expression was considered less robust than αVβ5 because staining was visually less intense for the former. Cells grown on Matrigel or fibronectin did not display specific staining for these integrins. This was expected in the case of Matrigel since PSCs interact with this substrate primarily through the laminin receptor α6β1 (Meng *et al.*, 2010). However, HUES7 attachment to fibronectin has previously been shown to require α5β1 engagement (Kalaskar *et al.*, 2013), thus the absence of specific staining on this substrate was unexpected. αVβ5 is a receptor for vitronectin (Smith *et al.*, 1990) and binds via the RGD motif located immediately C-terminal to the Somatomedin-B domain (Kim *et al.*, 1994; Schvartz *et al.*, 1999). Unlike fibronectin, the motif in vitronectin is positioned within an unstructured region of the protein (Mayasundari *et al.*, 2004). Human PSC attachment to both plasma-derived and recombinant vitronectin was mediated by αVβ5 (Braam *et al.*, 2008; Prowse *et al.*, 2010; Rowland *et al.*, 2010). hiPSCs were again found to interact with the vitronectin-derived peptide in Synthemax via αVβ5 (Jin *et al.*, 2012). Intriguingly, iPSCs exhibited broader actin filaments and an upregulation of zyxin on Synthemax compared to cells on Matrigel, the former of which is consistent with our observations of HUES7 cells engaging αVβ5 through $ZT^{Fn}$. There is no compelling evidence for the binding of fibronectin to αVβ5 either *in vitro* or *in vivo*. HUES1 cells have been shown to express α5, αVβ3, α6 and β1 but not αVβ5 when cultured on fibronectin (Soteriou *et al.*, 2013). Furthermore, unlike α5β1, which has a proven role in mechanotransduction and stress fibre formation via reactivation of

RhoA (Danen *et al.*, 2002), little is known about the effects of αVβ5 engagement on cytoskeletal remodelling.

Although immunostaining for αVβ5 was conclusive due to the presence of the heterodimer-specific β5 subunit, other αV-containing integrins known to bind the fibronectin RGD motif, αVβ1 and αVβ6 (Humphries *et al.*, 2006), were not investigated. Targeting the β1 subunit did not produce specific staining despite probing with three different monoclonal antibodies, suggesting that αVβ1 is not involved in adhesion to Matrigel, fibronectin or $ZT^{Fn}$. However, attachment to Matrigel via the hypothetical engagement of α6β1 and the presence of α5 staining in cells attached to $ZT^{Fn}$ is convincing evidence that the β1 subunit is present, thus positive staining would be expected. Therefore, $ZT^{Fn}$ induced expression of αVβ1 and αVβ6 in focal adhesions cannot be ruled out. It is interesting to note that cells on Matrigel appear to express more fibronectin than those attached to $ZT^{Fn}$, which on the former are assembled into fibrillar adhesions containing α5β1. Braam *et al.* (2008) observed the secretion of fibronectin by hESCs on feeder layers, but suggest that the majority was sourced from differentiated cells. The production of endogenous fibronectin is essential for murine ESC self-renewal on gelatine, to which the cells originally attach via fibronectin derived from serum (Hunt *et al.*, 2012). However, the role of fibronectin expression and fibrillation has not been explored in the context of hESC self-renewal. The results generated in the current study suggest that the level of fibronectin secretion observed on Matrigel is not necessary for maintenance of an undifferentiated phenotype on $ZT^{Fn}$. It may be that increased fibronectin expression is induced by factors present in Matrigel, since it is highly heterogeneous in nature and contains multiple ECM proteins and soluble factors.

The seemingly novel observation of FnIII 10 binding to αVβ5 poses many additional questions. Firstly, is the presentation of the RGD motif somehow altered in the context of $ZT^{Fn}$ to induce a preferential switch for αVβ5 engagement? Indeed, the specific conformations of adsorbed fibronectin on different synthetic surfaces were shown to have a dramatic effect on integrin specificity (Keselowsky *et al.*, 2003). It may be that the loop is structurally restrained within the assembly, or that the titin-derived components have a contributory effect on αVβ5 recruitment caused by the overall shape of the assembly or an unexpected synergistic interaction with the integrin. Secondly, is αVβ5 engagement alone responsible for the unique morphology observed on $ZT^{Fn}$ or is this a combinatorial effect of both αVβ5 and α5β1? It would be enlightening to inhibit αVβ5 with blocking antibodies to elucidate its contribution to HUES7 cell attachment to $ZT^{Fn}$ and determine whether α5β1 alone is sufficient for adhesion. Further, if the unique morphology is reverted to a more typical profile, one could conclude that αVβ5 is responsible for stress fibre formation. An alternative hypothesis is that $ZT^{Fn}$ is clustered upon deposition, making for discreet adhesion spots to which robust focal plaques are formed. This could account for the larger focal adhesions observed in cells attached to $ZT^{Fn}$, through which force could be propagated by actomyosin contraction and subsequent stress fibre formation. The distribution of $ZT^{Fn}$ on polystyrene surfaces could potentially be probed using a fluorophore-conjugated antibody against the titin component of the scaffold.

HUES7 cells were observed to form colonies on $ZT^{Fn}$ from single cell suspensions and the clonogenic potential of these cells was comparable to human plasma fibronectin, although colonies formed on $ZT^{Fn}$ were significantly smaller than those formed on fibronectin. This difference may be the result of a more

compact morphology of colonies induced by $ZT^{Fn}$, or could indicate a difference in cell growth rates between the substrates. Thus, proliferation assays are required to investigate HUES7 cell doubling time when cultured on $ZT^{Fn}$. Furthermore, ROCK inhibitor was not required for survival or self-renewal (Watanabe *et al.*, 2007). Encouraged by these results, we investigated the effects of long-term culture on $ZT^{Fn}$. The majority of cells continued to exhibit nuclear expression of OCT4 and NANOG whilst retaining a characteristic morphology over ten passages. Cells passaged five times on $ZT^{Fn}$ and fibronectin presented a slight decrease of *NANOG* and *SOX2* transcript levels compared to Matrigel, however, the differences were not significant. Unfortunately, RT-qPCR analysis at later passages (more than ten) was beyond the scope of this project. However, it would be enlightening to quantify pluripotency marker expression levels at later passages to determine whether they continue to decrease or stabilise as the cells adapt to the substrate.

HUES7 cells retained a pluripotent phenotype following prolonged (thirteen passages) culture on $ZT^{Fn}$, as demonstrated by the presence of lineages from all three embryonic germ layers following differentiation. However, cells in culture are prone to the development of chromosomal abnormalities and human PSCs are no exception. Many studies have investigated the effects of culture environments on the genetic stability of hESCs and hiPSCs, revealing a loss of heterozygosity under a variety of conditions (Maitra *et al.*, 2005; Mayshar *et al.*, 2010; Närvä *et al.*, 2010; Garitaonandia *et al.*, 2015). Aberrations are commonly observed in chromosomes 12, 17 and X that are similar to those found in germ cell tumours (Närvä *et al.*, 2010). Evidently, the genetic stability of PSCs cultured on novel substrates must be validated before such substrates could be utilised for scale-up and clinical application of stem cells. Therefore, cells grown on $ZT^{Fn}$ should be karyotyped to

ensure that the substrate is not inducing chromosomal abnormalities before concluding that this substrate is suitable for ESC culture. There are several techniques commonly employed in karyotype analysis. The most conventional method, G-banding, is the least sensitive and can detect aneuploidy, mosaicism and gross chromosomal aberration. More recently, fluorescence *in situ* hybridisation probes have allowed for the detection of chromosomal abnormalities at 1-2 Mb resolution. Higher resolution yet can be achieved by gene arrays, which can detect deletions, insertions, amplifications and duplications (Rebuzzini *et al*., 2015).

The fact that HUES7 cells have a propensity to aggregate when cultured on $ZT^{Fn}$ and fibronectin adsorbed on non-TCT plastic is problematic for cell propagation. It may be that the decrease in fibronectin secretion observed on $ZT^{Fn}$ is responsible, meaning that cells are not robustly anchored to the substrate by their own ECM. Alternatively, secreted ECM proteins may not adsorb sufficiently to the hydrophobic polystyrene surface, or a combination of both factors. Increasing the coating concentration of $ZT^{Fn}$ may help to mitigate this problem.

# Chapter 7

# General discussion and future perspectives

The design of biomaterials that best mimic the natural ECM is an ongoing pursuit in the fields of biotechnology and regenerative medicine. Due to their modular architecture and amenability to functionalisation, protein-based systems may be advantageous in this regard.

The current work has demonstrated the functionalisation potential of the ZT nanofibre system and its applicability to cell-based applications. An important attribute of this system is the heterologous expression of its components in bacteria, since *E. coli* high density fermentation is the method of choice for recombinant protein production at an industrial level (Sørensen and Mortensen, 2005; Sahdev *et al.*, 2008). By genetically encoding an RGD motif in the CD-loop of Z1, the potential of this site to successfully present a bioactive moiety in the context of $ZT^{RGD}$ could be evaluated *in vitro*. Additionally, protein domain exhibition was explored in the form of $ZT^{Fn}$ by the generation of a fusion chimera containing FnIII 10 from fibronectin. Crucially, these diversifications were well tolerated structurally and did not inhibit assembly. Furthermore, loop grafting and domain fusion did not negatively affect protein yield, an important factor when considering the need for a high ratio of protein to bacterial cell mass to feasibly translate the technology to cell-based applications.

In Chapter 4, the bioactivity and accessibility of adhesive motifs in ZT variants were investigated using mMSCs. Here, the successful exhibition of the RGD motifs were confirmed through mMSC attachment and focal adhesion formation when cultured on adsorbed $ZT^{RGD}$ and $ZT^{Fn}$. However, reduced cell

spreading and differences in cell morphology associated with the initial stages of mMSC attachment to $ZT^{RGD}$ were suggestive of reduced integrin avidity in this variant. By solving the partial crystal structure of $Z_{1212}{}^{RGD}$, it was envisioned that the specific conformation of the motif in the CD-loop could be determined and modified accordingly. Although the grafted loop could not be resolved, crystallisation of the protein emphasised the applicability of high resolution structural techniques to the system, which may allow for the structure-based rational improvement of future variants.

A specific goal of ZT nanofibre functionalisation was to induce MSC chondrogenesis for cartilage tissue engineering and treatment of osteoarthritis. Unfortunately, osteogenic differentiation of mMSCs was observed when cultured on $ZT^{RGD}$, and this phenotypic change appeared to be an artefact of the culture conditions rather than an effect of the substrate. These results highlighted the need for an alternative culture environment or additional chondroinductive cues for success in this aspect of the project. To this end, diversification of the Z1 CD-loop and β-strand B was undertaken to produce decorin and N-cadherin chimeras, respectively. However, due to time constraints, the bioactivity of $ZT^{HAVD}$ and $ZT^{KLER}$ was not characterised.

A disadvantage of the ZT nanofibre system in its current form is that it does not constitute a mechanically stable 3D scaffold for cell encapsulation. Such environments are often advantageous since they better replicate the *in vivo* situation (Ravi *et al.*, 2015). In the field of cartilage tissue engineering, 3D scaffolds (reviewed in section 4.1.2) have proven invaluable as customisable inducers of MSC chondrogenesis. Furthermore, such scaffolds are more applicable to clinical translation since they can be implanted at the site of injury. Therefore, a future

strategy for exploitation of bioactive ZT nanofibres could be their amalgamation with existing 3D scaffolds to generate nanocomposite materials.

During the initial design of ZT nanofibres, it was intended that each building block would incorporate multiple bioactivities, thereby imbuing a degree of tailorability on the system in terms of the topographical distribution and nature of functional moieties. In the current work, monofunctionalisation of $Z_{1212}$ components was achieved, but multifunctionalisation was not explored. Indeed, functionalities from fibronectin, N-cadherin and decorin were chosen with this objective in mind, because they represent a repertoire of cell-cell, cell-matrix and matrix-matrix interaction modulation involved in chondrogenic differentiation and cartilage homeostasis ( Oberlender and Tuan, 1994a; Oberlender and Tuan, 1994b; Bock *et al.*, 2001; Singh and Schwarzbauer, 2014). Although different monofunctionalised $Z_{1212}$ molecules could have been mixed to diversify the resultant assemblies, this route was not pursued since "doping" would remove control of functional group periodicity and may cause clustering. Therefore, it will be necessary to diversify different sites on the same module, for example the CD-loops of both Z1 and Z2 domains, to fully explore the multifunctionalisation potential of the system.

As discussed in Chapter 5, grafting the decorin KLER motif in the Z1 CD-loop was well tolerated in terms of recombinant protein yield and stability. However, the generation of $Z_{1212}^{HAVD}$ by β-strand B modification caused a significant quantity of the protein to become insoluble, most likely through domain destabilisation. This issue highlighted the sensitivity of certain sites in the Ig domains to residue substitution, and stimulated the contemplation of methods for more rationally devised chimeras. Computer software designed to predict the effects of residue

mutation on protein stability was not applied in the current work. However, algorithms have been developed to estimate energy changes upon residue mutations and alterations in fold stability, which could be implemented in the future generation of ZT variants (Topham *et al.*, 1997; Quan *et al.*, 2016). Experimentally, changes in protein stability could be observed by differential scanning fluorimetry, a high throughput technique that could quickly characterise multiple variants. Additionally, more intricate bioinformatics tools could be utilised to model the likely conformation of exogenous peptides, their dynamics, the effects of grafting location and influence of flanking residues (Bakan *et al.*, 2011; Jamroz *et al.*, 2013; Webb and Sali, 2014). These parameters could also be studied experimentally using biophysical techniques such as X-ray crystallography and NMR.

In Chapter 6, the self-renewal of hESCs when cultured on $ZT^{Fn}$ is described. It was found that HUES7 cells could attach and spread on $ZT^{Fn}$ at rates comparable to human plasma fibronectin, and that the cells acquired a unique morphology when cultured on the recombinant substrate. The formation of large focal adhesion foci and actin stress fibres in cells cultured on $ZT^{Fn}$ was likely caused by the engagement of αVβ5 and α5β1 integrins. These findings were highly interesting as there have been no in-depth studies into the role of αVβ5 in mechanotransduction and cytoskeletal remodelling. Thus, the HUES7-$ZT^{Fn}$ culture system could potentially be used to study the effects of αVβ5 engagement on Rac1 and RhoA dynamics. Importantly, changes in cell morphology did not correlate with a loss of embryonic phenotype. Following 5 passages on $ZT^{Fn}$, HUES7 cells expressed key pluripotency markers at levels comparable to cells grown on Matrigel and could differentiate to lineages from the three primary germ layers after 13 passages. These findings were highly supportive for the use of $ZT^{Fn}$ as an alternative substrate for ESC propagation.

Evidently, these conclusions will need to be validated using a range of ESC and iPSC lines with different media to ensure that the findings are not exclusive to HUES7 cells cultured in mTeSR™1 medium. If $ZT^{Fn}$ can support the self-renewal of a range of PSC lines, it is envisioned that production of the substrate could be scaled up by an industrial partner and marketed. Compared to currently available protein substrates produced in mammalian expression systems, the high yield production of $ZT^{Fn}$ in *E. coli* may make the substrate a cheaper alternative. As such, $ZT^{Fn}$ could be utilised in research for high throughput screening of PSCs, or possibly in the propagation of clinical-grade PSCs for therapeutic application.

On a final note, rapid advances in synthetic biology and recombinant protein production are fuelling a resurgence in protein-based technologies. The discrete functional architecture of polyproteins native to the ECM means that they may be dissected at the molecular level to produce novel substrates imbued with defined functions. However, such approaches are as yet underexploited but could represent a new generation of biomaterial scaffolds on the horizon.

# Bibliography

Adams, D. J. and Topham, P. D. (2010) 'Peptide conjugate hydrogelators', *Soft Matter*, 6(16), pp. 3707–3721.

Adams, P. D., Afonine, P. V., Bunkóczi, G., Chen, V. B., Davis, I. W., Echols, N., Headd, J. J., Hung, L. W., Kapral, G. J., Grosse-Kunstleve, R. W., McCoy, A. J., Moriarty, N. W., Oeffner, R., Read, R. J., Richardson, D. C., Richardson, J. S., Terwilliger, T. C. and Zwart, P. H. (2010) 'PHENIX: A comprehensive Python-based system for macromolecular structure solution', *Acta Crystallographica Section D: Biological Crystallography*, 66(2), pp. 213–221.

Ajeian, J. N., Horton, E. R., Astudillo, P., Byron, A., Askari, J. A., Millon-Frémillon, A., Knight, D., Kimber, S. J., Humphries, M. J. and Humphries, J. D. (2016) 'Proteomic analysis of integrin-associated complexes from mesenchymal stem cells', *Proteomics - Clinical Applications*, 10(1) pp. 51–57.

Akiyama, H., Chaboissier, M. C., Martin, J. F., Schedl, A. and De Crombrugghe, B. (2002) 'The transcription factor Sox9 has essential roles in successive steps of the chondrocyte differentiation pathway and is required for expression of Sox5 and Sox6', *Genes and Development*, 16(21), pp. 2813–2828.

Amet, N., Lee, H. F. and Shen, W. C. (2009) 'Insertion of the designed helical linker led to increased expression of Tf-based fusion proteins', *Pharmaceutical Research*, 26(3), pp. 523–528.

Angst, B. D., Marcozzi, C. and Magee, A. I. (2001) 'The cadherin superfamily: diversity in form and function', *Journal of Cell Science*, 114(4), pp. 629–641.

Aota, S. I., Nagai, T. and Yamada, K. M. (1991) 'Characterization of regions of fibronectin besides the arginine-glycine-aspartic acid sequence required for adhesive function of the cell-binding domain using site-directed mutagenesis', *Journal of Biological Chemistry*, 266(24), pp. 15938–15943.

Argos, P. (1990) 'An investigation of oligopeptides linking domains in protein tertiary structures and possible candidates for general gene fusion', *Journal of Molecular Biology*, 211(4), pp. 943–958.

Arikawa,-Hirasawa, E., Watanabe, H., Takami, H., Hassell, J. R. and Yamada, Y. (1999) 'Perlican is essential for cartilage and cephalic development', *Nature Genetics*, 23(3), pp. 354-358.

Arnaout, M. A., Mahalingam, B. and Xiong, J.-P. (2005) 'Integrin Structure, Allostery, and Bidirectional Signaling', *Annual Review of Cell and Developmental Biology*, 21, pp. 381–410.

Asakura, T., Nishi, H., Nagano, A., Yoshida, A., Nakazawa, Y., Kamiya, M. and Demura, M. (2011) 'NMR analysis of the fibronectin cell-adhesive sequence, Arg-Gly-Asp, in a recombinant silk-like protein and a model peptide', *Biomacromolecules*, 12(11), pp. 3910–3916.

Assenberg, R., Wan, P. T., Geisse, S. and Mayr, L. M. (2013) 'Advances in recombinant protein expression for use in pharmaceutical research', *Current Opinion in Structural Biology*, 23(3) pp. 393–402.

Aziz-Seible, R. S. and Casey, C. A. (2011) 'Fibronectin: Functional character and role in alcoholic liver disease', *World Journal of Gastroenterology*, 17(20), pp. 2482–2499.

Bakan, A., Meireles, L. M. and Bahar, I. (2011) 'ProDy: Protein dynamics inferred from theory and experiments', *Bioinformatics*, 27(11), pp. 1575–1577.

Baxter, M. A., Camarasa, M. V., Bates, N., Small, F., Murray, P., Edgar, D. and Kimber, S. J. (2009) 'Analysis of the distinct functions of growth factors and tissue culture substrates necessary for the long-term self-renewal of human embryonic stem cell lines', *Stem Cell Research*, 3(1), pp. 28–38.

Bergfors, T. (2003) 'Seeds to crystals', *Journal of Structural Biology*, 142(1), pp. 66–76.

Bertz, M., Wilmanns, M. and Rief, M. (2009) 'The titin-telethonin complex is a directed, superstable molecular bond in the muscle Z-disk.', *Proceedings of the National Academy of Sciences of the United States of America*, 106(32), pp. 13307–133310.

Bian, L., Guvendiren, M., Mauck, R. L. and Burdick, J. a (2013) 'Hydrogels that mimic developmentally relevant matrix and N-cadherin interactions enhance MSC chondrogenesis.', *Proceedings of the National Academy of Sciences of the United States of America*, 110(25), pp. 10117–22.

Bian, L., Hou, C., Tous, E., Rai, R., Mauck, R. L. and Burdick, J. A. (2013) 'The influence of hyaluronic acid hydrogel crosslinking density and macromolecular diffusivity on human MSC chondrogenesis and hypertrophy', *Biomaterials*, 34(2), pp. 413–421.

Bian, L., Zhai, D. Y., Tous, E., Rai, R., Mauck, R. L. and Burdick, J. A. (2011)

'Enhanced MSC chondrogenesis following delivery of TGF-β3 from alginate microspheres within hyaluronic acid hydrogels in vitro and in vivo', *Biomaterials*, 32(27), pp. 6425–6434.

Bilgen, B., Orsini, E., Aaron, R. K. and Ciombor, D. M. (2007) 'FBS suppresses TGF-β1-induced chondrogenesis in synoviocyte pellet cultures while dexamethasone and dynamic stimuli are beneficial', *Journal of Tissue Engineering and Regenerative Medicine*, 1(6), pp. 436–442.

Biswas, S., Kinbara, K., Oya, N., Ishii, N., Taguchi, H. and Aida, T. (2009) 'A tubular biocontainer: Metal ion-induced 1D assembly of a molecularly engineered chaperonin', *Journal of the American Chemical Society*, 131(22), pp. 7556–7557.

Blaschuk, O. W., Sullivan, R., David, S. and Pouliot, Y. (1990) 'Identification of a cadherin cell adhesion recognition sequence', *Developmental Biology*, 139(1), pp. 227–229.

Bock, H. C., Michaeli, P., Bode, C., Schultz, W., Kresse, H., Herken, R. and Miosge, N. (2001) 'The small proteoglycans decorin and biglycan in human articular cartilage of late-stage osteoarthritis', *Osteoarthritis and Cartilage*, 9(7), pp. 654–663.

Bodelón, G., Palomino, C. and Fernández, L. Á. (2013) 'Immunoglobulin domains in Escherichia coli and other enterobacteria: From pathogenesis to applications in antibody technologies', *FEMS Microbiology Reviews*, 37(2) pp. 204–250.

Boggon, T. J., Murray, J., Chappuis-Flament, S., Wong, E., Gumbiner, B. M. and Shapiro, L. (2002) 'C-cadherin ectodomain structure and implications for cell adhesion mechanisms.', *Science*, 296(5571), pp. 1308–13.

Boschetti, E., Girot, P. and Secheresse, J.P. (1981) 'Study of the molecular interaction between lysozyme and heparin and application in affinity chromatography', *Journal of Chromatography A*, 210(3), pp. 469-475.

Braam, S. R., Zeinstra, L., Litjens, S., Ward-van Oostwaard, D., van den Brink, S., van Laake, L., Lebrin, F., Kats, P., Hochstenbach, R., Passier, R., Sonnenberg, A. and Mummery, C. L. (2008) 'Recombinant vitronectin is a functionally defined substrate that supports human embryonic stem cell self-renewal via alphavbeta5 integrin.', *Stem cells*, 26(9), pp. 2257–2265.

Brafman, D. A., Chang, C. W., Fernandez, A., Willert, K., Varghese, S. and Chien, S. (2010) 'Long-term human pluripotent stem cell self-renewal on synthetic polymer surfaces', *Biomaterials*, 31(34), pp. 9135–9144.

Braman, J., Papworth, C. and Greener, a (1996) 'Site-directed mutagenesis using double-stranded plasmid DNA templates.', *Methods in Molecular Biology*, 57, pp. 31–44.

Bruning, M., Barsukov, I., Franke, B., Barbieri, S., Volk, M., Leopoldseder, S., Ucurum, Z. and Mayans, O. (2012) 'The intracellular Ig fold: A robust protein scaffold for the engineering of molecular recognition', *Protein Engineering, Design and Selection*, 25(5), pp. 205–212.

Bruning, M., Kreplak, L., Leopoldseder, S., Muller, S. A., Ringler, P., Duchesne, L., Fernig, D. G., Engel, A., Ucurum-Fotiadis, Z. and Mayans, O. (2010) 'Bipartite design of a self-fibrillating protein copolymer with nanopatterned peptide display capabilities', *Nano Letters*, 10(11), pp. 4533–4537.

Buckwalter, J. A. and Mankin, H. J. (1998) 'Articular cartilage: degeneration and osteoarthritis, repair, regeneration, and transplantation.', *Instructional Course Lectures*, 47, pp. 487–504.

Bunse, S., Garg, S., Junek, S., Vogel, D., Ansari, N., Stelzer, E. H. K. and Schuman, E. (2013) 'Role of N-cadherin cis and trans interfaces in the dynamics of adherens junctions in living cells', *PLoS ONE*, 8(12), e81517.

Burridge, K. and Wennerberg, K. (2004) 'Rho and Rac Take Center Stage', *Cell*, 116(2), pp. 167–179.

Burridge, K. and Wittchen, E. S. (2013) 'The tension mounts: Stress fibers as force-generating mechanotransducers', *Journal of Cell Biology*, 200(1), pp. 9–19.

Cai, L. and Heilshorn, S. C. (2014) 'Designing ECM-mimetic materials using protein engineering', *Acta Biomaterialia*, 10(4), pp. 1751–1760.

Caplan, a I. (1991) 'Mesenchymal stem cells.', *Journal of of Orthopaedic Research*, 9(5), pp. 641–50.

Carlson Scholz, J. A., Garg, R., Compton, S. R., Allore, H. G., Zeiss, C. J. and Uchio, E. M. (2011) 'Poliomyelitis in MuLV-infected ICR-SCID mice after injection of basement membrane matrix contaminated with lactate dehydrogenase-elevating virus', *Comparative Medicine*, 61(5), pp. 404–411.

Catalina, P., Cobo, F., Cortes, J.L., Nieto, A.I., Cabrera, C., Montes, R., Concha, A. and Menendez, P. (2007) 'Conventional and molecular cytogenetic diagnostic methods in stem cell research: a concise review', *Cell Biology International*, 31(9):861-9.

Celiz, A. D., Smith, J. G. W., Patel, A. K., Hook, A. L., Rajamohan, D., George, V. T., Flatt, L., Patel, M. J., Epa, V. C., Singh, T., Langer, R., Anderson, D. G., Allen, N. D., Hay, D. C., Winkler, D. A., Barrett, D. A., Davies, M. C., Young, L. E., Denning, C. and Alexander, M. R. (2015) 'Discovery of a Novel Polymer for Human Pluripotent Stem Cell Expansion and Multilineage Differentiation.', *Advanced Materials*, 27(27), pp. 4006–12.

Chen, V. B., Arendall, W. B., Headd, J. J., Keedy, D. A., Immormino, R. M., Kapral, G. J., Murray, L. W., Richardson, J. S. and Richardson, D. C. (2010) 'MolProbity: All-atom structure validation for macromolecular crystallography', *Acta Crystallographica Section D: Biological Crystallography*, 66(1), pp. 12–21.

Chen, X., Zaro, J. L. and Shen, W. C. (2013) 'Fusion protein linkers: Property, design and functionality', *Advanced Drug Delivery Reviews*, 65(10), pp. 1357–1369.

Chimal-Monroy, J. and De León, L. D. (1999) 'Expression of N-cadherin, N-CAM, fibronectin and tenascin is stimulated by TGF-β1, β2, β3 and β5 during the formation of precartilage condensations', *International Journal of Developmental Biology*, 43(1), pp. 59–67.

Chrzanowska-Wodnicka, M. and Burridge, K. (1996) 'Rho-stimulated contractility drives the formation of stress fibers and focal adhesions', *Journal of Cell Biology*, 133(6), pp. 1403–1415.

Chung, C. and Burdick, J. a (2009) 'Influence of three-dimensional hyaluronic acid microenvironments on mesenchymal stem cell chondrogenesis.', *Tissue Engineering. Part A*, 15(2), pp. 243–254.

Ciobanasu, C., Faivre, B. and Le Clainche, C. (2012) 'Actin dynamics associated with focal adhesions', *International Journal of Cell Biology*, 2012:941292.

Cobo, F., Navarro, J. M., Herrera, M. I., Vivo, A., Porcel, D., Hernández, C., Jurado, M., García-Castro, J. and Menendez, P. (2008) 'Electron microscopy reveals the presence of viruses in mouse embryonic fibroblasts but neither in human embryonic fibroblasts nor in human mesenchymal cells used for hESC maintenance: toward an implementation of microbiological quality assurance program i', *Cloning and Stem Cells*, 10(1), pp. 65–74.

Coburn, J. M., Gibson, M., Monagle, S., Patterson, Z. and Elisseeff, J. H. (2012) 'Bioinspired nanofibers support chondrogenesis for articular cartilage repair.', *Proceedings of the National Academy of Sciences of the United States of America*, 109(25), pp. 10012–7.

Costell, M., Gustafsson, E., Aszodi, A., Morgelin, M., Bloch, W., Hunziker, E.,

Addicks, K., Timpl, R. and Fassler, R. (1999) 'Perlican maintains the integrity of cartilage and some basement membranes', *Journal of Cell Biology*, 147(5), pp. 1109-1122.

Cs-Szabó, G., Melching, L. I., Roughley, P. J. and Glant, T. T. (1997) 'Changes in messenger RNA and protein levels of proteoglycans and link protein in human osteoarthritic cartilage samples.', *Arthritis & Rheumatism*, 40(6), pp. 1037–1045.

Csaki, C., Schneider, P. R. A. and Shakibaei, M. (2008) 'Mesenchymal stem cells as a potential pool for cartilage tissue engineering', *Annals of Anatomy*, 190(5), pp. 395–412.

Dalton, B.A., McFarland, C.D., Underwood, P.A. and Steele, J.G. (1995) 'Role of the heparin binding domain of fibronectin in attachment and spreading of human bone marrow-derived cells', *Journalof Cell Science*, 108(5), pp. 2083-2092.

Danen, E. H. J., Sonneveld, P., Brakebusch, C., Fässler, R. and Sonnenberg, A. (2002) 'The fibronectin-binding integrins α5β1 and αvβ3 differentially modulate RhoA-GTP loading, organization of cell matrix adhesions, and fibronectin fibrillogenesis', *Journal of Cell Biology*, 159(6), pp. 1071–1086.

DeLise, A. M., Fischer, L. and Tuan, R. S. (2000) 'Cellular interactions and signaling in cartilage development', *Osteoarthritis and Cartilage*, 8(5), pp. 309–334.

Delise, A. M. and Tuan, R. S. (2002) 'Analysis of N-cadherin function in limb mesenchymal chondrogenesis in vitro', *Developmental Dynamics*, 225(2), pp. 195–204.

Denning, C., Borgdorff, V., Crutchley, J., Firth, K. S. A., George, V., Kalra, S., Kondrashov, A., Hoang, M. D., Mosqueira, D., Patel, A., Prodanov, L., Rajamohan, D., Skarnes, W. C., Smith, J. G. W. and Young, L. E. (2016) 'Cardiomyocytes from human pluripotent stem cells: From laboratory curiosity to industrial biomedical platform', *Biochimica et Biophysica Acta - Molecular Cell Research*, 1863(7), pp. 1728–1748.

Derda, R., Li, L., Orner, B. P., Lewis, R. L., Thomson, J. A. and Kiessling, L. L. (2007) 'Defined substrates for human embryonic stem cell growth identified from surface arrays', *ACS Chemical Biology*, 2(5), pp. 347–355.

Dickhut, A., Pelttari, K., Janicki, P., Wagner, W., Eckstein, V., Egermann, M. and Richter, W. (2009) 'Calcification or dedifferentiation: Requirement to lock mesenchymal stem cells in a desired differentiation stage', *Journal of Cellular Physiology*, 219(1), pp. 219–226.

Diekman, B. O. and Guilak, F. (2013) ‘Stem cell-based therapies for osteoarthritis: challenges and opportunities.’, *Current opinion in rheumatology*, 25(1), pp. 119–26.

Djouad, F., Delorme, B., Maurice, M., Bony, C., Apparailly, F., Louis-Plence, P., Canovas, F., Charbord, P., Noël, D. and Jorgensen, C. (2007) ‘Microenvironmental changes during differentiation of mesenchymal stem cells towards chondrocytes.’, *Arthritis Research & Therapy*, 9(2), pp. R33.

Dong, R., Zhou, Y., Huang, X., Zhu, X., Lu, Y. and Shen, J. (2015) ‘Functional supramolecular polymers for biomedical applications’, *Advanced Materials*, 27(3), pp. 498–526.

Droguett, R., Cabello-Verrugio, C., Riquelme, C. and Brandan, E. (2006) ‘Extracellular proteoglycans modify TGF-β bio-availability attenuating its signaling during skeletal muscle differentiation’, *Matrix Biology*, 25(6), pp. 332–341.

Dy, P., Smits, P., Silvester, A., Penzo-Méndez, A., Dumitriu, B., Han, Y., la Motte, C. A. de, Kingsley, D. M. and Lefebvre, V. (2010) ‘Synovial joint morphogenesis requires the chondrogenic action of Sox5 and Sox6 in growth plate and articular cartilage’, *Developmental Biology*, 341(2), pp. 346–359.

Elliott, D. M., Robinson, P. S., Gimbel, J. A., Sarver, J. J., Abboud, J. A., Iozzo, R. V. and Soslowsky, L. J. (2003) ‘Effect of altered matrix proteins on quasilinear viscoelastic properties in transgenic mouse tail tendons’, *Annals of Biomedical Engineering*, 31(5), pp. 599–605.

Ellman, M. B., Yan, D., Ahmadinia, K., Chen, D., An, H. S. and Im, H. J. (2013) 'Fibroblast growth factor control of cartilage homeostasis', *Journal of Cellular Biochemistry*, 114(4), pp. 735-742.

Emsley, P., Lohkamp, B., Scott, W. G. and Cowtan, K. (2010) ‘Features and development of Coot’, *Acta Crystallographica Section D: Biological Crystallography*, 66(4), pp. 486–501.

Engler, C., Gruetzner, R., Kandzia, R. and Marillonnet, S. (2009) ‘Golden gate shuffling: A one-pot DNA shuffling method based on type ils restriction enzymes’, *PLoS ONE*, 4(5), e5553.

Enomoto, H., Enomoto-Iwamoto, M., Iwamoto, M., Nomura, S., Himeno, M., Kitamura, Y., Kishimoto, T. and Komori, T. (2000) ‘Cbfa1 is a positive regulatory factor in chondrocyte maturation’, *Journal of Biological Chemistry*, 275(12), pp. 8695–8702.

Erickson, I. E., Huang, A. H., Chung, C., Li, R. T., Burdick, J. A. and Mauck, R. L.

(2009) ‘Differential maturation and structure-function relationships in mesenchymal stem cell- and chondrocyte-seeded hydrogels.’, *Tissue Engineering. Part A*, 15(5), pp. 1041–52.

Evans, M. J. and Kaufman, M. H. (1981) ‘Establishment in culture of pluripotential cells from mouse embryos.’, *Nature*, 292(5819), pp. 154–156.

Even-Ram, S., Doyle, A. D., Conti, M. A., Matsumoto, K., Adelstein, R. S. and Yamada, K. M. (2007) ‘Myosin IIA regulates cell motility and actomyosin-microtubule crosstalk.’, *Nature Cell Biology*, 9(3), pp. 299–309.

Fadeev, A. G., Zhou, Y., Yang, J. and Catherine, a (2010) ‘Corning ® Synthemax ™ Surface : a tool for feeder-free , xeno-free culture of human embryonic stem cells’, *Nature Methods*, pp. 6–7.

Frantz, C., Stewart, K. M. and Weaver, V. M. (2010) ‘The extracellular matrix at a glance.’, *Journal of Cell Science*, 123(24), pp. 4195–4200.

French, M. M., Gomes, R. R., Timpl, R., Hook, M., Czymmek, K., Farach-Carson, M. C. and Carson, D. D. (2002) 'Chondrogenic activity of the heparan sulfate proteoglycan perlecan maps to the N-terminal domain I', *Journal of Bone and Mineral Research*, 17(1), pp. 48-55.

Friedenstein, A. J., Chailakhyan, R. K., Latsinik, N. V, Panasyuk, A. F. and Keiliss-Borok, I. V (1974) ‘Stromal cells responsible for transferring the microenvironment of the hematopoietic tissues : Cloning In Vitro and Retransplantation In Vivo.’, *Transplantation*, 17(4), pp. 331–40.

Garitaonandia, I., Amir, H., Boscolo, F. S., Wambua, G. K., Schultheisz, H. L., Sabatini, K., Morey, R., Waltz, S., Wang, Y. C., Tran, H., Leonardo, T. R., Nazor, K., Slavin, I., Lynch, C., Li, Y., Coleman, R., Romero, I. G., Altun, G., Reynolds, D., Dalton, S., Parast, M., Loring, J. F. and Laurent, L. C. (2015) ‘Increased risk of genetic and epigenetic instability in human embryonic stem cells associated with specific culture conditions’, *PLoS ONE*, 10(2), e0118307.

Geng, Y., McQuillan, D. and Roughley, P. J. (2006) ‘SLRP interaction can protect collagen fibrils from cleavage by collagenases’, *Matrix Biology*, 25(8), pp. 484–491.

Gehris, A. L., Stringa, E., Spina, J., Desmond, M. E., Tuan, R. S., and Bennett, V. D. (1997) 'The region encoded by the alternatively spliced exon IIIA in mesenchymal fibronectin appears essential for chondrogenesis at the level of cellular condensation', *Developmental Biology*. 190, pp. 191-205.

George, R. a and Heringa, J. (2002) ‘An analysis of protein domain linkers: their

classification and role in protein folding.', *Protein Engineering*, 15(11), pp. 871–879.

Gerecht, S., Burdick, J. A., Ferreira, L. S., Townsend, S. A., Langer, R. and Vunjak-Novakovic, G. (2007) 'Hyaluronic acid hydrogel for controlled self-renewal and differentiation of human embryonic stem cells.', *Proceedings of the National Academy of Sciences of the United States of America*, 104(27), pp. 11298–303.

Glennon-Alty, L., Williams, R., Dixon, S. and Murray, P. (2013) 'Induction of mesenchymal stem cell chondrogenesis by polyacrylate substrates', *Acta Biomaterialia*, 9(4), pp. 6041–6051.

Goldring, M. B., Tsuchimochi, K. and Ijiri, K. (2006) 'The control of chondrogenesis', *Journal of Cellular Biochemistry*, 97(1), pp. 33–44.

Gomes, S., Leonor, I. B., Mano, J. F., Reis, R. L. and Kaplan, D. L. (2012) 'Natural and genetically engineered proteins for tissue engineering', *Progress in Polymer Science*, 37(1), pp. 1–17.

Gould, S.E., Upholt, W. B. and Kosher, R .A. (1992) 'Syndecan-3: a member of the syndecan family of membrane-intercalated proteoglycans that is expressed in high amounts at the onset of chicken limb cartilage differentiation', *Proceedings of the National Academy of Sciences of the United States of America*', 89(8), pp. 3271-3275.

Granzier, H. L. and Labeit, S. (2004) 'The Giant Protein Titin: A Major Player in Myocardial Mechanics, Signaling, and Disease', *Circulation Research*, 94(3), pp. 284–295.

Gras, S. L., Tickler, A. K., Squires, A. M., Devlin, G. L., Horton, M. A., Dobson, C. M. and MacPhee, C. E. (2008) 'Functionalised amyloid fibrils for roles in cell adhesion', *Biomaterials*, 29(11), pp. 1553–1562.

Grueninger, D., Treiber, N., Ziegler, M. O. P., Koetter, J. W. A., Schulze, M.-S. and Schulz, G. E. (2008) 'Designed protein-protein association', *Science*, 319(5860), pp. 206–209.

Guinier, A. (1939) 'La diffraction des rayons X aux tres petits angles: applications a l'etude de phenomenes ultramicroscopiques', *Annales de physique*, 12, pp. 161–237.

Guo, L., Kawazoe, N., Fan, Y., Ito, Y., Tanaka, J., Tateishi, T., Zhang, X. and Chen, G. (2008) 'Chondrogenic differentiation of human mesenchymal stem cells on photoreactive polymer-modified surfaces', *Biomaterials*, 29(1), pp. 23–32.

Gupta, P. K., Das, A. K., Chullikana, A. and Majumdar, A. S. (2012) 'Mesenchymal stem cells for cartilage repair in osteoarthritis', *Stem Cell Research & Therapy*, 3(4), pp. 25.

Gustafsson, C., Govindarajan, S. and Minshull, J. (2004) 'Codon bias and heterologous protein expression', *Trends in Biotechnology*, 22(7), pp. 346–353.

Gwathmey, J. K., Tsaioun, K. and Hajjar, R. J. (2009) 'Cardionomics: a new integrative approach for screening cardiotoxicity of drug candidates', *Expert Opinion on Drug Metabolism & Toxicology*, 5(6), pp. 647–660.

Hallett, P. J., Deleidi, M., Astradsson, A., Smith, G. A., Cooper, O., Osborn, T. M., Sundberg, M., Moore, M. A., Perez-Torres, E., Brownell, A. L., Schumacher, J. M., Spealman, R. D. and Isacson, O. (2015) 'Successful function of autologous iPSC-derived dopamine neurons following transplantation in a non-human primate model of Parkinson's disease', *Cell Stem Cell*, 16(3), pp. 269–274.

Hallmann, R., Horn, N., Selg, M., Wendler, O., Pausch, F. and Sorokin, L. M. (2005) 'Expression and function of laminins in the embryonic and mature vasculature.', *Physiological Reviews*, 85(3), pp. 979–1000.

Handorf, A. M. and Li, W.-J. (2011) 'Fibroblast growth factor-2 primes human mesenchymal stem cells for enhanced chondrogenesis', *PloS ONE*, 6(7), pp. e22887.

Harrison, O. J., Jin, X., Hong, S., Bahna, F., Ahlsen, G., Brasch, J., Wu, Y., Vendome, J., Felsovalyi, K., Hampton, C. M., Troyanovsky, R. B., Ben-Shaul, A., Frank, J., Troyanovsky, S. M., Shapiro, L. and Honig, B. (2011) 'The extracellular architecture of adherens junctions revealed by crystal structures of type i cadherins', *Structure*, 19(2), pp. 244–256.

Hautanen, A., Gailit, J., Mann, D. M. and Ruoslahti, E. (1989) 'Effects of modifications of the RGD sequence and its context on recognition by the fibronectin receptor', *Journal of Biological Chemistry*, 264(3), pp. 1437–1442.

Hellingman, C. a, Koevoet, W., Kops, N., Farrell, E., Jahr, H., Liu, W., Baatenburg de Jong, R. J., Frenz, D. a and van Osch, G. J. V. M. (2010) 'Fibroblast growth factor receptors in in vitro and in vivo chondrogenesis: relating tissue engineering using adult mesenchymal stem cells to embryonic development.', *Tissue Engineering. Part A*, 16(2), pp. 545–56.

Hersel, U., Dahmen, C. and Kessler, H. (2003) 'RGD modified polymers: Biomaterials for stimulated cell adhesion and beyond', *Biomaterials*, 24(24), pp. 4385–4415.

Higuchi, A., Kao, S.-H., Ling, Q.-D., Chen, Y.-M., Li, H.-F., Alarfaj, A. A., Munusamy, M. A., Murugan, K., Chang, S.-C., Lee, H.-C., Hsu, S.-T., Kumar, S. S. and Umezawa, A. (2015) 'Long-term xeno-free culture of human pluripotent stem cells on hydrogels with optimal elasticity', *Scientific Reports*, 5, pp. 18136.

Holliger, P. and Hudson, P. J. (2005) 'Engineered antibody fragments and the rise of single domains.', *Nature Biotechnology*, 23(9), pp. 1126–1136.

Horwitz, E. M., Le Blanc, K., Dominici, M., Mueller, I., Slaper-Cortenbach, I., Marini, F. C., Deans, R. J., Krause, D. S. and Keating, a (2005) 'Clarification of the nomenclature for MSC: The International Society for Cellular Therapy position statement.', *Cytotherapy*, 7(5), pp. 393–5.

Hosse, R. J., Rothe, A. and Power, B. E. (2006) 'A new generation of protein display scaffolds for molecular recognition.', *Protein Science*, 15(1), pp. 14–27.

Huang, A. H., Farrell, M. J. and Mauck, R. L. (2010) 'Mechanics and mechanobiology of mesenchymal stem cell-based engineered cartilage', *Journal of Biomechanics*, 43(1), pp. 128–136.

Huang, A. H., Stein, A., Tuan, R. S. and Mauck, R. L. (2009) 'Transient exposure to transforming growth factor beta 3 improves the mechanical properties of mesenchymal stem cell-laden cartilage constructs in a density-dependent manner.', *Tissue Engineering. Part A*, 15(11), pp. 3461–72.

Humphries, J. D., Byron, A. and Humphries, M. J. (2006) 'Integrin ligands at a glance', *Journal of Cell Science*, 119(19), pp. 3901–3903.

Hung, I. H., Yu, K., Lavine, K. J. and Ornitz, D. M. (2007) 'FGF9 regulates early hypertrophic chondrocyte differentiation and skeletal vascularization in the developing stylopod', *Developmental Biology*, 307(2), pp. 300-313.

Hunt, G. C., Singh, P. and Schwarzbauer, J. E. (2012) 'Endogenous production of fibronectin is required for self-renewal of cultured mouse embryonic stem cells', *Experimental Cell Research*, 318(15), pp. 1820–1831.

Hynes, R. O. and Yamada, K. M. (1982) 'Fibronectins: Multifunctional modular glycoproteins', *Journal of Cell Biology*, 95(2), pp. 369–377.

Hyslop, L., Stojkovic, M., Armstrong, L., Walter, T., Stojkovic, P., Przyborski, S., Herbert, M., Murdoch, A., Strachan, T. and Lako, M. (2005) 'Downregulation of NANOG induces differentiation of human embryonic stem cells to extraembryonic lineages.', *Stem Cells*, 23(8), pp. 1035–1043.

Iozzo, R. V (1998) ‘Matrix proteoglycans: from molecular design to cellular function.’, *Annual Review of Biochemistry*, 67, pp. 609–52.

Irwin, E. F., Gupta, R., Dashti, D. C. and Healy, K. E. (2011) ‘Engineered polymer-media interfaces for the long-term self-renewal of human embryonic stem cells’, *Biomaterials*, 32(29), pp. 6912–6919.

Ivanova, N. B., Dimos, J. T., Schaniel, C., Hackney, J. a, Moore, K. a and Lemischka, I. R. (2002) ‘A stem cell molecular signature.’, *Science*, 298(5593), pp. 601–604.

Jackson, K. A., Majka, S. M., Wang, H., Pocius, J., Hartley, C. J., Majesky, M. W., Entman, M. L., Michael, L. H., Hirschi, K. K. and Goodell, M. A. (2001) ‘Regeneration of ischemic cardiac muscle and vascular endothelium by adult stem cells’, *Journal of Clinical Investigation*, 107(11), pp. 1395–1402.

Jamroz, M., Kolinski, A. and Kmiecik, S. (2013) ‘CABS-flex: Server for fast simulation of protein structure fluctuations.’, *Nucleic Acids Research*, 41, W427-31.

Janjanin, S., Li, W. J., Morgan, M. T., Shanti, R. M. and Tuan, R. S. (2008) ‘Mold-Shaped, Nanofiber Scaffold-Based Cartilage Engineering Using Human Mesenchymal Stem Cells and Bioreactor’, *Journal of Surgical Research*, 149(1), pp. 47–56.

Jayawarna, V., Ali, M., Jowitt, T. A., Miller, A. F., Saiani, A., Gough, J. E. and Ulijn, R. V. (2006) ‘Nanostructured hydrogels for three-dimensional cell culture through self-assembly of fluorenylmethoxycarbonyl-dipeptides’, *Advanced Materials*, 18(5), pp. 611–614.

Jin, R., Moreira Teixeira, L. S., Dijkstra, P. J., Van Blitterswijk, C. A., Karperien, M. and Feijen, J. (2011) ‘Chondrogenesis in injectable enzymatically crosslinked heparin/dextran hydrogels’, *Journal of Controlled Release*, 152(1), pp. 186–195.

Jin, S., Yao, H., Weber, J. L., Melkoumian, Z. K. and Ye, K. (2012) ‘A Synthetic, Xeno-Free Peptide Surface for Expansion and Directed Differentiation of Human Induced Pluripotent Stem Cells’, *PLoS ONE*, 7(11), e50880.

Johnstone, B., Hering, T.M., Caplan, A.I., Goldberg, V.M. and Yoo, J.U. (1998) 'In vitro chondrogenesis of bone marrow derived mesenchymal progenitor cells', *Experimental Cell Research*, 283(1), pp. 265-272.

Juffroy, O., Noël, D., Delanoye, A., Viltart, O., Wolowczuk, I. and Verwaerde, C. (2009) ‘Subcutaneous graft of D1 mouse mesenchymal stem cells leads to the formation of a bone-like structure’, *Differentiation*, 78(4), pp. 223–231.

Jung, J. P., Nagaraj, A. K., Fox, E. K., Rudra, J. S., Devgun, J. M. and Collier, J. H. (2009) 'Co-assembling peptides as defined matrices for endothelial cells', *Biomaterials*, 30(12), pp. 2400–2410.

Kabsch, W. (2010) 'XDS', *Acta Crystallographica Section D: Biological Crystallography*, 66(2), pp. 125–132.

Kalaskar, D. M., Downes, J. E., Murray, P., Edgar, D. H., Williams, R. L. and Interface, J. R. S. (2013) 'Characterization of the interface between adsorbed fibronectin and human embryonic stem cells Characterization of the interface between adsorbed fibronectin and human embryonic stem cells', *Journal of the Royal Society Interface*, 10(83):20130139.

Kanchanawong, P., Shtengel, G., Pasapera, A. M., Ramko, E. B., Davidson, M. W., Hess, H. F. and Waterman, C. M. (2010) 'Nanoscale architecture of integrin-based cell adhesions.', *Nature*, 468(7323), pp. 580–4.

Kavka, A. I. and Green, J. B. A. (1997) 'Tales of tails: Brachyury and the T-box genes', *Biochimica et Biophysica Acta - Reviews on Cancer*, 1333(2), pp. 73–84.

Kent, L. (2009) 'Culture and maintenance of human embryonic stem cells.', *Journal of visualized experiments : JoVE*, (34), pp. 2–5.

Keselowsky, B. G., Collard, D. M. and García, A. J. (2003) 'Surface chemistry modulates fibronectin conformation and directs integrin binding and specificity to control cell adhesion', *Journal of Biomedical Materials Research Part A*, 66A(2), pp. 247–259.

Kim, J. P., Zhang, K., Chen, J. D., Kramer, R. H. and Woodley, D. T. (1994) 'Vitronectin-driven human keratinocyte locomotion is mediated by the αvβ5 integrin receptor', *Journal of Biological Chemistry*, 269(43), pp. 26926–26932.

King, N. P. and Lai, Y. T. (2013) 'Practical approaches to designing novel protein assemblies', *Current Opinion in Structural Biology*, 23(4), pp. 632–638.

Kirsch, T., Koyama, E., Liu, M., Golub, E. E. and Pacifici, M. (2002) 'Syndecan-3 is a selective regulator of chondrocyte proliferation', *Journal of Biological Chemistry*, 277(44), pp. 42171-42177.

Knight, M. N. and Hankenson, K. D. (2013) 'Mesenchymal Stem Cells in Bone Regeneration.', *Advances in Wound Care*, 2(6), pp. 306–316.

Kolhar, P., Kotamraju, V. R., Hikita, S. T., Clegg, D. O. and Ruoslahti, E. (2010)

'Synthetic surfaces for human embryonic stem cell culture.', *Journal of Biotechnology*, 146(3), pp. 143–146.

Konarev, P. V., Volkov, V. V., Sokolova, A. V., Koch, M. H. J. and Svergun, D. I. (2003) 'PRIMUS: A Windows PC-based system for small-angle scattering data analysis', *Journal of Applied Crystallography*, 36(5), pp. 1277–1282.

Kopesky, P. W., Vanderploeg, E. J., Kisiday, J. D., Frisbie, D. D., Sandy, J. D. and Grodzinsky, A. J. (2011) 'Controlled delivery of transforming growth factor β1 by self-assembling peptide hydrogels induces chondrogenesis of bone marrow stromal cells and modulates Smad2/3 signaling.', *Tissue Engineering. Part A*, 17(1–2), pp. 83–92.

Koutsourakis, M., Langeveld, a, Patient, R., Beddington, R. and Grosveld, F. (1999) 'The transcription factor GATA6 is essential for early extraembryonic development.', *Development*, 126(9), pp. 723–32.

Koyama, E., Shimazu, A., Leatherman, J. L., Golden, E. B., Nah, H. D. and Pacifici, M. (1996) 'Expression of syndecan-3 and tenascin-C: possible involvement in posterium development', *Journal of Orthopaedic Research*, 14(3), pp. 403-412.

Krammer, A., Craig, D., Thomas, W. E., Schulten, K. and Vogel, V. (2002) 'A structural model for force regulated integrin binding to fibronectin's RGD-synergy site', *Matrix Biology*, 21(2), pp. 139–147.

Labeit, S. and Kolmerer, B. (1995) 'Titins: giant proteins in charge of muscle ultrastructure and elasticity', *Science*, 270(5234), pp. 293–296.

Leahy, D. J., Aukhil, I. and Erickson, H. P. (1996) '2.0 Å crystal structure of a four-domain segment of human fibronectin encompassing the RGD loop and synergy region', *Cell*, 84(1), pp. 155–164.

Lee, H. J., Yu, C., Chansakul, T., Hwang, N. S., Varghese, S., Yu, S. M. and Elisseeff, J. H. (2008) 'Enhanced Chondrogenesis of Mesenchymal Stem Cells in Collagen Mimetic Peptide-Mediated Microenvironment', *Tissue Engineering Part A*, 14(11), pp. 1843–1851.

Lee, N. K., Sowa, H., Hinoi, E., Ferron, M., Ahn, J. D., Confavreux, C., Dacquin, R., Mee, P. J., McKee, M. D., Jung, D. Y., Zhang, Z., Kim, J. K., Mauvais-Jarvis, F., Ducy, P. and Karsenty, G. (2007) 'Endocrine regulation of energy metabolism by the skeleton', *Cell*, 130(3), pp. 456–469.

Lee, S., Kim, J. H., Jo, C. H., Seong, S. C., Lee, J. C. and Lee, M. C. (2009) 'Effect of serum and growth factors on chondrogenic differentiation of synovium-derived

stromal cells.', *Tissue Engineering. Part A*, 15(11), pp. 3401–3415.

Lendahl, U., Zimmerman, L. B. and McKay, R. D. (1990) 'CNS stem cells express a new class of intermediate filament protein.', *Cell*, 60(4), pp. 585–595.

Li, W.-J. W.-J., Tuli, R., Okafor, C., Derfoul, A., Danielson, K. G. K. G., Hall, D. J. D. J. and Tuan, R. S. R. S. (2005) 'A three-dimensional nanofibrous scaffold for cartilage tissue engineering using human mesenchymal stem cells.', *Biomaterials*, 26(6), pp. 599–609.

Li, Z., Cao, B., Wang, X., Ye, K., Li, S. and Ding, J. (2015) 'Effects of RGD nanospacing on chondrogenic differentiation of mesenchymal stem cells', *Journal of Materials Chemistry. Part B*, 3(26), pp. 5197–5209.

Liu, Y., Song, Z., Zhao, Y., Qin, H., Cai, J., Zhang, H., Yu, T., Jiang, S., Wang, G., Ding, M. and Deng, H. (2006) 'A novel chemical-defined medium with bFGF and N2B27 supplements supports undifferentiated growth in human embryonic stem cells', *Biochemical and Biophysical Research Communications*, 346(1), pp. 131–139.

Liu, Z., Lavine, K. J., Hung, I. H. and Ornitz, D. M. (2007) 'FGF18 is required for early chondrocyte proliferation, hypertrophy and vascular invasion of the growth plate', *Developmental Biology*, 302(1), pp. 80-91.

Livak, K. J. and Schmittgen, T. D. (2001) 'Analysis of relative gene expression data using real-time quantitative PCR and the 2(-delta delta C(T)) method', *Methods*, 25(4), pp. 402–408.

Ludwig, T. E., Levenstein, M. E., Jones, J. M., Berggren, W. T., Mitchen, E. R., Frane, J. L., Crandall, L. J., Daigh, C. a, Conard, K. R., Piekarczyk, M. S., Llanas, R. a and Thomson, J. a (2006) 'Derivation of human embryonic stem cells in defined conditions.', *Nature Biotechnology*, 24(2), pp. 185–187.

Macneil, S., Rimmer, S., Perlin, L., Rimmer, S., Macneil, S. and Rimmer, S. (2008) 'Production and performance of biomaterials containing RGD peptides', *Soft Matter*, 4(12), pp. 2331-2349.

Main, A. L., Harvey, T. S., Baron, M., Boyd, J. and Campbell, I. D. (1992) 'The three-dimensional structure of the tenth type III module of fibronectin: An insight into RGD-mediated interactions', *Cell*, 71(4), pp. 671–678.

Maitra, A., Arking, D. E., Shivapurkar, N., Ikeda, M., Stastny, V., Kassauei, K., Sui, G., Cutler, D. J., Liu, Y., Brimble, S. N., Noaksson, K., Hyllner, J., Schulz, T. C., Zeng, X., Freed, W. J., Crook, J., Abraham, S., Colman, A., Sartipy, P., Matsui, S.-

I., Carpenter, M., Gazdar, A. F., Rao, M. and Chakravarti, A. (2005) 'Genomic alterations in cultured human embryonic stem cells.', *Nature Genetics*, 37(10), pp. 1099–103.

Mao, Y. and Schwarzbauer, J. E. (2005) 'Fibronectin fibrillogenesis, a cell-mediated matrix assembly process', *Matrix Biology*, 24(6), pp. 389–399.

Mardon, H. J. and Grant, K. E. (1994) 'The role of the ninth and tenth type III domains of human fibronectin in cell adhesion', *FEBS Letters*, 340(3), pp. 197–201.

Marino, M., Svergun, D. I., Kreplak, L., Konarev, P. V., Maco, B., Labeit, D. and Mayans, O. (2005) 'Poly-Ig tandems from I-band titin share extended domain arrangements irrespective of the distinct features of their modular constituents', *Journal of Muscle Research and Cell Motility*, 26(6-8), pp. 355–365.

Marino, M., Zou, P., Svergun, D., Garcia, P., Edlich, C., Simon, B., Wilmanns, M., Muhle-Goll, C. and Mayans, O. (2006) 'The Ig Doublet Z1Z2: A Model System for the Hybrid Analysis of Conformational Dynamics in Ig Tandems from Titin', *Structure*, 14(9), pp. 1437–1447.

Martin, G. R. (1981) 'Isolation of a pluripotent cell line from early mouse embryos cultured in medium conditioned by teratocarcinoma stem cells.', *Proceedings of the National Academy of Sciences of the United States of America*, 78(12), pp. 7634–7638.

Martin, M. J., Muotri, A., Gage, F. and Varki, A. (2005) 'Human embryonic stem cells express an immunogenic nonhuman sialic acid.', *Nature Medicine*, 11(2), pp. 228–232.

Matthews, B. W. (1968) 'Solvent content of protein crystals', *Journal of Molecular Biology*, 33(2), pp. 491–497.

Mayasundari, A., Whittemore, N. A., Serpersu, E. H. and Peterson, C. B. (2004) 'The solution structure of the N-terminal domain of human vitronectin: Proximal sites that regulate fibrinolysis and cell migration', *Journal of Biological Chemistry*, 279(28), pp. 29359–29366.

Mayshar, Y., Ben-David, U., Lavon, N., Biancotti, J.-C., Yakir, B., Clark, A. T., Plath, K., Lowry, W. E. and Benvenisty, N. (2010) 'Identification and classification of chromosomal aberrations in human induced pluripotent stem cells.', *Cell Stem Cell*, 7(4), pp. 521–531.

McCoy, A. J., Grosse-Kunstleve, R. W., Adams, P. D., Winn, M. D., Storoni, L. C. and Read, R. J. (2007) 'Phaser crystallographic software', *Journal of Applied*

*Crystallography*, 40(4), pp. 658–674.

Meinel, L., Hofmann, S., Karageorgiou, V., Zichner, L., Langer, R., Kaplan, D. and Vunjak-Novakovic, G. (2004) 'Engineering cartilage-like tissue using human mesenchymal stem cells and silk protein scaffolds', *Biotechnology and Bioengineering*, 88(3), pp. 379–391.

Meng, Y., Eshghi, S., Li, Y. J., Schmidt, R., Schaffer, D. V and Healy, K. E. (2010) 'Characterization of integrin engagement during defined human embryonic stem cell culture.', *FASEB Journal*, 24(4), pp. 1056–65.

Meyer, L. C. and Wright, N. T. (2013) 'Structure of giant muscle proteins', *Frontiers in Physiology*, 4:e16540

Mezey, E., Chandross, K. J., Harta, G., Maki, R. A., McKercher, S. R., Wright, W. E., Res, E. C., Vescovi, A. L., Snyder, E. Y., Pathol, B., Ray, J., Neurobiol, J., Mezey, E., Chandross, K. J., Harta, G., Maki, R. A. and McKercher, S. R. (2000) 'Turning Blood into Brain : Cells Bearing Neuronal Antigens Generated in Vivo from Bone', *Science*, 290(5497), pp. 1779–82.

Minina, E., Kreschel, C., Naski, M. C., Ornitz, D. M. and Vortkamp, A. (2002) 'Interaction of FGF, Ihh/Pthlh, and BMP signaling integrates chondrocyte proliferation and hypertrophic differentiation', *Developmental Cell*, 3(3), pp. 439–449.

Miyazaki, T., Futaki, S., Suemori, H., Taniguchi, Y., Yamada, M., Kawasaki, M., Hayashi, M., Kumagai, H., Nakatsuji, N., Sekiguchi, K. and Kawase, E. (2012) 'Laminin E8 fragments support efficient adhesion and expansion of dissociated human pluripotent stem cells.', *Nature Communications*, 3, pp. 1236.

Molténi, A., Modrowski, D., Hott, M. and Marie, P. J. (1999) 'Differential expression of fibroblast growth factor receptor-1, -2, and -3 and syndecan-1, -2, and -4 in neonatal rat mandibular condyle and calvaria during osteogenic differentiation in vitro', *Bone*, 24(4), pp. 337–347.

Morgan, M. R., Byron, A., Humphries, M. J. and Bass, M. D. (2009) 'Giving off mixed signals--distinct functions of alpha5beta1 and alphavbeta3 integrins in regulating cell behaviour.', *IUBMB life*, 61(7), pp. 731–8.

Moreth, K., Iozzo, R. V. and Schaefer, L. (2012) 'Small leucine-rich proteoglycans orchestrate receptor crosstalk during inflammation', *Cell Cycle*, 11(11), pp. 2084-2091.

Morrisey, E. E., Tang, Z., Sigrist, K., Lu, M. M., Jiang, F., Ip, H. S. and Parmacek,

M. S. (1998) ‘GATA6 regulates HNF4 and is required for differentiation of visceral endoderm in the mouse embryo’, *Genes and Development*, 12(22), pp. 3579–3590.

Murphy, J. M., Dixon, K., Beck, S., Fabian, D., Feldman, A. and Barry, F. (2002) ‘Reduced chondrogenic and adipogenic activity of mesenchymal stem cells from patients with advanced osteoarthritis’, *Arthritis and Rheumatism*, 46(3), pp. 704–713.

Myllyharju, J., Nokelainen, M., Vuorela, A. and Kivirikko, K. I. (2000) ‘Expression of recombinant human type I-III collagens in the yeast pichia pastoris’, *Biochemical Society Transactions*, 28(4), pp. 353–357.

Nagae, M., Re, S., Mihara, E., Nogi, T., Sugita, Y., and Takagi, J. (2012) 'Crystal structure of alpha 5 beta 1 integrin ectodomain: Atomic details of the fibronectin receptor', *Journal of Cell Biology*, 197(1), 131-140.

Närvä, E., Autio, R., Rahkonen, N., Kong, L., Harrison, N., Kitsberg, D., Borghese, L., Itskovitz-Eldor, J., Rasool, O., Dvorak, P., Hovatta, O., Otonkoski, T., Tuuri, T., Cui, W., Brüstle, O., Baker, D., Maltby, E., Moore, H. D., Benvenisty, N., Andrews, P. W., Yli-Harja, O. and Lahesmaa, R. (2010) ‘High-resolution DNA analysis of human embryonic stem cell lines reveals culture-induced copy number changes and loss of heterozygosity.’, *Nature Biotechnology*, 28(4), pp. 371–7.

Ng, E. S., Davis, R., Stanley, E. G. and Elefanty, A. G. (2008) ‘A protocol describing the use of a recombinant protein-based, animal product-free medium (APEL) for human embryonic stem cell differentiation as spin embryoid bodies.’, *Nature Protocols*, 3(5), pp. 768–776.

Ng, L. J., Wheatley, S., Muscat, G. E., Conway-Campbell, J., Bowles, J., Wright, E., Bell, D. M., Tam, P. P., Cheah, K. S. and Koopman, P. (1997) ‘Sox9 binds DNA, activates transcription, and coexpresses with type II collagen during chondrogenesis in the mouse.’, *Developmental Biology*, 183(1), pp. 108–121.

Nichols, J., Zevnik, B., Anastassiadis, K., Niwa, H., Klewe-Nebenius, D., Chambers, I., Scholer, H. and Smith, A. (1998) ‘Formation of pluripotent stem cells in the mammalian embryo depends on the POU transcription factor Oct4’, *Cell*, 95(3), pp. 379–391.

Nisbet, D. R. and Williams, R. J. (2012) ‘Self-assembled peptides: Characterisation and in vivo response’, *Biointerphases*, 7(1-4), pp. 1–14.

Noë, V., Willems, J., Vandekerckhove, J., Roy, F. V, Bruyneel, E. and Mareel, M. (1999) ‘Inhibition of adhesion and induction of epithelial cell invasion by HAV-containing E-cadherin-specific peptides.’, *Journal of Cell Science*, 112(1), pp. 127–

35.

Oberlender, S. A. and Tuan, R. S. (1994a) ‘Expression and functional involvement of N-cadherin in embryonic limb chondrogenesis.’, *Development*, 120(1), pp. 177–87.

Oberlender, S. A. and Tuan, R. S. (1994b) ‘Spatiotemporal profile of N-cadherin expression in the developing limb mesenchyme.’, *Cell Adhesion and Communication*, 2(6), pp. 521–37.

Ogawa, M., Kitamura, N., Kurokawa, T., Arakaki, K., Tanaka, Y., Gong, J. P. and Yasuda, K. (2012) ‘Poly(2-acrylamido-2-methylpropanesulfonic acid) gel induces articular cartilage regeneration in vivo: Comparisons of the induction ability between single- and double-network gels’, *Journal of Biomedical Materials Research - Part A*, 100(9), pp. 2244–2251.

Orgel, J. P. R. O., Eid, A., Antipova, O., Bella, J. and Scott, J. E. (2009) ‘Decorin core protein (decoron) shape complements collagen fibril surface structure and mediates its binding’, *PLoS ONE*, 4(9), e7028.

Ornitz, D. and Marie, P. J. (2002) 'FGF signaling pathways in endochondral and intramembranous bone development and human genetic disease', *Genes & Development*, 16(12), pp. 1446-1465.

Padilla, J. E., Colovos, C. and Yeates, T. O. (2001) ‘Nanohedra: using symmetry to design self assembling protein cages, layers, crystals, and filaments.’, *Proceedings of the National Academy of Sciences of the United States of America*, 98(5), pp. 2217–2221.

Pasapera, A. M., Schneider, I. C., Rericha, E., Schlaepfer, D. D. and Waterman, C. M. (2010) ‘Myosin II activity regulates vinculin recruitment to focal adhesions through FAK-mediated paxillin phosphorylation’, *Journal of Cell Biology*, 188(6), pp. 877–890.

Paszek, M. J., Zahir, N., Johnson, K. R., Lakins, J. N., Rozenberg, G. I., Gefen, A., Reinhart-King, C. A., Margulies, S. S., Dembo, M., Boettiger, D., Hammer, D. A. and Weaver, V. M. (2005) ‘Tensional homeostasis and the malignant phenotype’, *Cancer Cell*, 8(3), pp. 241–254.

Peister, A., Mellad, J.A., Larson, B.L., Hall, B.M., Gibson, L.F. and Prockop, D.J. (2004). 'Adult stem cells from the bone marrow (MSCs) isolated from different strains of inbred mice vary in surface epitopes, rates of proliferation, and differentiation potential', *Blood*, 103(5), pp. 1662-1668.

Pereira, D., Peleteiro, B., Araújo, J., Branco, J., Santos, R. A. and Ramos, E. (2011) 'The effect of osteoarthritis definition on prevalence and incidence estimates: A systematic review', *Osteoarthritis and Cartilage*, 19(11) pp. 1270–1285.

Perez, T. D. and Nelson, W. J. (2004) 'Cadherin adhesion: mechanisms and molecular interactions.', *Handbook of Experimental Pharmacology*, (165), pp. 3–21.

Petersen, B. E., Bowen, W. C., Patrene, K. D., Mars, W. M., Sullivan, a K., Murase, N., Boggs, S. S., Greenberger, J. S. and Goff, J. P. (1999) 'Bone marrow as a potential source of hepatic oval cells.', *Science*, 284(5417), pp. 1168–70.

Pierschbacher, M. D. and Ruoslahti, E. (1987) 'Influence of stereochemistry of the sequence Arg-Gly-Asp-Xaa on binding specificity in cell adhesion', *Journal of Biological Chemistry*, 262(36), pp. 17294–17298.

Pittenger, M. F., Mackay, a M., Beck, S. C., Jaiswal, R. K., Douglas, R., Mosca, J. D., Moorman, M. a, Simonetti, D. W., Craig, S. and Marshak, D. R. (1999) 'Multilineage potential of adult human mesenchymal stem cells.', *Science*, 284(5411), pp. 143–7.

Poole, A. R., Rosenberg, L. C., Reiner, A., Ionescu, M., Bogoch, E. and Roughley, P. J. (1996) 'Contents and distributions of the proteoglycans decorin and biglycan in normal and osteoarthritic human articular cartilage', *Journal of Orthopaedic Research*, 14(5), pp. 681–689.

Prowse, A. B. J., Doran, M. R., Cooper-White, J. J., Chong, F., Munro, T. P., Fitzpatrick, J., Chung, T. L., Haylock, D. N., Gray, P. P. and Wolvetang, E. J. (2010) 'Long term culture of human embryonic stem cells on recombinant vitronectin in ascorbate free media', *Biomaterials*, 31(32), pp. 8281–8288.

Putnam, C. D., Hammel, M., Hura, G. L. and Tainer, J. a (2007) 'X-ray solution scattering (SAXS) combined with crystallography and computation: defining accurate macromolecular structures, conformations and assemblies in solution.', *Quarterly Reviews of Biophysics*, 40(3), pp. 191–285.

Quan, L., Lv, Q. and Zhang, Y. (2016) 'STRUM: Structure-based prediction of protein stability changes upon single-point mutation', *Bioinformatics*, 32(19), pp. 2936-46.

Ragetly, G., Griffon, D. J. and Chung, Y. S. (2010) 'The effect of type II collagen coating of chitosan fibrous scaffolds on mesenchymal stem cell adhesion and chondrogenesis', *Acta Biomaterialia*, 6(10), pp. 3988–3997.

Ramsey, W. S., Hertl, W., Nowlan, E. D. and Binkowski, N. J. (1984) 'Surface

treatments and cell attachment', *In Vitro*, 20(10), pp. 802–808.

Ravi, M., Paramesh, V., Kaviya, S. R., Anuradha, E. and Paul Solomon, F. D. (2015) '3D cell culture systems: Advantages and applications', *Journal of Cellular Physiology*, 230(1), pp. 16–26.

Rebuzzini, P., Zuccotti., M, Reid, C.A. and Garagna, S. (2015) 'Chromosomal abnormalities in embryonic somatic stem cells', *Cytogenetics and Genome Research*, 147:1-9.

Re'em, T., Kaminer-Israeli, Y., Ruvinov, E. and Cohen, S. (2012) 'Chondrogenesis of hMSC in affinity-bound TGF-beta scaffolds', *Biomaterials*, 33(3), pp. 751–761.

Re'em, T., Tsur-Gang, O. and Cohen, S. (2010) 'The effect of immobilized RGD peptide in macroporous alginate scaffolds on TGFβ1-induced chondrogenesis of human mesenchymal stem cells', *Biomaterials*, 31(26), pp. 6746–6755.

Renner, J. N., Kim, Y. and Liu, J. C. (2012) 'Bone morphogenetic protein-derived peptide promotes chondrogenic differentiation of human mesenchymal stem cells.', *Tissue Engineering Part A*, 18(23–24), pp. 2581–2589.

Richardson, S. M., Kalamegam, G., Pushparaj, P. N., Matta, C., Memic, A., Khademhosseini, A., Mobasheri, R., Poletti, F. L., Hoyland, J. A. and Mobasheri, A. (2015) 'Mesenchymal stem cells in regenerative medicine: Focus on articular cartilage and intervertebral disc regeneration.', *Methods*, 99, pp. 69–80.

Ridley, A. J. and Hall, A. (1992) 'The small GTP-binding protein rho regulates the assembly of focal adhesions and actin stress fibers in response to growth factors', *Cell*, 70(3), pp. 389–399.

Rodin, S., Antonsson, L., Niaudet, C., Simonson, O. E., Salmela, E., Hansson, E. M., Domogatskaya, A., Xiao, Z., Damdimopoulou, P., Sheikhi, M., Inzunza, J., Nilsson, A.-S., Baker, D., Kuiper, R., Sun, Y., Blennow, E., Nordenskjöld, M., Grinnemo, K.-H., Kere, J., Betsholtz, C., Hovatta, O. and Tryggvason, K. (2014) 'Clonal culturing of human embryonic stem cells on laminin-521/E-cadherin matrix in defined and xeno-free environment.', *Nature Communications*, 5, pp. 3195.

Rodin, S., Domogatskaya, A., Ström, S., Hansson, E. M., Chien, K. R., Inzunza, J., Hovatta, O. and Tryggvason, K. (2010) 'Long-term self-renewal of human pluripotent stem cells on human recombinant laminin-511.', *Nature Biotechnology*, 28(6), pp. 611–615.

Rowland, T. J., Miller, L. M., Blaschke, A. J., Doss, E. L., Bonham, A. J., Hikita, S. T., Johnson, L. V and Clegg, D. O. (2010) 'Roles of integrins in human induced

pluripotent stem cell growth on Matrigel and vitronectin', *Stem Cells and Development*, 19(8), pp. 1231–1240.

Roy, D. C., Wilke-Mounts, S. J. and Hocking, D. C. (2011) 'Chimeric fibronectin matrix mimetic as a functional growth- and migration-promoting adhesive substrate', *Biomaterials*, 32(8), pp. 2077–2087.

Ruoslahti, E. (1996) 'RGD and other recognition sequences for integrins', *Annual Review of Cell and Developmental Biology*, 12(1), pp. 697–715.

Ruoslahti, E. and Obrink, B. (1996) 'Common principles in cell adhesion.', *Experimental Cell Research*, 227(1), pp. 1–11.

Sahdev, S., Khattar, S. K. and Saini, K. S. (2008) 'Production of active eukaryotic proteins through bacterial expression systems: A review of the existing biotechnology strategies', *Molecular and Cellular Biochemistry*, 307(1-2), pp. 249–264.

Sakiyama-Elbert, S. (2008) *Combining stem cells and biomaterial scaffolds for constructing tissues and cell delivery*, *StemBook*.

Salinas, C. N. and Anseth, K. S. (2008) 'The enhancement of chondrogenic differentiation of human mesenchymal stem cells by enzymatically regulated RGD functionalities', *Biomaterials*, 29(15), pp. 2370–2377.

Salinas, C. N. and Anseth, K. S. (2009) 'Decorin moieties tethered into PEG networks induce chondrogenesis of human mesenchymal stem cells', *Journal of Biomedical Materials Research - Part A*, 90(2), pp. 456–464.

Sanchez-Heras, E., Howell, F. V., Williams, G. and Doherty, P. (2006) The fibroblast growth factor receptor acid box is essential for interactions with N-cadherin and all of the major isoforms of neural cell adhesion molecule', *Journal of Biological Chemistry*, 281(46), pp. 35208-35216.

Sanjar, E. and Jin, S. (2015) 'Substrates for clinical applicability of stem cells', *World Journal of Stem Cells*, 7(2), pp. 243-252.

Schaefer, L., Tsalastra, W., Babelova, A., Minnerup, J., Sorokin, L., Grone, H., Reinhardt, D. P., Pfeilschifter, J., Iozzo, R. V. and Schaefer, R. M. (2007) 'Decorin-mediated regulation of fibrillin-1 in the kidney involves the insulin-like growth factor-1 receptor and mammalian target of rapamycin', *The American Journal of Pathology*, 170(1), pp. 301-315.

Schiller, H. B., Hermann, M.-R., Polleux, J., Vignaud, T., Zanivan, S., Friedel, C.

C., Sun, Z., Raducanu, A., Gottschalk, K.-E., Théry, M., Mann, M. and Fässler, R. (2013) 'beta1- and alphav-class integrins cooperate to regulate myosin II during rigidity sensing of fibronectin-based microenvironments', *Nature Cell Biology*, 15(6), pp. 625–636.

Schneider, C. a, Rasband, W. S. and Eliceiri, K. W. (2012) 'NIH Image to ImageJ: 25 years of image analysis', *Nature Methods*, 9(7), pp. 671–675.

Schuh, E., Hofmann, S., Stok, K., Notbohm, H., Müller, R. and Rotter, N. (2012) 'Chondrocyte redifferentiation in 3D: The effect of adhesion site density and substrate elasticity', *Journal of Biomedical Materials Research - Part A*, 100(1), pp. 38–47.

Schulze-Tanzil, G., De Souza, P., Villegas Castrejon, H., John, T., Merker, H. J., Scheid, A. and Shakibaei, M. (2002) 'Redifferentiation of dedifferentiated human chondrocytes in high-density cultures', *Cell and Tissue Research*, 308(3), pp. 371–379.

Schvartz, I., Seger, D. and Shaltiel, S. (1999) 'Vitronectin.', *The International Journal of Biochemistry & Cell Biology*, 31(5), pp. 539–544.

Scott, J. E. (1991) 'Proteoglycan:collagen interactions in connective tissues. Ultrastructural, biochemical, functional and evolutionary aspects', *International Journal of Biological Macromolecules*, 13(3), pp. 157–161.

Scott, J. E. (1996) 'Proteodermatan and proteokeratan sulfate (decorin, lumican/fibromodulin) proteins are horseshoe shaped. Implications for their interactions with collagen', *Biochemistry*, 35(27), pp. 8795–8799.

Scott, P. G., McEwan, P. A., Dodd, C. M., Bergmann, E. M., Bishop, P. N. and Bella, J. (2004) 'Crystal structure of the dimeric protein core of decorin, the archetypal small leucine-rich repeat proteoglycan.', *Proceedings of the National Academy of Sciences of the United States of America*, 101(44), pp. 15633–8.

Sela-Culang, I., Kunik, V. and Ofran, Y. (2013) 'The structural basis of antibody-antigen recognition', *Frontiers in Immunology*, 4:302.

Shapiro, L., Fannon, a M., Kwong, P. D., Thompson, a, Lehmann, M. S., Grübel, G., Legrand, J. F., Als-Nielsen, J., Colman, D. R. and Hendrickson, W. A. (1995) 'Structural basis of cell-cell adhesion by cadherins.', *Nature*, 375(6520), pp. 327–337.

Shekaran, A. and Garcia, A. J. (2011) 'Nanoscale engineering of extracellular matrix-mimetic bioadhesive surfaces and implants for tissue engineering',

*Biochimica et Biophysica Acta - General Subjects*, 1810(3), pp. 350–360.

Shimizu, A., Tada, K., Shukunami, C., Hiraki, Y., Kurokawa, T., Magane, N. and Kurokawa-Seo, M. (2001) 'A novel alternatively spliced fibroblast growth factor receptor 3 isoform lacking the acid box domain is expressed during chondrogenic differentiation of ATDC5 cells', *Journal of Biological Chemistry*, 276(14), pp. 11031-11040.

Shimizu, H., Yokoyama, S. and Asahara, H. (2007) 'Growth and differentiation of the developing limb bud from the perspective of chondrogenesis', *Development Growth and Differentiation*, 49(6), pp. 449–454.

Siani, A., Robert-Nicoud, G., Cellesi, F. and Tirelli, N. (2012) 'Quantitative descriptors for the effect of nature/mechanical properties of solid substrates on fibroblast morphology.', *Journal of Applied Biomaterials & Functional Materials*, 10(3), pp. 265–72.

Silverman, A. P., Levin, A. M., Lahti, J. L. and Cochran, J. R. (2009) 'Engineered Cystine-Knot Peptides that Bind αvβ3 Integrin with Antibody-Like Affinities', *Journal of Molecular Biology*, 385(4), pp. 1064–1075.

Sinclair, J. C., Davies, K. M., Vénien-Bryan, C. and Noble, M. E. M. (2011) 'Generation of protein lattices by fusing proteins with matching rotational symmetry.', *Nature Nanotechnology*, 6(9), pp. 558–62.

Singh, P. and Schwarzbauer, J. E. (2014) 'Fibronectin matrix assembly is essential for cell condensation during chondrogenesis.', *Journal of Cell Science*, 127(20), pp. 4420–4428.

Sinthuvanich, C., Haines-Butterick, L. A., Nagy, K. J. and Schneider, J. P. (2012) 'Iterative design of peptide-based hydrogels and the effect of network electrostatics on primary chondrocyte behavior', *Biomaterials*, 33(30), pp. 7478–7488.

Skerra, A. (2000) 'Engineered protein scaffolds for molecular recognition', *Journal of Molecular Recognition*, 13(4), pp. 167–187.

Smith, J. W., Vestal, D. J., Irwin, S. V, Burke, T. A. and Cheresh, D. A. (1990) 'Purification and functional characterization of integrin alphavbeta 5. An adhesion receptor for vitronectin.', *The Journal of Biological Chemistry*, 265(19), pp. 11008–13.

Smits, P., Li, P., Mandel, J., Zhang, Z., Deng, J. M., Behringer, R. R., De Crombrugghe, B. and Lefebvre, V. (2001) 'The Transcription Factors L-Sox5 and Sox6 Are Essential for Cartilage Formation', *Developmental Cell*, 1(2), pp. 277–

290.

Song, L., Baksh, D. and Tuan, R. S. (2004) ‘Mesenchymal stem cell-based cartilage tissue engineering: cells, scaffold and biology.’, *Cytotherapy*, 6(6), pp. 596–601.

Sørensen, H. P. and Mortensen, K. K. (2005) ‘Advanced genetic strategies for recombinant protein expression in Escherichia coli’, *Journal of Biotechnology*, 115(2), pp. 113–128.

Soteriou, D., Iskender, B., Byron, A., Humphries, J. D., Borg-Bartolo, S., Haddock, M.-C., Baxter, M. a, Knight, D., Humphries, M. J. and Kimber, S. J. (2013) ‘Comparative proteomic analysis of supportive and unsupportive extracellular matrix substrates for human embryonic stem cell maintenance.’, *The Journal of Biological Chemistry*, 288(26), pp. 18716–31.

Stadtfeld, M. and Hochedlinger, K. (2010) ‘Induced pluripotency: History, mechanisms, and applications’, *Genes and Development*, 24(20), pp. 2239–2263.

Su, N., Jin, M. and Chen, L. (2014) 'Role of FGF/FGFR signaling in skeletal development and homeostasis: learning from mouse models', *Bone Research*, 2:14003.

Svergun, D. I. (1992) ‘Determination of the Regularization Parameter in Indirect-Transform Methods Using Perceptual Criteria’, *Journal of Applied Crystallography*, 25, pp. 495–503.

Takahashi, K., Tanabe, K., Ohnuki, M., Narita, M., Ichisaka, T., Tomoda, K. and Yamanaka, S. (2007) ‘Induction of Pluripotent Stem Cells from Adult Human Fibroblasts by Defined Factors’, *Cell*, 131(5), pp. 861–872.

Takahashi, K. and Yamanaka, S. (2006) ‘Induction of pluripotent stem cells from mouse embryonic and adult fibroblast cultures by defined factors’, *Cell*, 126(4), pp. 663–676.

Tamura, K., Shan, W. S., Hendrickson, W. A., Colman, D. R. and Shapiro, L. (1998) ‘Structure-function analysis of cell adhesion by neural (N-) cadherin’, *Neuron*, 20(6), pp. 1153–1163.

Tavella, S., Bellese, G., Castagnola, P., Martin, I., Piccini, D., Doliana, R., Colombatti, A., Cancedda, R., and Tacchetti, C. (1997) 'Regulated expression of fibronectin, laminin and related integrin receptors during the early chondrocyte differentiation', *Journal of Cell Science*, 110(8), 2261-2270.

Thomson, J. A., Itskovitz-Eldor, J., Shapiro, S. S., Waknitz, M. A., Swiergiel, J. J.,

Marshall, V. S. and Jones, J. M. (1998) 'Embryonic stem cell lines derived from human blastocysts', *Science*, 282(5391), pp. 1145–1147.

Tojo, N., Miyagi, I., Miura, M. and Ohi, H. (2008) 'Recombinant human fibrinogen expressed in the yeast Pichia pastoris was assembled and biologically active.', *Protein Expression and Purification*, 59(2), pp. 289–296.

Topham, C. M., Srinivasan, N. and Blundell, T. L. (1997) 'Prediction of the stability of protein mutants based on structural environment-dependent amino acid substitution and propensity tables.', *Protein Engineering*, 10(1), pp. 7–21.

Turner, C. E. (2000) 'Paxillin interactions', *Journal of Cell Science*, 113(23), pp. 4139–4140.

Tuschong, L., Soenen, S. L., Blaese, R. M., Candotti, F. and Muul, L. M. (2002) 'Immune Response to Fetal Calf Serum by Two Adenosine Deaminase-Deficient Patients After T Cell Gene Therapy', *Human Gene Therapy*, 13(13), pp. 1605–1610.

Usui, K., Maki, T., Ito, F., Suenaga, A., Kidoaki, S., Itoh, M., Taiji, M., Matsuda, T., Hayashizaki, Y. and Suzuki, H. (2009) 'Nanoscale elongating control of the self-assembled protein filament with the cysteine-introduced building blocks', *Protein Science*, 18(5), pp. 960–969.

Valdes, a. M., Spector, T. D., Tamm, a., Kisand, K., Doherty, S. a., Dennison, E. M., Mangino, M., Kerna, I., Hart, D. J., Wheeler, M., Cooper, C., Lories, R. J., Arden, N. K. and Doherty, M. (2010) 'Genetic variation in the SMAD3 gene is associated with hip and knee osteoarthritis.', *Arthritis and Rheumatism*, 62(8), pp. 2347–52.

Veevers-Lowe, J., Ball, S. G., Shuttleworth, A. and Kielty, C. M. (2011) 'Mesenchymal stem cell migration is regulated by fibronectin through α5β1-integrin-mediated activation of PDGFR-β and potentiation of growth factor signals.', *Journal of Cell Science*, 124(8), pp. 1288–1300.

Vinardell, T., Sheehy, E. J., Buckley, C. T. and Kelly, D. J. (2012) 'A comparison of the functionality and in vivo phenotypic stability of cartilaginous tissues engineered from different stem cell sources.', *Tissue Engineering. Part A*, 18(11–12), pp. 1161–70.

Vinatier, C., Bouffi, C., Merceron, C., Gordeladze, J., Brondello, J.-M., Jorgensen, C., Weiss, P., Guicheux, J. and Noel, D. (2009) 'Cartilage Tissue Engineering: Towards a Biomaterial-Assisted Mesenchymal Stem Cell Therapy', *Current Stem Cell Research & Therapy*, 4(4), pp. 318–329.

Vincenti, M. P. and Brinckerhoff, C. E. (2002) 'Transcriptional regulation of collagenase (MMP-1, MMP-13) genes in arthritis: integration of complex signaling pathways for the recruitment of gene-specific transcription factors.', *Arthritis Research*, 4(3), pp. 157–64.

Wang, Y. and Gilmore, T. D. (2003) 'Zyxin and paxillin proteins: Focal adhesion plaque LIM domain proteins go nuclear', *Biochimica et Biophysica Acta - Molecular Cell Research*, pp. 115–120.

Wang, Z., Oron, E., Nelson, B., Razis, S. and Ivanova, N. (2012) 'Distinct lineage specification roles for NANOG, OCT4, and SOX2 in human embryonic stem cells', *Cell Stem Cell*, 10(4), pp. 440–454.

Watanabe, K., Ueno, M., Kamiya, D., Nishiyama, A., Matsumura, M., Wataya, T., Takahashi, J. B., Nishikawa, S., Nishikawa, S., Muguruma, K. and Sasai, Y. (2007) 'A ROCK inhibitor permits survival of dissociated human embryonic stem cells.', *Nature Biotechnology*, 25(6), pp. 681–6.

Webb, B. and Sali, A. (2014) 'Comparative protein structure modeling using MODELLER', *Current Protocols in Bioinformatics*, 2014, pp. 5.6.1-5.6.32.

Weber, I. T., Harrison, R. W. and Iozzo, R. V. (1996) 'Model structure of decorin and implications for collagen fibrillogenesis', *Journal of Biological Chemistry*, 271(50), pp. 31767–31770.

Widhe, M., Johansson, U., Hillerdahl, C. O. and Hedhammar, M. (2013) 'Recombinant spider silk with cell binding motifs for specific adherence of cells', *Biomaterials*, 34(33), pp. 8223–8234.

Williams, E. J., Furness, J., Walsh, F. S. and Doherty, P. (1994) 'Activation of the FGF receptor underlies neurite outgrowth stimulated by L1, N-CAM, and N-cadherin', *Neuron*, 13(3) pp. 583-594.

Williams, E., Williams, G., Gour, B. J., Blaschuk, O. W. and Doherty, P. (2000) 'A novel family of cyclic peptide antagonists suggests that N-cadherin specificity is determined by amino acids that flank the HAV motif', *Journal of Biological Chemistry*, 275(6), pp. 4007–4012.

Williamson, M. P. (1994) 'The structure and function of proline-rich regions in proteins.', *Biochemical Journal*, 297(2), pp. 249–260.

Winn, M. D., Ballard, C. C., Cowtan, K. D., Dodson, E. J., Emsley, P., Evans, P. R., Keegan, R. M., Krissinel, E. B., Leslie, A. G. W., McCoy, A., McNicholas, S. J., Murshudov, G. N., Pannu, N. S., Potterton, E. A., Powell, H. R., Read, R. J., Vagin,

A. and Wilson, K. S. (2011) 'Overview of the CCP4 suite and current developments', *Acta Crystallographica Section D: Biological Crystallography*, 67(4), pp. 235–242.

Wozniak, M. a, Desai, R., Solski, P. a, Der, C. J. and Keely, P. J. (2003) 'ROCK-generated contractility regulates breast epithelial cell differentiation in response to the physical properties of a three-dimensional collagen matrix.', *The Journal of Cell Biology*, 163(3), pp. 583–595.

Xu, J. and Mosher, D. (2011) 'Fibronectin and Other Adhesive Glycoproteins', in *The Extracellular Matrix: an Overview*, pp. 41–75.

Xu, J., Wang, W., Ludeman, M., Cheng, K., Hayami, T., Lotz, J. C. and Kapila, S. (2008) 'Chondrogenic differentiation of human mesenchymal stem cells in three-dimensional alginate gels.', *Tissue Engineering. Part A*, 14(5), pp. 667–680.

Yamada, T., Shimada, Y., Uyeda, A., Sugiyama, S. and Kikuchi, M. (1995) 'Construction of a divalent cell adhesive lysozyme by introducing the Arg-Gly-Asp sequence at two sites', *FEBS Letters*, 374(2), pp. 262–264.

Yang, M., Tanaka, C., Yamauchi, K., Ohgo, K., Kurokawa, M. and Asakura, T. (2008) 'Silklike materials constructed from sequences of Bombyx mori silk fibroin, fibronectin, and elastin', *Journal of Biomedical Materials Research - Part A*, 84(2), pp. 353–363.

Yoon, B. S., Ovchinnikov, D. A., Yoshii, I., Mishina, Y., Behringer, R. R. and Lyons, K. M. (2005) 'Bmpr1a and Bmpr1b have overlapping functions and are essential for chondrogenesis in vivo.', *Proceedings of the National Academy of Sciences of the United States of America*, 102(14), pp. 5062–7.

Yoshida, C. A., Yamamoto, H., Fujita, T., Furuichi, T., Ito, K., Inoue, K. I., Yamana, K., Zanma, A., Takada, K., Ito, Y. and Komori, T. (2004) 'Runx2 and Runx3 are essential for chondrocyte maturation, and Runx2 regulates limb growth through induction of Indian hedgehog', *Genes and Development*, 18(8), pp. 952–963.

Yoshigi, M., Hoffman, L. M., Jensen, C. C., Yost, H. J. and Beckerle, M. C. (2005) 'Mechanical force mobilizes zyxin from focal adhesions to actin filaments and regulates cytoskeletal reinforcement', *Journal of Cell Biology*, 171(2), pp. 209–215.

You, M., Peng, G., Li, J., Ma, P., Wang, Z., Shu, W., Peng, S. and Chen, G. Q. (2011) 'Chondrogenic differentiation of human bone marrow mesenchymal stem cells on polyhydroxyalkanoate (PHA) scaffolds coated with PHA granule binding protein PhaP fused with RGD peptide', *Biomaterials*, 32(9), pp. 2305–2313.

Yun, Y. R., Kim, H. W. and Jang, J. H. (2013) 'Impact of heparin-binding domain of recombinant human osteocalcin-fibronectinIII9-14 on the osteoblastic cell response', *Biotechnology Letters*, 35(12), pp. 2213–2220.

Zaidel-Bar, R., Ballestrem, C., Kam, Z. and Geiger, B. (2003) 'Early molecular events in the assembly of matrix adhesions at the leading edge of migrating cells.', *Journal of Cell Science*, 116(22), pp. 4605–4613.

Zhang, G., Ezura, Y., Chervoneva, I., Robinson, P. S., Beason, D. P., Carine, E. T., Soslowsky, L. J., Iozzo, R. V. and Birk, D. E. (2006) 'Decorin regulates assembly of collagen fibrils and acquisition of biomechanical properties during tendon development', *Journal of Cellular Biochemistry*, 98(6), pp. 1436–1449.

Zhang, Z., Morla, A. O., Vuori, K., Bauer, J. S., Juliano, R. L. and Ruoslahti, E. (1993) 'The αvβ1 integrin functions as a fibronectin receptor but does not support fibronectin matrix assembly and cell migration on fibronectin', *Journal of Cell Biology*, 122(1), pp. 235–242.

Zhou, M., Smith, A. M., Das, A. K., Hodson, N. W., Collins, R. F., Ulijn, R. V. and Gough, J. E. (2009) 'Self-assembled peptide-based hydrogels as scaffolds for anchorage-dependent cells', *Biomaterials*, 30(13), pp. 2523–2530.

Zhu, M., Lin, S., Sun, Y., Feng, Q., Li, G. and Bian, L. (2016) 'Hydrogels functionalized with N-cadherin mimetic peptide enhance osteogenesis of hMSCs by emulating the osteogenic niche', *Biomaterials*, 77, pp. 44–52.

Zollinger, A. J. and Smith, M. L. (2016) 'Fibronectin, the extracellular glue.', *Matrix Biology*, [Epub ahead of print].

Zou, P., Gautel, M., Geerlof, A., Wilmanns, M., Koch, M. H. J. and Svergun, D. I. (2003) 'Solution scattering suggests cross-linking function of telethonin in the complex with titin', *Journal of Biological Chemistry*, 278(4), pp. 2636–2644.

Zou, P., Pinotsis, N., Lange, S., Song, Y.-H., Popov, A., Mavridis, I., Mayans, O. M., Gautel, M. and Wilmanns, M. (2006) 'Palindromic assembly of the giant muscle protein titin in the sarcomeric Z-disk.', *Nature*, 439(7073), pp. 229–233.

# Appendix

## Nucleic acid sequences of protein constructs

Both the nucleotide and translated amino acid sequence (*yellow highlight*) encoding the construct is given. The position of stop codons is represented by a dash (-).

### Tel in the pETM-11 vector

```
ttaagaaggagatataccatgaaacatcaccatcaccatcaccccatgagcgattacgac
 L  R  R  R  Y  T  M  K  H  H  H  H  H  H  P  M  S  D  Y  D
atccccactactgagaatctttattttcagggcgccatggctacctcagagctgagcagc
 I  P  T  T  E  N  L  Y  F  Q  G  A  M  A  T  S  E  L  S  S
gaggtgtcggaggagaacagtgagcgccgggaggccttctgggcagaatggaaggatctg
 E  V  S  E  E  N  S  E  R  R  E  A  F  W  A  E  W  K  D  L
acactgtccacacggcccgaggagggcagctccctgcatgaggaggacacccagagacat
 T  L  S  T  R  P  E  E  G  S  S  L  H  E  E  D  T  Q  R  H
gagacctaccaccagcaggggcagagccaggtgctggtgcagcgctcgccctggctgatg
 E  T  Y  H  Q  Q  G  Q  S  Q  V  L  V  Q  R  S  P  W  L  M
atgaggatgggcatcctcggccgtgggctgcaggagtaccagctgccctaccagcggtga
 M  R  M  G  I  L  G  R  G  L  Q  E  Y  Q  L  P  Y  Q  R  -
```

### Tel$^{N\text{-}RGD}$13 in the pETM-13 vector

```
gagcggataacaattcccctctagaaataattttgtttaactttaagaaggagatatacc
 E  R  I  T  I  P  L  -  K  -  F  C  L  T  L  R  R  R  Y  T
atgggtcatcatcatcatcatcgcggcgatagcggccgcggcgatatggctacctca
 M  G  H  H  H  H  H  H  R  G  D  S  G  R  G  D  M  A  T  S
gagctgagcagcgaggtgtcggaggagaacagtgagcgccgggaggccttctgggcagaa
 E  L  S  S  E  V  S  E  E  N  S  E  R  R  E  A  F  W  A  E
tggaaggatctgacactgtccacacggcccgaggagggcagctccctgcatgaggaggac
 W  K  D  L  T  L  S  T  R  P  E  E  G  S  S  L  H  E  E  D
acccagagacatgagacctaccaccagcaggggcagagccaggtgctggtgcagcgctcg
 T  Q  R  H  E  T  Y  H  Q  Q  G  Q  S  Q  V  L  V  Q  R  S
ccctggctgatgatgaggatgggcatcctcggccgtgggctgcaggagtaccagctgccc
 P  W  L  M  M  R  M  G  I  L  G  R  G  L  Q  E  Y  Q  L  P
taccagcggtgaggtaccggatccgaattcgagctccgt
 Y  Q  R  -  G  T  G  S  E  F  E  L  R
```

### Tel$^{N\text{-}RGE}$13 in the pETM-13 vector

```
ctctagaaataattttgtttaactttaagaaggagatataccatgggtcatcatcatcat
 L  -  K  -  F  C  L  T  L  R  R  R  Y  T  M  G  H  H  H  H
catcatcgcggcgaaagcggccgcggcgaaatggctacctcagagctgagcagcgaggtg
 H  H  R  G  E  S  G  R  G  E  M  A  T  S  E  L  S  S  E  V
tcggaggagaacagtgagcgccgggaggccttctgggcagaatggaaggatctgacactg
 S  E  E  N  S  E  R  R  E  A  F  W  A  E  W  K  D  L  T  L
```

```
tccacacggcccgaggagggcagctccctgcatgaggaggacacccagagacatgagacc
 S  T  R  P  E  E  G  S  S  L  H  E  E  D  T  Q  R  H  E  T
taccaccagcaggggcagagccaggtgctggtgcagcgctcgccctggctgatgatgagg
 Y  H  Q  Q  G  Q  S  Q  V  L  V  Q  R  S  P  W  L  M  M  R
atgggcatcctcggccgtgggctgcaggagtaccagctgccctaccagcggtgaggtacc
 M  G  I  L  G  R  G  L  Q  E  Y  Q  L  P  Y  Q  R  -  G  T
```

## Tel$^{C\text{-}RGD}$13 in the pETM-13 vector

```
ttttgtttaactttaagaaggagatataccatggctacctcagagctgagcagcgaggtg
 F  C  L  T  L  R  R  R  Y  T  M  A  T  S  E  L  S  S  E  V
tcggaggagaacagtgagcgccgggaggccttctgggcagaatggaaggatctgacactg
 S  E  E  N  S  E  R  R  E  A  F  W  A  E  W  K  D  L  T  L
tccacacggcccgaggagggcagctccctgcatgaggaggacacccagagacatgagacc
 S  T  R  P  E  E  G  S  S  L  H  E  E  D  T  Q  R  H  E  T
taccaccagcaggggcagagccaggtgctggtgcagcgctcgccctggctgatgatgagg
 Y  H  Q  Q  G  Q  S  Q  V  L  V  Q  R  S  P  W  L  M  M  R
atgggcatcctcggccgtgggctgcaggagtaccagctgccctaccagcgcggcgatagc
 M  G  I  L  G  R  G  L  Q  E  Y  Q  L  P  Y  Q  R  G  D  S
ggccgcggcgatccgcatcatcatcatcattaaggtaccggatccgaattcgagctc
 G  R  G  D  P  H  H  H  H  H  H  -  G  T  G  S  E  F  E  L
```

## Tel$^{C\text{-}RGE}$13 in the pETM-13 vector

```
acaattcccctctagaaataattttgtttaactttaagaaggagatataccatggctacc
 T  I  P  L  -  K  -  F  C  L  T  L  R  R  R  Y  T  M  A  T
tcagagctgagcagcgaggtgtcggaggagaacagtgagcgccgggaggccttctgggca
 S  E  L  S  S  E  V  S  E  E  N  S  E  R  R  E  A  F  W  A
gaatggaaggatctgacactgtccacacggcccgaggagggcagctccctgcatgaggag
 E  W  K  D  L  T  L  S  T  R  P  E  E  G  S  S  L  H  E  E
gacacccagagacatgagacctaccaccagcaggggcagagccaggtgctggtgcagcgc
 D  T  Q  R  H  E  T  Y  H  Q  Q  G  Q  S  Q  V  L  V  Q  R
tcgccctggctgatgatgaggatgggcatcctcggccgtgggctgcaggagtaccagctg
 S  P  W  L  M  M  R  M  G  I  L  G  R  G  L  Q  E  Y  Q  L
ccctaccagcgcggcgaaagcggccgcggcgaaccgcatcatcatcatcattaaggt
 P  Y  Q  R  G  E  S  G  R  G  E  P  H  H  H  H  H  H
```

## Tel$^{C\text{-}RGD}$11 in the pETM-11 vector

```
nnnnnnnnnnnnnctagaataattttgttnnctttaagaaggagatataccatgaaacat
 X  X  X  X  X  R  I  I  L  X  X  L  R  R  R  Y  T  M  K  H
caccatcaccatcaccccatgagcgattacgacatccccactactgagaatctttatttt
 H  H  H  H  H  P  M  S  D  Y  D  I  P  T  T  E  N  L  Y  F
cagggcgccatggcaacctcagagctgagcagcgaggtgtcggaggagaacagtgagcgc
 Q  G  A  M  A  T  S  E  L  S  S  E  V  S  E  E  N  S  E  R
cgggaggccttctgggcagaatggaaggatctgacactgtccacacggcccgaggagggc
 R  E  A  F  W  A  E  W  K  D  L  T  L  S  T  R  P  E  E  G
agctccctgcatgaggaggacacccagagacatgagacctaccaccagcaggggcagagc
 S  S  L  H  E  E  D  T  Q  R  H  E  T  Y  H  Q  Q  G  Q  S
caggtgctggtgcagcgctcgccctggctgatgatgaggatgggcatcctcggccgtggg
 Q  V  L  V  Q  R  S  P  W  L  M  M  R  M  G  I  L  G  R  G
ctgcaggagtaccagctgccctaccagagtggtcgcggcgatagcccctgaggtaccgga
 L  Q  E  Y  Q  L  P  Y  Q  S  G  R  G  D  S  P  -  G  T  G
```

## Tel$^{C\text{-}RGE}$11 in the pETM-11 vector

```
nnnnnnnnnnctagnaatattttgtttnctttaagaaggagatataccatgaaacatcac
 X  X  X  X  X  N  I  L  F  X  L  R  R  R  Y  T  M  K  H  H
catcaccatcaccccatgagcgattacgacatccccactactgagaatctttatttttcag
 H  H  H  H  P  M  S  D  Y  D  I  P  T  T  E  N  L  Y  F  Q
ggcgccatggcaacctcagagctgagcagcgaggtgtcggaggagaacagtgagcgccgg
 G  A  M  A  T  S  E  L  S  S  E  V  S  E  E  N  S  E  R  R
gaggccttctgggcagaatggaaggatctgacactgtccacacggcccgaggagggcagc
 E  A  F  W  A  E  W  K  D  L  T  L  S  T  R  P  E  E  G  S
tccctgcatgaggaggacacccagagacatgagacctaccaccagcaggggcagagccag
 S  L  H  E  E  D  T  Q  R  H  E  T  Y  H  Q  Q  G  Q  S  Q
gtgctggtgcagcgctcgccctggctgatgatgaggatgggcatcctcggccgtgggctg
 V  L  V  Q  R  S  P  W  L  M  M  R  M  G  I  L  G  R  G  L
caggagtaccagctgccctaccagagtggtcgcggcgaaagcccctgaggtaccggatcc
 Q  E  Y  Q  L  P  Y  Q  S  G  R  G  E  S  P  -  G  T  G  S
```

## Z1Z2 in the pETM-11 vector

```
ttaactttaagaaggagatataccatgaaacatcaccatcaccatcaccccatgagcgat
 L  T  L  R  R  R  Y  T  M  K  H  H  H  H  H  H  P  M  S  D
tacgacatccccactactgagaatctttatttttcagggcgccatggcaactcaagcaccg
 Y  D  I  P  T  T  E  N  L  Y  F  Q  G  A  M  A  T  Q  A  P
acgtttacgcagccgttacaaagcgttgtggtactggagggtagtaccgcaacctttgag
 T  F  T  Q  P  L  Q  S  V  V  V  L  E  G  S  T  A  T  F  E
gctcacattagtggttttccagttcctgaggtgagctggtttagggatggccaggtgatt
 A  H  I  S  G  F  P  V  P  E  V  S  W  F  R  D  G  Q  V  I
tccacttccactctgcccggcgtgcagatctcctttagcgatggccgcgctaaactgacg
 S  T  S  T  L  P  G  V  Q  I  S  F  S  D  G  R  A  K  L  T
atccccgccgtgactaaagccaacagtggacgatattccctgaaagccaccaatggatct
 I  P  A  V  T  K  A  N  S  G  R  Y  S  L  K  A  T  N  G  S
ggacaagcgactagtactgctgagcttctcgtgaaagctgagacagcaccacccaacttc
 G  Q  A  T  S  T  A  E  L  L  V  K  A  E  T  A  P  P  N  F
gttcaacgactgcagagcatgaccgtgagacaaggaagccaagtgagactccaagtgaga
 V  Q  R  L  Q  S  M  T  V  R  Q  G  S  Q  V  R  L  Q  V  R
gtgactggaatccctacacctgtggtgaagttctaccgggatggagccgaaatccagagt
 V  T  G  I  P  T  P  V  V  K  F  Y  R  D  G  A  E  I  Q  S
tcccttgatttccaaatttcacaagaaggcgacctctacagcttactgattgcagaagca
 S  L  D  F  Q  I  S  Q  E  G  D  L  Y  S  L  L  I  A  E  A
taccctgaggactcagggacctattcagtaaatgccaccaatagcgttggaagagctact
 Y  P  E  D  S  G  T  Y  S  V  N  A  T  N  S  V  G  R  A  T
tcgactgctgagctccttgtgcagggcgagacatgaggtaccggatccgaattcgagctc
 S  T  A  E  L  L  V  Q  G  E  T  -  G  T  G  S  E  F  E  L
```

## Z1Z2 in the pET-15b vector

```
nnnnnnnnnnnntccccnctnnnntaattttgtttaactttaagaaggagatataccatg
 X  X  X  X  S  X  X  X  -  F  C  L  T  L  R  R  R  Y  T  M
gcaactcaagcaccgacgtttacgcagccgttacaaagcgttgtggtactggagggtagt
 A  T  Q  A  P  T  F  T  Q  P  L  Q  S  V  V  V  L  E  G  S
accgcaacctttgaggctcacattagtggttttccagttcctgaggtgagctggtttagg
 T  A  T  F  E  A  H  I  S  G  F  P  V  P  E  V  S  W  F  R
gatggccaggtgatttccacttccactctgcccggcgtgcagatctcctttagcgatggc
 D  G  Q  V  I  S  T  S  T  L  P  G  V  Q  I  S  F  S  D  G
cgcgctaaactgacgatccccgccgtgactaaagccaacagtggacgatattccctgaaa
```

```
 R  A  K  L  T  I  P  A  V  T  K  A  N  S  G  R  Y  S  L  K
gccaccaatggatctggacaagcgactagtactgctgagcttctcgtgaaagctgagaca
 A  T  N  G  S  G  Q  A  T  S  T  A  E  L  L  V  K  A  E  T
gcaccacccaacttcgttcaacgactgcagagcatgaccgtgagacaaggaagccaagtg
 A  P  P  N  F  V  Q  R  L  Q  S  M  T  V  R  Q  G  S  Q  V
agactccaagtgagagtgactggaatccctacacctgtggtgaagttctaccgggatgga
 R  L  Q  V  R  V  T  G  I  P  T  P  V  V  K  F  Y  R  D  G
gccgaaatccagagttcccttgatttccaaatttcacaagaaggcgacctctacagctta
 A  E  I  Q  S  S  L  D  F  Q  I  S  Q  E  G  D  L  Y  S  L
ctgattgcagaagcataccctgaggactcagggacctattcagtaaatgccaccaatagc
 L  I  A  E  A  Y  P  E  D  S  G  T  Y  S  V  N  A  T  N  S
gttggaagagctacttcgactgctgagctccttgtgcagggcgagacatgaggtaccgga
 V  G  R  A  T  S  T  A  E  L  L  V  Q  G  E  T  -  G  T  G
```

## $Z_{1212}$ in the pETM-11 vector

```
ccntngctagaatantttgtttaactttaagaaggagatataccatgaaacatcaccat
 X  X  L  E  X  F  C  L  T  L  R  R  R  Y  T  M  K  H  H  H
caccatcaccccatgagcgattacgacatccccactactgagaatctttattttcagggc
 H  H  H  P  M  S  D  Y  D  I  P  T  T  E  N  L  Y  F  Q  G
gccatggcgactcaagcaccgacgtttacgcagccgttacaaagcgttgtggtactggag
 A  M  A  T  Q  A  P  T  F  T  Q  P  L  Q  S  V  V  V  L  E
ggtagtaccgcaacctttgaggctcacattagtggttttccagttcctgaggtgagctgg
 G  S  T  A  T  F  E  A  H  I  S  G  F  P  V  P  E  V  S  W
tttagggatggccaggtgatttccacttccactctgcccggcgtgcagatctcctttagc
 F  R  D  G  Q  V  I  S  T  S  T  L  P  G  V  Q  I  S  F  S
gatggccgcgctaaactgacgatccccgccgtgactaaagccaacagtggacgatattcc
 D  G  R  A  K  L  T  I  P  A  V  T  K  A  N  S  G  R  Y  S
ctgaaagccaccaatggatctggacaagcgactagtactgctgagcttctcgtgaaagct
 L  K  A  T  N  G  S  G  Q  A  T  S  T  A  E  L  L  V  K  A
gagacagcaccacccaacttcgttcaacgactgcagagcatgaccgtgagacaaggaagc
 E  T  A  P  P  N  F  V  Q  R  L  Q  S  M  T  V  R  Q  G  S
caagtgagactccaagtgagagtgactggaatccctacacctgtggtgaagttctaccgg
 Q  V  R  L  Q  V  R  V  T  G  I  P  T  P  V  V  K  F  Y  R
gatggagccgaaatccagagttcccttgatttccaaatttcacaagaaggcgacctctac
 D  G  A  E  I  Q  S  S  L  D  F  Q  I  S  Q  E  G  D  L  Y
agcttactgattgcagaagcataccctgaggactcagggacctattcagtaaatgccacc
 S  L  L  I  A  E  A  Y  P  E  D  S  G  T  Y  S  V  N  A  T
aatagcgttggaagagctacttcgactgctgagctccttgtgcagggcgagacaactcaa
 N  S  V  G  R  A  T  S  T  A  E  L  L  V  Q  G  E  T  T  Q
gcaccgacgtttacgcagccgttacaaagcgttgtggtactggagggtagtaccgcaacc
 A  P  T  F  T  Q  P  L  Q  S  V  V  V  L  E  G  S  T  A  T
tttgaggctcacattagtggttttccagttcctgaggtgagctggtttagggatggccag
 F  E  A  H  I  S  G  F  P  V  P  E  V  S  W  F  R  D  G  Q
gtgatttccacttccactctgcccggcgtgcagatctcctttagcgatggccgcgctaaa
 V  I  S  T  S  T  L  P  G  V  Q  I  S  F  S  D  G  R  A  K
ctgacgatccccgccgtgactaaagccaacagtggacgatattccctgaaagccaccaat
 L  T  I  P  A  V  T  K  A  N  S  G  R  Y  S  L  K  A  T  N
ggatctggacaagcgactagtactgctgagcttctcgtgaaagctgagacagcaccaccc
 G  S  G  Q  A  T  S  T  A  E  L  L  V  K  A  E  T  A  P  P
aacttcgttcaacgactgcagagcatgaccgtgagacaaggaagccaagtgagactccaa
 N  F  V  Q  R  L  Q  S  M  T  V  R  Q  G  S  Q  V  R  L  Q
gtgagagtgactggaatccctacacctgtggtgaagttctaccgggatggagccgaaatc
 V  R  V  T  G  I  P  T  P  V  V  K  F  Y  R  D  G  A  E  I
cagagttcccttgatttccaaatttcacaagaaggcgacctctacagcttactgattgca
 Q  S  S  L  D  F  Q  I  S  Q  E  G  D  L  Y  S  L  L  I  A
gaagcataccctgaggactcagggacctattcagtaaatgccaccaatagcgttggaaga
 E  A  Y  P  E  D  S  G  T  Y  S  V  N  A  T  N  S  V  G  R
gctacttcgactgctgaattactggttcaaggtgaatgaaagcttgcggccgcactcgag
 A  T  S  T  A  E  L  L  V  Q  G  E  -  K  L  A  A  A  L  E
```

## Z1Z2$^{RGD}$ in the pETM-11 vector

```
nnnnnnnnnnnnnnnnnntctnnnannattttgtttaactttaagaaggagatataccatg
 X  X  X  X  X  X  X  X  X  F  C  L  T  L  R  R  R  Y  T  M
aaacatcaccatcaccatcaccccatgagcgattacgacatccccactactgagaatctt
 K  H  H  H  H  H  H  P  M  S  D  Y  D  I  P  T  T  E  N  L
tattttcagggcgccatggcaactcaagcaccgacgtttacgcagccgttacaaagcgtt
 Y  F  Q  G  A  M  A  T  Q  A  P  T  F  T  Q  P  L  Q  S  V
gtggtactggagggtagtaccgcaacctttgaggctcacattagtggttttccagttcct
 V  V  L  E  G  S  T  A  T  F  E  A  H  I  S  G  F  P  V  P
gaggtgagctggtttagggatggccaggtgatttccagtggtcgcggcgatagcagtccc
 E  V  S  W  F  R  D  G  Q  V  I  S  S  G  R  G  D  S  S  P
ggcgtgcagatctcctttagcgatggccgcgctaaactgacgatccccgccgtgactaaa
 G  V  Q  I  S  F  S  D  G  R  A  K  L  T  I  P  A  V  T  K
gccaacagtggacgatattccctgaaagccaccaatggatctggacaagcgactagtact
 A  N  S  G  R  Y  S  L  K  A  T  N  G  S  G  Q  A  T  S  T
gctgagcttctcgtgaaagctgagacagcaccacccaacttcgttcaacgactgcagagc
 A  E  L  L  V  K  A  E  T  A  P  P  N  F  V  Q  R  L  Q  S
atgaccgtgagacaaggaagccaagtgagactccaagtgagagtgactggaatccctaca
 M  T  V  R  Q  G  S  Q  V  R  L  Q  V  R  V  T  G  I  P  T
cctgtggtgaagttctaccgggatggagccgaaatccagagttcccttgatttccaaatt
 P  V  V  K  F  Y  R  D  G  A  E  I  Q  S  S  L  D  F  Q  I
tcacaagaaggcgacctctacagcttactgattgcagaagcataccctgaggactcaggg
 S  Q  E  G  D  L  Y  S  L  L  I  A  E  A  Y  P  E  D  S  G
acctattcagtaaatgccaccaatagcgttggaagagctacttcgactgctgaattactg
 T  Y  S  V  N  A  T  N  S  V  G  R  A  T  S  T  A  E  L  L
gttcaaggtgaatgaaagcttgcggccgcactcgagcaccaccaccaccaccactgagat
 V  Q  G  E  -  K  L  A  A  A  L  E  H  H  H  H  H  H  -  D
```

## Z1Z2$^{RGD}$ in the pET-15b vector

```
atgacaactcaagcaccgacgtttacgcagccgttacaaagcgttgtggtactggagggt
 M  T  T  Q  A  P  T  F  T  Q  P  L  Q  S  V  V  V  L  E  G
agtaccgcaacctttgaggctcacattagtggttttccagttcctgaggtgagctggttt
 S  T  A  T  F  E  A  H  I  S  G  F  P  V  P  E  V  S  W  F
agggatggccaggtgatttccagtggtcgcggcgatagcagtcccggcgtgcagatctcc
 R  D  G  Q  V  I  S  S  G  R  G  D  S  S  P  G  V  Q  I  S
tttagcgatggccgcgctaaactgacgatccccgccgtgactaaagccaacagtggacga
 F  S  D  G  R  A  K  L  T  I  P  A  V  T  K  A  N  S  G  R
tattccctgaaagccaccaatggatctggacaagcgactagtactgctgagcttctcgtg
 Y  S  L  K  A  T  N  G  S  G  Q  A  T  S  T  A  E  L  L  V
aaagctgagacagcaccacccaacttcgttcaacgactgcagagcatgaccgtgagacaa
 K  A  E  T  A  P  P  N  F  V  Q  R  L  Q  S  M  T  V  R  Q
ggaagccaagtgagactccaagtgagagtgactggaatccctacacctgtggtgaagttc
 G  S  Q  V  R  L  Q  V  R  V  T  G  I  P  T  P  V  V  K  F
taccgggatggagccgaaatccagagttcccttgatttccaaatttcacaagaaggcgac
 Y  R  D  G  A  E  I  Q  S  S  L  D  F  Q  I  S  Q  E  G  D
ctctacagcttactgattgcagaagcataccctgaggactcagggacctattcagtaaat
 L  Y  S  L  L  I  A  E  A  Y  P  E  D  S  G  T  Y  S  V  N
gccaccaatagcgttggaagagctacttcgactgctgaattactggttcaaggtgaatga
 A  T  N  S  V  G  R  A  T  S  T  A  E  L  L  V  Q  G  E  -
```

## $Z_{1212}^{RGD}$ in the pETM-11 vector

```
nnnnnnnnntnccctctannnnnntttgtttaactttaagaaggagatataccatgaaa
 X  X  X  X  P  L  X  X  F  C  L  T  L  R  R  R  Y  T  M  K
catcaccatcaccatcaccccatgagcgattacgacatccccactactgagaatctttat
 H  H  H  H  H  H  P  M  S  D  Y  D  I  P  T  T  E  N  L  Y
tttcagggcgccatggcgactcaagcaccgacgtttacgcagccgttacaaagcgttgtg
 F  Q  G  A  M  A  T  Q  A  P  T  F  T  Q  P  L  Q  S  V  V
gtactggagggtagtaccgcaacctttgaggctcacattagtggttttccagttcctgag
 V  L  E  G  S  T  A  T  F  E  A  H  I  S  G  F  P  V  P  E
gtgagctggtttagggatggccaggtgatttccacttccactctgcccggcgtgcagatc
 V  S  W  F  R  D  G  Q  V  I  S  T  S  T  L  P  G  V  Q  I
tcctttagcgatggccgcgctaaactgacgatccccgccgtgactaaagccaacagtgga
 S  F  S  D  G  R  A  K  L  T  I  P  A  V  T  K  A  N  S  G
cgatattccctgaaagccaccaatggatctggacaagcgactagtactgctgagcttctc
 R  Y  S  L  K  A  T  N  G  S  G  Q  A  T  S  T  A  E  L  L
gtgaaagctgagacagcaccacccaacttcgttcaacgactgcagagcatgaccgtgaga
 V  K  A  E  T  A  P  P  N  F  V  Q  R  L  Q  S  M  T  V  R
caaggaagccaagtgagactccaagtgagagtgactggaatccctacacctgtggtgaag
 Q  G  S  Q  V  R  L  Q  V  R  V  T  G  I  P  T  P  V  V  K
ttctaccgggatggagccgaaatccagagttcccttgatttccaaatttcacaagaaggc
 F  Y  R  D  G  A  E  I  Q  S  S  L  D  F  Q  I  S  Q  E  G
gacctctacagcttactgattgcagaagcataccctgaggactcagggacctattcagta
 D  L  Y  S  L  L  I  A  E  A  Y  P  E  D  S  G  T  Y  S  V
aatgccaccaatagcgttggaagagctacttcgactgctgagctccttgtgcagggcgag
 N  A  T  N  S  V  G  R  A  T  S  T  A  E  L  L  V  Q  G  E
acaactcaagcaccgacgtttacgcagccgttacaaagcgttgtggtactggagggtagt
 T  T  Q  A  P  T  F  T  Q  P  L  Q  S  V  V  V  L  E  G  S
accgcaacctttgaggctcacattagtggttttccagttcctgaggtgagctggtttagg
 T  A  T  F  E  A  H  I  S  G  F  P  V  P  E  V  S  W  F  R
gatggccaggtgatttccagtggtcgcggcgatagcagtcccggcgtgcagatctccttt
 D  G  Q  V  I  S  S  G  R  G  D  S  S  P  G  V  Q  I  S  F
agcgatggccgcgctaaactgacgatccccgccgtgactaaagccaacagtggacgatat
 S  D  G  R  A  K  L  T  I  P  A  V  T  K  A  N  S  G  R  Y
tccctgaaagccaccaatggatctggacaagcgactagtactgctgagcttctcgtgaaa
 S  L  K  A  T  N  G  S  G  Q  A  T  S  T  A  E  L  L  V  K
gctgagacagcaccacccaacttcgttcaacgactgcagagcatgaccgtgagacaagga
 A  E  T  A  P  P  N  F  V  Q  R  L  Q  S  M  T  V  R  Q  G
agccaagtgagactccaagtgagagtgactggaatccctacacctgtggtgaagttctac
 S  Q  V  R  L  Q  V  R  V  T  G  I  P  T  P  V  V  K  F  Y
cgggatggagccgaaatccagagttcccttgatttccaaatttcacaagaaggcgacctc
 R  D  G  A  E  I  Q  S  S  L  D  F  Q  I  S  Q  E  G  D  L
tacagcttactgattgcagaagcataccctgaggactcagggacctattcagtaaatgcc
 Y  S  L  L  I  A  E  A  Y  P  E  D  S  G  T  Y  S  V  N  A
accaatagcgttggaagagctacttcgactgctgaattactggttcaaggtgaatgaaag
 T  N  S  V  G  R  A  T  S  T  A  E  L  L  V  Q  G  E  -  K
```

## $Z1Z2^{RGE}$ in the pETM-11 vector

```
nnnnnnnnnnnccnnctannnnnntttgtttaactttaagaaggagatataccatgaaa
 X  X  X  X  X  L  X  X  F  C  L  T  L  R  R  R  Y  T  M  K
catcaccatcaccatcaccccatgagcgattacgacatccccactactgagaatctttat
 H  H  H  H  H  H  P  M  S  D  Y  D  I  P  T  T  E  N  L  Y
tttcagggcgccatggcaactcaagcaccgacgtttacgcagccgttacaaagcgttgtg
 F  Q  G  A  M  A  T  Q  A  P  T  F  T  Q  P  L  Q  S  V  V
gtactggagggtagtaccgcaacctttgaggctcacattagtggttttccagttcctgag
 V  L  E  G  S  T  A  T  F  E  A  H  I  S  G  F  P  V  P  E
gtgagctggtttagggatggccaggtgatttccagtggtcgcggcgagagcagtcccggc
 V  S  W  F  R  D  G  Q  V  I  S  S  G  R  G  E  S  S  P  G
```

```
gtgcagatctcctttagcgatggccgcgctaaactgacgatccccgccgtgactaaagcc
 V  Q  I  S  F  S  D  G  R  A  K  L  T  I  P  A  V  T  K  A
aacagtggacgatattccctgaaagccaccaatggatctggacaagcgactagtactgct
 N  S  G  R  Y  S  L  K  A  T  N  G  S  G  Q  A  T  S  T  A
gagcttctcgtgaaagctgagacagcaccacccaacttcgttcaacgactgcagagcatg
 E  L  L  V  K  A  E  T  A  P  P  N  F  V  Q  R  L  Q  S  M
accgtgagacaaggaagccaagtgagactccaagtgagagtgactggaatccctacacct
 T  V  R  Q  G  S  Q  V  R  L  Q  V  R  V  T  G  I  P  T  P
gtggtgaagttctaccgggatggagccgaaatccagagttcccttgatttccaaatttca
 V  V  K  F  Y  R  D  G  A  E  I  Q  S  S  L  D  F  Q  I  S
caagaaggcgacctctacagcttactgattgcagaagcataccctgaggactcagggacc
 Q  E  G  D  L  Y  S  L  L  I  A  E  A  Y  P  E  D  S  G  T
tattcagtaaatgccaccaatagcgttggaagagctacttcgactgctgaattactggtt
 Y  S  V  N  A  T  N  S  V  G  R  A  T  S  T  A  E  L  L  V
caaggtgaatgaaagcttgcggccgcactcgagcaccaccaccaccaccactgagatccg
 Q  G  E  -  K  L  A  A  A  L  E  H  H  H  H  H  H  -  D  P
```

## $Z_{1212}^{RGD}$ in the pETM-11 vector

```
nnnnnnntnnnnnctagnntnntttgtttaactttaagaaggagatataccatgaaacat
 X  X  X  X  X  X  X  X  C  L  T  L  R  R  R  Y  T  M  K  H
caccatcaccatcaccccatgagcgattacgacatccccactactgagaatctttatttt
 H  H  H  H  H  P  M  S  D  Y  D  I  P  T  T  E  N  L  Y  F
cagggcgccatggcgactcaagcaccgacgtttacgcagccgttacaaagcgttgtggta
 Q  G  A  M  A  T  Q  A  P  T  F  T  Q  P  L  Q  S  V  V  V
ctggagggtagtaccgcaacctttgaggctcacattagtggttttccagttcctgaggtg
 L  E  G  S  T  A  T  F  E  A  H  I  S  G  F  P  V  P  E  V
agctggtttagggatggccaggtgatttccacttccactctgcccggcgtgcagatctcc
 S  W  F  R  D  G  Q  V  I  S  T  S  T  L  P  G  V  Q  I  S
tttagcgatggccgcgctaaactgacgatccccgccgtgactaaagccaacagtggacga
 F  S  D  G  R  A  K  L  T  I  P  A  V  T  K  A  N  S  G  R
tattccctgaaagccaccaatggatctggacaagcgactagtactgctgagcttctcgtg
 Y  S  L  K  A  T  N  G  S  G  Q  A  T  S  T  A  E  L  L  V
aaagctgagacagcaccacccaacttcgttcaacgactgcagagcatgaccgtgagacaa
 K  A  E  T  A  P  P  N  F  V  Q  R  L  Q  S  M  T  V  R  Q
ggaagccaagtgagactccaagtgagagtgactggaatccctacacctgtggtgaagttc
 G  S  Q  V  R  L  Q  V  R  V  T  G  I  P  T  P  V  V  K  F
taccgggatggagccgaaatccagagttcccttgatttccaaatttcacaagaaggcgac
 Y  R  D  G  A  E  I  Q  S  S  L  D  F  Q  I  S  Q  E  G  D
ctctacagcttactgattgcagaagcataccctgaggactcagggacctattcagtaaat
 L  Y  S  L  L  I  A  E  A  Y  P  E  D  S  G  T  Y  S  V  N
gccaccaatagcgttggaagagctacttcgactgctgagctccttgtgcagggcgagaca
 A  T  N  S  V  G  R  A  T  S  T  A  E  L  L  V  Q  G  E  T
actcaagcaccgacgtttacgcagccgttacaaagcgttgtggtactggagggtagtacc
 T  Q  A  P  T  F  T  Q  P  L  Q  S  V  V  V  L  E  G  S  T
gcaacctttgaggctcacattagtggttttccagttcctgaggtgagctggtttagggat
 A  T  F  E  A  H  I  S  G  F  P  V  P  E  V  S  W  F  R  D
ggccaggtgatttccagtggtcgcggcgagagcagtcccggcgtgcagatctcctttagc
 G  Q  V  I  S  S  G  R  G  E  S  S  P  G  V  Q  I  S  F  S
gatggccgcgctaaactgacgatccccgccgtgactaaagccaacagtggacgatattcc
 D  G  R  A  K  L  T  I  P  A  V  T  K  A  N  S  G  R  Y  S
ctgaaagccaccaatggatctggacaagcgactagtactgctgagcttctcgtgaaagct
 L  K  A  T  N  G  S  G  Q  A  T  S  T  A  E  L  L  V  K  A
gagacagcaccacccaacttcgttcaacgactgcagagcatgaccgtgagacaaggaagc
 E  T  A  P  P  N  F  V  Q  R  L  Q  S  M  T  V  R  Q  G  S
caagtgagactccaagtgagagtgactggaatccctacacctgtggtgaagttctaccgg
 Q  V  R  L  Q  V  R  V  T  G  I  P  T  P  V  V  K  F  Y  R
gatggagccgaaatccagagttcccttgatttccaaatttcacaagaaggcgacctctac
 D  G  A  E  I  Q  S  S  L  D  F  Q  I  S  Q  E  G  D  L  Y
```

```
agcttactgattgcagaagcataccctgaggactcagggacctattcagtaaatgccacc
 S  L  L  I  A  E  A  Y  P  E  D  S  G  T  Y  S  V  N  A  T
aatagcgttggaagagctacttcgactgctgaattactggttcaaggtgaatgaaagctt
 N  S  V  G  R  A  T  S  T  A  E  L  L  V  Q  G  E  -  K  L
```

## Z1Z2$^{Fn}$ in the pET-15b vector

```
ctactgagaatctttattttcagggcgccatggatgacaactcaagcaccgacgtttacg
 L  L  R  I  F  I  F  R  A  P  W  M  T  T  Q  A  P  T  F  T
cagccgttacaaagcgttgtggtactggagggtagtaccgcaacctttgaggctcacatt
 Q  P  L  Q  S  V  V  V  L  E  G  S  T  A  T  F  E  A  H  I
agtggttttccagttcctgaggtgagctggtttagggatggccaggtgatttccacttcc
 S  G  F  P  V  P  E  V  S  W  F  R  D  G  Q  V  I  S  T  S
actctgcccggcgtgcagatctcctttagcgatggccgcgctaaactgacgatccccgcc
 T  L  P  G  V  Q  I  S  F  S  D  G  R  A  K  L  T  I  P  A
gtgactaaagccaacagtggacgatattccctgaaagccaccaatggatctggacaagcg
 V  T  K  A  N  S  G  R  Y  S  L  K  A  T  N  G  S  G  Q  A
actagtactgctgagcttctcgtgaaagctgagacagcaccacccaacttcgttcaacga
 T  S  T  A  E  L  L  V  K  A  E  T  A  P  P  N  F  V  Q  R
ctgcagagcatgaccgtgagacaaggaagccaagtgagactccaagtgagagtgactgga
 L  Q  S  M  T  V  R  Q  G  S  Q  V  R  L  Q  V  R  V  T  G
atccctacacctgtggtgaagttctaccgggatggagccgaaatccagagttcccttgat
 I  P  T  P  V  V  K  F  Y  R  D  G  A  E  I  Q  S  S  L  D
ttccaaatttcacaagaaggcgacctctacagcttactgattgcagaagcataccctgag
 F  Q  I  S  Q  E  G  D  L  Y  S  L  L  I  A  E  A  Y  P  E
gactcagggacctattcagtaaatgccaccaatagcgttggaagagctacttcgactgct
 D  S  G  T  Y  S  V  N  A  T  N  S  V  G  R  A  T  S  T  A
gaattactggttcaaggtgaaactactcaatctgatgttccgagggacctggaagttgtt
 E  L  L  V  Q  G  E  T  T  Q  S  D  V  P  R  D  L  E  V  V
gctgcgacccccaccagcctactgatcagctgggatgctcctgctgtcacagtgagatat
 A  A  T  P  T  S  L  L  I  S  W  D  A  P  A  V  T  V  R  Y
tacaggatcacttacggagaaacaggaggaaatagccctgtccaggagttcactgtgcct
 Y  R  I  T  Y  G  E  T  G  G  N  S  P  V  Q  E  F  T  V  P
gggagcaagtctacagctaccatcagcggccttaaacctggagttgattataccatcact
 G  S  K  S  T  A  T  I  S  G  L  K  P  G  V  D  Y  T  I  T
gtgtatgctgtcactggccgtggagacagccccgcaagcagcaagccaatttccattaat
 V  Y  A  V  T  G  R  G  D  S  P  A  S  S  K  P  I  S  I  N
taccgaacagaaattgactgaggtaccggatccgaattcgagctccgtcgacaagcttgc
 Y  R  T  E  I  D  -  G  T  G  S  E  F  E  L  R  R  Q  A  C
```

## $Z_{1212}$$^{Fn}$ in the pETM-11 vector

```
nnnnnnnncccnctnnnnnaattttgtttaactttaagaaggagatataccatgaaacat
 X  X  X  X  X  X  X  F  C  L  T  L  R  R  R  Y  T  M  K  H
caccatcaccatcaccccatgagcgattacgacatccccactactgagaatctttatttt
 H  H  H  H  H  P  M  S  D  Y  D  I  P  T  T  E  N  L  Y  F
cagggcgccatggcaactcaagcaccgacgtttacgcagccgttacaaagcgttgtggta
 Q  G  A  M  A  T  Q  A  P  T  F  T  Q  P  L  Q  S  V  V  V
ctggagggtagtaccgcaacctttgaggctcacattagtggttttccagttcctgaggtg
 L  E  G  S  T  A  T  F  E  A  H  I  S  G  F  P  V  P  E  V
agctggtttagggatggccaggtgatttccacttccactctgcccggcgtgcagatctcc
 S  W  F  R  D  G  Q  V  I  S  T  S  T  L  P  G  V  Q  I  S
tttagcgatggccgcgctaaactgacgatccccgccgtgactaaagccaacagtggacga
 F  S  D  G  R  A  K  L  T  I  P  A  V  T  K  A  N  S  G  R
tattccctgaaagccaccaatggatctggacaagcgactagtactgctgagcttctcgtg
 Y  S  L  K  A  T  N  G  S  G  Q  A  T  S  T  A  E  L  L  V
aaagctgagacagcaccacccaacttcgttcaacgactgcagagcatgaccgtgagacaa
```

```
 K  A  E  T  A  P  P  N  F  V  Q  R  L  Q  S  M  T  V  R  Q
ggaagccaagtgagactccaagtgagagtgactggaatccctacacctgtggtgaagttc
 G  S  Q  V  R  L  Q  V  R  V  T  G  I  P  T  P  V  V  K  F
taccgggatggagccgaaatccagagttcccttgatttccaaatttcacaagaaggcgac
 Y  R  D  G  A  E  I  Q  S  S  L  D  F  Q  I  S  Q  E  G  D
ctctacagcttactgattgcagaagcataccctgaggactcagggacctattcagtaaat
 L  Y  S  L  L  I  A  E  A  Y  P  E  D  S  G  T  Y  S  V  N
gccaccaatagcgttggaagagctacttcgactgctgagctccttgtgcagggcgagaca
 A  T  N  S  V  G  R  A  T  S  T  A  E  L  L  V  Q  G  E  T
actcaagcaccgacgtttacgcagccgttacaaagcgttgtggtactggagggtagtacc
 T  Q  A  P  T  F  T  Q  P  L  Q  S  V  V  V  L  E  G  S  T
gcaacctttgaggctcacattagtggttttccagttcctgaggtgagctggtttagggat
 A  T  F  E  A  H  I  S  G  F  P  V  P  E  V  S  W  F  R  D
ggccaggtgatttccacttccactctgcccggcgtgcagatctcctttagcgatggccgc
 G  Q  V  I  S  T  S  T  L  P  G  V  Q  I  S  F  S  D  G  R
gctaaactgacgatccccgccgtgactaaagccaacagtggacgatattccctgaaagcc
 A  K  L  T  I  P  A  V  T  K  A  N  S  G  R  Y  S  L  K  A
accaatggatctggacaagcgactagtactgctgagcttctcgtgaaagctgagacagca
 T  N  G  S  G  Q  A  T  S  T  A  E  L  L  V  K  A  E  T  A
ccacccaacttcgttcaacgactgcagagcatgaccgtgagacaaggaagccaagtgaga
 P  P  N  F  V  Q  R  L  Q  S  M  T  V  R  Q  G  S  Q  V  R
ctccaagtgagagtgactggaatccctacacctgtggtgaagttctaccgggatggagcc
 L  Q  V  R  V  T  G  I  P  T  P  V  V  K  F  Y  R  D  G  A
gaaatccagagttcccttgatttccaaatttcacaagaaggcgacctctacagcttactg
 E  I  Q  S  S  L  D  F  Q  I  S  Q  E  G  D  L  Y  S  L  L
attgcagaagcataccctgaggactcagggacctattcagtaaatgccaccaatagcgtt
 I  A  E  A  Y  P  E  D  S  G  T  Y  S  V  N  A  T  N  S  V
ggaagagctacttcgactgctgaattactggttcaaggtgaaactactcaatctgatgtt
 G  R  A  T  S  T  A  E  L  L  V  Q  G  E  T  T  Q  S  D  V
ccgagggacctggaagttgttgctgcgacccccaccagcctactgatcagctgggatgct
 P  R  D  L  E  V  V  A  A  T  P  T  S  L  L  I  S  W  D  A
cctgctgtcacagtgagatattacaggatcacttacggagaaacaggaggaaatagccct
 P  A  V  T  V  R  Y  Y  R  I  T  Y  G  E  T  G  G  N  S  P
gtccaggagttcactgtgcctgggagcaagtctacagctaccatcagcggccttaaacct
 V  Q  E  F  T  V  P  G  S  K  S  T  A  T  I  S  G  L  K  P
ggagttgattataccatcactgtgtatgctgtcactggccgtggagacagccccgcaagc
 G  V  D  Y  T  I  T  V  Y  A  V  T  G  R  G  D  S  P  A  S
agcaagccaatttccattaattaccgaacagaaattgactgaggtaccggatccgaattc
 S  K  P  I  S  I  N  Y  R  T  E  I  D  -  G  T  G  S  E  F
```

**Fibronectin FnIII 8-11 in the pETM-11 vector**

```
ttcagggcgccatggatcatcccagctgttcctcctcccactgacctgcgattcaccaac
 F  R  A  P  W  I  I  P  A  V  P  P  P  T  D  L  R  F  T  N
attggtccagacaccatgcgtgtcacctgggctccacccccatccattgatttaaccaac
 I  G  P  D  T  M  R  V  T  W  A  P  P  P  S  I  D  L  T  N
ttcctggtgcgttactcacctgtgaaaaatgaggaagatgttgcagagttgtcaatttct
 F  L  V  R  Y  S  P  V  K  N  E  E  D  V  A  E  L  S  I  S
ccttcagacaatgcagtggtcttaacaaatctcctgcctggtacagaatatgtagtgagt
 P  S  D  N  A  V  V  L  T  N  L  L  P  G  T  E  Y  V  V  S
gtctccagtgtctacgaacaacatgagagcacacctcttagaggaagacagaaaacaggt
 V  S  S  V  Y  E  Q  H  E  S  T  P  L  R  G  R  Q  K  T  G
cttgattccccaactggcattgacttttctgatattactgccaactcttttactgtgcac
 L  D  S  P  T  G  I  D  F  S  D  I  T  A  N  S  F  T  V  H
tggattgctcctcgagccaccatcactggctacaggatccgccatcatcccgagcacttc
 W  I  A  P  R  A  T  I  T  G  Y  R  I  R  H  H  P  E  H  F
agtgggagacctcgagaagatcgggtgccccactctcggaattccatcaccctcaccaac
 S  G  R  P  R  E  D  R  V  P  H  S  R  N  S  I  T  L  T  N
ctcactccaggcacagagtatgtggtcagcatcgttgctcttaatggcagagaggaaagt
```

```
 L  T  P  G  T  E  Y  V  V  S  I  V  A  L  N  G  R  E  E  S
ccctttattgattggccaacaatcaacagtttctgatgttccgagggacctggaagttgtt
 P  L  L  I  G  Q  Q  S  T  V  S  D  V  P  R  D  L  E  V  V
gctgcgacccccaccagcctactgatcagctgggatgctcctgctgtcacagtgagatat
 A  A  T  P  T  S  L  L  I  S  W  D  A  P  A  V  T  V  R  Y
tacaggatcacttacggagaaacaggaggaaatagccctgtccaggagttcactgtgcct
 Y  R  I  T  Y  G  E  T  G  G  N  S  P  V  Q  E  F  T  V  P
gggagcaagtctacagctaccatcagcggccttaaacctggagttgattataccatcact
 G  S  K  S  T  A  T  I  S  G  L  K  P  G  V  D  Y  T  I  T
gtgtatgctgtcactggccgtggagacagccccgcaagcagcaagccaatttccattaat
 V  Y  A  V  T  G  R  G  D  S  P  A  S  S  K  P  I  S  I  N
taccgaacagaaattgacaaaccatcccagatgcaagtgaccgatgttcaggacaacagc
 Y  R  T  E  I  D  K  P  S  Q  M  Q  V  T  D  V  Q  D  N  S
attagtgtcaagtggctgccttcaagttcccctgttactggttacagagtaaccaccact
 I  S  V  K  W  L  P  S  S  S  P  V  T  G  Y  R  V  T  T  T
cccaaaaatggaccaggaccaacaaaaactaaaactgcaggtccagatcaaacagaaatg
 P  K  N  G  P  G  P  T  K  T  K  T  A  G  P  D  Q  T  E  M
actattgaaggcttgcagcccacagtggagtatgtggttagtgtctatgctcagaatcca
 T  I  E  G  L  Q  P  T  V  E  Y  V  V  S  V  Y  A  Q  N  P
agcggagagagtcagcctctggttcagactgcagtaaccaacattgatcgccctaaagga
 S  G  E  S  Q  P  L  V  Q  T  A  V  T  N  I  D  R  P  K  G
```

## Z1Z2$^{HAVD}$ in the pETM-11 vector

```
nattcccctctngatattttgtttactttaagaaggagatataccatgaaacatcaccat
 X  S  P  X  D  I  L  F  T  L  R  R  R  Y  T  M  K  H  H  H
caccatcaccccatgagcgattacgacatccccactactgagaatctttattttcagggc
 H  H  H  P  M  S  D  Y  D  I  P  T  T  E  N  L  Y  F  Q  G
gccatggcaactcaagcaccgacgtttacgcagccgttacaaagcgttgtggtactggag
 A  M  A  T  Q  A  P  T  F  T  Q  P  L  Q  S  V  V  V  L  E
ggtagtaccgcaacctttgaggctcacgctgttgattttccagttcctgaggtgagctgg
 G  S  T  A  T  F  E  A  H  A  V  D  F  P  V  P  E  V  S  W
tttagggatggccaggtgatttccacttccactctgcccggcgtgcagatctcctttagc
 F  R  D  G  Q  V  I  S  T  S  T  L  P  G  V  Q  I  S  F  S
gatggccgcgctaaactgacgatccccgccgtgactaaagccaacagtggacgatattcc
 D  G  R  A  K  L  T  I  P  A  V  T  K  A  N  S  G  R  Y  S
ctgaaagccaccaatggatctggacaagcgactagtactgctgagcttctcgtgaaagct
 L  K  A  T  N  G  S  G  Q  A  T  S  T  A  E  L  L  V  K  A
gagacagcaccacccaacttcgttcaacgactgcagagcatgaccgtgagacaaggaagc
 E  T  A  P  P  N  F  V  Q  R  L  Q  S  M  T  V  R  Q  G  S
caagtgagactccaagtgagagtgactggaatccctacacctgtggtgaagttctaccgg
 Q  V  R  L  Q  V  R  V  T  G  I  P  T  P  V  V  K  F  Y  R
gatggagccgaaatccagagttcccttgatttccaaatttcacaagaaggcgacctctac
 D  G  A  E  I  Q  S  S  L  D  F  Q  I  S  Q  E  G  D  L  Y
agcttactgattgcagaagcataccctgaggactcagggacctattcagtaaatgccacc
 S  L  L  I  A  E  A  Y  P  E  D  S  G  T  Y  S  V  N  A  T
aatagcgttggaagagctacttcgactgctgagctccttgtgcagggcgagacatgaggt
 N  S  V  G  R  A  T  S  T  A  E  L  L  V  Q  G  E  T  -  G
accggatccgaattcgagctccgtcgacaagcttgcggccgcactcgagcaccaccacca
 T  G  S  E  F  E  L  R  R  Q  A  C  G  R  T  R  A  P  P  P
```

## $Z_{1212}$$^{HAVD}$ in the pETM-11 vector

```
aaacatcaccatcaccatcaccccatgagcgattacgacatccccactactgagaatctt
 K  H  H  H  H  H  H  P  M  S  D  Y  D  I  P  T  T  E  N  L
tattttcagggcgccatggcaactcaagcaccgacgtttacgcagccgttacaaagcgtt
 Y  F  Q  G  A  M  A  T  Q  A  P  T  F  T  Q  P  L  Q  S  V
gtggtactggagggtagtaccgcaacctttgaggctcacgctgttgattttccagttcct
```

```
 V  V  L  E  G  S  T  A  T  F  E  A  H  A  V  D  F  P  V  P
gaggtgagctggtttagggatggccaggtgatttccacttccactctgcccggcgtgcag
 E  V  S  W  F  R  D  G  Q  V  I  S  T  S  T  L  P  G  V  Q
atctcctttagcgatggccgcgctaaactgacgatccccgccgtgactaaagccaacagt
 I  S  F  S  D  G  R  A  K  L  T  I  P  A  V  T  K  A  N  S
ggacgatattccctgaaagccaccaatggatctggacaagcgactagtactgctgagctt
 G  R  Y  S  L  K  A  T  N  G  S  G  Q  A  T  S  T  A  E  L
ctcgtgaaagctgagacagcaccacccaacttcgttcaacgactgcagagcatgaccgtg
 L  V  K  A  E  T  A  P  P  N  F  V  Q  R  L  Q  S  M  T  V
agacaaggaagccaagtgagactccaagtgagagtgactggaatccctacacctgtggtg
 R  Q  G  S  Q  V  R  L  Q  V  R  V  T  G  I  P  T  P  V  V
aagttctaccgggatggagccgaaatccagagttcccttgatttccaaatttcacaagaa
 K  F  Y  R  D  G  A  E  I  Q  S  S  L  D  F  Q  I  S  Q  E
ggcgacctctacagcttactgattgcagaagcataccctgaggactcagggacctattca
 G  D  L  Y  S  L  L  I  A  E  A  Y  P  E  D  S  G  T  Y  S
gtaaatgccaccaatagcgttggaagagctacttcgactgctgagctccttgtgcagggc
 V  N  A  T  N  S  V  G  R  A  T  S  T  A  E  L  L  V  Q  G
gagacaactcaagcaccgacgtttacgcagccgttacaaagcgttgtggtactggagggt
 E  T  T  Q  A  P  T  F  T  Q  P  L  Q  S  V  V  V  L  E  G
agtaccgcaacctttgaggctcacattagtggttttccagttcctgaggtgagctggttt
 S  T  A  T  F  E  A  H  I  S  G  F  P  V  P  E  V  S  W  F
agggatggccaggtgatttccacttccactctgcccggcgtgcagatctcctttagcgat
 R  D  G  Q  V  I  S  T  S  T  L  P  G  V  Q  I  S  F  S  D
ggccgcgctaaactgacgatccccgccgtgactaaagccaacagtggacgatattccctg
 G  R  A  K  L  T  I  P  A  V  T  K  A  N  S  G  R  Y  S  L
aaagccaccaatggatctggacaagcgactagtactgctgagcttctcgtgaaagctgag
 K  A  T  N  G  S  G  Q  A  T  S  T  A  E  L  L  V  K  A  E
acagcaccacccaacttcgttcaacgactgcagagcatgaccgtgagacaaggaagccaa
 T  A  P  P  N  F  V  Q  R  L  Q  S  M  T  V  R  Q  G  S  Q
gtgagactccaagtgagagtgactggaatccctacacctgtggtgaagttctaccgggat
 V  R  L  Q  V  R  V  T  G  I  P  T  P  V  V  K  F  Y  R  D
ggagccgaaatccagagttcccttgatttccaaatttcacaagaaggcgacctctacagc
 G  A  E  I  Q  S  S  L  D  F  Q  I  S  Q  E  G  D  L  Y  S
ttactgattgcagaagcataccctgaggactcagggacctattcagtaaatgccaccaat
 L  L  I  A  E  A  Y  P  E  D  S  G  T  Y  S  V  N  A  T  N
agcgttggaagagctacttcgactgctgaattactggttcaaggtgaatgaaagcttgcg
 S  V  G  R  A  T  S  T  A  E  L  L  V  Q  G  E  -  K  L  A
```

## Z1Z2$^{KLER}$ in pETM-11 vector

```
nnnnnnnnnnnnnnctagantnntttgttnnnnttaagaaggagatataccatgaaacat
 X  X  X  X  X  -  X  X  L  X  X  L  R  R  R  Y  T  M  K  H
caccatcaccatcaccccatgagcgattacgacatccccactactgagaatctttatttt
 H  H  H  H  H  P  M  S  D  Y  D  I  P  T  T  E  N  L  Y  F
cagggcgccatggcaactcaagcaccgacgtttacgcagccgttacaaagcgttgtggta
 Q  G  A  M  A  T  Q  A  P  T  F  T  Q  P  L  Q  S  V  V  V
ctggagggtagtaccgcaacctttgaggctcacattagtggttttccagttcctgaggtg
 L  E  G  S  T  A  T  F  E  A  H  I  S  G  F  P  V  P  E  V
agctggtttagggatggccaggtgaaactcgaacgcctgcccggcgtgcagatctccttt
 S  W  F  R  D  G  Q  V  K  L  E  R  L  P  G  V  Q  I  S  F
agcgatggccgcgctaaactgacgatccccgccgtgactaaagccaacagtggacgatat
 S  D  G  R  A  K  L  T  I  P  A  V  T  K  A  N  S  G  R  Y
tccctgaaagccaccaatggatctggacaagcgactagtactgctgagcttctcgtgaaa
 S  L  K  A  T  N  G  S  G  Q  A  T  S  T  A  E  L  L  V  K
gctgagacagcaccacccaacttcgttcaacgactacagagcatgaccgtgagacaagga
 A  E  T  A  P  P  N  F  V  Q  R  L  Q  S  M  T  V  R  Q  G
agccaagtgagactccaagtgagagtgactggaatccctacacctgtggtgaagttctac
 S  Q  V  R  L  Q  V  R  V  T  G  I  P  T  P  V  V  K  F  Y
cgggatggagccgaaatccagagttcccttgatttccaaatttcacaagaaggcgacctc
```

```
 R  D  G  A  E  I  Q  S  S  L  D  F  Q  I  S  Q  E  G  D  L
tacagcttactgattgcagaagcataccctgaggactcagggacctattcagtaaatgcc
 Y  S  L  L  I  A  E  A  Y  P  E  D  S  G  T  Y  S  V  N  A
accaatagcgttggaagagctacttcgactgctgagctccttgtgcagggcgagacatga
 T  N  S  V  G  R  A  T  S  T  A  E  L  L  V  Q  G  E  T  -
```

## $Z_{1212}^{KLER}$ in the pETM-11 vector

```
nnnnnnnnnnnnnncnntnnngaataatttgtttaactttaagaaggagatataccatg
 X  X  X  X  X  X  X  E  -  F  C  L  T  L  R  R  R  Y  T  M
aaacatcaccatcaccatcaccccatgagcgattacgacatccccactactgagaatctt
 K  H  H  H  H  H  H  P  M  S  D  Y  D  I  P  T  T  E  N  L
tattttcagggcgccatggcaactcaagcaccgacgtttacgcagccgttacaaagcgtt
 Y  F  Q  G  A  M  A  T  Q  A  P  T  F  T  Q  P  L  Q  S  V
gtggtactggagggtagtaccgcaacctttgaggctcacattagtggttttccagttcct
 V  V  L  E  G  S  T  A  T  F  E  A  H  I  S  G  F  P  V  P
gaggtgagctggtttagggatggccaggtgaaactcgaacgcctgcccggcgtgcagatc
 E  V  S  W  F  R  D  G  Q  V  K  L  E  R  L  P  G  V  Q  I
tcctttagcgatggccgcgctaaactgacgatccccgccgtgactaaagccaacagtgga
 S  F  S  D  G  R  A  K  L  T  I  P  A  V  T  K  A  N  S  G
cgatattccctgaaagccaccaatggatctggacaagcgactagtactgctgagcttctc
 R  Y  S  L  K  A  T  N  G  S  G  Q  A  T  S  T  A  E  L  L
gtgaaagctgagacagcaccacccaacttcgttcaacgactgcagagcatgaccgtgaga
 V  K  A  E  T  A  P  P  N  F  V  Q  R  L  Q  S  M  T  V  R
caaggaagccaagtgagactccaagtgagagtgactggaatccctacacctgtggtgaag
 Q  G  S  Q  V  R  L  Q  V  R  V  T  G  I  P  T  P  V  V  K
ttctaccgggatggagccgaaatccagagttcccttgatttccaaatttcacaagaaggc
 F  Y  R  D  G  A  E  I  Q  S  S  L  D  F  Q  I  S  Q  E  G
gacctctacagcttactgattgcagaagcataccctgaggactcagggacctattcagta
 D  L  Y  S  L  L  I  A  E  A  Y  P  E  D  S  G  T  Y  S  V
aatgccaccaatagcgttggaagagctacttcgactgctgagctccttgtgcagggcgag
 N  A  T  N  S  V  G  R  A  T  S  T  A  E  L  L  V  Q  G  E
acaactcaagcaccgacgtttacgcagccgttacaaagcgttgtggtactggagggtagt
 T  T  Q  A  P  T  F  T  Q  P  L  Q  S  V  V  V  L  E  G  S
accgcaacctttgaggctcacattagtggttttccagttcctgaggtgagctggtttagg
 T  A  T  F  E  A  H  I  S  G  F  P  V  P  E  V  S  W  F  R
gatggccaggtgatttccacttccactctgcccggcgtgcagatctcctttagcgatggc
 D  G  Q  V  I  S  T  S  T  L  P  G  V  Q  I  S  F  S  D  G
cgcgctaaactgacgatccccgccgtgactaaagccaacagtggacgatattccctgaaa
 R  A  K  L  T  I  P  A  V  T  K  A  N  S  G  R  Y  S  L  K
gccaccaatggatctggacaagcgactagtactgctgagcttctcgtgaaagctgagaca
 A  T  N  G  S  G  Q  A  T  S  T  A  E  L  L  V  K  A  E  T
gcaccacccaacttcgttcaacgactgcagagcatgaccgtgagacaaggaagccaagtg
 A  P  P  N  F  V  Q  R  L  Q  S  M  T  V  R  Q  G  S  Q  V
agactccaagtgagagtgactggaatccctacacctgtggtgaagttctaccgggatgga
 R  L  Q  V  R  V  T  G  I  P  T  P  V  V  K  F  Y  R  D  G
gccgaaatccagagttcccttgatttccaaatttcacaagaaggcgacctctacagctta
 A  E  I  Q  S  S  L  D  F  Q  I  S  Q  E  G  D  L  Y  S  L
ctgattgcagaagcataccctgaggactcagggacctattcagtaaatgccaccaatagc
 L  I  A  E  A  Y  P  E  D  S  G  T  Y  S  V  N  A  T  N  S
gttggaagagctacttcgactgctgaattactggttcaaggtgaatgaaagcttgcggcc
 V  G  R  A  T  S  T  A  E  L  L  V  Q  G  E  -  K  L  A  A
```